Role of FABP7 and DHA in Glioblastoma Cell Migration

by

Xia Xu

A thesis submitted in partial fulfillment of the requirements for the degree of

Doctor of Philosophy

In

Cancer Sciences

Department of Oncology

University of Alberta

Abstract

Glioblastoma (GBM) is the most common primary brain malignancy and has a dismal prognosis. Despite advanced therapies, including surgery and concurrent radiotherapy with temozolomide (TMZ), GBM patients only have a 14.6-month median survival time. This dismal outcome can be attributed to the highly infiltrative nature and tumour heterogeneity in GBM, with the tumour cells infiltrating surrounding brain parenchyma at early stages of the disease. Brain fatty acid binding protein (B-FABP or FABP7) is highly expressed in GBM neural stem-like cells (GSCs), correlating with increased GBM cell migration/invasion and a poor clinical prognosis. Long chain polyunsaturated fatty acids (PUFAs) such as docosahexaenoic acid (DHA) and arachidonic acid (AA) are abundant in GBM tissues, with a considerably lower DHA content compared to normal adult brain. DHA and AA are preferred ligands of FABP7, with DHA having the stronger affinity for FABP7. Our combined studies have revealed that FABP7 affects GBM migration through several possible PUFA-dependent mechanisms, including membrane lipid remodeling, PUFA storage and energy production, and FABP7 cargo transport via GBM microtubes.

FABP7 is involved in both DHA and AA transport from membrane to cytosol. In Chapter 2, we used a quantitative fluorescence microscopy technique (Laurdan) and super-resolution STED microscopy to investigate FABP7-mediated DHA effect on the GBM cell membrane fluidity, GBM cell membrane FABP7 nanoscale domain formation and the impact of these biophysical properties on GBM cell migration. Our results demonstrate that FABP7 expression in GBM cells correlates with increased membrane

lipid order and punctate FABP7 nanodomains, which are particularly enriched at the migrating front of GBM cells. High-DHA/low-AA supplemented culture conditions result in dramatically diminished lipid order and disrupted FABP7 nanodomains.

In Chapter 3, we examine the role of FABP7 in the uptake of DHA from the culture medium. Using gas-chromatography and FABP7-depleted GSCs, we show that FABP7 expression facilitates: (i) uptake of DHA into GSC lipids, (ii) formation of lipid droplets, (iii) increasing the ω-3:ω-6 ratio in lipids (2-fold, $p < 0.0001$), and (iv) mitigating migration of GSCs. DHA supplementation in FABP7-expressing GSCs also inhibits their migration. Our results demonstrate that it may be possible to increase the DHA content in GSCs which are believed to drive GBM infiltrative properties.

Experiments in Chapters 2 and 4 also show that a preferred FABP7 subcellular localization in GBM cells is mitochondria, suggesting a role for FABP7 in mitochondrial PUFA β-oxidation and energy production. Using a highly aggressive patient-derived GSC line, A4-007N, we show that FABP7 affects GSC microtube formation. Microtubes serve as intercellular communication channels in GBM tumours. We propose that microtubes may also facilitate the transport of FABP7/PUFA across the tumour and perhaps into neighboring brain parenchyma.

We propose a model whereby FABP7 and relative levels of DHA versus AA in the tumour microenvironment determines GBM migratory/invasive properties, particularly in GBM patient-derived GSCs. The mechanistic insight into the role of FABP7 and its ligands provided by our study suggests that dietary intervention using a DHA-rich diet combined

with the current standard therapy, may benefit GBM patients by slowing down infiltration

of GSCs in the brain.

Preface

This thesis is original work by Xia Xu.

This work received research ethics approval from the Cross Cancer Institute Animal Care Committee, protocol #AC15220. GBM tissues from patients were consented prior to surgery under Health Research Ethics Board of Alberta Cancer Committee Protocol #HREBA.CC-14-0070.

Chapter 2 has been published as **Xia Xu***, Yixiong Wang*, Won-Shik Choi, Xuejun Sun, Roseline Godbout. *Super resolution microscopy reveals DHA-dependent alterations in glioblastoma membrane remodelling and cell migration.* **Nanoscale, (2021)** Jun 3;13(21):9706-9722. doi: 10.1039/d1nr02128a. *These authors contributed equally to this work. I was involved in all experimental aspects of the study, including study design, tissue culture, fatty acid treatments, confocal/super-resolution microscopy and writing the manuscript. Dr. Yixiong Wang was responsible for the direct conjugation of FABP7 antibody, image processing, quantification, statistical analysis and writing the manuscript. Dr. Xuejun Sun taught me super-resolution microscopy and supervised this aspect of the project. Won-Shik Choi did the western blot. Dr. Roseline Godbout was involved in all stages of the project and in writing the manuscript.

Chapter 3 has been published as Won-Shik Choi[*], **Xia Xu**[*], Susan Goruk, Yixiong Wang, Samir Patel, Michael Chow, Catherine J. Field and Roseline Godbout. *FABP7 Facilitates Uptake of Docosahexaenoic Acid in Glioblastoma Neural Stem-like Cells.* **Nutrients**. **(2021)** 13(8), 2664; https://doi.org/10.3390/nu13082664. *These authors contributed equally to this work. Won-Shik Choi and I were involved in all experimental

aspects of the study, including study design, fatty acid extraction, gas chromatography, data analysis and writing the manuscript. In addition, Won-Shik Choi carried out the tissue culture, RT-qPCR and Transwell assays. I established the stable GBM cell lines, and did the confocal microscopy and statistical analysis. Susan Goruk did the gas chromatography data analysis. Dr. Yixiong Wang was responsible for imaging analysis. Dr. Samir Patel and Dr. Michael Chow provided the GBM tumour tissue. Dr. Catherine J. Field supervised the gas chromatography study. Dr. Roseline Godbout was involved in all stages of the project and in writing the manuscript.

Acknowledgement

Table of Contents

List of Figures

List of Tables

Abbreviations

ΔΨm	Mitochondrial membrane potential
AA	Arachidonic acid
ABC	ATP-binding cassette
ACBP	Acyl-CoA-binding protein
ACLY	ATP-citrate lyase
ACSBG1	Acyl-CoA synthetase bubblegum family, member 1
ACSL	Acyl-CoA synthetase long chain family
ADA	Adrenic acid
ADC	Antibody drug conjugate
ALA	Alpha-linolenic acid
ATP	Adenosine triphosphate
ATX	Autotaxin
α-KG	α-ketoglutarate
B-FABP/FABP7	Brain fatty acid-binding protein
CNS	Central nervous system
COX	Cyclooxygenase
COX8A	Cytochrome C oxidase subunit 8A
cPLA$_2$	Ca^{2+}-dependent cytosolic PLA$_2$
CPT1c	Carnitine palmitoyltransferase 1, isoform c
CYP450	Cytochrome P450
D-2-HG	D-2-hydroxyglutarate
DHA	Docosahexaenoic acid
DMEM	Dulbecco's modified eagle medium
DPA	Docosapentaenoic acid
EDP	Epoxy-docosapentaenoic acid
EET	Epoxy-eicosatrienoic acid

EGF	Epidermal growth factor
EGFR	Epidermal growth factor receptor
EGFRvIII	Epidermal growth factor receptor variant III
EPA	Eicosapentaenoic acid
ER	Endoplasmic reticulum
ESR	Electron spin resonance
FA	Fatty acid
F-actin	Filamentous-actin
FABP	Fatty acid binding protein
FCS	Fluorescence correlation spectroscopy
FCS	Fetal calf serum
FGF	Fibroblast growth factor
FPKM	Fragments per kilobase million
FRET	Förster resonance energy transfer
GABRA1	Gamma-aminobutyric acid type A receptor alpha1
GDC	Genomic Data Commons
GFAP	Glial fibrillary acidic protein
GBM	Glioblastoma multiforme
GP	Generalized polarization
GSC	GBM neural stem-like cell
HBSS	Hank's balanced salt solution
HETE	Hydroxy-eicosatetraenoic fatty acid
HIF-1α	Hypoxia-inducible factor-1α
HpETE	Hydroperoxyeicosatetraenoic acid
IDH	Isocitrate dehydrogenase
IL	Interleukin
iPLA$_2$	Ca^{2+}-independent PLA$_2$
L1CAM	L1 cell adhesion molecule

LA	Linoleic acid
LCFA	Long chain fatty acid
LD	Lipid droplets
Ld	Liquid-disordered
LDLR	Low-density lipoprotein receptor
Lo	Liquid-ordered
LOX	Lipoxygenase
LPA	Lysophosphatidic acid
LPCAT3	Lysophosphatidylcholine acyltransferase 3
LPEAT2	Lysophosphatidylethanolamine acyltransferase 2
LPLAT	Lysophospholipid acyltransferase
LT	Leukotriene
LysoPtdCho	Lysophosphatidylcholine
LysoPtdEtn	Lysophosphatidylethanolamine
MaR	Maresin
MβCD	Methyl-β-cyclodextrin
Mfsd2a	Major facilitator superfamily domain containing 2a
MGMT	O-6-methylguanine-DNA methyltransferase
MRI	Magnetic resonance imaging
MUFA	Monounsaturated fatty acid
NAO	10-Nonyl acridine orange
NEFL	Neurofilament light polypeptide
NES	Nestin
NMR	Nuclear magnetic resonance
NND	Nearest neighbour distance
NOS	Not otherwise specified
NPD	Neuroprotection D
NSAIDs	Nonsteroidal anti-inflammatory drugs

NSC	Neural stem-like cell
NSG	NOD.Cg-PrkdcscidIl2rg
OA	Oleic acid
OPC	Oligodendrocyte precursor or progenitor cell
OXPHOS	Oxidative phosphorylation
PALM	Photoactivated localization microscopy
PC	phosphatidylcholine
PD	Protectin
PDGFRA	Platelet-derived growth factor receptor A
PDGFβ	Platelet-derived growth factor β
PDX	Patient-derived xenograft
PE	Phosphatidylethanolamine
PET	Polyethylene terephthalate
PFA	Paraformaldehyde
PG	Prostaglandin
PGE_2	Prostaglandin E_2
PI	Phosphatidylinositol
PL	Phospholipid
PLA	Phospholipase A
PPAR	Peroxisome proliferator-activated receptor
PS	Phosphatidylserine
PTG	Prostaglandin-endoperoxide synthase
PUFA	Polyunsaturated fatty acid
ROI	Regions of interest
ROS	Reactive oxygen specie
Rv	Resolvin
SA	Stearic acid
SD	Standard deviation

SDS-PAGE	Sodium dodecyl sulfate-polyacrylamide gel electrophoresis
SFA	Saturated fatty acid
SGZ	Subgranular zone
sn	Stereo-specifically number
sPLA$_2$	Ca^{2+}-dependent secretory phospholipase A$_2$
SPM	Specialized pro-resolving mediator
SREBP1	Sterol regulatory element-binding protein 1
STED	Stimulated emission depletion microscopy
STORM	Stochastic optical reconstruction microscopy
SVZ	Subventricular zone
TAM	Tumour-associated macrophage
TCA	Tricarboxylic acid
TL	Total lipid
TMRE	Tetramethylrhodamine ethyl ester
TMZ	Temozolomide
VEGFA	Vascular endothelial growth factor A
WGA	Wheat germ agglutinin
WHO	World Health Organization

Chapter 1.

Introduction

1.1 Glioblastoma

1.1.1 Classification and epidemiology of gliomas

Brain tumours are characterized by their high mortality rates due to their location and/or infiltrative/invasive growth properties. The average annual incidence of primary brain tumours and other central nervous system (CNS) tumours in the United States between 2013 and 2017 was 23.79 per 100,000 Individuals, approximately 29.7% of which were malignant (Ostrom et al., 2020). Malignant brain and CNS cancers were the 3rd most common cause of cancer death during this period of time. Meningioma and glioma were the most common adult primary brain tumours, while embryonal tumours were the most common histologic types for children and adolescents with primary brain tumours (Ostrom et al., 2020).

Glioma accounts for approximately 25.1% of all primary brain tumours and 80.8% of brain malignancies (Ostrom et al., 2020). Based on US cancer statistics (CBTRUS Statistical Report 2013-2017), the majority of gliomas occur in the supra-tentorium regions (includes frontal 26.8%, temporal 20.2%, parietal 11.6%, and occipital 2.8%), which accounts for 61.4% of glioma cases. Only a small proportion of glioma occur in CNS regions other than brain, such as spinal cord (4.1%) (Ostrom et al., 2020).

Under the World Health Organization (WHO) classification system, glioma is graded into four histological grades based on the increasing degree of undifferentiation and aggressiveness. Grade I is the least aggressive with the best prognosis, and grade IV is the most aggressive with the worst prognosis (Louis et al., 2007). According to the histological features, glioma can also be classified into several major groups, including astrocytoma (e.g., glioblastoma multiforme (GBM)), oligodendroglioma, ependymomas,

2

and mixed glioma (e.g., oligoastrocytoma) (Louis et al., 2007). Further classification can include featured differentiation patterns (e.g., pilocytic), tumour location (e.g., brain stem) and features of anaplasia (e.g., mitotic activity, microvascular proliferation and necrosis). Most gliomas, the so-called 'diffuse gliomas' (WHO grade II to grade IV), are featured by more diffuse infiltrative growth in the neuropil, compared to 'non-diffuse gliomas' (e.g., pilocytic astrocytoma) that have a circumscribed growth pattern (Weller et al., 2015b).

According to the 2013-2017 CBTRUS Statistical Report (5-year statistics for 104,103 glioma cases in both adults and children), 57.7% of gliomas are GBM, 7.1% are diffuse astrocytomas, 6.8% are anaplastic astrocytomas and 5.3% are oligodendrogliomas (Ostrom et al., 2020). In adults, the common gliomas are infiltrative astrocytomas (WHO grades II to IV), while pilocytic astrocytoma (WHO grade I) and diffuse midline gliomas (WHO grade IV) are the most common gliomas in children and young adults (Weller et al., 2015b).

In the 20th century, the glioma histological classification and grading system were the "gold standard" for glioma diagnosis and treatment, which is summarized in WHO Classification of CNS tumours published in 2007 (Louis et al., 2007). This histological classification is based on light microscopy features, such as levels of differentiation and cell-of-origin based on immunohistochemistry (IHC) analysis of different lineage protein markers (Louis et al., 2007). Based on this system, gliomas are mainly classified into three groups: oligodendroglioma, astrocytoma, and oligoastrocytoma. Even though this system has served clinicians well, it is associated with inter-observer variation, particularly in the classification of infiltrative gliomas (van den Bent, 2010; Weller et al., 2015a).

Over the last decade, more dedicated research in genomic, transcriptomic and epigenetic profiling of glioma has improved our understanding of the molecular pathogenesis of glioma in both adults and children (Weller et al., 2015b). In 2014, a meeting held in Haarlem, Netherlands, sponsored by the International Society of Neuropathology, reached the decision to incorporate the molecular parameters of CNS tumour diagnosis into a new classification scheme (Hainfellner et al., 2014). The combination of histological and molecular features to classify gliomas established better diagnostic criteria than the purely histological-based classification, particularly for infiltrative gliomas (Chen et al., 2017a). The new WHO classification that was published in 2016 changed the century-old principle of classifying gliomas based entirely on histology, thus allowing more precise tumour categorization (Komori et al., 2016).

Under the 2016 WHO classification for primary brain tumours, gliomas are classified based on multilayered parameters which include histological tumour type, WHO tumour grade (I to IV) and molecular information. For the first time, classification of diffuse glioma incorporates testing for isocitrate dehydrogenase (*IDH*) mutation, chromosome 1p/19q deletion, and histone mutations (Louis et al., 2016; Reifenberger et al., 2017). For example, diffuse astrocytoma, anaplastic astrocytoma and GBM are divided into *IDH*-mutant and *IDH*-wild type, and oligodendrogliomas are defined as *IDH*-mutant and 1p/19q co-deleted. Diffuse midline gliomas, more commonly occurring in children, are defined by histone H3 K27M mutations (Komori et al., 2016). When molecular testing is not available, a diagnostic designation of NOS (not otherwise specified) is allowed for some glioma types (Louis et al., 2016). (**Figure 1.1**). The mechanisms underlying these molecular alterations and their correlation with patient outcome are described in the next section. A

better understanding of glioma pathogenesis at the molecular level will improve the discovery of new therapeutic targets that offer the potential for improving patient outcome.

GBM accounts for 57.7% of all glioma cases, and has the lowest five-year survival (5%) amongst all CNS tumours (Ostrom et al., 2020) (**Figure 1.2**). According to several contemporary clinical trials (Chinot et al., 2014; Gilbert et al., 2014), the median survival for GBM patients is approximately 14-17 months. Under the 2016 WHO classification, GBM is divided into *IDH*-mutant type and *IDH*-wild type. Patients with mutations in *IDH-1* or *IDH-2* (~10% of GBM cases) are generally younger, with a history of lower grade glioma and a better prognosis than *IDH*-wild-type GBM patients (Ohgaki and Kleihues, 2013; Sturm et al., 2012). *IDH*-wild-type GBM manifests as 'primary tumour' with a short onset (less than three months) before diagnosis, without a pre-existing lower-grade glioma (Louis et al., 2016). In addition to the two GBM variants already listed in the 2007 classification (i.e., giant cell GBM and gliosarcoma), epithelioid GBM was introduced in the 2016 classification of *IDH*-wild-type GBM. This new variant is characterized by large epithelioid cells with abundant eosinophilic cytoplasm, large melanoma-like nucleoli, limited glial fibrillary acidic protein (GFAP) immunostaining, and is more common in children and young adults (Louis et al., 2016).
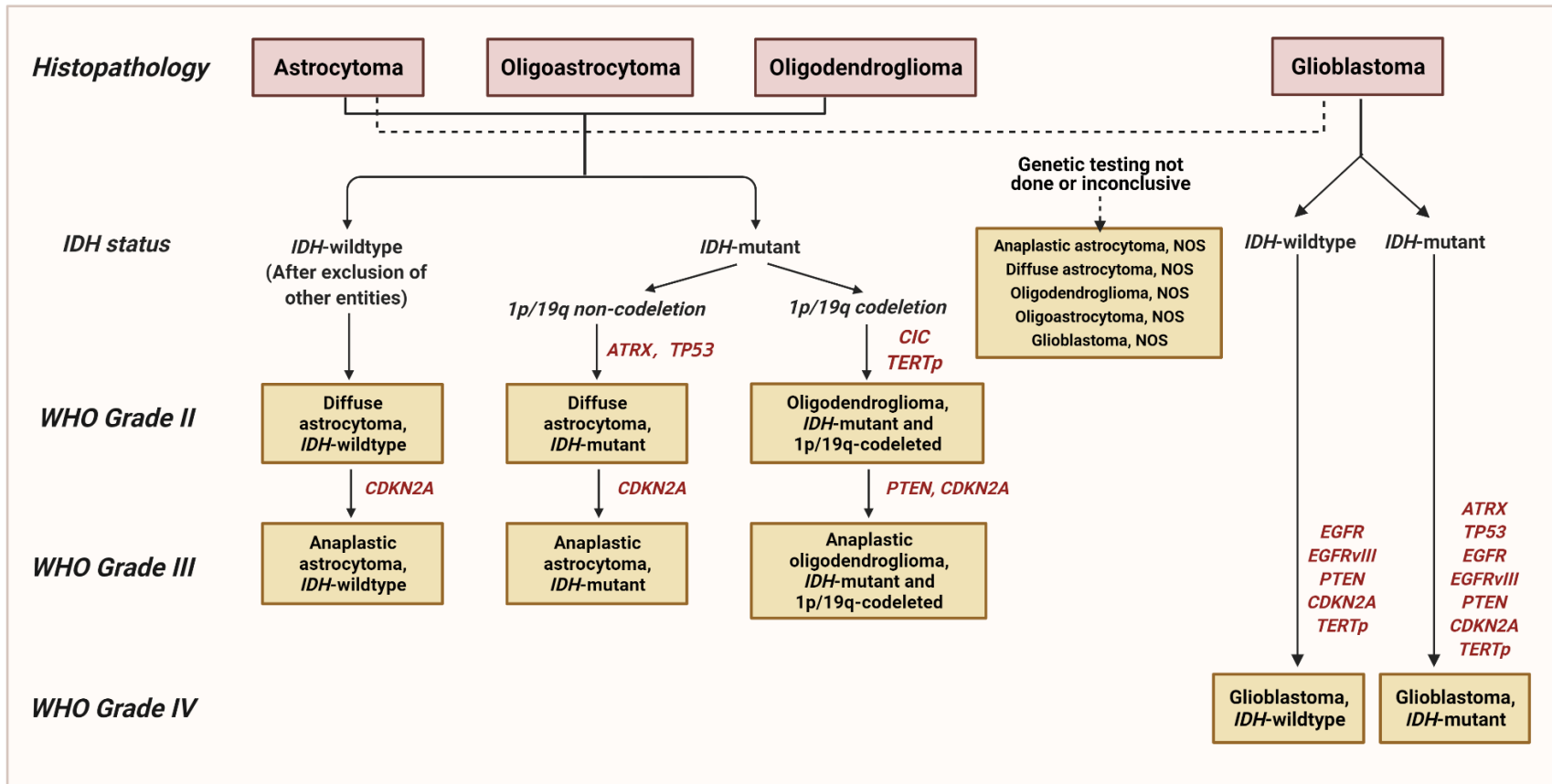
Figure 1.1 Classification of diffuse gliomas based on histological and genetic features.

Abbreviations; *ATRX*, α-thalassemia mental retardation X-linked; *IDH*, Isocitrate dehydrogenase; *Tp53*, Tumor protein p53; *CDKN2A*, Cyclin dependent kinase inhibitor 2A; *CIC*, capicua transcriptional repressor; *TERTp*, Telomerase reverse transcriptase; *PTEN*, Phosphatase and tensin homolog; *EGFR*, Epidermal growth factor receptor; *EGFRvIII*, Epidermal growth factor receptor variant III; *NOS*, Not otherwise specified; (Modified from 2016 WHO CNS tumour classification) (Louis et al., 2016).
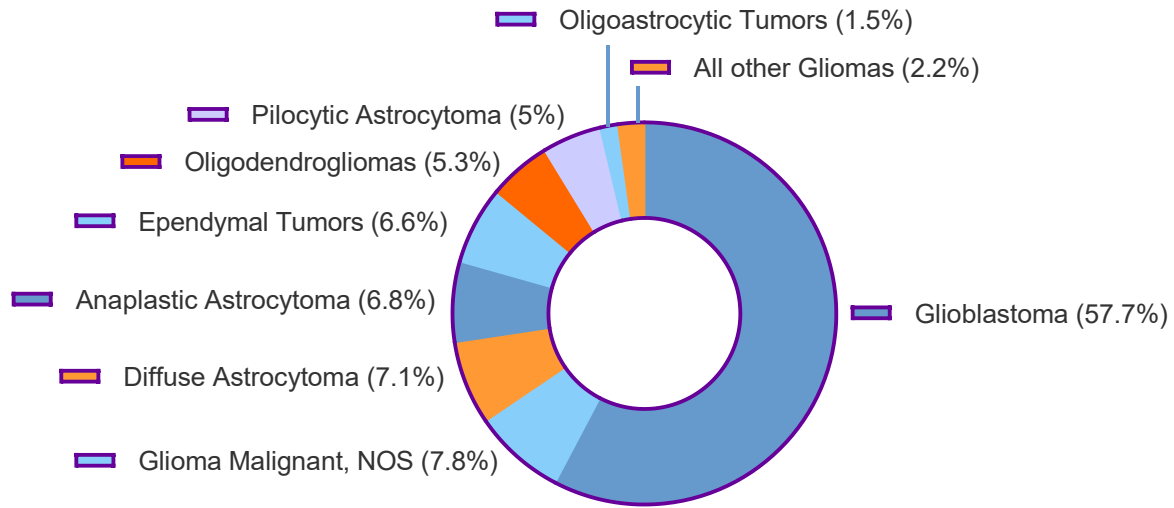
Figure 1.2 Percentages of primary gliomas in humans.

(Data obtained from CBTRUS Statistical Report 2020) (Ostrom et al., 2020)

Clinical presentation of GBM includes persistent headaches (~50%) (Forsyth and Posner, 1993), new onset of seizures (20% to 40%) (Glantz et al., 2000), as well as cognitive difficulties and personality changes (e.g., when tumour is located in specific prefrontal areas) (Zwinkels et al., 2016). Brain magnetic resonance imaging (MRI) with and without contrast (i.e., gadolinium) is the diagnostic approach when a patient has a suspected brain tumour such as GBM. The MRI typically reveals a necrotic core surrounded by white matter edema (Shukla et al., 2017).

Over the last two decades, several molecular target therapies have failed in phase III clinical trials. Thus, the classical treatment for GBM remains maximal surgical resection, radiotherapy and chemotherapy (Reifenberger et al., 2017). After neuroimaging, patients with a suspected GBM will be scheduled for surgical resection or stereotactic biopsy (i.e.,

inoperable tumours), aiming at relieving mass effect and providing tumour tissue for histologic diagnosis. As surgical resection is not curative, it is followed by radiation therapy (i.e., total dose of 60 Gy, divided into 30 fractions) and concomitant administration of temozolomide (TMZ) (i.e., 75 mg daily per square meter of body-surface area for 42 days). Addition of temozolomide to the treatment regimen increased GBM patient overall median survival to 14.6 months compared to 12.1 months with radiotherapy alone (Davis, 2016; Stupp et al., 2005). The 2-year survival rate increased to 26.5% with TMZ concomitant with radiotherapy, compared to 10.4% for radiotherapy alone (Stupp et al., 2005). Unfortunately, clinical trials have shown that neither dose-intensified TMZ (Gilbert et al., 2013) nor the vascular endothelial growth factor A (VEGFA)-specific antibody bevacizumab (Chinot et al., 2014; Gilbert et al., 2014) improves overall GBM patient survival. As GBM tumours are infiltrative and incompletely resectable, tumour progression and recurrence typically occur. The treatment options for recurrent GBM depend on pattern of failure and the type of initial treatment (Reifenberger et al., 2017).

1.1.2 GBM molecular biomarkers, subtypes, and their related therapies

Determining the molecular biomarkers and subtypes of GBM is increasingly requested by neuro-oncologists for guiding post-surgery therapy in GBM patients. In addition to important diagnostic biomarkers such as *IDH* mutation for glioma classification, other predictive biomarkers are showing promise for GBM management: e.g., *MGMT*-promoter methylation for predicting response to TMZ (Gilbert et al., 2013); *IDH* mutation to guide treatment with IDH inhibitors (Rohle et al., 2013; Schumacher et al., 2014); and epidermal growth factor receptor (*EGFR)* amplification/*EGFRvIII* positivity to guide

treatment with EGFR inhibitors or antibody-based therapies (Sampson et al., 2014; Zahonero et al., 2015).

O^6-methylguanine-DNA methyltransferase (MGMT) is a DNA repair protein that diminishes DNA damage induced by the alkylating agent temozolomide (TMZ), which is the standard drug used in GBM therapy (Hegi et al., 2005). Approximately 40% of *IDH*-wild-type GBM have hypermethylation of an MGMT-associated 5´-CpG island (Wick et al., 2014), which is known as *MGMT* promoter methylation. *MGMT* promoter methylation is closely correlated with benefits from TMZ and better survival in *IDH* wild-type glioma patients (Gilbert et al., 2013).

The phase 3 clinical trial conducted by Stupp, Mason *et al.* showed the benefit of combined radiation therapy and TMZ (i.e., median survival: 14.6 months) compared to radiation therapy alone (i.e., median survival: 12.1 months), which is the guideline for GBM treatment (Stupp et al., 2005). However, this trial only included GBM patients 70 years of age or younger. The standard of care for GBM patients >70 years remained surgical resection followed by radiation therapy (Keime-Guibert et al., 2007). In 2012, phase III clinical trials showed benefits in elderly patients from TMZ therapy alone (i.e., median survival: 9 months) compared to radiation therapy alone (i.e., median survival: 5.2 months) (Malmstrom et al., 2012; Wick et al., 2012). Similar results were observed when TMZ combined with radiation therapy was compared to a short-course of radiation therapy alone (Perry et al., 2017). Thus, *MGMT* promoter methylation has become a predictive marker to select patients for TMZ treatment, with particular benefits in elderly patients. Currently, the *MGMT* promoter methylation status is determined by methylation-

specific PCR and the Infinium (Illumina) methylation bead array technique (Wick et al., 2014).

IDH mutations are common in WHO grade II and WHO grade III gliomas (>80%), as well as secondary GBM malignancies (73%), but rarely occur in primary GBM malignancies (3.7%) (Nobusawa et al., 2009; Parsons et al., 2008; Yan et al., 2009). *IDH* enzymes catalyse the oxidative decarboxylation of isocitrate, playing essential roles in the tricarboxylic acid (TCA) cycle and cellular energy homoeostasis. The catalytic sites of IDH1 (located in the cytoplasm and peroxisomes) and IDH2 (located in mitochondria) exhibit affinity for the substrate isocitrate, and catalyze its oxidative decarboxylation, resulting in the formation of α-ketoglutarate (α-KG). The frequently mutated active sites in gliomas are arginine 132 (R132) for *IDH1*, R140 or R172 for *IDH2*, resulting in the failure of substrate recognition (Hurley et al., 1991; Yan et al., 2009). Mutant IDH enzymes promote conversion of a-KG for D-2-hydroxyglutarate (D-2-HG). The impact of *IDH* mutation and D-2-HG accumulation in GBM includes reprogrammed metabolism (i.e., inhibiting a-KG-dependent dioxygenases) (Xu et al., 2011), epigenome alterations (i.e., wide-spread global DNA hypermethylation and histone methylation) (Unruh et al., 2019) and redox homoeostasis [i.e., accumulation of reactive oxygen species (ROS) and oxidative damage] (Han et al., 2020; Turkalp et al., 2014).

Rohle *et al.* reported the first synthetic small-molecule inhibitor of mutant IDH1 (R132H), called AGI-5198, which decreased production of D-2-HG and reduced *IDH*1-mutated patient-derived anaplastic oligodendroglioma (WHO grade III) tumour growth in murine xenografts (Rohle et al., 2013). A recent phase I clinical trial reported that AG-881 (a dual inhibitor of both mutant IDH1 and IDH2) was associated with a favorable safety

profile (at doses <100 mg) in glioma patients (K. et al., 2019; K. et al., 2018). In a study using a U87 GBM cell line transfected with a mutated *IDH1* (R132H) expression construct, both *in vitro* and *in vivo* U87 tumour proliferation was reduced; however, the cells were still able to form tumours in a xenograft mouse model (Bralten et al., 2011). This result suggests some challenges to the development of IDH-targeted therapies.

GBM is a highly heterogeneous tumour. To better understand determinants of GBM tumour evolution and therapeutic resistance, genome-wide expression studies were carried out with hundreds of GBM patients. Using these data, a GBM transcriptome-based classification was established that displayed features of four distinct GBM molecular subtypes: classical, mesenchymal, proneural, and neural (Verhaak et al., 2010) (**Figure 1.3**).

	Classical	Mesenchymal	Proneural	Neural
Genetic aberrations	• *EGFR* amplification • *EGFRvIII* mutation • Lack of *TP53* mutations • Chr. 7 gain • Chr. 10 loss	• *NF1* mutation and loss • Presence of mesenchymal and astrocyte markers (MET and CD44)	• *PDGFRA* overexpression/mutaion • *IDH* mutation • Proneural and oligodendrocytic markers (SOX2, DCX and OLIG2)	• Neuron markers (GABRA1, NEFL)
Clinical Features	• Older adults • Median OS 12-14 months • Clinical outcome improved with TMZ/radiation	• Older adults • Median OS 12-14 months • Clinical outcome improved with TMZ/radiation	• Younger adults • Secondary GBM • *IDH* mutation patients have better median OS	Not validated in recent GBM cluster analysis*

Figure 1.3 Glioblastoma molecular subtypes based on key genes.

Abbreviations; GBM, Glioblastoma; *IDH*, Isocitrate dehydrogenase; *Tp53*, Tumor protein p53; *PTEN*, Phosphatase and tensin homolog; *EGFR*, Epidermal growth factor receptor; *EGFRvIII*, Epidermal growth factor receptor variant III; *NF1*, Neurofibromin 1; *PDGFRA*, Platelet-derived growth factor receptor A; GABRA1, Gamma-aminobutyric acid type A receptor alpha1; NEFL, Neurofilament light polypeptide; OS, Overall survival; TMZ, Temozolomide; MET, MET proto-oncogene; SOX2, SRY-box transcription factor 2; DCX, Doublecortin; OLIG2, Oligodendrocyte transcription factor 2; Summarized from (Verhaak et al., 2010; Wang et al., 2017)

The classical subtype showed the highest expression of *EGFR* amplification compared to the other subtypes. The mesenchymal subtype was associated with a high frequency of *NF1* mutations/loss. Loss/mutations of *NF1* (observed in ~13% of GBM patients) is correlated with increased invasion, proliferation, and tumour aggressiveness in GBM (Fadhlullah et al., 2019). Both primary and recurrent tumours of the mesenchymal subtype showed worse patient survival than classical and proneural subtypes (Verhaak et al., 2010; Wang et al., 2017). The proneural subtype is found primarily in younger patients, particularly in lower grade glioma and secondary GBM, and features high platelet-derived growth factor receptor A (*PDGFRA*) gene expression and *IDH* mutation. Patients with the proneural subtype of GBM have better survival rates than the other subtypes (Phillips et al., 2006; Verhaak et al., 2010). However, when patients with *IDH* mutations are excluded from the analysis, the proneural subtype has a worse prognosis than the other subtypes (Sturm et al., 2012). The neural subtype is characterized by high levels of neuronal markers [e.g., *GABRA1* (gamma-aminobutyric acid type A receptor alpha1*) and NEFL* (Neurofilament light polypeptide)] (Verhaak et al., 2010). More recently, further cluster analysis re-classified GBM in three subtypes (i.e., classical, mesenchymal and proneural). It was deemed that the neural signature was associated with non-tumourigenic cells in the tumour microenvironment (Behnan et al., 2019; Wang et al., 2017). Recent GBM tumour single cell RNA-sequencing analyses demonstrated that GBM bulk tumours consist of 2 or 3 GBM subtypes (Patel et al., 2014; Wang et al., 2017). Thus, subtype switching from primary to recurrent GBM is common, such as proneural to mesenchymal transition (Wang et al., 2017).

Epidermal Growth Factor Receptor (*EGFR*) is a transmembrane receptor tyrosine kinase enriched in the classical subtype of GBM. *EGFR* amplification is detected in 57.4% of GBM tumours (Brennan et al., 2013), and is correlated with poor clinical prognosis in GBM patients (Li et al., 2018). The most common mutated form of *EGFR* found in GBM shows deletion of exons 2–7 (i.e., *EGFRvIII*, found in 20–25% of *IDH* wild-type GBM) (Nishikawa et al., 1994). *EGFRvIII* lacks 268 amino acids (from 6 to 273), resulting from an in-frame deletion of 801 base pairs in the extracellular domain. As a result, EGFRvIII is constitutively active without ligand binding (An et al., 2018). Both *EGFR* amplification and *EGFRvIII* can enhance GBM angiogenesis and tumour invasion (Keller and Schmidt, 2017).

The most widely studied EGFR inhibitors in GBM are small molecule tyrosine kinase inhibitors and monoclonal antibodies. First-generation (e.g., gefitinib and erlotinib), second-generation (e.g., afatinib) (An et al., 2018), third-generation EGFR (e.g., panitumumab) inhibitors, as well as EGFR monoclonal antibody (e.g., cetuximab) (Neyns et al., 2009) have not shown efficacy as a mono-therapy in clinical trials due to multiple resistance mechanisms (Saleem et al., 2019). The two main mechanisms of resistance to EGFR inhibitors/monoclonal antibodies are target independence (i.e., alterations in expression/structure of the target, such as *EGFRvIII* mutants) and target compensation (i.e., alternative signaling pathways are activated, such as platelet-derived growth factor β (*PDGFβ*)) (Saleem et al., 2019). Thus, overcoming resistance to EGFR-based therapies may require combination with *EGFR* co-occurred mutation targets or EGFR downstream specific targets.

Multi-target therapies for *EGFR* amplification may provide excellent strategies to move forward, such as antibody drug conjugates (ADCs). For example, a new ADC, depatuxizumab mafodotin (ABT-414) that targets both EGFR and EGFRvIII, releases a potent anti-microtubule agent inside targeted cancer cells (Phillips et al., 2016). A recent phase II clinical trial for recurrent GBM reported that combined ABT-414 and TMZ can slightly improve median overall patient survival (9.6 months), compared to ABT-414 alone (7.9 months) and chemotherapy alone (8.2 months) (van den Bent et al., 2020).

1.1.3 GBM cell-of-origin and stem-like cells

Identification of the cell-of-origin in GBM is key to our understanding of disease etiology and development of new therapies. There has been controversy about the cell-of-origin of GBM for decades. Currently, there are two main hypotheses for the cell-of-origin of GBM: (i) neural stem-like cells (NSCs), and (ii) oligodendrocyte precursor or progenitor cells (OPCs). The evidence supporting NSCs versus OPCs as the cell-of-origin is based on the following: (i) similarity of cell surface markers and gene profiling, and (ii) tumorigenic capacity in xenograft mouse models.

Neural stem cells (NSCs) are self-renewing, multipotent cells that generate the multiple cell types in the nervous system, including neurons and glia (astrocytes and oligodendrocytes) during embryonic development (Gage, 2000; Reynolds and Weiss, 1992). NSCs divide symmetrically to self-renew or divide asymmetrically to generate progenitor cells that have limited self-renewal potential (Morrison and Kimble, 2006). In mammalian brain, NCSs persist into adulthood and contribute to brain plasticity throughout life, with a primary site of plasticity being the dentate gyrus of the hippocampus.

In adult rodent brain, there are two major niches for NSCs: the subventricular zone (SVZ) and the subgranular zone (SGZ) (Bond et al., 2015).

Adult SVZ NSCs (radial glia-like cells, also named type B cells) give rise to transient amplifying progenitors (type C cells), which undergo several divisions before becoming neuroblasts (type A cells) (Doetsch et al., 1999). SVZ astrocytes express GFAP and maintain stem cell characteristics (Doetsch et al., 1999). The hypothesis that GBMs may originate from SVZ NSCs that have undergone malignant transformation has been investigated in a study by Lee *et al.* in 2018 (Lee et al., 2018). This study showed that normal SVZ tissue distantly located from the tumour carries low levels of GBM driver mutations, which are present at high levels in their matching GBM. These authors also presented evidence from genome-edited mouse models showing that astrocyte-like NSCs carrying driver mutations can migrate from the SVZ and develop GBM in distant brain regions (Lee et al., 2018). In terms of clinical implications for GBM management, several clinical studies have already shown that radiotherapy targeting the SVZ NSC niches significantly improves progression-free survival (e.g., from 7.2 months to 15 months in one study) (Evers et al., 2010; Nourallah et al., 2017).

In contract to NSCs, OPCs are generally considered as lineage-restricted precursor cells, which also share expression profile markers with GBM cells (e.g., Olig2 and NG2). Liu *et al.* provided the first convincing evidence in support of OPCs serving as the cell-of-origin for GBM, by studying concurrent *p53/Nf1* mutations in mice to model gliomagenesis (Liu et al., 2011; Zong et al., 2005). More evidence supporting OPCs as the GBM cells-of-origin comes from OPC-specific conditional knock-out mice (e.g., *NG2-CreERT*) (Alcantara Llaguno et al., 2015). Using their mouse model, Alcantara *et al.*

showed that both NSCs and OPCs can function as cells-of-origin for GBMs, giving rise to different GBM subtypes and contributing to the intertumoral heterogeneity characteristic of GBMs (Alcantara Llaguno et al., 2015). With the tremendous progress recently made in high throughput technologies (i.e., drug screening, deep sequencing, single-cell analysis), a better understanding of the cell-of-origin of GBM can help in the development of novel targeted therapeutic strategies.

To date, many GBM mouse models have been developed using disease-relevant initiating mutations in tumour suppressors (e.g., *PTEN*, *Trp53* and *Nf1*) and oncogenes (e.g., *EGFRvIII* and *PDGFRA*) (Huse and Holland, 2009). For example, Alcantara *et al.* used a transgenic mouse strain carrying tamoxifen-inducible Cre (*Nestin-CreER^{T2}*) to target neural stem/progenitor cells *in vivo* and drive *PTEN*, *p53* and *Nf1* deletion specifically in postnatal SVZ. *Nestin-CreER^{T2}* transgenic mice were injected with tamoxifen at either embryonic day (E13.5) or adult (4 weeks of age). Similar to E13.5 mouse, adult transgenic mice showed regionally restricted Cre activity, particularly in neural stem and progenitor cells located at the SVZ and the SGZ. Tamoxifen induction in both E13.5 and adult transgenic mice resulted in diffusely infiltrating grade III or IV astrocytomas. (Alcantara Llaguno et al., 2009). Other studies using different approaches to target neural stem-like cells or progenitor cells have shown similar results (Chow et al., 2011; Holland et al., 2000). A study aimed at addressing whether more mature neural cells may also serve as cells-of-origin for GBM suggest that increased lineage restriction is accompanied by decreased susceptibility to GBM transformation (Alcantara Llaguno et al., 2019).

GBM is characterized by tumour heterogeneity and therapeutic resistance, which are thought to be promoted by a subpopulation of GBM stem cells (Bao et al., 2006; Chen et al., 2012). Human NSCs were first isolated in 2000 (Uchida et al., 2000). This was followed by a burst of reports showing that GBM stem cells share features with NSCs including expression of NSC markers such as CD133, SSEA1, FABP7 and SOX-2, and the ability to generate multi-lineage progeny (Berezovsky et al., 2014; De Rosa et al., 2012; Singh et al., 2004; Son et al., 2009). GBM stem cells are defined based on three principal functional features that include sustained self-renewal, tumour initiation and persistent proliferation. Several methods have been used for GBM stem cell isolation. These include neurosphere cultures (based on inclusion of epidermal growth factor and fibroblast growth factor in culture medium (Pastrana et al., 2011) and flow cytometry (based on expression by GBM stem cells of drug efflux transporters like ATP-binding cassette (ABC) transporters) (Bleau et al., 2009). Recent studies are more focused on the interactions of GBM stem cells with their microenvironment and the metabolic reprogramming of cancer stem cells. The formation of hypoxic-necrotic niches enriched in GSC cells is one of the main characteristics of GBM (Hambardzumyan and Bergers, 2015). Hypoxia facilitates the maintenance of GSCs through both hypoxia-inducible factor-1α (HIF-1α) and HIF2α in the nutrient-restricted microenvironment, driving GBM progression and resistance to therapy (Li et al., 2009; Qiang et al., 2012; Semenza, 2013). Emerging evidence has demonstrated that compared to their more differentiated counterparts, GBM stem cells are less glycolytic and preferentially utilize mitochondrial oxidative phosphorylation for their energy needs (Hoang-Minh et al., 2018; Lin et al., 2017). Thus, the tumour microenvironment and metabolism-targeting approaches are

upcoming potential therapeutic avenues for GBM, in particular when combined with conventional treatment (Garnier et al., 2019).

1.2 Brain fatty acid binding protein

1.2.1 FABPs family

Long chain fatty acids (LCFAs) are highly hydrophobic molecules, so their intracellular transportation is highly dependent on fatty acid transporters. Fatty acid binding proteins (FABPs) are small protein vehicles that facilitate fatty acid uptake and transport. FABPs transport fatty acids to specific intracellular organelles such as lipid droplets for lipid storage, mitochondria or peroxisome for fatty acid β-oxidation, endoplasmic reticulum (ER) for lipid metabolism and phospholipid synthesis, or nucleus for lipid-mediated transcriptional factor activation (Coe and Bernlohr, 1998; Liu et al., 2010; Storch and Corsico, 2008). Since the discovery of the first FABP in 1972, 9 additional FABPs have been identified in humans*.*

FABPs exhibit tissue-specific expression patterns, different lipid binding affinities and different mechanisms for binding to their lipid ligands (Furuhashi and Hotamisligil, 2008). Using X-ray crystallography, nuclear magnetic resonance and other biochemical and biophysical techniques on isolated recombinant proteins, these ~15 kDa FABPs have been shown to have highly conserved structures, which consist of two orthogonal β-sheets (i.e.,10-stranded antiparallel β-barrel structure) and an α-helical cap (Chmurzynska, 2006). The fatty acid binding pocket is located inside the β-barrel, and the N-terminal helix–loop–helix 'cap' serves as the fatty acid (FA) entry site (Chmurzynska, 2006).

FAs from the extracellular milieu are known to diffuse across phospholipid bilayers in cell membranes (Kamp et al., 1995). FAs can also be generated via hydrolysis of phospholipids by phospholipases (Bazinet and Laye, 2014). FABPs not only promote uptake of FAs from the microenvironment via FABP-phospholipid interactions (Falomir-Lockhart et al., 2011; Hsu and Storch, 1996), but also serve as intracellular FA transporters, which at least in theory, requires their direct ligand transfer from a donor membrane to a targeted acceptor membrane (Zamarreno et al., 2012). The helical N-terminus of unliganded FABPs associates with membranes via electrostatic interactions. Nuclear Magnetic Resonance (NMR) and Electron Spin Resonance (ESR) were used to show that FABP7 binding to its polyunsaturated fatty acid (PUFA) ligands induces a conformational alteration resulting in its dissociation from the membrane   FABPs   not only promote FA uptake from the microenvironment, but also transport FAs to the specific compartments within the cell, such as nucleus, ER and mitochondria (Furuhashi and Hotamisligil, 2008). Intestinal-FABP (I-FABP) and liver-FABP (L-FABP)) have been shown to transport their FA ligands to mitochondria, ER and/or Golgi (Karsenty et al., 2009; Thumser and Storch, 2007). Such a role for FABP7 has not been investigated to date.

1.2.2 FABPs in the brain

Three of the ten mammalian FABPs (FABP3, FABP5 and FABP7) are highly expressed in the developing and/or adult brain (Liu et al., 2010). Unlike FABP3 which mainly participates in synaptogenesis and myelinogenesis after birth until adulthood, both FABP5 and FABP7 are primarily expressed during embryonic brain development, with a

gradual decrease in expression after birth (Owada et al., 1996). FABP7 is specifically expressed in radial glial cells, also recognized as NSCs (Feng et al., 1994; Kurtz et al., 1994; Xu et al., 1996). Functional studies have revealed many different roles for FABP5 and FABP7, such as neuronal/glial cell generation (De Leon et al., 1996) and radial glial fiber system establishment (FABP7) (Feng et al., 1994; Kurtz et al., 1994), and progenitor cell differentiation and migration (both FABP5 and FABP7) (Owada, 2008).

FABP3, FABP5 and FABP7 have preferences for specific FA ligands (Liu et al., 2010). For example, human FABP3 shows highest binding affinity for ω-6 PUFA (e.g., arachidonic acid (AA)), whereas human FABP5 and FABP7 show the highest binding affinity to saturated fatty acids (e.g. stearic acid (SA)) and ω-3 PUFA (e.g., docosahexaenoic acid (DHA)), respectively (Balendiran et al., 2000).

FABP3 is mainly expressed after birth until adulthood, and is involved in neurite formation and synapse maturation (Owada et al., 1996). *FABP3* gene-ablated mice show a 24% reduction in ω-6 FA incorporation into the brain (Murphy et al., 2005). Interestingly, recent studies have demonstrated that FABP5 may also transport DHA across the blood-brain barrier. In a *FABP5* knock-out mice model, there was a 15% reduction in brain DHA compared to wild-type mice (Pan et al., 2015b; Pan et al., 2016). The same group of investigators further demonstrated that DHA supplementation can induce an upregulation of FABP5 protein expression in human brain microvascular brain endothelial cells and C57BL/6 mice brain micro-vessels (Pan et al., 2018).

During mammalian brain development, FABP7 is specifically expressed in radial glial cells (Feng et al., 1994; Kurtz et al., 1994). FABP7 serves as a transporter protein for both DHA and AA in the developing brain (Liu et al., 2010). FABP7 dramatically

declines after birth, while it is highly expressed in GBM and particularly in GBM stem-like cells (De Rosa et al., 2012). FABP7 knockout resulted in reduced neural progenitor cells numbers and attenuated neurogenesis in developing mouse brain (Watanabe et al., 2007), with neonatal mice showing a small reduction in brain DHA (Owada et al., 2006).

1.2.3 Roles of FABP7 in GBM

FABP7 expression in developing brain is important for neuronal migration and neurogenesis (Liu et al., 2010; Owada, 2008). Neutralization of FABP7 in co-cultures of immature cerebellar neurons and radial glia cells revealed a role for FABP7 in the establishment of the radial glial fiber system, which is necessary for the migration of immature neurons to establish cortical layers (Feng et al., 1994). A subsequent study by the same group showed that FABP7 expression in radial glial cells was induced by co-culture with differentiating neurons (Feng and Heintz, 1995), with *FABP7* up-regulated through activation of the Notch signalling pathway (Anthony et al., 2005).

High levels of FABP7 correlate with increased GBM tumour invasion, and poor prognosis in GBM patients (De Rosa et al., 2012; Kaloshi et al., 2007; Liang et al., 2005; Mita et al., 2007). Ectopic expression of FABP7 in non-FABP7 expressing GBM cells increases GBM cell migration, whereas FABP7 knockdown in FABP7-expressing GBM cells inhibits migration (Liang et al., 2005; Mita et al., 2007). These findings suggest an important role for FABP7 in the highly infiltrative and invasive properties of GBM tumours. In addition to GBM, FABP7 has also been shown to be associated with increased migratory/invasive properties and poor patient outcome in breast cancer, renal cell carcinoma and melanoma (Liu et al., 2012; Slipicevic et al., 2008; Tolle et al., 2011).

Furthermore, a recent study has shown that FABP7 expression in HER2+ breast cancers is associated with a higher incidence of brain metastasis with FABP7 driving metabolic reprogramming to allow better survival in the brain environment (Cordero et al., 2019).

Similar to brain, GBM tissue is rich in PUFAs, including ω-6 AA and ω-3 DHA (Martin et al., 1996). However, DHA levels are reduced by ~50% in GBM tumour samples compared to adult brain tissue, with AA levels remaining unchanged (Marszalek et al., 2010; Martin et al., 1996). We previously reported that ectopic expression of FABP7 in the U87 GBM cell line increased cell migration (Mita et al., 2007). We further showed that cell migration was inhibited by supplementing culture medium with DHA (Mita et al., 2010). We found that AA-mediated cell migration was dependent on activation of the AA/COX-2-pathway and prostaglandin E_2 (PGE_2) production (Mita et al., 2010).

In GBM patient tissue studies, nuclear expression of FABP7 was more specifically correlated with *EGFR* amplification and more invasive GBM tumours (Kaloshi et al., 2007; Liang et al., 2006). Nuclear FABP7 and its FA ligands are believed to play a role in gene regulation by activating peroxisome proliferator-activated receptors (PPARs) which have been implicated in multiple disease models (Adida and Spener, 2006; Kwong et al., 2019; Tripathi et al., 2017). In support of FABP7/PPARs playing a role in the regulation of GBM cell migration, De Rosa *et al*. found that PPARγ inhibition by PPAR antagonists resulted in inhibition of the migration of FABP7-expressing GBM patient-derived neurosphere cells (De Rosa et al., 2012). Conversely, PPARγ depletion in DHA-supplemented FABP7-expressing cells increased cell migration (Mita et al., 2010). These results suggest the FABP7 expression and the DHA/AA ratio play key roles in PPARγ-mediated regulation of GBM cell migration (Elsherbiny et al., 2013).

GBM, similar to other cancers, have long been thought to primarily use anaerobic glucose metabolism for energy production; however, emerging studies have revealed that FAs can also be important sources of energy production in cancer cells (Lin et al., 2017). Fatty acid oxidation has been shown to be a major contributor to aerobic respiration in GBM primary cells cultured under serum-free conditions (Lin et al., 2017). Furthermore, FABP7 depletion in GBM cell lines significantly decreased the formation of lipid droplets (LDs) after hypoxia, suggesting a role for FABP7 in LD formation (Bensaad et al., 2014). More recently, high levels of FABP7 in GBM slow-cycling cells (likely NSCs) was found to correlate with reduced glycolysis, increased LD formation, increased mitochondria oxidative phosphorylation and higher ATP levels compared to the more differentiated/low FABP7-expressing GBM cells (Hoang-Minh et al., 2018). These investigators did not examine the subcellular localization of FABP7 or possible roles for FABP7 and its ligands in metabolic reprogramming.

In addition to FABP7/PUFA-mediated PPARγ activation and possible effects on mitochondrial reprogramming, FABP7 also appears to play a role in plasma membrane remodelling. In a previous publication, we showed that FABP7 co-localizes with filamentous (F)-actin at the leading edge of GBM cells cultured in AA-rich medium (Mita et al., 2007). More recently, FABP7 was found to transcriptionally regulate the expression of caveolin-1 in membrane rafts of primary astrocytes in culture (Kagawa et al., 2015). As plasma membrane ordered domain formation is a key determinant in cancer cell migration/invasion (Erazo-Oliveras et al., 2018), further studies focused on the role of FABP7 in GBM membrane lipid remodeling will help to elucidate the role of FABP7 in driving GBM cell migration and invasion.

1.3 Fatty acids

1.3.1 Polyunsaturated fatty acids (PUFAs) in the brain

Fatty acids are classified based on their carbon chain length and degree of saturation. Polyunsaturated fatty acids (PUFAs) are fatty acids that contain more than one double bond in their carbon backbone. Some PUFAs are defined as essential fatty acids, which means that they must be provided in the diet. Two essential PUFAs are alpha-linolenic acid (ALA, C18:3ω-3) and linoleic acid (LA, C18:2ω-6), precursors of docosahexaenoic acid (DHA) and arachidonic acid (AA), respectively (Czapski et al., 2016; Simopoulos, 1999). It is recommended that DHA and eicosapentaenoic acid (EPA) should also be included in the diet because of their low conversion rates from ALA.

LA is the most abundant PUFA in nature, and is mainly found in seed oils (e.g., soybean, sunflower, and in wheat germ), meat and eggs (Whelan and Fritsche, 2013). LA is also the most abundant PUFA in Western diets, comprising between 40 to 50% of PUFA intake (Whelan and Fritsche, 2013). ALA is mostly found in leafy green vegetables, canola oil and flaxseeds (Moghadasian, 2008). Dietary ALA and LA are precursor fatty acids that undergo further desaturation and elongation steps and are converted into longer chain PUFAs such as C22:6ω-3 DHA and C20:5ω-3 EPA, and C20:4ω-3 AA) (Wiktorowska-Owczarek et al., 2015) (**Figure 1.4**).
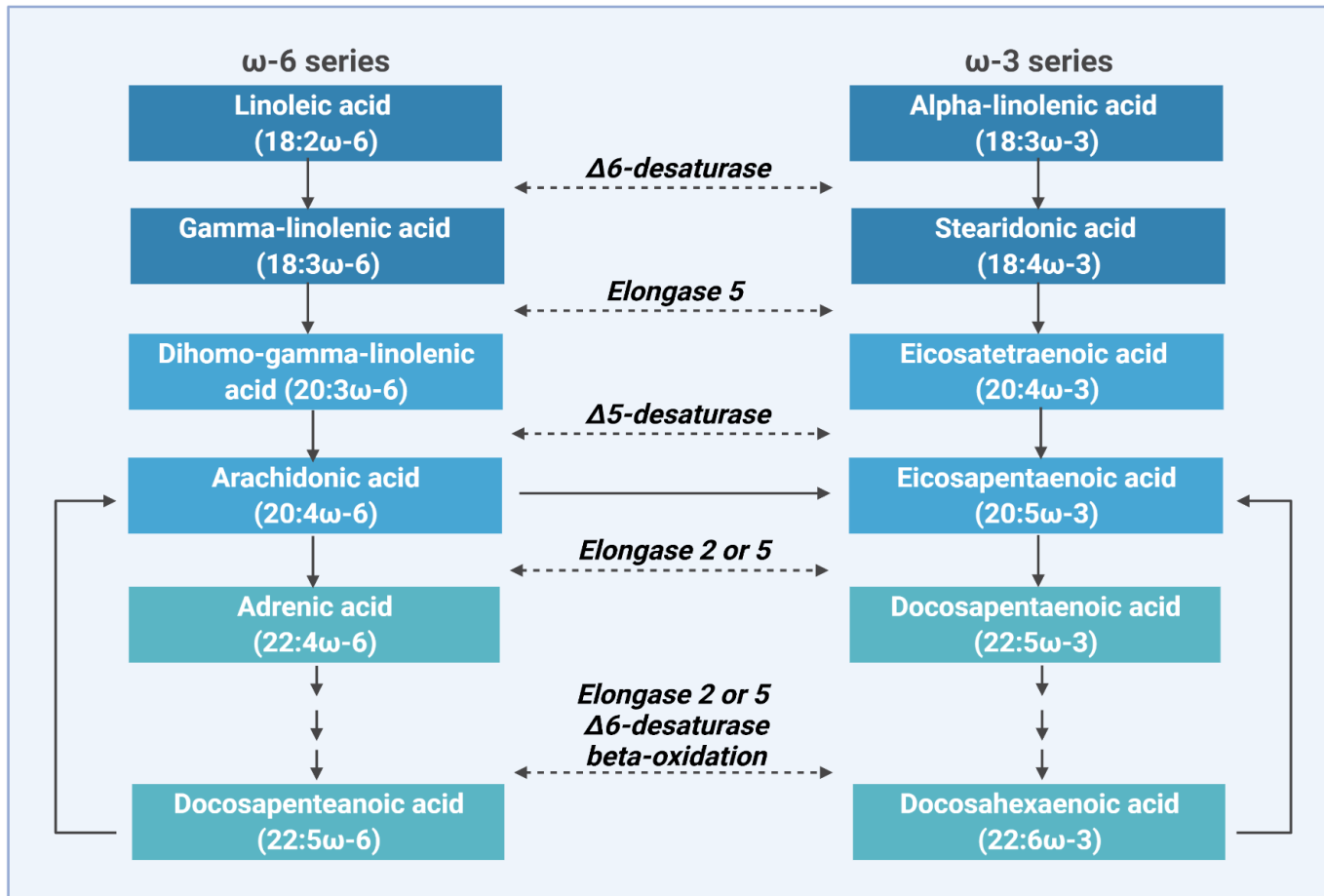
Figure 1.4 Polyunsaturated fatty acid synthesis pathways in humans.

Modified from (Bird et al., 2018; Laye et al., 2018)

Less than 5% of dietary ALA is converted to DHA based on radiotracer studies using labeled ALA (Brenna, 2002). If diet has a high content of ω-6 PUFAs, this conversion rate is further reduced by 50% because of the competition between ω-3 and ω-6 PUFAs for the same metabolic enzymes (Gerster, 1998). Even though dietary ALA enters the brain, less than 0.2% of brain ALA is eventually converted into DHA due to the very low levels of PUFA elongases and desaturases in the brain (Demar et al., 2005). As a result, the brain relies on the constant supply of DHA and AA from the plasma (Bazinet and Laye, 2014).

The two predominant PUFAs in the adult brain are AA and DHA, which are esterified to the cell membrane phospholipid bilayers and regulate the function of neurons, glial cells and signal transduction at synapses. AA and DHA each make up ~10% of brain total lipids and total phospholipid fractions (Martin et al., 1996). In healthy adult brain, >80% of DHA is esterified into phospholipids (Taha et al., 2013). However, in GBM tissue, DHA levels are reduced by ~50% resulting in 2-fold higher levels of AA relative to DHA (Martin et al., 1996). Other PUFAs, such as ω-6 LA, ω-3 EPA and ALA, are either not detectable in the brain or are present at much lower concentrations than AA and DHA.

There are 4 different phospholipid classes in the cell membrane including phosphatidylethanolamine (PE), phosphatidylcholine (PC), phosphatidylserine (PS) and phosphatidylinositol (PI). Brain DHA is primarily esterified into PE and PS, whereas AA is preferentially esterified into PE and PI (Green and Yavin, 1993; Svennerholm, 1968). The distinct distribution of DHA or AA across phospholipid classes is believed to be regulated by specific enzymes involved in the *de novo* phospholipid synthesis and phospholipid remodelling pathways (Lacombe et al., 2018).

PUFAs have been proposed to cross the blood-brain-barrier through several potential mechanisms, including transmembrane lipid transporter proteins (e.g., major facilitator superfamily domain containing 2a (Mfsd2a)), lipoprotein receptors (e.g., low-density lipoprotein receptor (LDLR)) and passive diffusion (e.g., flip-flop mechanism) across the endothelial membrane (Bazinet and Laye, 2014; Lacombe et al., 2018; Montecillo-Aguado et al., 2020). PUFA cytosolic transport in the brain (e.g., endothelial cells, astrocytes and neurons) relies on fatty acid binding proteins (e.g., FABP3, FABP5 and FABP7) (Liu et al., 2010).

The enrichment of brain PUFA starts from conversion of non-esterified-fatty acids into fatty acid-CoA by long chain fatty acid CoA synthetase (Watkins, 1997). The most common forms of plasma DHA are the non-esterified-DHA, as well as the esterified-DHA, the most common of which are triacylglycerol-bound DHA found within lipoproteins and lysophosphatidylcholine (LysoPtdCho or LPC)-DHA (Nguyen et al., 2014). Both non-esterified-DHA and LysoPtdCho-DHA can be complexed with albumin, serving as the main circulating lipid pools for brain DHA supply. Upon reaching the endothelial luminal plasma membrane, non-esterified-DHA can passively diffuse across these blood-brain-barrier plasma membranes.In contrast, the incorporation of LysoPtdCho-DHA into the brain endothelium is facilitated by the LysoPtdCho transporter, Mfsd2a (Bazinet and Laye, 2014; Lacombe et al., 2018) (**Figure 1.5**). Recently, both Mfsd2a (Nguyen et al., 2014) and Acyl-CoA synthetase long chain family, member 6 (ACSL6) have been linked to enrichment of DHA in brain (Fernandez et al., 2018).
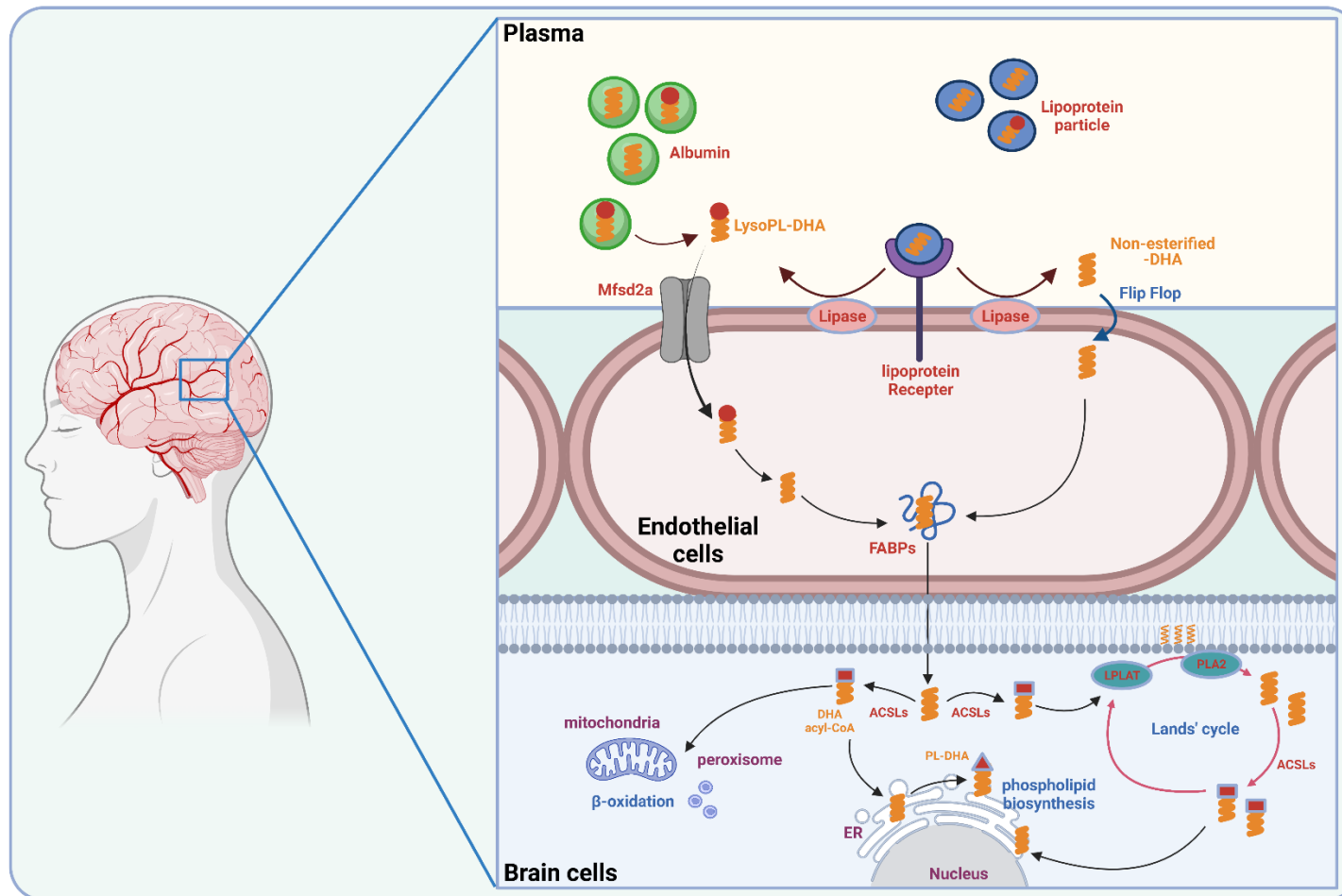
Figure 1.5 DHA uptake into normal brain.

Abbreviations; ACSL, long-chain acyl-CoA synthetase; acyl-CoA, acyl-Coenzyme A; DHA, docosahexaenoic acid; FABP, fatty acid binding protein; LPLAT, lysophospholipid acyltransferase; Mfsd2a, major facilitator superfamily domain-containing protein 2a; PLA$_2$, phospholipase A$_2$; LysoPL, lysophospholipid; Modified from (Lacombe, Chouinard-Watkins et al. 2018)

Mfsd2a belongs to the major facilitator superfamily, which is expressed exclusively in the brain endothelium of the blood-brain-barrier. Mfsd2a has been proposed to play an essential role in the uptake of LysoPtdCho-DHA across the luminal plasma membrane of brain microvessel endothelial cells (Alakbarzade et al., 2015; Guemez-Gamboa et al., 2015). *Mfsd2a* knockout mice have a 50% decrease in brain DHA content compared to wildtype mice (Nguyen et al., 2014). Mfsd2a also shows some affinity for other esterified-DHA, such as lysophosphatidylethanolamine-DHA (LysoPtdEtn-DHA and lysophosphatidylserine-DHA (LysoPtdSer-DHA) (Nguyen et al., 2014)

In contrast to Mfsd2a which functions as a DHA transporter, ACSL6 converts non-esterified DHA into DHA acyl-CoA in neurons and astrocytes (Soupene and Kuypers, 2008). DHA acyl-CoA can be further re-esterified to a lysophospholipid and re-incorporated into the cell membrane phospholipid bilayer (Kornberg and Pricer, 1953). ACSL6 is highly abundant in the brain (Fujino and Yamamoto, 1992) and has a substrate preference for DHA compared to other PUFAs, MUFAs and SFAs (Van Horn et al., 2005). Brain DHA-containing lipids are decreased by 22–71% in *ACSL6-/-* mice, along with accompanying increases in AA-containing lipids (Fernandez et al., 2018). Besides ACSL6, the other predominant ACSL isoforms expressed in the brain are ACSL3 and ACSL4 (Pelerin, Jouin et al. 2014). ACSL3 has high substrate preference for ALA, LA, and AA (Van Horn, Caviglia et al. 2005, Fernandez and Ellis 2020). ACSL4 was reported to be important for neuronal differentiation in the brain and shows preference for AA in brain neuronal cells (Shimshoni, Basselin et al. 2011, Cho 2012, Kuwata and Hara 2019).

1.3.2 PUFA metabolism in the brain and their roles in GBM

1.3.2.1 PLA$_2$-mediated PUFA membrane turnover

Unlike other PUFAs (such as LA, ALA and EPA) which quickly undergo β-oxidation, DHA and AA are converted into fatty acid acyl-CoA, and then esterified into membrane phospholipids. There are 2 stereo-specifically numbered (sn) carbon positions in the glycerol backbone of phospholipids, sn-1 and sn-2. The sn-1 position fatty acids (typically saturated fatty acids) can be de-esterified by phospholipase A1 (PLA$_1$), whereas the sn-2 position fatty acids (typically unsaturated fatty acids including DHA or AA) are de-esterified by phospholipase A2 (PLA$_2$) (Bazinet and Laye, 2014). Several different PLA$_2$ enzymes have been characterized in the brain and neuronal tissue, and are classified into two subtypes, calcium-dependent and calcium-independent, based on their catalytic dependence on calcium (Farooqui et al., 1997). For example, Ca^{2+}-dependent cytosolic PLA$_2$ (cPLA$_2$) triggers AA hydrolysis from the sn-2 position of phospholipids (Alonso et al., 1986; Mouchlis et al., 2018), but rarely hydrolyses DHA (Mouchlis et al., 2018). In turn, DHA is mainly hydrolysed by Ca^{2+}-independent PLA$_2$ (iPLA$_2$) (Strokin et al., 2003).

cPLA$_2$ knockout mice are characterized by reduced AA incorporation rates into brain ethanolamine glycerophospholipid and choline glycerophospholipid from both the plasma non-esterified-AA and brain AA acyl-CoA pools (Rosenberger et al., 2003). AA and AA-derived eicosanoids have been widely investigated for their pro-inflammatory roles in many neurodegenerative diseases as well as GBM (Dennis et al., 2011; Farooqui et al., 1997; Sun et al., 2010). Recent studies revealed that high expression of cPLA2 is associated with poor prognosis and chemotherapy resistance in GBM patients (Wu et al., 2019; Yang and Zhang, 2018). Inhibition of brain cPLA$_2$ pathways reduces AA-related

neuroinflammation (Tajuddin et al., 2014) and therapeutic resistance in GBM (Bhave et al., 2013).

Apart from AA, $cPLA_2$ catalysis also generates lysophosphatidylcholine (LPC). LPC can be subsequently converted to lysophosphatidic acid (LPA) by autotaxin (ATX), an enzyme with lysophospholipase D activity. ATX is widely overexpressed in GBM tissue, which contributes to GBM tumour migration/invasion (Hoelzinger et al., 2008; Kishi et al., 2006). Emerging evidence points to inhibition of ATX and LPA playing a role in sensitizing GBM to radiation therapy and attenuating GBM cell migration/invasion (Bhave et al., 2013).

In normal rat brain, $iPLA_2$ mRNA levels are significantly higher than cPLA2 mRNA levels in all brain regions (Ong et al., 2010). Six isoforms of iPLA2 (group VI) has been identified in humans (Vasquez et al., 2018), with two $iPLA_2$-hydrolyzing DHA isoforms found in brain, $iPLA_2\beta$ and $iPLA_2\gamma$ (Strokin et al., 2007). In neuronal cells, inhibition of $iPLA_2\gamma$ can selectively reduce ATP-induced DHA release (Strokin et al., 2004). Using *in vivo* quantitative autoradiography to image DHA incorporation from plasma into brain, $iPLA_2\beta$ was found to be critical for brain DHA metabolism and neurotransmission pathways (Rapoport et al., 2011). There appears to be a direct link between brain DHA content and iPLA2 levels, with rats fed an ω-3 PUFA-deficient diet showing up-regulation of iPLA2 protein levels (Rapoport et al., 2007). Another study showed dietary DHA can selectively reverse $iPLA_2\beta$ inhibition in mice (Mazzocchi-Jones, 2015).

In addition to $cPLA_2$ and $iPLA_2$, Ca^{2+}-dependent secretory phospholipase A_2 ($sPLA_2$) has also been identified in the brain, which suggests that sPLA2 may also play some role in PUFA metabolism (Sun et al., 2010). In a rat brain AA metabolism study,

both cPLA$_2$ and sPLA$_2$, as well as AA and PGE$_2$ were upregulated upon lipopolysaccharide–activated neuroinflammation (Rosenberger et al., 2004). Furthermore, a study using human astrocytoma cells demonstrated that cPLA$_2$ was involved in inflammatory induction of sPLA$_2$ (Hernandez et al., 1998). Because sPLA$_2$ shows very low affinity towards phosphatidylethanolamine (Singer et al., 2002), the main DHA-incorporated phospholipid pool, sPLA$_2$ may only play a small role in brain DHA metabolism.

Crosstalk between sPLA$_2$, cPLA$_2$ and iPLA$_2$ is an important characteristic of this protein family (Sun et al., 2010). In an *in vivo* brain PUFA metabolism study, downregulation of iPLA$_2$ activity was accompanied by increased cPLA$_2$ and sPLA$_2$ activities, reflecting elevated brain ω-6 PUFA turnover upon graded dietary ω-3 PUFA deprivation (Kim et al., 2011). In iPLA$_2$β-deficient mice, brain DHA metabolism could not be totally abolished, which suggests that other PLA2's such as iPLA$_2$γ contribute to DHA membrane release (Rapoport et al., 2011). These findings support a homeostatic relationship between PLA$_2$-mediated membrane turnover of ω-3 PUFAs and ω-6 PUFAs in the brain.

After release from membrane phospholipids, brain AA and DHA are quickly re-esterified into phospholipids via acyl-CoA synthetases ACSLs. ACSLs are responsible for the phospholipid re-incorporation of 90% of membrane released PUFAs (Chen et al., 2008; Robinson et al., 1992). This PUFA recycling pathway is called Land's cycle, which is believed to be key to maintaining the high levels of PUFAs in brain (Lands, 1958). As for the PUFAs that are released into the cytoplasm, most are converted into lipid mediators (also called lipid derivatives) in brain cells. The enzymes involved in PUFA

metabolism pathways include cyclooxygenases (COXs), lipoxygenases (LOXs) and cytochrome P450 (CYP450). These enzymes reside mainly in ER and have been widely studied in many CNS physiological conditions, neurological diseases and cancers (Iliff et al., 2010; Montecillo-Aguado et al., 2020; Tassoni et al., 2008).

1.3.2.2 Cyclooxygenases

COXs, or prostaglandin-endoperoxide synthases (PTGS), catalyze the first committed step of the conversion of AA into prostaglandins (PGs) and thromboxanes. Different from the constitutive expression of COX-1 in most brain tissues for normal physiological functions, COX-2 levels are specifically elevated in cortical and hippocampus neurons undergoing normal synaptic activities (Yamagata et al., 1993), as well as in microglial cells in response to pathological inflammatory conditions (Minghetti, 2004; Yang and Chen, 2008). COX-2 has been implicated in the pathogenesis of neurodegenerative diseases, traumatic brain injury and brain tumours (Hewett et al., 2006; Hickey et al., 2007; Minghetti, 2004; Pan et al., 2016). PGs include different biologically active compounds (e.g. PGD_2, PGE_2, PGI_2) (Minghetti, 2004), with PGE_2 being the principal metabolite of AA in COX-2-driven tumour progression, including GBM (Jiang et al., 2017; Wang and Dubois, 2010).

There is extensive data demonstrating COX-2 expression in human gliomas. COX-2 and its main metabolite PGE_2, are expressed at higher levels in high-grade gliomas, and have been proposed to facilitate tumorigenesis, inflammation, invasion and tumour recurrence in GBM (Joki et al., 2000; Lalier et al., 2007; Shono et al., 2001). Immunohistochemical analysis of 66 GBM tumour specimens revealed that high COX-2

expression correlates with clinical aggressiveness and poor survival in GBM patients (Shono et al., 2001).

Inhibition of COX-2 by its selective inhibitor NS*398* has been shown to inhibit the growth of human GBM cell lines (Bernardi et al., 2006; Joki et al., 2000; Matsuo et al., 2004). In a recent study, Lombardi *et al.* collected extracellular vesicles released from NS*398*-treated GBM neurospheres. They found that these vesicles had significant inhibitory effects on GBM cell migration (Palumbo et al., 2020). Our lab previously showed that FABP7/AA-mediated U87 GBM cell migration is dependent on activation of COX-2 (5-fold increase) and PGE_2 production (>6-fold increase) (Mita et al., 2010). NS*398* treatment significantly reduced PGE_2 levels and FABP7/AA/COX-2-mediated migration in our GBM cell lines (Mita et al., 2010).

In the last 20 years, many case-control studies and cohort studies have been conducted to investigate the association between the use of COX inhibitors and the risk of glioma/GBM [e.g., nonsteroidal anti-inflammatory drugs (NSAIDs) and the selective COX-2 inhibitor Celecoxib] (Daugherty et al., 2011; Gaist et al., 2013; Sivak-Sears et al., 2004). However, inconsistent results from these clinical studies have reduced the prospect of using COX-2 inhibitors as a direct therapeutic target for GBM (Qiu et al., 2017). As the COX-2 tumour-promoting pathway is widely up-regulated in GBM, either upstream diet intervention (e.g., reduced ω-6 PUFA dietary uptake) (Montecillo-Aguado et al., 2020) or the use of downstream PGE_2 synthases/receptors (Jiang et al., 2017) may represent alternative therapeutic targets for GBM.

1.3.2.3 LOXs metabolism pathways

LOXs are a group of iron-containing lipid-peroxidation enzymes that catalyze the peroxidation of different PUFAs, such as LA, AA and DHA. There are six LOX genes in the human genome, with three LOX genes expressed in the brain, including 5-LOX, 12-LOX, 15-LOX (Phillis et al., 2006). The main lipid substrates for LOXs in the brain are AA and DHA that are released from plasma membrane phospholipids by PLA_2 enzymes (Bazinet and Laye, 2014).

LOXs show different positional specificity for AA oxygenation (Kuhn and Thiele, 1999). The catalytic products of AA by LOXs are hydroperoxyeicosatetraenoic acids (HpETEs), which are subsequently converted into pro-inflammatory lipid mediators such as hydroxy-eicosatetraenoic fatty acids (5-,12- and 15-HETEs) and 4-series leukotrienes (LTB_4, LTC_4, and LTD_4) (Hanna and Hafez, 2018). These AA derivatives can be further metabolized into lipoxins in inflammatory diseases and cancers (Janakiram et al., 2011; Weylandt et al., 2007). Various AA derivatives from LOX-mediated pathways have been identified in the brain (Bazinet and Laye, 2014; Bosetti, 2007). 5-LOX expression has been associated with increased proliferation in human GBM and poor prognosis in GBM patients (Nathoo et al., 2006; Wang et al., 2015b). Furthermore, many *in vitro* studies have found that 5-LOX inhibitors (e.g., MK886) and 15-LOX inhibitors [e.g., luteolin and nordihydroguaiaretic acid] exhibit potent inhibitory effects on GBM cell proliferation/migration (Lim et al., 2010; Souza et al., 2020; Wang et al., 2016; Woo et al., 2013).

Compared to the pro-inflammatory effect of AA derivatives, DHA-derived bioactive mediators [e.g., neuroprotection D1 (NPD1), resolvins D (RvDs), and maresin1 (MaR1)]

are characterized as specialized pro-resolving mediators (SPMs), which exhibit anti-inflammatory/pro-resolving effects in various neurological diseases and cancers (Lacombe et al., 2018; Laye et al., 2018). In an Alzheimer's disease *in vitro* model that uses primary neural cell cultures, SPMs can reduce pro-inflammatory gene expression and promote neural cell survival (Lukiw et al., 2005; Zhu et al., 2016).

Even though there are no published studies investigating the effect of SPMs on GBM tumour growth, recent work on other cancers indicate that RvDs exhibit many anti-tumorigenic effects and enhance benefits from cancer therapy (Moro et al., 2016). In a prostate cancer cell-macrophage co-culture system, RvD1 and RvD2 reduced cell proliferation by inhibiting tumour-associated macrophage (TAM) polarization (Shan et al., 2020). Another critical mechanism for RvDs is to stimulate macrophage phagocytosis in cancer (Serhan, 2014). In a Lewis lung carcinoma animal model, RvD treatment (e.g., RvD1, RvD2 and RvE1) stimulated macrophage phagocytosis of tumour debris resulting from chemotherapy (Sulciner et al., 2018). This combined evidence points to a potential anti-tumorigenic role for LOX-derived DHA metabolites, such as RvD, mediated through macrophage function.

1.3.2.4 CYP450 metabolism pathways

Cytochromes P450 (CYP450) are a superfamily of enzymes that function as monooxygenases. CYP450 metabolize PUFAs to either hydroxy-PUFAs (with hydroxylase activity) or Ep-PUFAs (epoxygenase activity). Both AA and DHA have been shown to be substrates for CYP450 metabolism pathways in human (Konkel and Schunck, 2011). CYP450 enzymes with epoxygenase activity (mainly CYP2C and CYP2J)

generate AA-derived Ep-PUFAs (epoxy-eicosatrienoic acids (EETs)) and DHA-derived Ep-PUFAs (epoxy-docosapentaenoic acid (EDPs)) (Spector and Kim, 2015). CYP450 enzymes with hydroxylase activity (mainlyCYP1A and CYP2E) hydroxylate AA at the terminal methyl group to produce 20-HETE (Chuang et al., 2004; Spector and Kim, 2015). All of the major AA-metabolizing CYP450 enzymes can metabolize ω-3 PUFAs, such as EPA and DHA as efficient alternative substrates to AA,,generating products with different catalytic activities from those derived from AA (Fer et al., 2008; Konkel and Schunck, 2011)

A few CYP450 enzymes have been reported to regulate GBM tumour growth. In U251 GBM cells, overexpression of CYP4A1 increases the production of AA-derived 20-HETE (by 60-fold), which stimulates *in vitro* cell proliferation and *in vivo* orthotopic tumour growth (Guo et al., 2008). CYP2J2 overexpression increases production of AA-derived EETs and enhances cancer cell migration in different cancer types (Jiang et al., 2007). A recent study shows that CYP2J2 knockdown reduces the production of AA-derived 11,12-EET in a U87 orthotopic xenograft mouse model, through inhibition of microglia M2 (pro-immunosuppressive) polarization (Lei et al., 2020). CYP2J2's higher metabolizing activity towards EPA (by 9-fold) and DHA (by 4-fold) compared to AA (Arnold et al., 2010) suggests a potential anti-tumorigenic effect of pro-resolving DHA-derived lipid mediators on GBM tumour growth (Elsherbiny et al., 2013).

1.3.3 Roles of PUFAs in GBM

1.3.3.1 GBM risk and dietary intake of PUFAs

The right amounts and a balanced ratio of dietary ω-3 and ω-6 PUFAs are required for optimal brain health, since it is widely accepted that ω-3 and ω-6 PUFAs have opposing metabolic functions. AA-derived eicosanoids are generally pro-inflammatory, pro-tumorigenic, and are involved in various pathological processes in the CNS system, including neural trauma, neuroinflammation and brain tumours (Iliff et al., 2010; Montecillo-Aguado et al., 2020; Tassoni et al., 2008). On the other hand, DHA-derived metabolites (e.g., RvDs and neuroprotection NPD1) are predominantly anti-inflammatory, anti-tumorigenic, and have neuroprotective and therapeutic effect in some neurological diseases (Li et al., 2020; Serhan and Levy, 2018; Serhan and Petasis, 2011). For example, many epidemiological studies in the past 30 years have shown that dietary intake of ω-3 PUFAs is inversely correlated with the prevalence of neurodegenerative diseases (e.g., Parkinson's disease and Alzheimer's Disease) (Abbott et al., 2003; Huang et al., 2005; Kalmijn et al., 1997). Based on these findings, numerous clinical trials have investigated the effect of ω-3 PUFA-enriched diets on the prevention/occurrence of neurodegenerative diseases (Avallone et al., 2019).

GBM is the most aggressive type of primary brain tumour. Both in vitro and in vivo studies support potential therapeutic effects of ω-3 supplements in GBM (Montecillo-Aguado et al., 2020). Recent meta-analyses of both case-control and cohort studies indicate that high consumption of fish may be associated with lower risk of brain cancer (Lee et al., 2020; Lian et al., 2017). These studies included 4428 brain cancer cases and 501,617 participants and spanned 20 years (from 1986 to 2006). In 2020, a summary

study which included 57 meta-analyses demonstrated that brain cancer is one of four cancer types (along with liver cancer, breast cancer and prostate cancer) that showed an association between ω-3 PUFA dietary intake and lower risk of cancer (Lee et al., 2020). In the context of GBM, emerging studies now focus on the effect of ω-3 PUFAs on GBM immune environment modulation, inhibition of infiltrative/invasive properties and mitochondrial function regulation (detailed below).

1.3.3.2 Effects of PUFAs on GBM infiltrative/invasive properties

GBM is characterized by highly infiltrative/invasive properties (Aum et al., 2014; Vehlow and Cordes, 2013). The diffuse infiltration of GBM to neighboring brain parenchyma contributes to surgical escape, resistance to GBM standard therapies and tumour recurrence (Osuka and Van Meir, 2017). Several studies have shown that PUFAs contribute to GBM infiltrative/invasive properties. For example, AA-derivatives (e.g., PGs and LTs) are pro-tumorigenic, promoting GBM tumour infiltration and invasion (Jiang et al., 2017; Nathoo et al., 2004). Furthermore, activation of the AA/COX-2/PGE_2 pathway stimulates the migration and invasion of U87 and U251 cells (Chiu et al., 2010; Wang et al., 2015a). Ferreira *et al*. reported increased prostaglandin D_2 (PGD_2) production in GBM tumour samples compared to lower grade gliomas (Ferreira et al., 2018). More recently, Leukotriene B4 (LTB4) receptor 1 has been reported to be highly expressed in a subset of GBM cell lines, and inhibition of the AA/15-LOX/leukotriene-pathway reduced A172, U87 and U251 cell migration (Souza et al., 2020). With regards to DHA, our lab previously showed that DHA inhibits the migration of FABP7-expressing GBM cells (Mita et al., 2010), with Ruan *et al.* also showing inhibition of GBM cell migration by DHA (Ruan et al., 2019).

Nasrollahzadeh *et al.* have shown that intravenously-injected radioactively-labeled fatty acids or dietary PUFA supplements can be incorporated into intracranially-implanted rat C6 glioma tumour tissue (Nasrollahzadeh et al., 2008). Although no animal study has been published regarding PUFAs' effects on GBM tumour infiltration/invasion, some studies have shown opposing roles for ω-6 and ω-3 PUFAs on melanoma brain metastasis using both melanoma cell lines and patient-derived xenografts (PDX). Denkins *et al.* demonstrated that AA/COX-2/PGE$_2$ activation promotes melanoma metastasis to the brain, whereas DHA and EPA supplementation abolished this effect (Denkins et al., 2005). More recently, Zou *et al.* reported that astrocyte-mediated PPARγ activation promotes melanoma metastasis to the brain in an AA-enriched tumour microenvironment (Zou et al., 2019). Interestingly, a higher content of AA has been detected in peritumoral astrocytes compared to metastatic melanoma cells, suggesting that surrounding astrocytes could be an alternative target of dietary PUFAs (Zou et al., 2019). As GBM tumours also have a highly heterogeneous microenvironment, PUFAs could potential affect tumour cells and peritumoral cells to influence GBM growth properties.

1.3.3.3 Effects of PUFAs on GBM mitochondrial function

In the adult brain, the main source of ATP is from glucose oxidation, with a secondary source of ATP being fatty acid β-oxidation (Schonfeld and Reiser, 2013). The oxidization of long chain fatty acids for energy production is known to enhance mitochondrial reactive oxygen species (ROS) production in the normal brain (Schonfeld and Reiser, 2013, 2017). Thus, it is hypothesized that the low levels of fatty acid β-

oxidation in the brain protects against increased oxidative stress (Schonfeld and Reiser, 2017).

In contrast to brain, the ω-6 PUFA, LA, has been shown to increase mitochondrial oxygen consumption rate in primary GBM cultures under serum-free conditions, suggesting dysregulated fatty acid metabolism in GBM cells compared to normal brain (Lin et al., 2017). A recent study further shows that elevated levels of FABP7 in GBM neural stem-like cells are associated with increased mitochondrial oxidative phosphorylation and ATP production (Hoang-Minh et al., 2018). Therefore, it will be very interesting to investigate how FABP7's ligands, especially DHA, affects mitochondria function in GBM cells.

In addition to a possible role in mitochondrial respiration, DHA may also affect mitochondrial function by altering the fatty acid composition of GBM cell membranes. Emerging data from cardiomyocytes and colon cancer cells indicate that DHA incorporates into cardiolipin (Hofmanova et al., 2017; Raza Shaikh and Brown, 2013). Cardiolipin is a mitochondrial-specific phospholipid located at the inner mitochondrial membrane which functions as a platform for anchoring and clustering mitochondrial proteins (e.g., cytochrome C) (Dudek, 2017). In some cancer cells, DHA-rich cardiolipin has been shown to alter mitochondrial membrane lipid organization, enhance mitochondrial oxidative stress, and trigger cytochrome-C release and apoptosis (Hofmanova et al., 2017; Ng et al., 2005).

1.4 GBM membrane lipid remodelling

1.4.1 Plasma membrane lipid order and nanoclusters

Plasma membranes are composed of heterogeneous mixtures of lipids, proteins, and carbohydrates. The different biophysical properties of saturated lipids and unsaturated lipids allows separation of plasma membranes into two distinct liquid phases, highly condensed/rigid liquid-ordered (Lo) domains (also called membrane rafts), and disordered/fluid liquid-disordered (Ld) domains (Kaiser et al., 2009). Lo domains/membrane rafts which are enriched in cholesterol, sphingolipids and saturated phospholipids, have been postulated to drive the formation of functionally important and relatively ordered membrane nanodomains (10-200 nm in diameter) that recruit other lipids and proteins (Pike, 2006; Simons and Ikonen, 1997). In contrast to Lo domains, Ld domains are enriched in unsaturated lipids.

Regional enrichment of hydrophobic components with distinct physical properties (i.e., increased lipid packing and lipid order), allows the formation of functional platforms for the regulation of cellular processes (Lingwood and Simons, 2010). The first evidence of heterogeneity within membranes came from the separation of differentially solubilized membrane lipid fractions by detergents in the 1970s (Yu et al., 1973). Using biochemical tools, plasma membranes were later separated into distinct fractions, containing detergent-soluble membranes and detergent-insoluble membranes (Hanada et al., 1995; Schroeder et al., 1994). However, experimental variations in plasma membrane fractionation and inconsistencies in protein composition of membrane fractions (Schuck et al., 2003), resulted in unresolved controversies regarding Lo and Ld domains in membranes (Klotzsch and Schutz, 2013).

Emerging biophysical technical approaches (e.g. mimetic membranes such as giant plasma membrane vesicles, lipophilic probes such as DiO, DiI and DiD and lipid environment-sensitive probes such as Laurdan and di-4-ANEPPDHQ) (Sezgin et al., 2017) provided strong support for the presence of Lo domain/membrane rafts on plasma membranes. The use of combined biomimetic membranes and lipophilic probes clearly demonstrated that certain lipids interact preferentially with one another, and generate large scale lateral domains as a consequence of phase separation (Simons and Vaz, 2004). However, the lack of a live cell environment and disruption of cytoskeleton actin scaffold remained the main weaknesses of these methods.

Imaging of membrane lipid packing state in phospholipid bilayers using Laurdan probe has been widely applied to investigate membrane heterogeneity in live cells and tissues (Owen et al., 2011). There is a shift in the emission spectra of membrane-bound Laurdan depending on the polarity of the phospholipid environment, with shorter emission wavelengths observed when there is a lower aqueous content (i.e., membrane Lo domain). Thus, by ratiometrically calculating alterations in Laurdan intensity at both ordered phase and disordered phase, it is possible to quantitate the extent of plasma membrane lipid order (Owen et al., 2011).

Although membrane domains can be defined as lipid clusters, in most physiologically states, they also contain proteins. In addition to the membrane lipid and protein components, cortical actin cytoskeleton is also an important factor in Lo domain/membrane raft maintenance and lipid remodelling (Honigmann et al., 2014b; Saha et al., 2015). The most well-studied membrane lipid-anchored proteins are RAC1 and RAS, which are capable of binding directly to actin and forming nanoclusters (Nan et

al., 2015; Remorino et al., 2017). The molecular machinery that generates actin-based nanoclusters and associated membrane Lo domains has not been identified, and further study is required to understand the functional significance of these processes.

Super-resolution microscopy, including photoactivated localization microscopy (PALM), stimulated emission depletion (STED) microscopy and stochastic optical reconstruction microscopy (STORM), all allow images to be taken at resolutions below the diffraction limit (~250 nm), enabling the direct observation of membrane rafts/Lo domains (Sezgin, 2017). Both PLAM and STORM use mathematical models to reconstruct super-resolution images form diffraction limited images. STED microscopy creates super-resolution images by the selective deactivation of fluorophores using depletion lasers, thereby enhancing the achievable resolution to 70-90 nm (Vicidomini et al., 2018). When STED is combined with deconvolution processing or fluorescence correlation spectroscopy (FCS), the resolution of nanoclusters can reach ~30-60 nm, which further reveals underlying nanoscopic features of the plasma membrane (Eggeling et al., 2009).

By using STED microscopy, several plasma membrane proteins (e.g., TrKB) (Angelov and Angelova, 2017) and mitochondrial proteins (e.g., Tom20) (Singh et al., 2012) were found to be distributed as nanoscale clusters. Furthermore, STED microscopy also allows the visualization of the plasma membrane and other organelles in live cells. For example, by combining FCS with STED microscopy, sphingolipids and glycosylphosphatidylinositol-anchored proteins associated with membrane raft domain formation were found to be transiently trapped in cholesterol-mediated molecular complexes within a nanoscale area (~30 nm) (Eggeling et al., 2009). Future critical

developments in the field of super-resolution microscopy will involve enhanced use of lipophilic probes and lipid environment-sensitive probes.

1.4.2 Membrane lipid remodelling in GBM

The membrane lipid composition of cancer cells is dramatically altered compared to that of normal cells, which is driven by dysregulated lipid metabolism pathways. Cancer cell membrane lipids are characterized by an increased degree of saturation and a relatively lower content of polyunsaturated lipids, which protects cancer cells from oxidative stress-induced cell death (Rysman et al., 2010). Membrane rafts/Lo domains, which are enriched in cholesterol and saturated phospholipids, play essential roles in cancer cell migration, invasion and metastasis pathways, and many proteins involved in these processes are localized in membrane rafts, such as tyrosine kinase receptor families. Both *EGFR*-amplified and *EGFR*-mutated GBM cells have been shown to undergo remarkable alterations in membrane biophysical dynamics and membrane phospholipid composition (Bi et al., 2019; Martin et al., 1996). Several membrane lipid remodelling processes have been found to promote GBM tumour growth, such as increased saturated phospholipids in plasma membranes (Bi et al., 2019) and formation of membrane rafts/Lo domains (i.e., caveolin-1 pathway) (Martin et al., 2009).

Kambach *et al.* reported a correlation between upregulation of cholesterol biosynthesis and poor survival in GBM patients (Kambach et al., 2017). GBM cells take up exogenous cholesterol that is secreted by astrocytes in the tumour microenvironment, which can be upregulated by sterol regulatory element-binding protein 1 (SREBP1) activation, providing an abundant supply of cholesterol for membrane formation (Griffiths

et al., 2013; Guo et al., 2009). The membrane cholesterol content can also regulate GBM membrane protein functions. CD44 is a cell surface adhesion molecule, which activates RAC1 for actin remodelling and plays an important role in tumour invasion/metastasis (Murai et al., 2004). Cholesterol depletion using methyl-β-cyclodextrin (MβCD)/statin agents increases membrane rafts/Lo domain-dependent CD44 shedding and suppresses GBM cell migration (Murai, 2012; Murai et al., 2011).

Activation of the intracellular kinase domain of EGFR upon extracellular ligand binding is crucial to oncogenic signalling pathways. EFGR activates *de novo* fatty acid synthesis and increases the content of saturated fatty acids (Guo et al., 2009). On the other hand, the EGFR pathway is also affected by the lipid composition of the plasma membrane (Arkhipov et al., 2013). For example, EGFR upregulates lysophosphatidylcholine acyltransferase 1 (LPCAT1), a key enzyme that is overexpressed in GBM and is used for synthesizing saturated PC. Enhanced saturated PC content leads to plasma membrane remodelling, which in turn, is required for EGFR-mediated oncogenic signalling transduction (Bi et al., 2019). Using the Laurdan assay, Bi *et al.* further showed that increased membrane lipid saturation affected the biophysical properties of membranes, such as membrane lipid order (Bi et al., 2019).

Several membrane proteins localize to membrane rafts/Lo domains and promote GBM migration/invasion. One of these, the gap junction protein Connexin 43 interacts with caveolin-1 in membrane rafts/Lo domains, promoting invasion of human U251 GBM cells (Strale, Clarhaut et al. 2012). As well, transient receptor potential canonical channels can localize to membrane rafts/Lo domains at the leading edge of migrating D54MG GBM

cells, which is essential for GBM chemotaxis in response to EGF (Bomben, Turner et al. 2011).

1.4.3 Effect of DHA on GBM membrane remodelling

The most common strategy to modify membrane rafts/Lo domain function and diminish its downstream migration/invasion signaling pathways is the alteration of membrane lipid composition, such as increasing the degree of plasma membrane lipid unsaturation (i.e., dietary ω-3 PUFAs, DHA and EPA) and cholesterol depletion (i.e., MβCD). As mentioned earlier, membrane rafts/Lo domains are required for efficient EGFR signaling. ω-3 PUFA supplementation has been shown to alter the membrane localization of EGFR in different cancer models (Fuentes et al., 2018a; Schley et al., 2007). More recently, combined biophysical methods [e.g., Förster resonance energy transfer (FRET)] and super-resolution microscopy (e.g., dSTORM and STED) revealed that DHA supplementation/dietary DHA can induce alterations in membrane rafts/Lo domain-mediated membrane protein nanoclustering (e.g., KRas, TrkB) in colon cancer and neuroblastoma cells (Angelov and Angelova, 2017; Fuentes et al., 2018b; Fuentes et al., 2021).

In further support of DHA altering membrane properties, Fuentes *et al.* reported that DHA can be incorporated into colonic cell phospholipid membranes and increase plasma membrane fluidity using di-4-ANEPPDHQ, a lipid environment-sensitive probe (Fuentes et al., 2021). These investigators further demonstrated that both DHA treatment and cholesterol depletion can significantly decrease EGFR nanocluster formation in mouse epithelial colonic cells using STED microscopy (Fuentes et al., 2021). The similar

effects of DHA and cholesterol depletion on membrane protein nanodomain formation/nanoclustering suggest that DHA and cholesterol possess a mutual aversion to each other that induces the lateral segregation of DHA-containing phospholipids into cholesterol-free Ld domains (Wassall and Stillwell, 2009). DHA membrane incorporation into phospholipid bilayers has been reported in both U87 GBM cells and a GBM mouse model (Harvey et al., 2015; Nasrollahzadeh et al., 2008). Thus, it will be very important to investigate the effect of DHA and its transporter protein FABP7 on the inhibition of GBM migration in the context of GBM membrane lipid remodelling.

1.5 Thesis hypothesis

We propose that FABP7 and its PUFA ligands DHA and AA regulate GBM migratory properties through multiple mechanisms, including PUFA uptake, plasma membrane remodelling and mitochondrial function.

1.6 Thesis objectives

1.6.1 Chapter 2

The goals of Chapter 2 were to examine: (i) the relationship between GBM cell migration, plasma membrane lipid order and FABP7/DHA presence, and (ii) the effect of DHA supplementation on membrane-localized FABP7 nanoscale domain formation in migratory GBM cells.

1.6.2 Chapter 3

The goals of Chapter 3 were to examine: (i) the difference in fatty acid incorporation in GBM neural stem-like cells versus their paired adherent counterparts upon DHA supplementation, (ii) the effect of FABP7/DHA on fatty acid incorporation in GBM neural stem-like cells, and (iii) the impact of FABP7-facilitated DHA uptake on GBM lipid droplet formation and cell migration.

1.6.3 Chapter 4

The goals of Chapter 4 were to examine: (i) the effect of FABP7 on mitochondrial fatty acid β-oxidation genes and expression of phospholipases in GBM neural stem-like cells, (ii) the importance of FABP7 in GBM microtube formation, and (iii) the distribution of FABP7 within microtubes.

1.7 Thesis summaries

1.7.1 Chapter 2

Brain fatty acid binding protein (FABP7; B-FABP) promotes glioblastoma (GBM) cell migration and is associated with tumour infiltration, properties associated with a poor prognosis in GBM patients. FABP7-expressing neural stem-like cells are known to drive tumour migration/infiltration and resistance to treatment. We have previously shown that FABP7's effects on cell migration can be reversed when GBM cells are cultured in medium supplemented with the omega-3 fatty acid, docosahexaenoic acid (DHA). Here, we use super-resolution imaging on patient-derived GBM stem-like cells to examine the

importance ofFABP7 and its fatty acid ligands in mitigating GBM cell migration. As FABPs are involved in fatty acid transport from membrane to cytosol, we focus on the effect of FABP7 and its ligand DHA on GBM membrane remodeling, as well as FABP7 nanoscale domain formation on GBM membrane. Using quantitative plasma membrane lipid order imaging, we show that FABP7 expression in GBM cells correlates with increased membrane lipid order, with DHA dramatically decreasing lipid order. Using super-resolution stimulated emission depletion (STED) microscopy, we observe non-uniform distribution of FABP7 on the surface of GBM cells, with FABP7 forming punctate nanoscale domains of ~100 nm in diameter. These nanodomains are particularly enriched at the migrating front of GBM cells. Interestingly, FABP7 nanodomains are disrupted when GBM cells are cultured in DHA-supplemented medium. We demonstrate a tight link between cell migration, a higher membrane lipid order and increased FABP7 nanoscale domains. We propose that DHA-mediated disruption of membrane lipid order and FABP7 nanodomains forms the basis of FABP7/DHA-mediated inhibition of cell migration in GBM.

1.7.2 Chapter 3

Glioblastoma (GBM) is an aggressive tumor with a dismal prognosis. Neural stem-like cells contribute to GBM's poor prognosis by driving drug resistance and maintaining cellular heterogeneity. GBM neural stem-like cells express high levels of brain fatty acid-binding protein (FABP7), which binds to polyunsaturated fatty acids (PUFAs) ω-6 arachidonic acid (AA) and ω-3 docosahexaenoic acid (DHA). Similar to brain, GBM tissue is enriched in AA and DHA. However, DHA levels are considerably lower in GBM tissue

compared to adult brain. Therefore, it is possible that increasing DHA content in GBM, particularly in neural stem-like cells, might have therapeutic value. Here, we examine the fatty acid composition of patient-derived GBM neural stem-like cells grown as neurosphere cultures. We also investigate the effect of AA and DHA treatment on the fatty acid profiles of GBM neural stem-like cells with or without FABP7 knockdown. We show that DHA treatment increases DHA levels and the DHA:AA ratio in GBM neural stem-like cells, with FABP7 facilitating the DHA uptake. We also found that an increased uptake of DHA inhibits the migration of GBM neural stem-like cells. Our results suggest that increasing DHA content in the GBM microenvironment may reduce the migration/infiltration of FABP7-expressing neural stem-like cancer cells.

1.7.3 Chapter 4

Chapters 2 and 3 focus on the effects of FABP7 and its PUFA ligands, especially DHA, on membrane remodelling (e.g., phospholipid fatty acid composition, plasma membrane lipid order and membrane FABP7 nanodomain formation) and the interplay between these factors and cell migration, particular in GBM neural stem-like cells. Emerging evidence from other labs highlights the roles of FABP7 in regulating lipid droplet storage and mitochondrial fatty acid metabolism. GBM neural stem-like cells (GSCs) exhibit distinct metabolic profiles compared to the more differentiated adherent GBM cells, including upregulated mitochondria ATP production. In Chapter 4, we investigate possible mechanisms for increased mitochondrial activity in GBM neural stem-like cells. We identify mitochondrial fatty acid β-oxidation genes (e.g., *Cpt1c*, *ACSL6* and *ACSBG1*) that are upregulated in GBM neural stem-like cells compared to their paired adherent

differentiated cells. We report that FABP7 depletion down-regulates both *Cpt1c* and *ACSL6* expression, along with a reduction in GBM mitochondrial ATP production. Using A4-007N, a highly infiltrative/invasive GBM neurosphere culture characterized by the formation of long intertumoral connections (i.e., microtubes), we observed FABP7 localization at mitochondria, with increased localization to mitochondria when cells were cultured in DHA-supplemented medium. Intriguingly, we also found abundant FABP7 localization in mitochondria located in A4-007N microtubes when cells were cultured under neurosphere conditions and *in vivo* using an orthotopic xenograft mouse model of GBM. Depletion of FABP7 in A4-007N cells resulted in loss of microtube formation. We propose that FABP7 plays an essential role in regulating GBM mitochondria fatty acid β-oxidation metabolism and may mediate mitochondria intra-tumoral transfer via GBM microtubes. The novel observations presented in Chapter 4 may lead to a better understanding of how FABP7 and its ligands can be used to inhibit GBM infiltration/invasion.

Chapter 2.

Super Resolution Microscopy Reveals DHA-dependent Alterations in Glioblastoma Membrane Remodelling and Cell Migration

2.1 Introduction

GBM is the most common and malignant primary brain cancer. Despite aggressive treatment and extensive research, GBM remains one of the most deadly cancers, with the majority of patients dying within 15 months of their diagnosis (Wen and Kesari, 2008). The highly infiltrative/invasive properties of GBM and treatment-resistant cancer stem cells are believed to be responsible for the high recurrence rates observed after radiation treatment and chemotherapy (Vehlow and Cordes, 2013). Brain fatty acid binding protein (B-FABP or FABP7) is normally expressed in neural stem cells during development (Feng et al., 1994; Kurtz et al., 1994). FABP7 is also expressed in GBM stemlike cells and is preferentially found at the infiltrative edges of GBM tumors (De Rosa et al., 2012; Mita et al., 2007; Morihiro et al., 2013). FABP7, whose preferred ligands are polyunsaturated fatty acids (PUFAs), has previously been shown to localize to the nucleus of GBM cells where its expression is associated with epidermal growth factor receptor (EGFR) (Kaloshi et al., 2007) and the transfer of PUFAs to transcription factors such as peroxisome proliferator associated receptors (PPARs) (Adida and Spener, 2006). However, FABP7 is also found in the cytoplasm and plasma membrane of GBM cells (Mita et al., 2010; Mita et al., 2007).

The main components of the plasma membrane are phospholipids (van Meer et al., 2008). The plasma membrane order refers to physical phase segregation of phospholipid bilayers, with the liquid-ordered (Lo) phase co-existing with the liquid-disordered (Ld) phase (Sezgin et al., 2017) . The ordered lipid domain (Lo phase), also referred to as tightly packed membrane nanodomains, is characterized by clustering of

membrane proteins and lipids, including sphingolipids, cholesterol and saturated phospholipids. However, the presence of unsaturated phospholipids impairs lipid packing, resulting in a lower state of lipid order (Ld phase) (Sezgin et al., 2017). In addition to lipid composition, plasma membrane order is also determined by actin cytoskeletal activity (Gomez-Llobregat et al., 2013). GBM cell migration is accompanied by protrusion and retraction of cell membranes, processes that require cytoskeleton remodelling (Prahl et al., 2018). Interestingly, FABP7 co-localizes with actin at the edge of lamellipodial protrusions in FABP7-expressing GBM cells (Mita et al., 2007). These results, combined with the fact that polyunsaturated fatty acids (PUFAs) are the preferred ligands of FABP7, suggest that FABP7's role in promoting GBM cell migration is related to plasma membrane order. Relevant to our study, Laurdan (6-dodecanoyl-2-dimethylaminonaphthalene), a lipid phase sensitive fluorescent probe (Owen et al., 2011), reveals increased plasma membrane order resulting from increased lipid saturation in GBM cells (Bi et al., 2019).

Lipid-mediated protein membrane nanodomain formation is responsible for alterations in plasma membrane lipid order (Gomez-Llobregat et al., 2013). However, the mechanism behind these changes remained poorly understood until the emergence of super-resolution microscopy. Super-resolution microscopy, including direct stochastic optical reconstruction microscopy (dSTORM), photoactivated localization microscopy (PALM) (Sengupta et al., 2011) and stimulated emission depletion microscopy (STED), have allowed visualization and quantification of membrane protein distribution in the nanoscale (Sezgin, 2017). In recent years, several membrane lipid-anchored proteins have been reported to form nanoscale domains, including PKCα, Ras and Rac1, which

play essential roles in membrane protein-initiated signalling pathways (i.e., Ca^{2+}-dependent signalling, Ras-driven proliferation pathway and Rac1 cell migration pathway, respectively) (Bonny et al., 2016; Nan et al., 2015; Remorino et al., 2017). As super-resolution microscopy overcomes the limitation of conventional optical microscopes, it allows direct visualization of membrane-anchored cytoskeletal protein nanodomains which is essential to our understanding of the mechanism underlying cell migration (Garcia-Parajo et al., 2014; Remorino et al., 2017).

Similar to brain, GBM tumors are rich in PUFAs, including ω-6 arachidonic acid (AA) and ω-3 docosahexaenoic acid (DHA) (Martin et al., 1996). As both AA and DHA are highly hydrophobic molecules, their transport within GBM cells relies on fatty acid transport proteins, such as FABP7 (Elsherbiny et al., 2013). DHA, a preferred ligand of FABP7, attenuates KRas-driven proliferation in colon cancer cells by altering KRas protein membrane nanodomain formation (Fuentes et al., 2018b). FABPs have been shown to increase the uptake of fatty acids from the cellular microenvironment (Furuhashi and Hotamisligil, 2008). FABP7's affinity for DHA and AA (Balendiran et al., 2000; Xu et al., 1996), combined with its localization at the plasma membrane, cytoplasm and nucleus (Mita et al., 2010; Mita et al., 2007), suggest a role for FABP7 in both the uptake of DHA and AA from the microenvironment and its subsequent intracellular distribution. In agreement with this, using Nuclear Magnetic Resonance (NMR) and Electron Spin Resonance (ESR), FABP7 was found to undergo a conformational alteration upon binding to fatty acid ligands, resulting in its dissociation from biomimetic model membranes (Cheng et al., 2019; Dyszy et al., 2013). Our previous work has shown that DHA inhibits GBM cell migration in a FABP7-dependent manner (Mita et al., 2010). With its 6

unsaturated bonds and very long carbon chain (Stillwell and Wassall, 2003), DHA's inhibitory effect on GBM cell migration may be a direct consequence of its increased FABP7-dependent uptake and incorporation into plasma membrane phospholipids, thereby altering plasma membrane lipid order.

In this study, we use quantitative plasma membrane lipid order imaging to demonstrate an association between FABP7 expression in GBM cells and the formation of highly ordered plasma membrane lipid domains. We further show that increased plasma membrane lipid order correlates with increased GBM cell migration. DHA supplementation in culture medium has a dramatic effect on the plasma membrane lipid order of FABP7-expressing, but not non-FABP7-expressing, GBM cells. FABP7 imaging using super-resolution microscopy indicates that FABP7 forms nanodomains on the membranes of both established GBM cell lines and patient-derived GBM stem-like cells. DHA supplementation inhibits cell migration and disrupts these FABP7 nanodomains. This is in contrast to AA and saturated stearic acid (SA) which have no effect on FABP7 nanodomains. Our results suggest that DHA inhibits GBM cell migration by decreasing membrane lipid order and disrupting FABP7 nanodomains.

2.2 Materials and methods

2.2.1 Cell lines and transfections

The established human GBM cell lines have been previously described (Brun et al., 2018; Mita et al., 2010). GBM cells (e.g., U251, M049, T98 and A172) were cultured in Dulbecco's modification of Eagle's minimum essential medium (DMEM) supplemented with 10% fetal calf serum (FCS). Clonal populations of U87 cells stably transfected with pREP4 vector (U87-Control or U87C) or a pREP4-FABP7 expression construct (U87B or U87-FABP7) have previously been described (Mita et al., 2007). Patient-derived GBM neurosphere cultures (A4-004N) were prepared by enzymatic and mechanical dissociation of GBM tissues and plating the cells in DMEM/F12 medium supplemented with B-27 (Life Technologies, Carlsbad, CA, USA), epidermal growth factor (EGF), and fibroblast growth factor (FGF). ED501 GBM neurosphere (ED501N) cultures were obtained from Drs. Hua Chen and Kenneth Petruk, University of Alberta. GBM tissues from patients were consented prior to surgery under Health Research Ethics Board of Alberta Cancer Committee Protocol #HREBACC-14-0070.

2.2.2 Fatty acid preparation and treatment

Fatty acids (DHA and AA) (Sigma) were dissolved in ethanol, then complexed to BSA (Sigma) over a steady stream of nitrogen gas and stored at −80 °C under reducing conditions. Both GBM neurosphere cultures and GBM adherent cells were maintained at 37 °C in a humidified 5% CO_2 atmosphere. For fatty acid supplementation, cells (at 60-70% confluency) were cultured under serum-free conditions and supplemented with BSA

(vehicle control), 30 µM or 60 µM DHA, AA, or SA in their regular growth medium (neurosphere medium for A4-004N and ED501N and DMEM for U251) for 24 hours.

2.2.3 shRNA knockdown and siRNA knockdown

Lentivirus shRNA packaging plasmids and control plasmids were purchased from Sigma. The two lentivirus FABP7 shRNA constructs used for our experiments were obtained from the University of Alberta RNAi Core Facility, with the following shRNA sequences: CCGGGAAACTGTAAGTCTGTTGTTACTCGAGTAACAACAGACTTACAG-TTTCTTTTTG (shFABP7-1) and CCGGGTGACCAAACCAACGGTAATTCTCGAGAA-TTACCGTTGGTTTGGTCACTTTTTG (shFABP7-2). Control vector was MISSION pLKO.1 (Sigma-Aldrich, SHC002). For virus production, lentiviral plasmids were transfected into HEK293T cells along with lentivirus packaging vectors (Sigma Mission), and virus-containing supernatant was collected 48 hours after transfection. U251 GBM cells were infected with lentivirus overnight and medium was changed after infection. Infected cells were selected in 1 µg mL^{-1} puromycin. GBM neurosphere cultures (ED501N) were transfected with 10 nM scrambled siRNA (control) or FABP7 siRNAs (5′-CAAACCAACGGUAAUUAUCAGUCAA-3′ (NM_001446_stealth_405) and 5′-GCUUU-CUGUGCUACCUGGAAGCUGA-3′ (NM_001446_stealth_304) (Invitrogen) using LipofectamineTM RNAiMAX (Invitrogen). siRNA-transfected cells used for the Laurdan assay were seeded onto coverslips 48 hours post-transfection.

2.2.4 Western blot analysis

Whole cell lysates were prepared as previously described (Liu et al., 2020b). Lysates (50 µg per lane) were separated by sodium dodecyl sulfate-polyacrylamide gel electrophoresis (SDS-PAGE) and transferred to nitrocellulose membranes. Membranes were immunoblotted with rabbit anti-FABP7 (prepared in-house; 1:1000) (Mita et al., 2007) and mouse anti-GAPDH (Thermo Fisher Scientific; 1:1000) antibodies, followed by anti-rabbit or anti-mouse secondary antibodies (Invitrogen, 1:50000).

2.2.5 Quantitative analysis of cell membrane lipid order using Laurdan

Quantification imaging of GBM cell membrane lipid order was carried out using the Laurdan dye (Thermo Fisher Scientific) as described previously (Owen et al., 2011). GBM cells were plated on coverslips in 24-well dishes and cultured to ~70% confluency. The Laurdan dye was diluted in serum free DMEM medium to a final concentration of 5 µM. Live cells were washed with 1×PBS and stained with 5 µM Laurdan dye in a humidified incubator (37 °C with 5% CO_2) for 30 minutes. Laurdan-stained cells were then fixed in 4% paraformaldehyde (PFA) for 10 minutes. For co-immunofluorescence of FABP7 and Laurdan dye, fixed cells were labelled with anti-FABP7 antibody (Santa Cruz, 1:400, sc-374588) and anti-mouse Alexa 647 secondary antibody (1:400, Invitrogen).

Images were acquired with a Zeiss LSM 710 confocal microscope (excitation at 405 nm; emission at 400–460 nm for ordered phase imaging and 470–530 nm for disordered phase imaging) with a 40×/1.3 oil-immersion objective as described previously (Owen et al., 2011). For co-immunofluorescence of FABP7 and Laurdan dye, a Zeiss

confocal 40×/1.3 oil objective and a Leica confocal 100×/1.40 oil objective were used. Liquid-ordered and liquid-disordered phase images were acquired and analyzed using ImageJ software following published guidelines (Owen et al., 2011). Merged mean intensity and rainbow RGB pseudo-colored generalized polarization (GP) images are shown. GP values of 8–10 images (total of 30–40 cells analyzed) were quantified from GP images for generation of GP scatter plot histograms using GraphPad Prism 8 software (GraphPad Software, Inc. San Diego, CA, USA). Statistical analyses for the Laurdan assay are presented using the merged mean GP values for each image.

2.2.5 Immunofluorescence assay

For co-immunofluorescence analysis of FABP7 and cell membrane dye wheat germ agglutinin (WGA) Texas Red™, the WGA dye was diluted to 5 µg mL^{-1} using Hank's balanced salt solution (HBSS). GBM cells adhering to coverslips were incubated in WGA dye for 15 minutes at 37 °C. Labelled cells were washed two times with HBSS, then fixed with 4% paraformaldehyde (PFA) for 10 minutes at room temperature, followed by immunostaining with anti-FABP7 antibody (Santa Cruz, 1:400, sc-374588) and anti-mouse Alexa 488 secondary antibody (1:400, Invitrogen).

To enhance the FABP7 cell membrane nanoscale domain immunofluorescence signal for super-resolution microscopy imaging, we used glyoxal to fix cells along with fluorophore-conjugated primary antibody, as described (Richter et al., 2018). Cells were cultured on high performance coverslips (D = 0.17 mm ± 0.005 mm, Carl Zeiss) for analysis using the STED microscope. The coverslips were coated with laminin (50 µg

mL^{-1}, Sigma- Aldrich) to improve attachment of cells cultured under neurosphere conditions (Rahman et al., 2015). GBM cells were fixed in 3% glyoxal pH 4 (Sigma-Aldrich) for 30 minutes on ice, followed by 30 minutes at room temperature. Fixation was then quenched with 100 mM NH$_4$Cl for 20 minutes, and cells were blocked with 2.5% BSA in 1× PBS for 15 minutes. Cells were then incubated with Atto 550-conjugated affinity-purified rabbit primary anti-FABP7 antibody (1:20; conjugation was with the Atto 550 Protein Labeling Kit from Sigma-Aldrich) or Alexa 546-conjugated primary anti-FABP7 antibody (1:20; Santa Cruz, sc-374588) for 60 minutes. For EGFR detection, U251 cells were immunostained with anti-EGFR antibody (Cell signalling, 1:400, #4267) and anti-rabbit Alexa 555 secondary antibody (1:400, Invitrogen). Cells were washed in high-salt PBS (500 mM NaCl), then 1× PBS, and embedded in Prolong Diamond Antifade Mountant (Thermo Fisher Scientific). The cells were imaged using a STED microscope.

For co-staining of FABP7 and mitochondria, live cells were stained with 200 nM MitoTracker® Deep Red FM (Thermo Fisher Scientific) for 30 minutes at 37 °C, followed by 4% PFA or 3% glyoxal pH 4 fixation and quenching with 100 Mm NH$_4$Cl as described (Richter et al., 2018). Cells were permeabilized in 2.5% BSA and 0.1% Triton-X 100 in 1× PBS for 15 minutes and labelled with Atto 550-conjugated primary anti-FABP7 antibody (1:100, conjugation was with the Atto 550 Protein Labeling Kit from Sigma-Aldrich) for 60 minutes for dual-color STED microscopy imaging or Zeiss confocal microscopy imaging. For quantitative analysis upon BSA control/DHA treatment, raw images (n = 15, 70–80 cells) were acquired using a Zeiss LSM 710 confocal microscope with a 40×/1.3 oil-immersion objective. The average mitochondrial FABP7 intensity of each image and quantitative analysis were carried out using ImageJ software.

2.2.6 STED microscopy imaging and data analysis

A Leica TCS SP8 Falcon STED microscope was used for our experiments. The inverted microscope was operated with a 100×/1.40 oil objective (HC Plan APO CS2). Quantitative imaging was achieved using Leica HyD detectors HyD 562 nm–648 nm and HyD 660 nm–768 nm. For single-color STED imaging, a laser wavelength of 557 nm was used for excitation of the Atto 550 or Alexa 546-conjugated primary anti-FABP7 antibodies and the depletion laser was set at a wavelength of 660 nm. For dual-color STED imaging (FABP7 co-stained with MitoTracker® Deep Red), MitoTracker® Deep Red images were scanned first (excitation laser wavelength 660 nm, depletion laser wavelength 775 nm), followed by acquisition of FABP7 images with Atto 550-conjugated primary anti-FABP7 antibody (excitation laser wavelength 557 nm, depletion laser wavelength 660 nm). Images with a pixel size set to 23.75 nm were scanned at 100 Hz. For each image data set, a 100 nm Z-stack (at 20 nm intervals) was collected and processed with the LAS X Lightning package for deconvolution to reduce out-of-focus signal and to enhance the signal-to-noise ratio of the final images.

ImageJ software was used for quantitative analysis of FABP7 cell membrane nanoscale domain size, density, intensity, shape, and inter-domain distance. For intensity statistics, maximum intensity projections of the deconvolved images were exported to ImageJ software. Thirty to forty images of 100 pixels × 100 pixels were randomly selected from each image and exported to ImageJ. The pixel intensity of the images had a range of 0–255 (pixel intensity) and the number of pixels at each intensity level was counted.

The intensity of each STED image is represented by the average pixel count at each intensity level. Ten images from each of 3 independent experiments were analyzed.

For nanoscale domain size quantification, the maximum intensity projections of the deconvolved images were exported and thresholded for particle analysis. A threshold was established for each cell line based on the most accurate representation of the immunostained images. The threshold established for each cell line was used for all treatment conditions. Images were saved and processed with ImageJ software. The Nearest Neighbour Distance (NND) ImageJ plugin script was used for inter-domain distance calculation (Mao, 2016). Statistical analyses for inter-domain distance and nanodomain density are presented using the average mean values of each image for comparison. ImageJ particle analyzer was used for nanoscale domain distribution and shape analysis (an area with more than 2 pixel^2 was counted as a particle). Frequencies with different interdomain distance and size were summarized. Both circularity and solidity of the nanodomains measured with ImageJ particle analyzer are based on differences in nanodomain shape. Circularity is defined as the degree to which the particle is similar to a circle (ranges from 0 to 1, with 1 indicating a perfect circle). Solidity measures overall concavity of a particle (ranges from 0 to 1, with 1 indicating a solid particle with regular boundary). The average particle circularity and solidity values for each image were used for comparison.

2.2.7 Transswell and scratch assays for isolating migratory GBM cells

We used a previously published method to isolate migratory GBM cells (Adamski et al., 2017). Briefly, GBM cells were trypsinized and counted (Coulter Counter). Twenty-five thousand cells in serum-free DMEM (U251 cells) or in DMEM/F12/B-27/EGF/FGF (A4-004N cells) were seeded in Transswell inserts (pore size: 8 μm; Falcon Cell Culture Inserts) placed in a 24-well plate. Cells were allowed to migrate through the Transswell membrane towards the bottom reservoir containing DMEM or DMEM/F12/B-27/ EGF/FGF supplemented with 10% FCS. Cells that remained in the top chamber after 20 hours were considered to be nonmigratory, whereas cells that had migrated across the membrane were considered to be migratory. Non-migratory and migratory cells were removed from two different reservoirs, using a Q-tip to discard the migratory and non-migratory cells, respectively. The remaining cells (top chamber in one case and bottom chamber in the other case) were stained with Laurdan dye and fixed with 4% PFA for quantitative membrane lipid order staining as described above. Transswell membranes (top membranes for non-migratory cells and bottom membranes for migratory cells) were released from the inserts using a scalpel. Released membranes were mounted onto glass slides and covered with coverslips for imaging.

The scratch assay (Liang et al., 2007) was used to study FABP7 plasma membrane nanoscale domain formation in GBM migratory cells versus non-migratory cells. Previous work from other labs has shown that cells that migrate away from the scratch margin into the cell-free scratch zones are migratory, whereas cells found farthest from the scratch margins are non-migratory (Yang et al., 2012). FABP7 immunofluorescence analysis was carried out using STED microscopy. U251, ED501N

and A4-004N cells were cultured on high performance laminin-coated cover glasses (D = 0.17 mm ± 0.005 mm, Carl Zeiss) until they reached 70%–80% confluence. A top-to-bottom scratch was introduced in the middle of the coverslip with a P20 pipet tip, and cells were incubated for an additional 24 hours. Cells were washed with 1× PBS and fixed in glyoxal using the immunostaining method described in above. For FABP7 membrane nanoscale domain analysis, images of cells in the migratory zones and non-migratory zones were collected using a Leica TCS SP8-gated STED microscope. Quantitative data analysis was as described above.

2.2.8 Statistical analysis

Two-tailed unpaired t-test was used to assess the significance of differences between two experimental groups. If more than two experimental groups are present in a graph, either multiple t-test with Holm-Sidak method (alpha = 0.05) or one-way ANOVA with Dunnett multiple comparisons test was used to evaluate the statistical significance depending on the experimental design. The exact statistical methods used for each experiment is indicated in the figure legends. Prism 8 (GraphPad Software, Inc. San Diego, CA, USA) was used for statistical analysis of data. A p-value or adjusted p-value of <0.05 was considered significantly different. All experiments were done in triplicate (technical replicates) and were repeated at least three times (biological replicates). All imaging data analysis was based on an average of eight to ten images for each experiment.

2.3 Results

2.3.1 FABP7 expression increases GBM cell membrane lipid order

We have previously reported correlation between FABP7 expression and increased migration in GBM cells (Mita et al., 2007). Others have shown that the leading edge of migrating cells has high membrane order regions based on quantitative membrane lipid order analysis (Aranda et al., 2011; Golfetto et al., 2013). To examine the lipid packing state, an indication of hydration level, in GBM cell membrane phospholipids, we used the Laurdan dye. Ratiometrically measured alterations in membrane-bound Laurdan dye intensity at two different spectral channels (liquid-ordered (Lo) channel and liquid-disordered (Ld channel)), represented by the generalized polarization (GP) value, was used to quantitate plasma membrane lipid order (Owen et al., 2011). We first examined the effect of FABP7 expression on GBM membrane lipid order. For these experiments, we used our previously described U87 stable transfectants (Mita et al., 2007) (U87-Control and U87-FABP7 cell lines) (**Figure 2.1A**). The GP distribution obtained for each cell line is represented as pseudo-colored images, normalized histograms and average GP index values. Our results show that U87-FABP7 cells have a higher plasma membrane order (right shifting of GP histograms and higher GP index values) compared to U87-Control cells (**Figure 2.1B-D**). These results indicate that FABP7 expression promotes highly ordered/rigid plasma membrane formation in GBM cells.

We also carried out Laurdan experiments with U251 control cells (U251-shControl) which naturally express FABP7 and U251 cells depleted of FABP7 using lentiviral shRNA constructs (U251-shFABP7) (**Figure 2.1A**). Consistent with our U87 data, FABP7-

depleted U251 cells (U251-shFABP7-2) have a lower plasma membrane order (left shifting of GP histograms and lower GP index values) compared to U251-Control cells (**Figure 2.1B-D**). No significant effect was observed with U251-shFABP7-1, in keeping with the lower FABP7 knockdown efficiency observed in these cells.

Patient derived GBM cells cultured under conditions that promote the growth of cells with neural-stem like properties express high levels of FABP7 (Morihiro et al., 2013). When we repeated our Laurdan experiments with FABP7-expressing patient-derived ED501N GBM neurosphere cells, we observed similar results as with our U87 and U251 cell lines, with ED501N siControl cells showing a higher plasma membrane order compared to FABP7-depleted ED501N cells (both ED501N siFABP7-1 and siFABP7-2) (**Figure 2.1B-D**). These combined results are particularly noteworthy in the context of FABP7 localization to cell protrusions in migratory cells and suggest a link between FABP7- induced ordered plasma membrane and GBM cell migration.
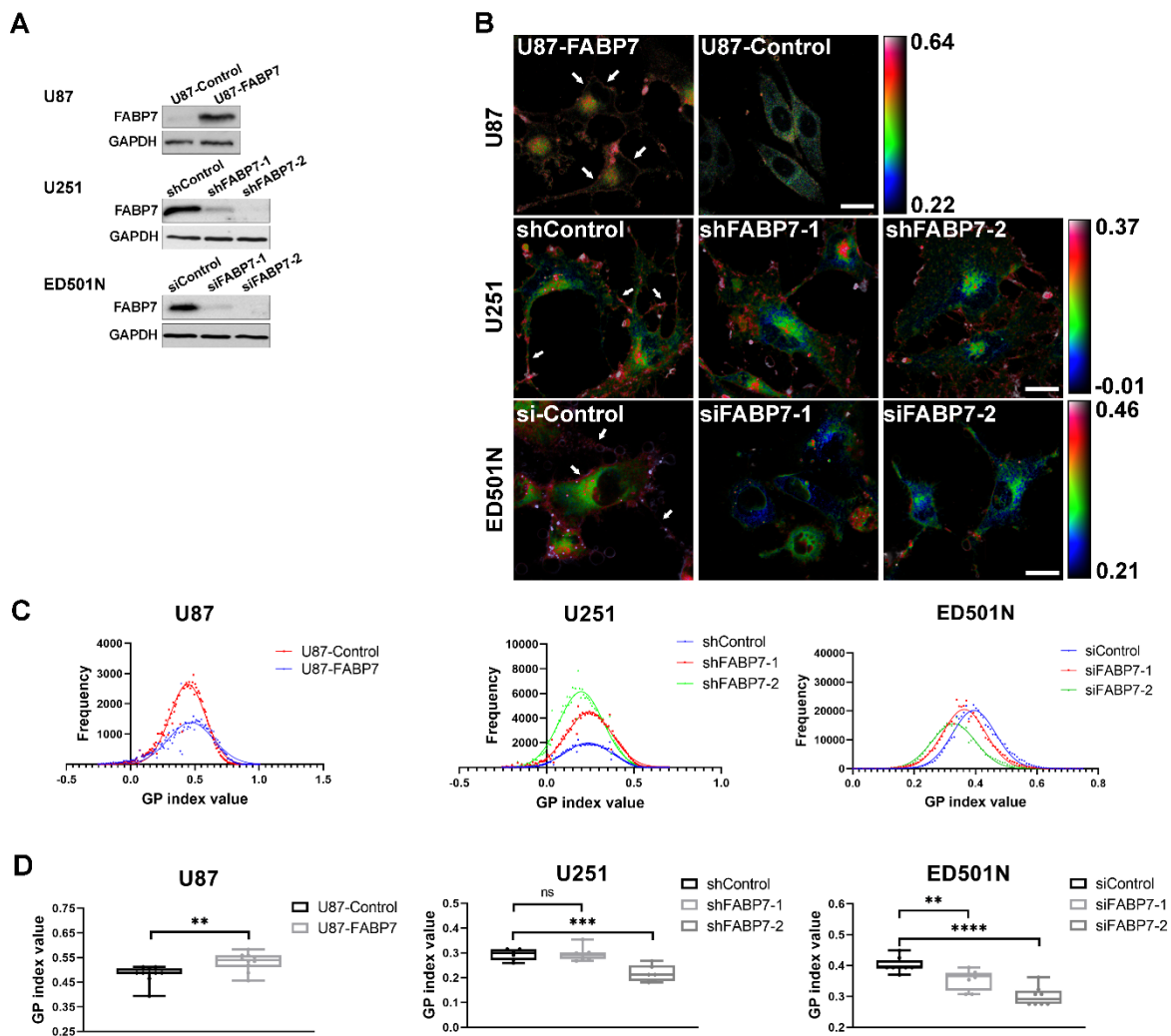
Figure 2.1 FABP7 increases membrane lipid order in GBM cells and neurosphere cultures.

(A) Western blot analysis showing FABP7 expression in stable U87-Control and U87-FABP7 transfected cells, stable U251-shControl and U251-shFABP7-1 & U251-shFABP7-2 transfected cells, and transient ED501N control and siFABP7-1 and siFABP7-2 transfected cells. (B) Laurdan imaging analysis of membrane lipid order in U87 and U251 stable transfectants, and ED501N transient transfectants. Representative

merged pseudo-colored GP images are shown, with color range indicated by the color bar. Purple-red colors (arrows point to plasma membrane) indicate high membrane order and lower fluidity, whereas green-blue colors indicate low membrane order and increased fluidity. Scale bars = 20 μm. (C) Distribution of the GP index values in GBM cells described in A and B. The histograms for U87-FABP7 cells are shifted to the right (higher GP value) compared to U87-Control cells. FABP7-depleted U251 and ED501N cells are shifted to the left (lower GP value). (D) Average GP index values in GBM cells were calculated from several images including the ones shown in panel B (n = 7–10). Statistical analysis of U87 was performed using the two-tailed unpaired t-test. Statistical analysis of U251 and ED501N was performed with one-way ANOVA and Dunnett multiple comparisons test. Center line, median; box limits, 25th and 75th percentiles; whiskers, minimum to maximum with all points shown. ** indicates $p < 0.01$, *** indicates $p < 0.001$, **** indicates $p < 0.0001$, and ns indicates $p > 0.05$. GP, generalized polarization.

2.3.2 Migratory GBM cells have higher membrane lipid order

A previous study using the Laurdan assay showed an association between cell migration in HeLa cells and membrane lipid order (Aranda et al., 2011). To address whether this also applies to GBM cells, we used Transwell inserts to separate migratory cells from non-migratory cells using FABP7-expressing U251 and A4-004N cells. Of note, migratory GBM cells have already been shown to express high levels of GBM neural stem cell-like markers compared to their non-migratory counterparts (Adamski et al., 2017).

Cells (25 000 per well) were seeded in Transwell inserts and allowed to migrate across the porous membrane towards the bottom reservoir containing 10% FCS over a period of 20 hours. After removal of either the non-migratory (retained on top of the membrane) or migratory cells (located at the bottom of the membrane) from duplicate inserts, the remaining cells (bottom membrane representing migratory cells in one case and top membrane representing non-migratory cells in the other case) were stained with the Laurdan dye. Our results indicate that migratory GBM cells have a higher plasma membrane order (higher GP value) compared to non-migratory cells. This was observed for both U251 and A4-004N cells (**Figure 2.2A-C**). Increased migration therefore positively correlates with a more rigid and less fluid plasma membrane in FABP7-expressing GBM cells.
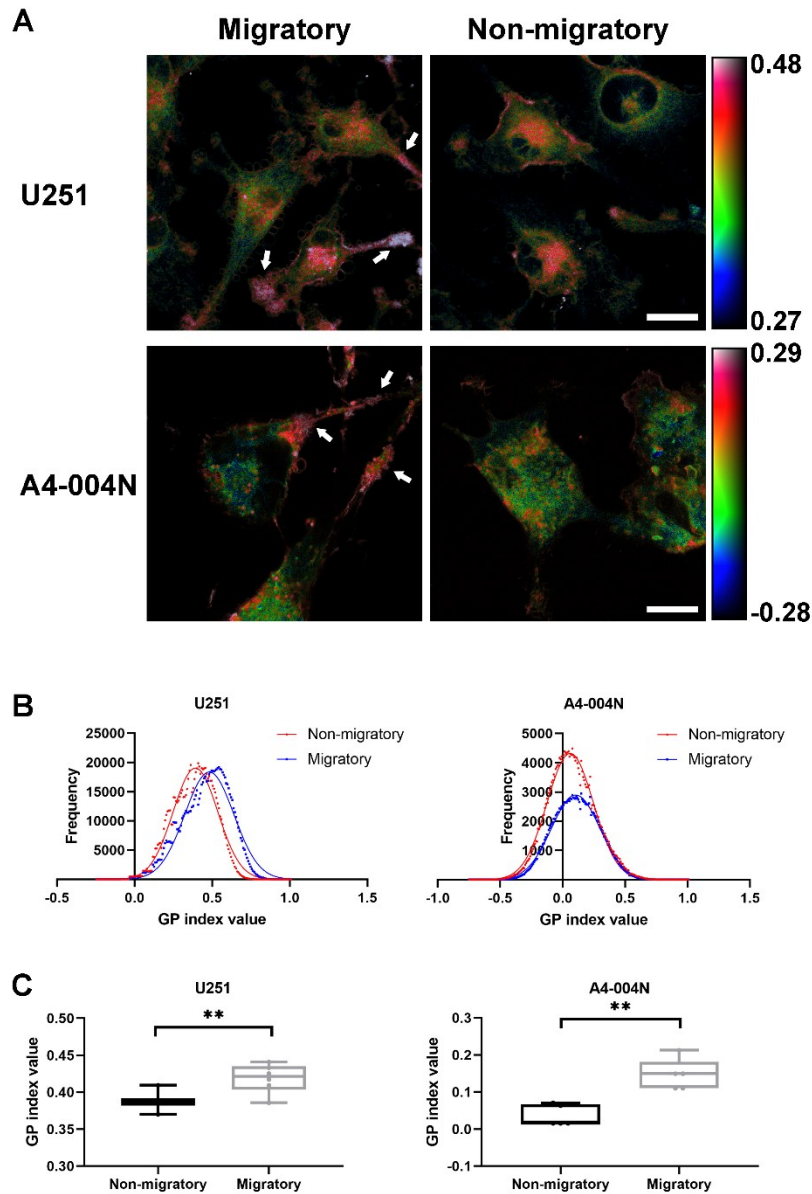
Figure 2.2 Migratory GBM cells have a higher membrane order.

Laurdan imaging analysis of membrane lipid order in migratory U251 and A4- 004N cells (bottom of Transwell inserts) and their non-migratory counterparts (top of Transwell inserts). (A) Representative merged pseudo-colored GP images are shown, with the color range indicated by the color bar. Scale bars = 20 μm. (B) Distribution of GP index values

in GBM cells described in panel A. The histograms of migratory U251 and A4-004N cells are shifted to the right (higher GP value), whereas their non-migratory counterparts are shifted to the left (lower GP value). (C) Average GP index values in migratory and non-migratory GBM cells were calculated from several images including the ones shown in panel a (n = 6). Statistical analysis was performed using the two-tailed unpaired *t*-test. Center line, median; box limits, 25th and 75th percentiles; whiskers, minimum to maximum with all points shown. ** indicates $p < 0.01$. GP, generalized polarization.

2.3.3 DHA decreases membrane lipid order in FABP7-expressing GBM cells

A defining property of membrane liquid-ordered domains is their tight packing of lipids which is usually associated with high levels of tightly-stacking saturated fatty acids and cholesterol (Sezgin et al., 2017). In contrast, fatty acids with multiple double bonds reduce the tight interaction between phospholipid tails, thereby increasing the fluidity of the plasma membrane. Thus, the fatty acid composition of plasma membrane phospholipids can dramatically alter cell membrane order/fluidity as well as membrane-localized growth factor receptor activity and signal transduction (Bi et al., 2019).

We have already shown that DHA inhibits GBM migration in a FABP7-dependent manner (Mita et al., 2010). Furthermore, DHA is rapidly incorporated into cell membrane phospholipid bilayers in DHA-supplemented cells, thereby disrupting saturated lipids/cholesterol-dependent lipid domains (Wassall and Stillwell, 2009). In light of FABP7's affinity for DHA and likely role in DHA uptake from the extracellular microenvironment, we examined the impact of FABP7 on DHA-mediated changes in

membrane lipid order. For these experiments, we used the following pairs of established GBM cell lines: U251-shControl and U251-shFABP7; U87-Control and U87-FABP7. Cells were cultured in 60 µM DHA for 24 hours and stained with the Laurdan dye. DHA supplementation decreased membrane lipid order (i.e., reduced membrane GP index value) in FABP7-expressing GBM cells (U251-shControl and U87-FABP7); however, little effect on lipid order was observed in FABP7-depleted and negative cells (U251-shFABP7-2 and U87-Control) (**Figure 2.3A–C**).

To further document the role of FABP7 in DHA-mediated changes in GBM membrane lipid order, we carried out the Laurdan assay on additional established GBM cell lines (unmanipulated FABP7-expressing U251 and M049; unmanipulated FABP7-negative T98 and A172) as well as patient-derived FABP7-expressing neurosphere cultures (ED501N and A4-004N, both of which naturally express high levels of FABP7). Similar to what was observed in our paired U87 and U251 cell lines, DHA supplementation significantly decreased membrane lipid order (i.e., decreased GP index value) over the entire cell membrane and abolished high-GP regions in all FABP7-expressing GBM cell lines/neurosphere cultures, but had little effect on FABP7-negative GBM cells (**Figure S2.1A–C**). Thus, our results support a role for FABP7 in increasing the incorporation of DHA in membrane phospholipids, thereby disrupting GBM plasma membrane rigidity and ability to migrate.

Like DHA, AA is a PUFA, but with only four double bonds compared to DHA's six double bonds. As FABP7 can also bind AA, albeit with lesser affinity than DHA, and AA is generally associated with pro-tumorigenic properties, we were particularly interested in whether AA can also alter GBM plasma membrane lipid order. For these experiments, we

analysed FABP7-expressing U251 cells cultured in 60 μM AA, compared to BSA control or 60 μM DHA. In contrast to DHA supplementation, AA supplementation had no effect on membrane GP values in GBM cells, generating results similar to BSA control cells (**Figure S2.2A-C**).
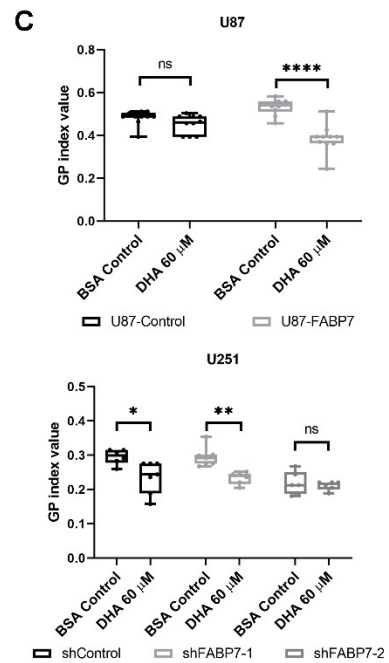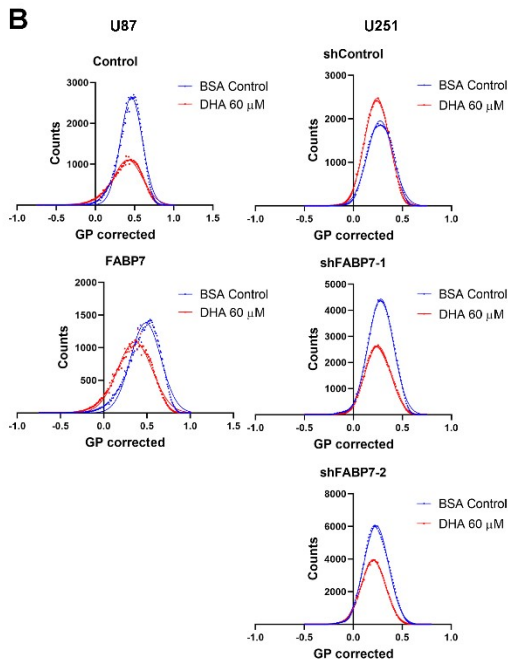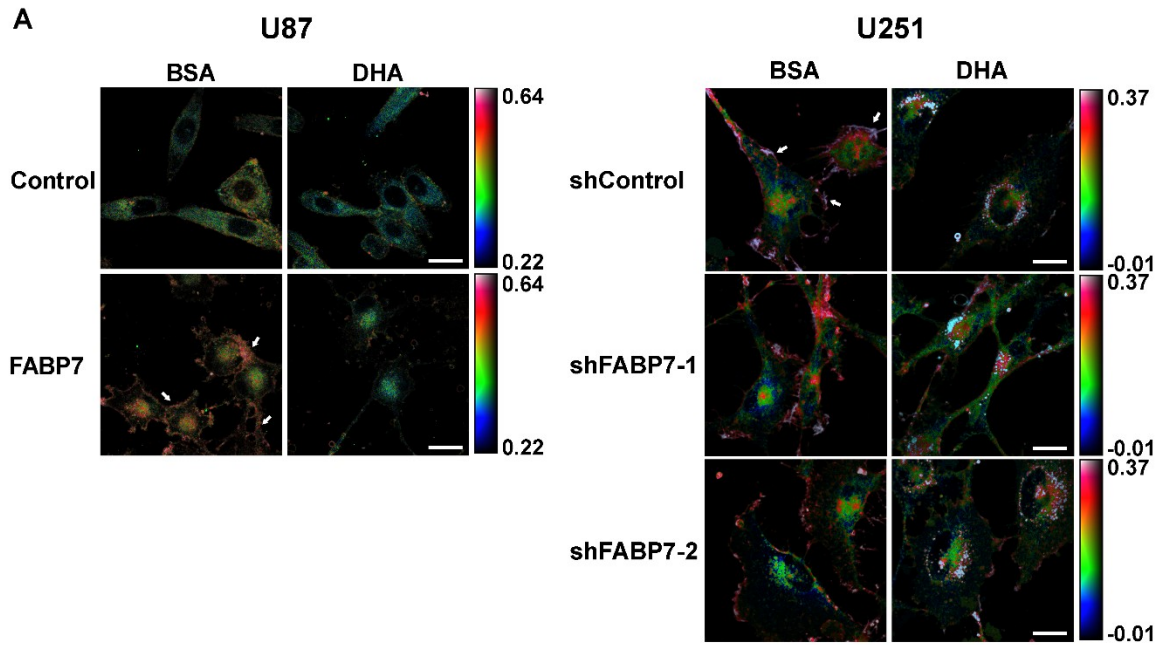
Figure 2.3 DHA decreases membrane lipid order in FABP7-expressing GBM cells.

(A) Laurdan imaging analysis of membrane lipid order in U87 and U251 stable transfectants (U87-Control & U87-FABP7, U251-shControl & U251-shFABP7) treated with BSA control or 60 µM DHA for 24 hours. Representative merged pseudo-colored GP images are shown, with color range indicated by the color bar. Scale bars = 20 µm. (B) Histograms of FABP7-expressing GBM cells (U87-FABP7 and U251-shControl) are shifted to the left (lower GP value) upon DHA treatment, whereas histograms of FABP7-depleted GBM cells (U87-Control and U251-shFABP7) show no shift upon DHA treatment. (C) Average GP index values were calculated from several images including the ones shown in panel A (n = 6–10). Statistical analysis was performed with multiple t-test using the Holm-Sidak method, with alpha = 0.05. Center line, median; box limits, 25th and 75th percentiles; whiskers, minimum to maximum with all points shown. * indicates $p < 0.05$, ** indicates $p < 0.001$, **** indicates $p < 0.0001$, and ns indicates $p > 0.05$. GP, generalized polarization.

2.3.4 FABP7 localizes to the highly ordered lipid regions of GBM plasma membrane

FABP7 co-localizes with actin at the leading edge of GBM cells cultured in AA-rich medium, suggesting a role for FABP7 in cell migration (Mita et al., 2007). Unliganded FABP7 has been shown to directly associate with the plasma membrane (Cheng et al., 2019; Dyszy et al., 2013). Once bound by fatty acids, FABP7 dissociates from the plasma membrane, presumably to take its cargo inside the cell (Cheng et al., 2019; Dyszy et al., 2013). We therefore used the Texas Red-conjugated Wheat Germ Agglutinin (WGA)

membrane marker to investigate whether FABP7 is located at the plasma membrane. Co-staining U251 cells with WGA-Texas Red and anti-FABP7 antibody revealed FABP7 at the leading edge of membrane protrusions (filopodia and lamellipodia; indicated by arrows). As well, FABP7 was observed in the cytoplasm, nucleus and perinuclear region (**Figure 2.4A**).

Actin accumulation at cell membrane protrusions is tightly associated with membrane bound protein distribution, and activation of cytoskeleton remodelling proteins as well as cell signaling pathways (Mattila et al., 2016). The Laurdan assay has already been used to confirm that cytoskeleton remodelling proteins preferentially localize to highly ordered membrane regions with a high GP value in cancer cells (Aranda et al., 2011; Chichili and Rodgers, 2009). To pursue the relationship between FABP7 located at the leading edge of membrane protrusions and membrane order, we stained U251 cells with anti-FABP7 antibody and the Laurdan dye. Confocal images show that FABP7 accumulates at highly ordered plasma membrane regions (with a high GP values) (**Figure 2.4B**).
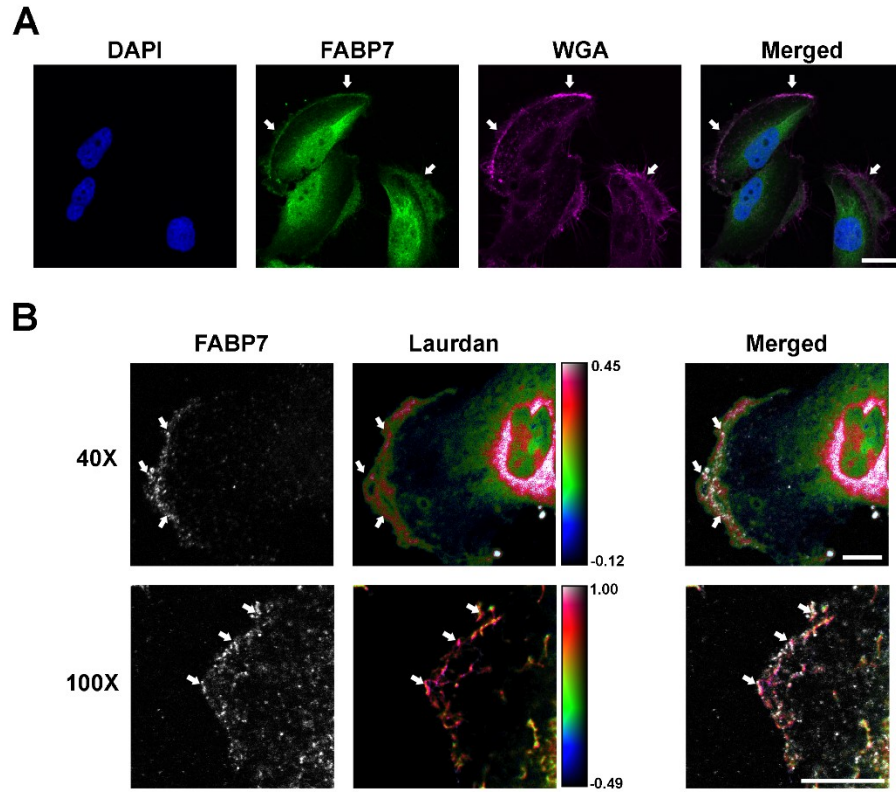
Figure 2.4 FABP7 localizes to highly ordered regions of GBM plasma membrane.

(A) U251 cells were co-stained with anti-FABP7 antibody (detected with Alexa 488 anti-mouse secondary antibody) and plasma membrane marker WGA-Texas Red. Arrows point to plasma membrane regions. Scale bar = 20 μm. (B) U251 cells were co-stained with anti-FABP7 antibody (detected with Alexa 647 anti-mouse secondary antibody) and Laurdan dye. Images were taken using either a Zeiss confocal microscope (40× oil lens) or a Leica confocal microscope (100× oil lens). Representative merged pseudo-colored GP images are shown for the Laurdan assay. The color range is indicated by the color bar. Arrows point to FABP7 located at highly ordered plasma membrane regions. Scale bars = 10 μm.

2.3.5 FABP7 forms membrane nanoscale domains in GBM cells

Membrane liquid-ordered domains are believed to be nanoscale domains (<200 nm), thus conventional optical microscopy cannot be used to directly investigate nanoscale domain structures because of the limit of its resolution (~250 nm) (Sezgin et al., 2017). To overcome this limitation, several super-resolution optical tools have been developed to address membrane lipid-mediated protein nanoscale organization (Sezgin, 2017). Using these new tools, actin cytoskeleton protein (i.e., Rac1) has been shown to form nanoscale domains at the plasma membrane in migrating cells (Maxwell et al., 2018; Remorino et al., 2017).

To address the nanoscale distribution of membrane-localized FABP7, we used STED super-resolution microscopy in conjunction with fluorophore-conjugated antibodies which allows a spatial resolution of 30–60 nm with deconvolution. U251 cells were cultured on high-performance coverslips, and immunostained with Atto 550- or Alexa 546-conjugated primary anti-FABP7 antibodies. The localization of FABP7 on the basal surface (closest to the coverslip) of cell membrane protrusions was examined by Z-stack scanning (~100 nm stack thickness) with deconvolution. Our results indicate that FABP7 forms nanoscale domains on the plasma membrane in the submicron range (with diameters ranging from 50–150 nm) (**Figure S2.3**).

2.3.6 DHA disrupts FABP7 nanoscale domain formation in GBM cell membrane

DHA supplementation affects membrane-associated protein organization and downstream signaling pathways based on super-resolution microscopy. For example,

DHA has been shown to alter KRas and neurotrophin receptor TrkB nanoscale distribution by re-arranging or disrupting membrane protein nanoscale domains (Angelov and Angelova, 2017; Fuentes et al., 2018b).When FABP7 binds to its preferred ligand DHA (Balendiran et al., 2000; Xu et al., 1996), it undergoes a conformational change that causes it to dissociate from the plasma membrane (Cheng et al., 2019; Dyszy et al., 2013). We were therefore interested in investigating the effect of DHA on the nanoscale domain properties of membrane FABP7, including size, density, inter-domain distance, intensity and shape.

FABP7-expressing U251, ED501N and A4-004N cells were cultured in 60 μM (U251 cells) or 30 μM (ED501N and A4-004N neurosphere cultures) DHA, AA or saturated stearic acid (SA) for 24 hours, with BSA serving as the fatty acid treatment control. Our results revealed reduced FABP7 nanoscale domain formation when the three cell lines were cultured in DHA-supplemented medium compared to BSA-, AA- or SA-supplemented medium (**Figure 2.5A**). The sizes of the majority of FABP7 nanoscale domains ranged from 0.01–0.015 μm^2 (100 nm in diameter) when cells were cultured in their normal (non fatty acid-supplemented) growth medium (DMEM for U251 cells and DMEM/F12/B-27/EGF/FGF neurosphere medium for ED501N and A4-004N). However, upon DHA supplementation, a decrease in membrane FABP7 nanoscale domain size was observed in all three GBM cell lines compared to BSA control. While AA- and SA-supplementation also resulted in a decrease in FABP7 nanodomain size in U251 cells, this decrease was of much lower magnitude compared to that observed with DHA supplementation (**Figure 2.5B**).

In addition to a reduction in size, we observed a significant reduction in the average density of membrane FABP7 nanoscale domains upon DHA supplementation (6-fold decrease in U251 cells, 10-fold decrease in both ED501N and A4-004N) (**Figure 2.5C**). To gain more insight into the spatial distribution of membrane FABP7, we calculated the distance between nearest nanoscale domains using a nearest neighbour distance (NND) analysis algorithm. The overall FABP7 interdomain distance distribution (**Figure 2.4A**) and the average interdomain distance (**Figure 2.5D**) were significantly increased in DHA-supplemented U251, ED501N and A4-004N cells compared BSA-supplemented cells. Quantitative analyses revealed a >2-fold increase in the average interdomain distance of FABP7 (500–600 nm) upon DHA treatment compared to ~200–250 nm in BSA-supplemented cells (**Figure 2.5D**). Again, the strongest effects were observed in ED501N and A4-004N cultures. Neither AA- nor SA- supplementation affected the FABP7 interdomain distance of FABP7-expressing U251, ED501N and A4-004N, with the exception of SA-supplementation in U251 cells which increased the FABP7 interdomain distance to ~150 nm (**Figure 2.5D**). Similarly, quantitative analysis of FABP7 nanoscale domain intensity also showed attenuation in all three cell lines upon DHA supplementation compared to BSA control based on immunofluorescence intensity scores (**Figure S2.4B**). AA and SA supplementation had no effect on FABP7 nanoscale domain intensity.

Finally, we studied the circularity and solidity of membrane FABP7 nanoscale domains in GBM cells cultured in BSA (control) versus DHA supplemented medium. The latter induced a more circular and solid FABP7 membrane distribution pattern compared to control cells. In particular, DHA supplementation increased average FABP7 nanodomain circularity and solidity in ED501N by 7% and 10%, respectively, and in A4-

004N cells by 19% and 14%, respectively, compared to BSA control. In comparison, there was no change in circularity and solidity upon AA and SA supplementation in ED501N and A4-004N cells (**Figure S2.4C-D**). In contrast to neurosphere cultures, DHA, AA and SA supplementation in U251 cells all had effects on the circularity and solidity of FABP7 nanoscale domains, although effects were strongest with DHA supplementation. Regions selected for shape analysis are shown in **Figure S2.5**. Our results indicate an important role for DHA in the disassembly of FABP7 nanodomains which has broad implications for the regulation of GBM cell migration.

EGFR is a well-characterized protein expressed in GBM cells that forms well-defined membrane nanodomains (Boyd et al., 2016). We next asked whether other membrane-associated proteins are also affected by DHA supplementation in GBM cells. For this experiment, we cultured U251 cells in serum-free DMEM supplemented with 60 µM DHA for 24 hours. We then immunostained the cells with anti-EGFR antibody. STED microscopy showed that DHA supplementation did not disrupt EGFR nanodomain organization, indicating that not all membrane proteins are susceptible to DHA-mediated disruption of nanodomains (**Figure S2.6**).
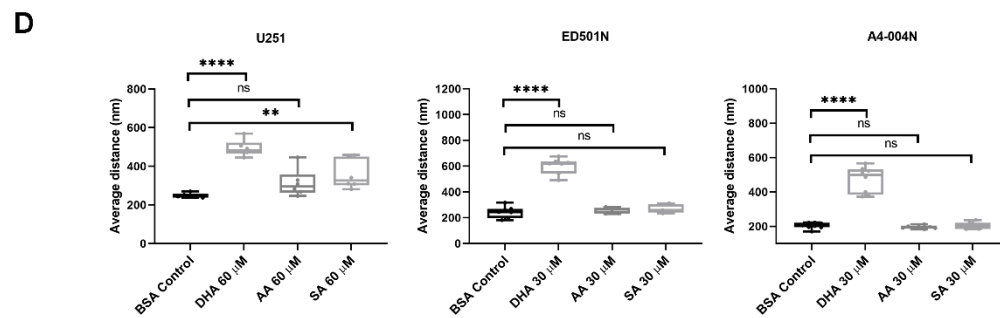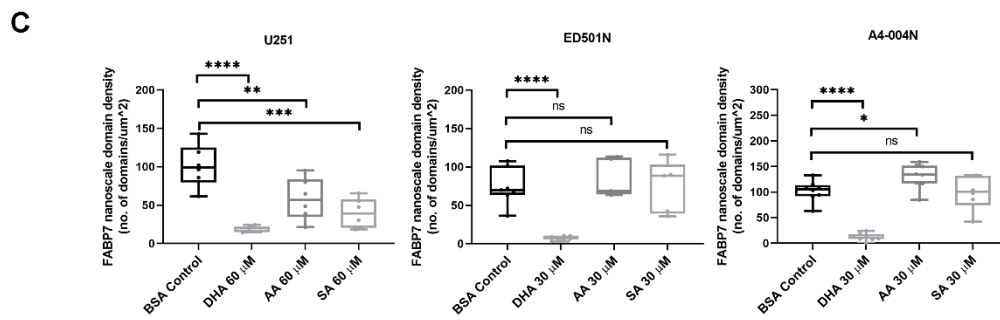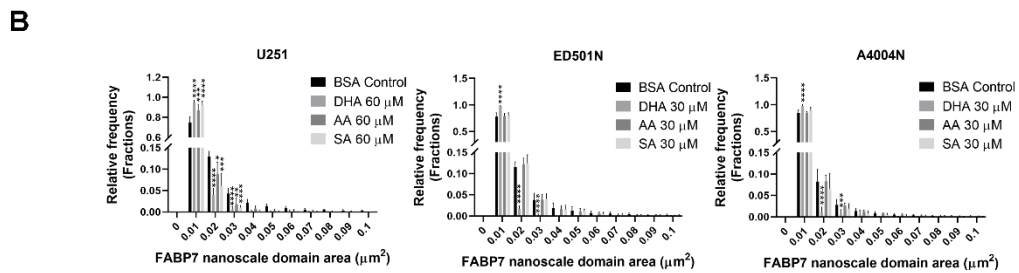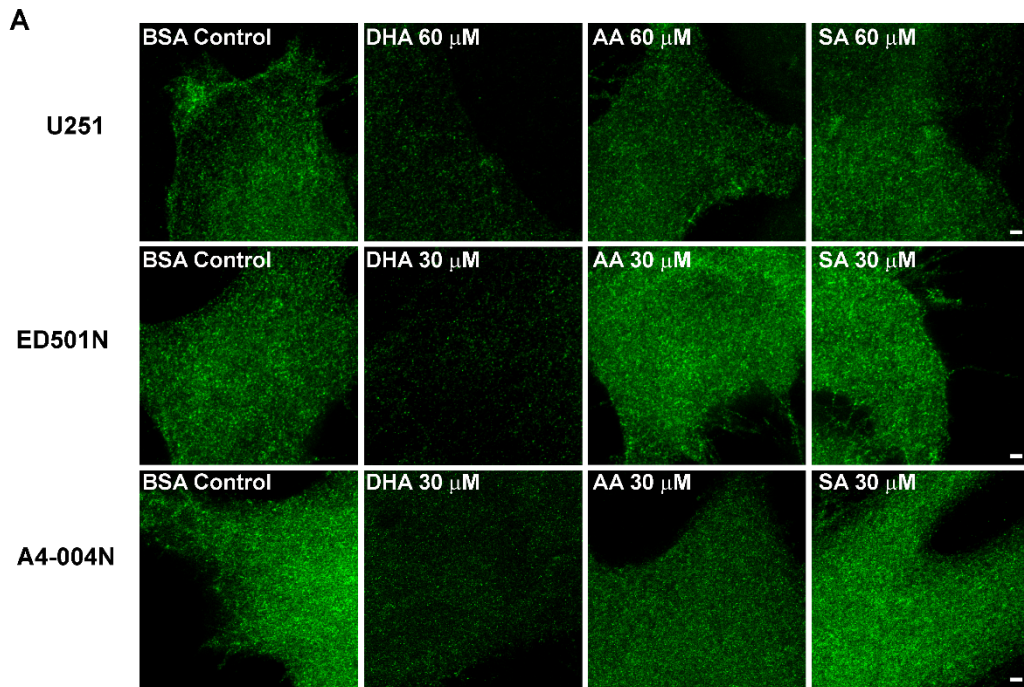
Figure 2.5 DHA disrupts FABP7 membrane nanoscale domains in GBM cells.

U251, ED501N and A4-004N GBM cells were supplemented with BSA (Control), 60 µM

or 30 µM DHA, AA, or SA for 24 hours, then labelled with Atto 550-conjugated primary

anti-FABP7 antibody for STED microscopy. Images were taken in Z-stack mode and

processed using deconvolution. Maximum intensity projections are shown for the different

fatty acid treatment conditions. (A) Membrane FABP7 nanoscale domains in GBM cells

show reduced density distribution upon DHA treatment compared to BSA control and

supplementation with AA or SA. Scale bars = 1 µm. (B) The size distribution of membrane

FABP7 nanoscale domains are significantly decreased upon DHA supplementation

compared to BSA control, and supplementation with AA or SA ($p < 0.0001$, n = 6 to 8 for

all three GBM cell lines tested). Statistical analysis was performed with multiple *t*-test

using the Holm-Sidak method, with alpha = 0.05. Error bars represent standard deviation.

(C) The membrane FABP7 nanoscale domain average density in DHA-supplemented

cells is significantly decreased compared to BSA control and supplementation with AA or

SA ($p < 0.0001$, n = 6 to 8 for all three GBM cell lines tested). Nearest neighbour distance

analysis (NND) was performed to determine the distance between a FABP7 nanoscale

domain and its five nearest neighbors. (D) DHA supplementation increases the average

distance between FABP7 nanodomains compared to BSA control and supplementation

with AA or SA ($p < 0.0001$, n = 6 to 8 for all three GBM cell lines tested). Statistical analysis

of (C) and (D) was performed with one-way ANOVA and Dunnett multiple comparisons

test. Center line, median; box limits, 25th and 75th percentiles; whiskers, minimum to

maximum with all points shown. * indicates $p < 0.05$, ** indicates $p < 0.01$, *** indicates p

< 0.001, **** indicates $p < 0.0001$, and ns indicates $p > 0.05$.
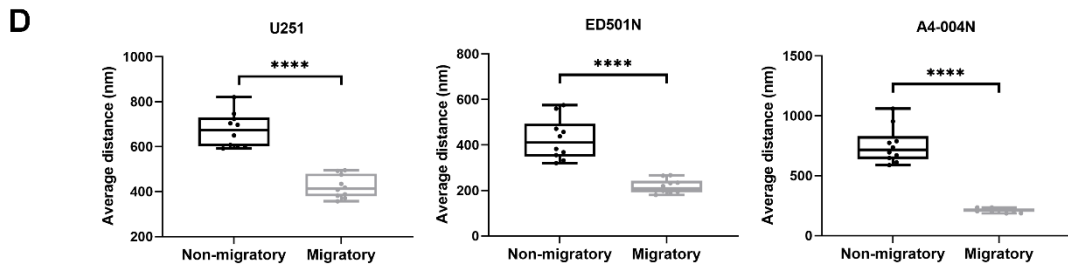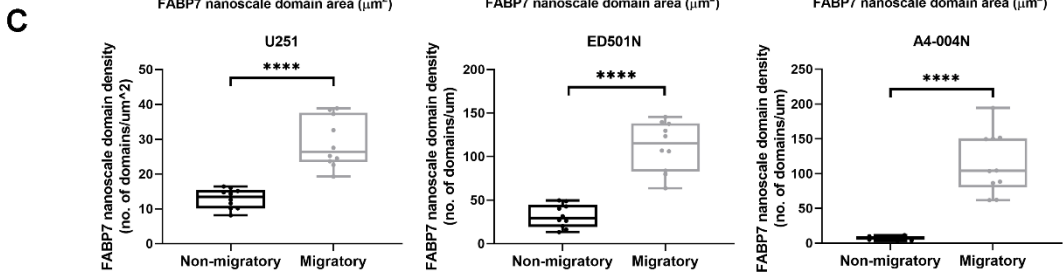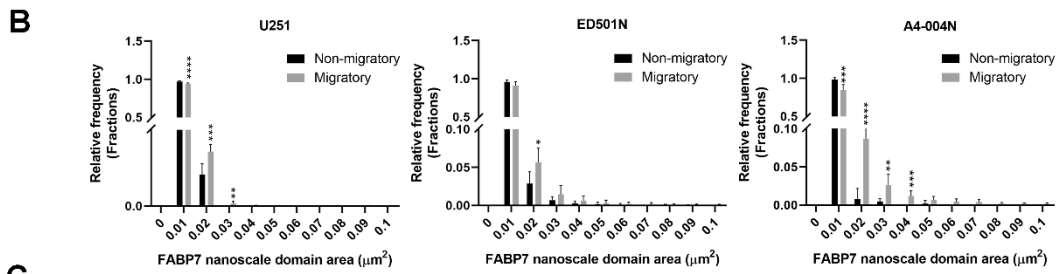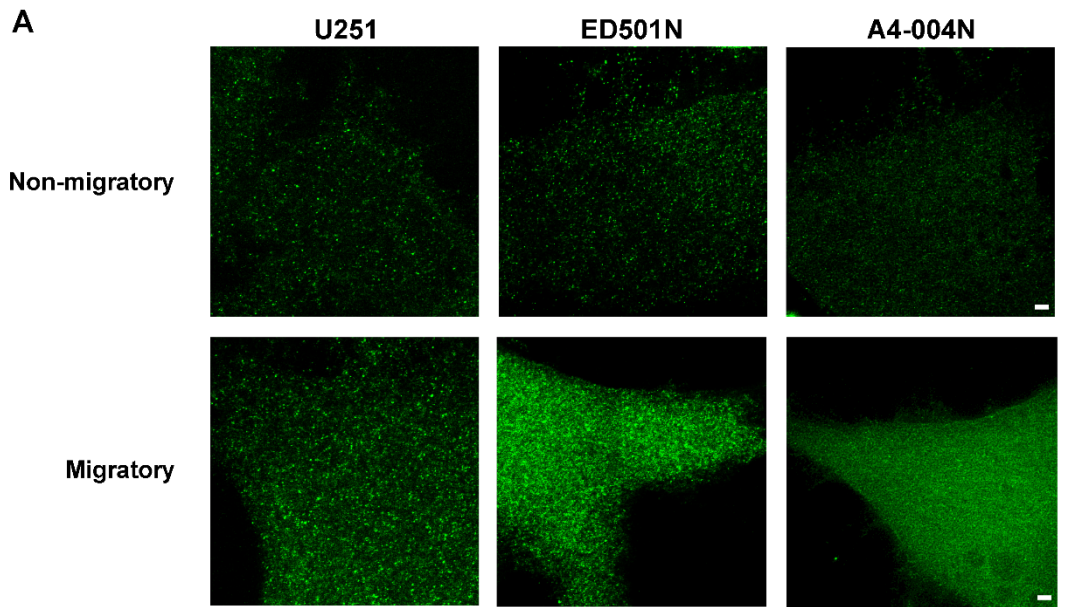
Figure 2.6 FABP7 nanoscale domains on GBM membranes are differentially distributed in migratory and non-migratory cells.

U251, ED501N and A4-004N were cultured on high-performance coverslips, and the scratch assay carried out to separate GBM migratory cells (migrating fronts) from non-migratory cells (control areas). Cells were then immunostained with Atto 550-conjugated primary anti-FABP7 antibody for STED microscopy. Images were taken in Z-stack mode and processed using deconvolution. Maximum intensity projections are shown for migratory cells and non-migratory cells. Scale bars = 1 μm. (A) Membrane FABP7 nanoscale domains in migratory GBM cells show a more condensed distribution compared to cells in control regions. (B) The size of membrane FABP7 nanoscale domains increases in cells located in the migrating front compared to control regions (n = 10 for all three GBM cell lines tested). Statistical analysis was performed with multiple t-test using the Holm-Sidak method, with alpha = 0.05. Error bars represent standard deviation. (C) The membrane FABP7 nanoscale domain average density in migratory cells is significantly increased compared to cells located in control regions ($p < 0.0001$, n = 10 for all three GBM cell lines tested). Nearest neighbour distance analysis (NND) was performed to determine the distance between a FABP7 nanoscale domain and its five nearest neighbors. (D) The average inter-domain distance is decreased in migratory cells compared to cells located in control regions ($p < 0.0001$, n = 10 for all three GBM cell lines tested). Statistical analysis of (C) and (D) was performed with two-tailed unpaired t-test. Center line, median; box limits, 25th and 75th percentiles; whiskers, minimum to maximum with all points shown. ** indicates $p < 0.01$, *** indicates $p < 0.001$, and **** indicates $p < 0.0001$.

2.3.7 Migratory GBM cells show increased FABP7 membrane nanoscale domain formation

Migrating/motile cancer stem cells define a subgroup of cells with properties associated with a more invasive/metastatic phenotype (Brabletz et al., 2005). Notably, stem cell markers (CD44 and ALDH1) are expressed at elevated levels in the cells located at the leading edges of invasive breast cancer tumors (Pan et al., 2015a; Yang et al., 2019), as well as migrating front of breast cancer cells using the in vitro scratch assay (Saha et al., 2014). Similar to CD44 and ALDH1 in breast cancer, FABP7 can be found at the leading edge of GBM tumors (Mita et al., 2007). As our results indicate that FABP7 forms nanoscale domains at the GBM plasma membrane, we next investigated whether there was a correlation between FABP7 membrane distribution and GBM cell migration. U251, ED501N and A4-004N cells were cultured on high performance cover glass and a scratch introduced pre-confluency. Cells were allowed to migrate into the scratch over a period of 24 hours. Cells were then fixed, immunostained with anti-FABP7 antibody and super-resolution STED microscopy carried out at both the migrating front and control areas. STED deconvolution images showed higher expression of FABP7 (right shifting of intensity score curve) at the migrating front compared to control areas for all three GBM cell lines (**Figure S2.7A**). We also found that migratory GBM cells have a higher density of FABP7 nanodomains which are also larger compared to those observed in non-migrating cells in all three GBM cell lines (**Figure 2.6A-B**). The increase in FABP7 average nanodomain density at migrating fronts ranged from 2.5× for U251 and 5× for ED501N, to 16× for A4-004N (**Figure 2.6C**). Consistent with our density analysis, there was also a significantly decreased inter-domain distance, ranging from ~35–50%,

between FABP7 nanodomains in the migrating fronts of all three GBM cell lines based on NND analysis (**Figure 2.6D and Figure S2.7B**). Interestingly, migratory cells also showed less circular FABP7 membrane signals compared to non-migrating cells (~6% and 13% decreases in ED501N and A4-004N cells, respectively), in agreement with highly migratory GBM cells forming more condensed, and thus more irregular FABP7 nanoscale domains at plasma membranes associated with migrating fronts (**Figure S2.7C-D**).
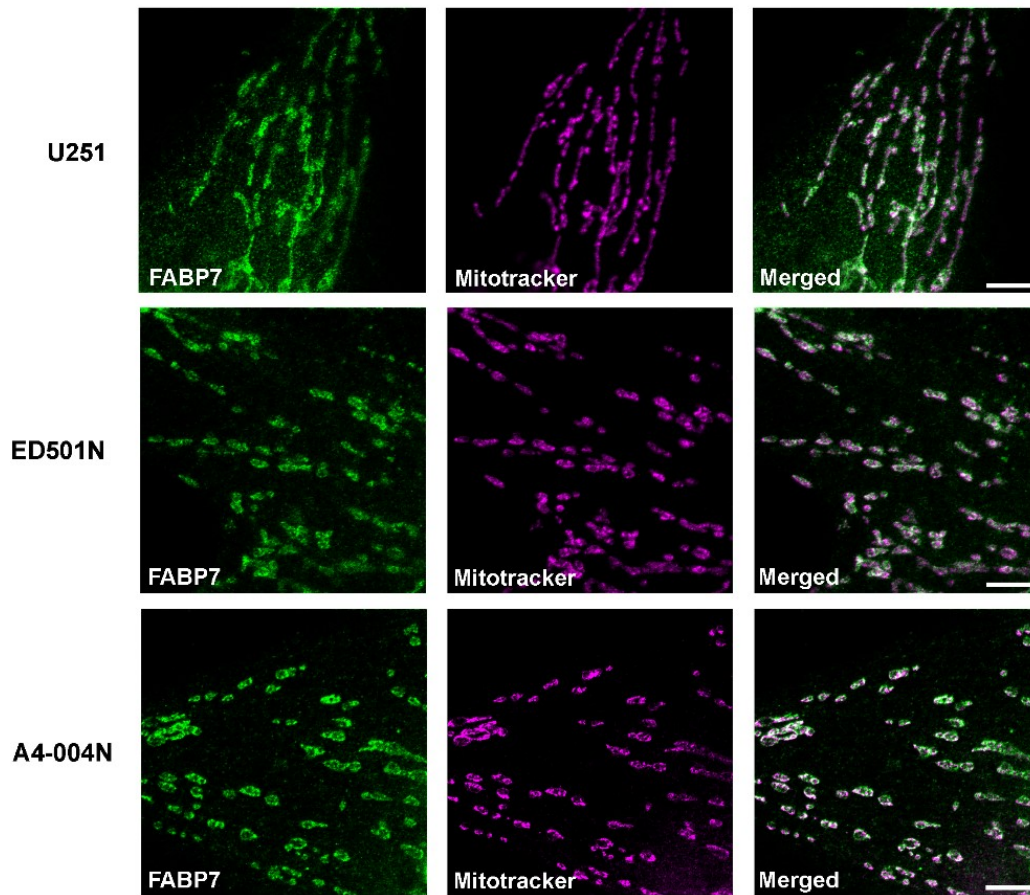
Figure 2.7 FABP7 localizes to the mitochondria of GBM cells.

Dual-color STED microscopy shows cytoplasmic FABP7 (detected with Atto 550 conjugated primary anti-FABP7 antibody) co-compartmentalizes with mitochondria (MitoTracker® Deep Red) in U251, ED501N and A4-004N cells. Scale bars = 5 µm.

2.3.8 FABP7 translocates from plasma membrane to mitochondria upon DHA supplementation

Similar to DHA-treated cells, non-migratory GBM cells form fewer FABP7 nanodomains compared to cells cultured in DHA-poor medium. To address whether reduced FABP7 nanodomain formation is the result of reduced overall FABP7 levels or redistribution of FABP7 within the cells, we examined the overall levels of FABP7 in U251, ED501N and A4-004N cells cultured for 24 hours in DHA-supplemented medium. DHA supplementation had no effect on FABP7 protein levels based on western blot analysis of whole cell lysates (**Figure S2.8A-C**), consistent with our published data in U87-FABP7 cells (Mita et al., 2010).

FABPs are lipid chaperones that not only facilitate lipid uptake but transport lipids to different sites within the cell including mitochondria, ER and nucleus (Furuhashi and Hotamisligil, 2008). We still have a poor understanding of the role of fatty acid ligands in regulating the subcellular localization of FABPs. When we used confocal microscopy to visualize U251 cells immunostained with anti-FABP7 Atto 550-conjugated primary antibody, we observed a punctate immunostaining pattern throughout the cytoplasm that was reminiscent of mitochondria staining (**Figure S2.9**). To further address the localization of FABP7 in the cytoplasm of GBM cells, we carried out co-staining analysis of U251, ED501N and A4-004N cells with Atto 550-conjugated primary anti-FABP7 antibody and MitoTracker® Deep Red followed by STED microscopy. As we were particularly interested in the possible localization of FABP7 to the mitochondria, we fixed the cells with glyoxal to maximize the preservation of mitochondria (Richter et al., 2018).

Images acquired by dual-color STED microscopy showed FABP7 co-compartmentalization with MitoTracker® Deep Red in all three GBM cell lines (**Figure 2.7**). For quantification analysis, we acquired confocal microscopy images at lower magnification using a 40×/NA1.3 oil lens in order to capture more representative pictures. FABP7 signal was quantified with masks selected by MitoTracker® Deep Red staining pattern in ImageJ (**Figure 2.8A**). We found that FABP7 intensity increased ~1.5 to 2-fold in all three DHA-supplemented GBM cell lines compared to control cells (**Figure 2.8B**). Thus, a preferred site for DHA intracellular transport by FABP7 is mitochondria.
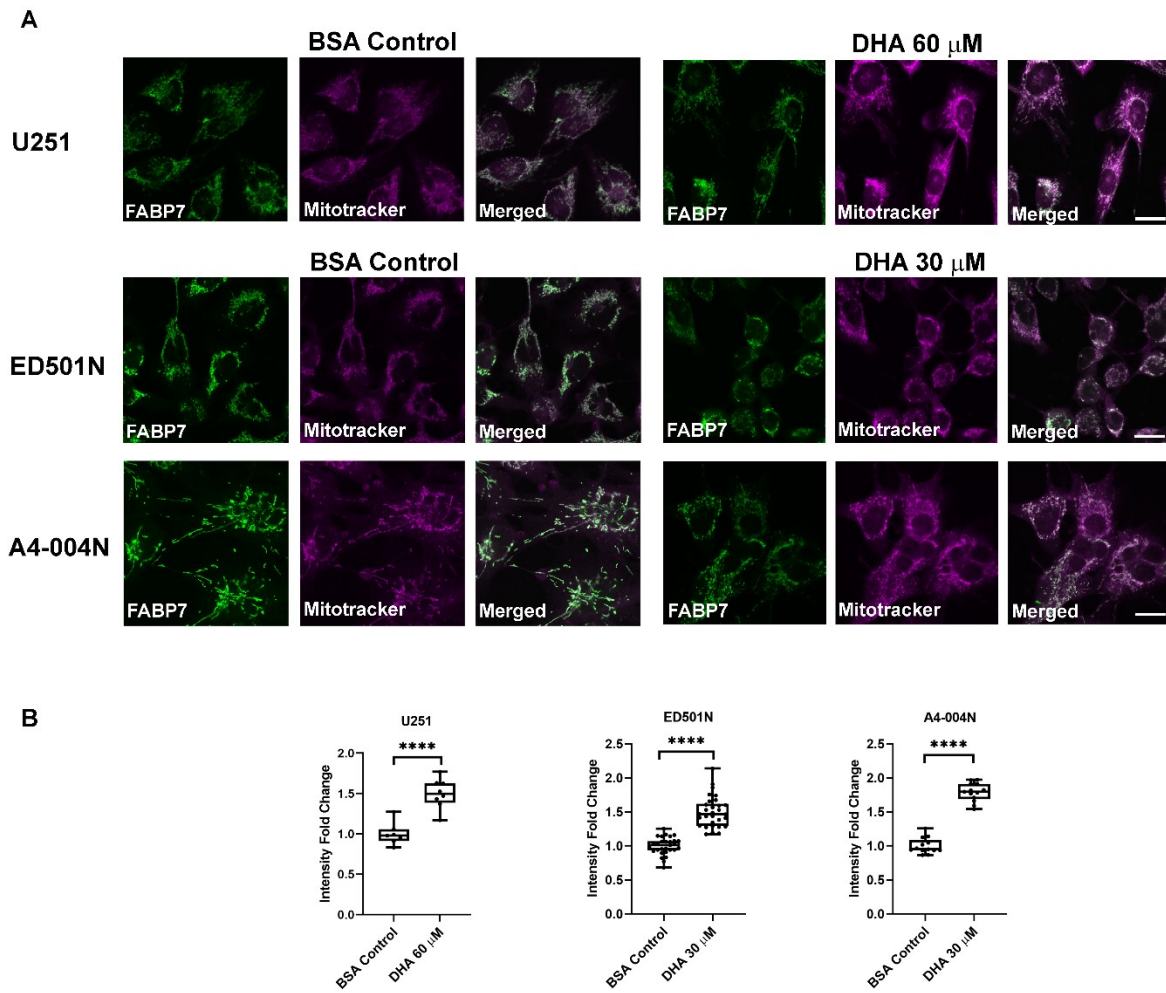
Figure 2.8 DHA supplementation relocates FABP7 to mitochondria in GBM cells.

(A) Confocal images of FABP7 and MitoTracker® Deep Red co-staining in U251, ED501N and A4-004N cells cultured under BSA Control or DHA 60 µM (U251)/30 µM (ED501N and A4-004N) supplemented conditions. Scale bars = 20 µm. (B) Quantification analysis of mitochondrial FABP7 average intensity in U251 cells, ED501N and A4-004N cells cultured under control (BSA) or DHA 60 µM (U251)/30 µM (ED501N and A4-004N) supplemented conditions. Statistical analysis was performed with two-tailed unpaired *t*-

test. Center line, median; box limits, 25th and 75th percentiles; whiskers, minimum to maximum with all points shown. **** indicates $p < 0.0001$.

2.4 Discussion

High membrane lipid order and nanoscale domain formation are tightly associated with increased cell migration and infiltrative properties in different cancer types, including GBM (Bi et al., 2019; Erazo-Oliveras et al., 2018). Plasma membrane components assemble into well-defined nanoscale domains at the leading edges of cells, with the migrating front exhibiting distinct biophysical properties (i.e., increased membrane rigidity) and cytoskeleton remodelling (Gomez-Llobregat et al., 2013), key determinants of tumor migratory/infiltrative signalling events (Erazo-Oliveras et al., 2018). FABP7 is an important marker of poor survival in GBM patients (Kaloshi et al., 2007) (Hoang-Minh et al., 2018; Liang et al., 2005) and is preferentially expressed at sites of infiltration in GBM tumors (Mita et al., 2007). FABP7 drives cell migration in GBM cells, a property that can be reversed by supplementing the culture medium with DHA (Mita et al., 2010). Previously described roles for FABP7 include cytoplasmic lipid droplet formation (Bensaad et al., 2014) and activation of nuclear receptors (Adida and Spener, 2006; Mita et al., 2010). Here, we used a combination of Laurdan assay, FABP7 manipulation and super-resolution microscopy to show that FABP7 expression is associated with increased lipid membrane order, with FABP7 forming nanodomains at the membrane protrusions of GBM cells. By examining migratory versus non-migratory cells, we observed a correlation between a highly ordered FABP7 membrane nanoscale assemblies and increased migration in GBM cells. These results were observed in both GBM cell lines and patient-derived GBM cells cultured under conditions that select for neural stem-like cells.

DHA is a very long (22 carbon chain) and flexible (6 double bonds) fatty acid (Stillwell and Wassall, 2003). Incorporation of DHA in cell membranes can dramatically affect membrane properties, with accompanying effects on membrane protein function (Fuentes et al., 2018a). As an example, dietary DHA inhibits oncogenic KRas-driven cell proliferation in vivo by rearranging KRas nanoscale domain organization (Fuentes et al., 2018b). A striking finding of our study is that DHA supplementation, specifically in FABP7-expressing GBM cells, caused remodelling of membrane lipids to a less ordered state. This membrane lipid remodelling was accompanied by a reduced density of FABP7 nanoscale domains in the plasma membrane and decreased GBM cell migration. These DHA-mediated effects were not observed when cells were cultured in either AA-supplemented or saturated fatty acid-supplemented medium. Furthermore, DHA-supplementation of non-FABP7- expressing GBM cells had no effect on either membrane lipid order or cell migration.

FABP7's preferred ligands are long chain PUFAs, with an ~4× stronger binding affinity for ω-3 PUFA DHA compared to ω-6 PUFA AA (Balendiran et al., 2000; Xu et al., 1996). DHA is generally linked to anti-tumorigenic properties (Larsson et al., 2004) whereas AA is generally linked to pro-tumorigenic properties (Azrad et al., 2013). For example, AA supplementation in vitro induces Rho-GTPase-mediated cytoskeleton remodelling and cell migration in metastatic human prostate cancer and melanoma cell (Brown et al., 2014; Garcia et al., 2009). In GBM cells, AA supplementation in vitro induces cyclooxygenase 2 and the formation of prostaglandin E2, promoting cell migration (Mita et al., 2010). The brain is a fat-rich tissue with exceptionally high levels of AA and DHA. In adult brain, DHA levels are higher than AA (Owada, 2008). GBM tissue,

on the other hand, has higher levels of AA than DHA (Martin et al., 1996). As the availability of AA in GBM tumor tissue may be greater than that of DHA, FABP7 may be primarily bound to AA in these tumors, a condition that may promote cell migration and tumor invasion. It's already known that DHA can be rapidly incorporated into phospholipid bilayers to replace saturated fatty acids and disrupt cholesterol-dependent lipid domains (Stillwell et al., 2005; Wassall and Stillwell, 2009). Thus, our results suggest that FABP7, when bound to DHA, induces membrane remodelling properties associated with inhibition of GBM cell migration.

Plasma membranes are composed of a heterogeneous mixture of lipids and proteins, which can be organized to form specific nanoscale domains (10–200 nm), facilitating cellular signaling transduction (Sezgin et al., 2017). In recent years, increased accessibility of super-resolution microscopy has helped to resolve the nanoscale organization of a number of membrane proteins, including EGFR and TrkB (Angelov and Angelova, 2017; Boyd et al., 2016). Addition of DHA to SH-SY5Y neuroblastoma culture medium caused a significant disruption of TrkB receptor nanoscale clusters on the cell surface. To the best of our knowledge, no one has studied FABP membrane nanoscale distribution to date. Compared to the traditional optical microscope, our STED super-resolution images combined with directly conjugated primary FABP7 antibodies revealed non-uniform distribution of FABP7 on the plasma membrane of GBM cells, with FABP7 localized to highly ordered irregular nanoscale domains <150 nm in diameter. These FABP7 nanoscale domains were most abundant at the basal surface of GBM cell membrane protrusions.

Our results indicate that FABP7 nanodomains have increased size/intensity/domain density and lower circularity/solidity under low-DHA/high-AA culture conditions, suggesting greater FABP7 membrane accumulation as well as coalescing of individual FABP7 nanoscale domains into larger domains, particular in more migratory GBM cells. In GBM cells cultured in DHA-supplemented medium, we observed notably reduced numbers of FABP7 membrane nanodomains as well as reduced membrane FABP7 expression (i.e., decreased intensity and size) and increased membrane FABP7 lateral segregation (i.e., increased inter-domain distance and circularity). These altered properties would likely inhibit any FABP7-dependent GBM migration events. In contrast to FABP7 nanodomains, EGFR nanodomains were not affected by DHA supplementation, indicating a specific role for FABP7 nanodomains in inhibiting cell migration when bound to DHA.

FABPs not only promote fatty acid/lipid uptake from the microenvironment, but also transport lipids to specific compartments within the cell, such as nucleus, ER and mitochondria (Furuhashi and Hotamisligil, 2008). For example, both I-FABP and L-FABP have been shown to transport their fatty acid ligands to mitochondria (Karsenty et al., 2009; Schley et al., 2007). In support of FABP7 playing a role in mitochondria, FABP7 is expressed at high levels in GBM slow-cycling cells (likely neural stem-like cells) which are characterized by increased mitochondria oxidative phosphorylation (Hoang-Minh et al., 2018). Our data indicate that, like I-FABP and L-FABP, FABP7 also co-compartmentalizes with mitochondria. Intriguingly, growth of GBM cells in DHA-supplemented medium increased the overall intensity of the FABP7 signal localizing to mitochondria. These results are surprising as DHA is not normally recognized as a

preferred substrate for fatty acid β-oxidation, although there is evidence from the literature that DHA can localize to the mitochondria. For example, fluorescent-tagged DHA (DHA-BODIPY) localizes to mitochondria in lymphoma cells (Raza Shaikh and Brown, 2013; Teague et al., 2013). One possibility is that FABP7 and its fatty acid ligands, and especially DHA, affects mitochondrial function by altering the composition of fatty acids in its membranes. Emerging data from cardiomyocytes and colon cancer cells indicate that DHA incorporates into cardiolipin (Hofmanova et al., 2017; Raza Shaikh and Brown, 2013), a mitochondrial-specific phospholipid located at the inner mitochondrial membrane which functions as a platform for anchoring and clustering mitochondrial proteins (e.g., cytochrome C) (Dudek, 2017). In some cancer cells, DHA-rich cardiolipin has been shown to alter mitochondrial membrane lipid organization, enhance oxidative stress, and trigger cytochrome-C release and apoptosis (Hofmanova et al., 2017; Ng et al., 2005).

We propose the following model to explain the role of FABP7 in GBM cell migration. When GBM cells are cultured under standard conditions or in AA-supplemented medium, FABP7 forms nanoscale domains at the plasma membrane, promoting membrane lipid order and cell migration. We postulate that FABP7 exists in a primarily unliganded state under these conditions, as liganded FABP7 has previously been shown to dissociate from biomimetic model membranes (Cheng et al., 2019; Dyszy et al., 2013). When bound to AA, FABP7 may be rapidly recycled back to the plasma membrane after releasing AA in the cytoplasm for conversion to bioactive metabolites such as prostaglandins (Mita et al., 2010) that promote GBM cell migration and tumorigenic properties (**Figure 2.9 left**). In contrast to AA, when cells are cultured in DHA-supplemented medium, FABP7 nanodomains and cell membrane lipid order are disrupted, and cell migration in inhibited.

We propose that recycling of DHA-liganded FABP7 is much slower than that of AA-liganded FABP7 because of FABP7's greater affinity for DHA (Balendiran et al., 2000; Xu et al., 1996). DHA-bound FABP7 relocates to the mitochondria (shown here) and possibly other structures in the cell such as the nucleus(Mita et al., 2010) (**Figure 2.9 right**).

In conclusion, we provide evidence that FABP7 expression has a profound effect on the biophysical properties of GBM cell membranes. FABP7's effect on GBM membranes is dependent on the relative levels of its preferred fatty acid ligands in the extracellular microenvironment. Under non-DHA-supplemented growth conditions, FABP7 increases lipid order and formation of nanoscale domains in the plasma membrane of GBM cells, processes accompanied by increased cell migration; however, lipid order, FABP7 nanodomains and cell migration are all disrupted when cells are cultured in DHA-rich medium. These results are observed in both FABP7-expressing established GBM cell lines and in patient-derived GBM neurosphere cultures. Intriguingly, membrane dissociated FABP7 accumulates at mitochondria when GBM cells are cultured in DHA-supplemented medium, suggesting a link between DHA, mitochondria and decreased cell migration. Our findings point to FABP7-dependent lipid remodelling as being a critically important determinant of cell migration in GBM. Based on our results, we postulate that increasing DHA content in the GBM microenvironment is a valid strategy for reducing GBM infiltration in brain.
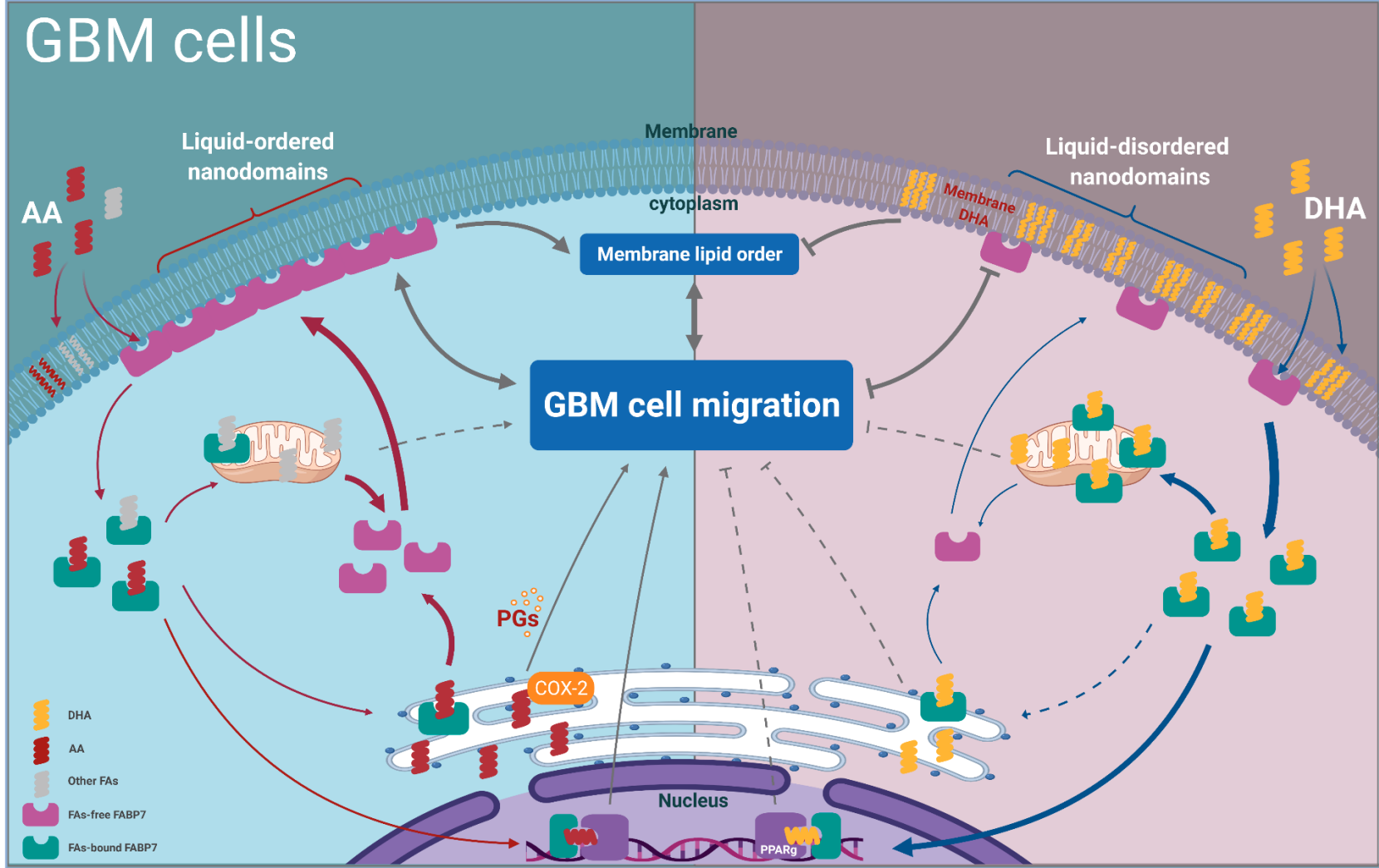
Figure 2.9 Schematic model showing the effect of DHA on GBM plasma membrane remodelling and FABP7 distribution.

(Left) Under AA-rich culture conditions, FABP7 rapidly cycles between liganded and unliganded states, releasing AA in the cytoplasm for conversion to bioactive metabolites such as prostaglandins (PGs) or fatty acid β-oxidation. Unliganded FABP7 is found in nanoscale liquid-ordered domains, promoting membrane lipid order and cell migration. (Right) Under DHA-rich culture conditions, FABP7 binds to DHA, and liganded FABP7 dissociates from the cell membrane. The high affinity of FABP7 for DHA prevents rapid release of DHA and rapid cycling of FABP7 back to the cell membrane, thereby disrupting FABP7 membrane nanoscale domains, decreasing membrane lipid order and inhibiting GBM cell migration. At least some of the DHA-liganded FABP7 locates to the mitochondria, where it may alter mitochondrial membrane properties. Although not tested here, DHA-liganded FABP7 may also relocate to the nucleus with DHA then activating nuclear factors such as PPARs.

2.5 Acknowledgements

2.6 Conflicts of interest

The authors declare no conflict of interest.

2.7 References

Adamski, V., Schmitt, A.D., Fluh, C., Synowitz, M., Hattermann, K., Held-Feindt, J., 2017. Isolation and Characterization of Fast-Migrating Human Glioma Cells in the Progression of Malignant Gliomas. Oncol Res 25, 341-353.

Adida, A., Spener, F., 2006. Adipocyte-type fatty acid-binding protein as inter-compartmental shuttle for peroxisome proliferator activated receptor gamma agonists in cultured cell. Biochim Biophys Acta 1761, 172-181.

Angelov, B., Angelova, A., 2017. Nanoscale clustering of the neurotrophin receptor TrkB revealed by super-resolution STED microscopy. Nanoscale 9, 9797-9804.

Aranda, J.F., Reglero-Real, N., Kremer, L., Marcos-Ramiro, B., Ruiz-Saenz, A., Calvo, M., Enrich, C., Correas, I., Millan, J., Alonso, M.A., 2011. MYADM regulates Rac1 targeting to ordered membranes required for cell spreading and migration. Mol Biol Cell 22, 1252-1262.

Azrad, M., Turgeon, C., Demark-Wahnefried, W., 2013. Current evidence linking polyunsaturated Fatty acids with cancer risk and progression. Front Oncol 3, 224.

Balendiran, G.K., Schnutgen, F., Scapin, G., Borchers, T., Xhong, N., Lim, K., Godbout, R., Spener, F., Sacchettini, J.C., 2000. Crystal structure and thermodynamic analysis of human brain fatty acid-binding protein. J Biol Chem 275, 27045-27054.

Bensaad, K., Favaro, E., Lewis, C.A., Peck, B., Lord, S., Collins, J.M., Pinnick, K.E., Wigfield, S., Buffa, F.M., Li, J.L., Zhang, Q., Wakelam, M.J.O., Karpe, F., Schulze, A., Harris, A.L., 2014. Fatty acid uptake and lipid storage induced by HIF-1alpha contribute to cell growth and survival after hypoxia-reoxygenation. Cell Rep 9, 349-365.

Bi, J., Ichu, T.A., Zanca, C., Yang, H., Zhang, W., Gu, Y., Chowdhry, S., Reed, A., Ikegami, S., Turner, K.M., Zhang, W., Villa, G.R., Wu, S., Quehenberger, O., Yong, W.H., Kornblum, H.I., Rich, J.N., Cloughesy, T.F., Cavenee, W.K., Furnari, F.B., Cravatt, B.F., Mischel, P.S., 2019. Oncogene Amplification in Growth Factor Signaling Pathways Renders Cancers Dependent on Membrane Lipid Remodeling. Cell Metab 30, 525-538 e528.

Bonny, M., Hui, X., Schweizer, J., Kaestner, L., Zeug, A., Kruse, K., Lipp, P., 2016. C2-domain mediated nano-cluster formation increases calcium signaling efficiency. Sci Rep 6, 36028.

Boyd, P.S., Struve, N., Bach, M., Eberle, J.P., Gote, M., Schock, F., Cremer, C., Kriegs, M., Hausmann, M., 2016. Clustered localization of EGFRvIII in glioblastoma cells as detected by high precision localization microscopy. Nanoscale 8, 20037-20047.

Brabletz, T., Jung, A., Spaderna, S., Hlubek, F., Kirchner, T., 2005. Opinion: migrating cancer stem cells - an integrated concept of malignant tumour progression. Nat Rev Cancer 5, 744-749.

Brown, M., Roulson, J.A., Hart, C.A., Tawadros, T., Clarke, N.W., 2014. Arachidonic acid induction of Rho-mediated transendothelial migration in prostate cancer. Br J Cancer 110, 2099-2108.

Brun, M., Jain, S., Monckton, E.A., Godbout, R., 2018. Nuclear Factor I Represses the Notch Effector HEY1 in Glioblastoma. Neoplasia 20, 1023-1037.

Cheng, Y.Y., Huang, Y.F., Lin, H.H., Chang, W.W., Lyu, P.C., 2019. The ligand-mediated affinity of brain-type fatty acid-binding protein for membranes determines the directionality of lipophilic cargo transport. Biochim Biophys Acta Mol Cell Biol Lipids 1864, 158506.

Chichili, G.R., Rodgers, W., 2009. Cytoskeleton-membrane interactions in membrane raft structure. Cell Mol Life Sci 66, 2319-2328.

De Rosa, A., Pellegatta, S., Rossi, M., Tunici, P., Magnoni, L., Speranza, M.C., Malusa, F., Miragliotta, V., Mori, E., Finocchiaro, G., Bakker, A., 2012. A Radial Glia Gene Marker, Fatty Acid Binding Protein 7 (FABP7), Is Involved in Proliferation and Invasion of Glioblastoma Cells. PLoS One 7, e52113.

Dudek, J., 2017. Role of Cardiolipin in Mitochondrial Signaling Pathways. Front Cell Dev Biol 5, 90.

Dyszy, F., Pinto, A.P., Araujo, A.P., Costa-Filho, A.J., 2013. Probing the interaction of brain fatty acid binding protein (B-FABP) with model membranes. PLoS One 8, e60198.

Elsherbiny, M.E., Emara, M., Godbout, R., 2013. Interaction of brain fatty acid-binding protein with the polyunsaturated fatty acid environment as a potential determinant of poor prognosis in malignant glioma. Prog Lipid Res 52, 562-570.

Erazo-Oliveras, A., Fuentes, N.R., Wright, R.C., Chapkin, R.S., 2018. Functional link between plasma membrane spatiotemporal dynamics, cancer biology, and dietary membrane-altering agents. Cancer Metastasis Rev 37, 519-544.

Feng, L., Hatten, M.E., Heintz, N., 1994. Brain lipid-binding protein (BLBP): a novel signaling system in the developing mammalian CNS. Neuron 12, 895-908.

Fuentes, N.R., Kim, E., Fan, Y.Y., Chapkin, R.S., 2018a. Omega-3 fatty acids, membrane remodeling and cancer prevention. Mol Aspects Med 64, 79-91.

Fuentes, N.R., Mlih, M., Barhoumi, R., Fan, Y.Y., Hardin, P., Steele, T.J., Behmer, S., Prior, I.A., Karpac, J., Chapkin, R.S., 2018b. Long-Chain n-3 Fatty Acids Attenuate Oncogenic KRas-Driven Proliferation by Altering Plasma Membrane Nanoscale Proteolipid Composition. Cancer Res 78, 3899-3912.

Furuhashi, M., Hotamisligil, G.S., 2008. Fatty acid-binding proteins: role in metabolic diseases and potential as drug targets. Nat Rev Drug Discov 7, 489-503.

Garcia-Parajo, M.F., Cambi, A., Torreno-Pina, J.A., Thompson, N., Jacobson, K., 2014. Nanoclustering as a dominant feature of plasma membrane organization. J Cell Sci 127, 4995-5005.

Garcia, M.C., Ray, D.M., Lackford, B., Rubino, M., Olden, K., Roberts, J.D., 2009. Arachidonic acid stimulates cell adhesion through a novel p38 MAPK-RhoA signaling pathway that involves heat shock protein 27. J Biol Chem 284, 20936-20945.

Golfetto, O., Hinde, E., Gratton, E., 2013. Laurdan fluorescence lifetime discriminates cholesterol content from changes in fluidity in living cell membranes. Biophys J 104, 1238-1247.

Gomez-Llobregat, J., Buceta, J., Reigada, R., 2013. Interplay of cytoskeletal activity and lipid phase stability in dynamic protein recruitment and clustering. Sci Rep 3, 2608.

Hoang-Minh, L.B., Siebzehnrubl, F.A., Yang, C., Suzuki-Hatano, S., Dajac, K., Loche, T., Andrews, N., Schmoll Massari, M., Patel, J., Amin, K., Vuong, A., Jimenez-Pascual, A., Kubilis, P., Garrett, T.J., Moneypenny, C., Pacak, C.A., Huang, J., Sayour, E.J., Mitchell, D.A., Sarkisian, M.R., Reynolds, B.A., Deleyrolle, L.P., 2018. Infiltrative and drug-resistant slow-cycling cells support metabolic heterogeneity in glioblastoma. EMBO J 37.

Hofmanova, J., Slavik, J., Ovesna, P., Tylichova, Z., Vondracek, J., Strakova, N., Vaculova, A.H., Ciganek, M., Kozubik, A., Knopfova, L., Smarda, J., Machala, M., 2017. Dietary fatty acids specifically modulate phospholipid pattern in colon cells with distinct differentiation capacities. Eur J Nutr 56, 1493-1508.

Kaloshi, G., Mokhtari, K., Carpentier, C., Taillibert, S., Lejeune, J., Marie, Y., Delattre, J.Y., Godbout, R., Sanson, M., 2007. FABP7 expression in glioblastomas: relation to prognosis, invasion and EGFR status. J Neurooncol 84, 245-248.

Karsenty, J., Helal, O., de la Porte, P.L., Beauclair-Deprez, P., Martin-Elyazidi, C., Planells, R., Storch, J., Gastaldi, M., 2009. I-FABP expression alters the intracellular distribution of the BODIPY C16 fatty acid analog. Mol Cell Biochem 326, 97-104.

Kurtz, A., Zimmer, A., Schnutgen, F., Bruning, G., Spener, F., Muller, T., 1994. The expression pattern of a novel gene encoding brain-fatty acid binding protein correlates with neuronal and glial cell development. Development 120, 2637-2649.

Larsson, S.C., Kumlin, M., Ingelman-Sundberg, M., Wolk, A., 2004. Dietary long-chain n-3 fatty acids for the prevention of cancer: a review of potential mechanisms. Am J Clin Nutr 79, 935-945.

Liang, C.C., Park, A.Y., Guan, J.L., 2007. In vitro scratch assay: a convenient and inexpensive method for analysis of cell migration in vitro. Nat Protoc 2, 329-333.

Liang, Y., Diehn, M., Watson, N., Bollen, A.W., Aldape, K.D., Nicholas, M.K., Lamborn, K.R., Berger, M.S., Botstein, D., Brown, P.O., Israel, M.A., 2005. Gene expression profiling reveals molecularly and clinically distinct subtypes of glioblastoma multiforme. Proc Natl Acad Sci U S A 102, 5814-5819.

Liu, R.Z., Choi, W.S., Jain, S., Dinakaran, D., Xu, X., Han, W.H., Yang, X.H., Glubrecht, D.D., Moore, R.B., Lemieux, H., Godbout, R., 2020. The FABP12/PPARgamma pathway promotes metastatic transformation by inducing epithelial-to-mesenchymal transition and lipid-derived energy production in prostate cancer cells. Mol Oncol 14, 3100-3120.

Mao, Y., 2016. Nearest Neighbor Distances Calculation with ImageJ.

Martin, D.D., Robbins, M.E., Spector, A.A., Wen, B.C., Hussey, D.H., 1996. The fatty acid composition of human gliomas differs from that found in nonmalignant brain tissue. Lipids 31, 1283-1288.

Mattila, P.K., Batista, F.D., Treanor, B., 2016. Dynamics of the actin cytoskeleton mediates receptor cross talk: An emerging concept in tuning receptor signaling. J Cell Biol 212, 267-280.

Maxwell, K.N., Zhou, Y., Hancock, J.F., 2018. Rac1 Nanoscale Organization on the Plasma Membrane Is Driven by Lipid Binding Specificity Encoded in the Membrane Anchor. Mol Cell Biol 38.

Mita, R., Beaulieu, M.J., Field, C., Godbout, R., 2010. Brain fatty acid-binding protein and omega-3/omega-6 fatty acids: mechanistic insight into malignant glioma cell migration. J Biol Chem 285, 37005-37015.

Mita, R., Coles, J.E., Glubrecht, D.D., Sung, R., Sun, X., Godbout, R., 2007. B-FABP-expressing radial glial cells: the malignant glioma cell of origin? Neoplasia 9, 734-744.

Morihiro, Y., Yasumoto, Y., Vaidyan, L.K., Sadahiro, H., Uchida, T., Inamura, A., Sharifi, K., Ideguchi, M., Nomura, S., Tokuda, N., Kashiwabara, S., Ishii, A., Ikeda, E., Owada, Y., Suzuki, M., 2013. Fatty acid binding protein 7 as a marker of glioma stem cells. Pathol Int 63, 546-553.

Nan, X., Tamguney, T.M., Collisson, E.A., Lin, L.J., Pitt, C., Galeas, J., Lewis, S., Gray, J.W., McCormick, F., Chu, S., 2015. Ras-GTP dimers activate the Mitogen-Activated Protein Kinase (MAPK) pathway. Proc Natl Acad Sci U S A 112, 7996-8001.

Ng, Y., Barhoumi, R., Tjalkens, R.B., Fan, Y.Y., Kolar, S., Wang, N., Lupton, J.R., Chapkin, R.S., 2005. The role of docosahexaenoic acid in mediating mitochondrial membrane lipid oxidation and apoptosis in colonocytes. Carcinogenesis 26, 1914-1921.

Owada, Y., 2008. Fatty acid binding protein: localization and functional significance in the brain. Tohoku J Exp Med 214, 213-220.

Owen, D.M., Rentero, C., Magenau, A., Abu-Siniyeh, A., Gaus, K., 2011. Quantitative imaging of membrane lipid order in cells and organisms. Nat Protoc 7, 24-35.

Pan, H., Wu, N., Huang, Y., Li, Q., Liu, C., Liang, M., Zhou, W., Liu, X., Wang, S., 2015. Aldehyde dehydrogenase 1 expression correlates with the invasion of breast cancer. Diagn Pathol 10, 66.

Prahl, L.S., Bangasser, P.F., Stopfer, L.E., Hemmat, M., White, F.M., Rosenfeld, S.S., Odde, D.J., 2018. Microtubule-Based Control of Motor-Clutch System Mechanics in Glioma Cell Migration. Cell Rep 25, 2591-2604 e2598.

Rahman, M., Reyner, K., Deleyrolle, L., Millette, S., Azari, H., Day, B.W., Stringer, B.W., Boyd, A.W., Johns, T.G., Blot, V., Duggal, R., Reynolds, B.A., 2015. Neurosphere and adherent culture conditions are equivalent for malignant glioma stem cell lines. Anat Cell Biol 48, 25-35.

Raza Shaikh, S., Brown, D.A., 2013. Models of plasma membrane organization can be applied to mitochondrial membranes to target human health and disease with polyunsaturated fatty acids. Prostaglandins Leukot Essent Fatty Acids 88, 21-25.

Remorino, A., De Beco, S., Cayrac, F., Di Federico, F., Cornilleau, G., Gautreau, A., Parrini, M.C., Masson, J.B., Dahan, M., Coppey, M., 2017. Gradients of Rac1 Nanoclusters Support Spatial Patterns of Rac1 Signaling. Cell Rep 21, 1922-1935.

Richter, K.N., Revelo, N.H., Seitz, K.J., Helm, M.S., Sarkar, D., Saleeb, R.S., D'Este, E., Eberle, J., Wagner, E., Vogl, C., Lazaro, D.F., Richter, F., Coy-Vergara, J., Coceano, G., Boyden, E.S., Duncan, R.R., Hell, S.W., Lauterbach, M.A., Lehnart, S.E., Moser, T., Outeiro, T.F., Rehling, P., Schwappach, B., Testa, I., Zapiec, B., Rizzoli, S.O., 2018. Glyoxal as an alternative fixative to formaldehyde in immunostaining and super-resolution microscopy. EMBO J 37, 139-159.

Saha, A., Shree Padhi, S., Roy, S., Banerjee, B., 2014. Method of detecting new cancer stem cell-like enrichment in development front assay (DFA). J Stem Cells 9, 235-242.

Schley, P.D., Brindley, D.N., Field, C.J., 2007. (n-3) PUFA alter raft lipid composition and decrease epidermal growth factor receptor levels in lipid rafts of human breast cancer cells. J Nutr 137, 548-553.

Sengupta, P., Jovanovic-Talisman, T., Skoko, D., Renz, M., Veatch, S.L., Lippincott-Schwartz, J., 2011. Probing protein heterogeneity in the plasma membrane using PALM and pair correlation analysis. Nat Methods 8, 969-975.

Sezgin, E., 2017. Super-resolution optical microscopy for studying membrane structure and dynamics. J Phys Condens Matter 29, 273001.

Sezgin, E., Levental, I., Mayor, S., Eggeling, C., 2017. The mystery of membrane organization: composition, regulation and roles of lipid rafts. Nat Rev Mol Cell Biol 18, 361-374.

Stillwell, W., Shaikh, S.R., Zerouga, M., Siddiqui, R., Wassall, S.R., 2005. Docosahexaenoic acid affects cell signaling by altering lipid rafts. Reprod Nutr Dev 45, 559-579.

Stillwell, W., Wassall, S.R., 2003. Docosahexaenoic acid: membrane properties of a unique fatty acid. Chem Phys Lipids 126, 1-27.

Teague, H., Ross, R., Harris, M., Mitchell, D.C., Shaikh, S.R., 2013. DHA-fluorescent probe is sensitive to membrane order and reveals molecular adaptation of DHA in ordered lipid microdomains. The Journal of nutritional biochemistry 24, 188-195.

van Meer, G., Voelker, D.R., Feigenson, G.W., 2008. Membrane lipids: where they are and how they behave. Nat Rev Mol Cell Biol 9, 112-124.

Vehlow, A., Cordes, N., 2013. Invasion as target for therapy of glioblastoma multiforme. Biochim Biophys Acta 1836, 236-244.

Wassall, S.R., Stillwell, W., 2009. Polyunsaturated fatty acid-cholesterol interactions: domain formation in membranes. Biochim Biophys Acta 1788, 24-32.

Wen, P.Y., Kesari, S., 2008. Malignant gliomas in adults. N Engl J Med 359, 492-507.

Xu, L.Z., Sanchez, R., Sali, A., Heintz, N., 1996. Ligand specificity of brain lipid-binding protein. J Biol Chem 271, 24711-24719.

Yang, C., Cao, M., Liu, Y., He, Y., Du, Y., Zhang, G., Gao, F., 2019. Inducible formation of leader cells driven by CD44 switching gives rise to collective invasion and metastases in luminal breast carcinomas. Oncogene 38, 7113-7132.

Yang, C., Iyer, R.R., Yu, A.C., Yong, R.L., Park, D.M., Weil, R.J., Ikejiri, B., Brady, R.O., Lonser, R.R., Zhuang, Z., 2012. beta-Catenin signaling initiates the activation of astrocytes and its dysregulation contributes to the pathogenesis of astrocytomas. Proc Natl Acad Sci U S A 109, 6963-6968.

2.8 Supplementary figures

A

B

U251

M049

T98

A172

ED501N

A4-004N

C

GBM cell lines Laurdan assay

GBM neurosphere Laurdan assay
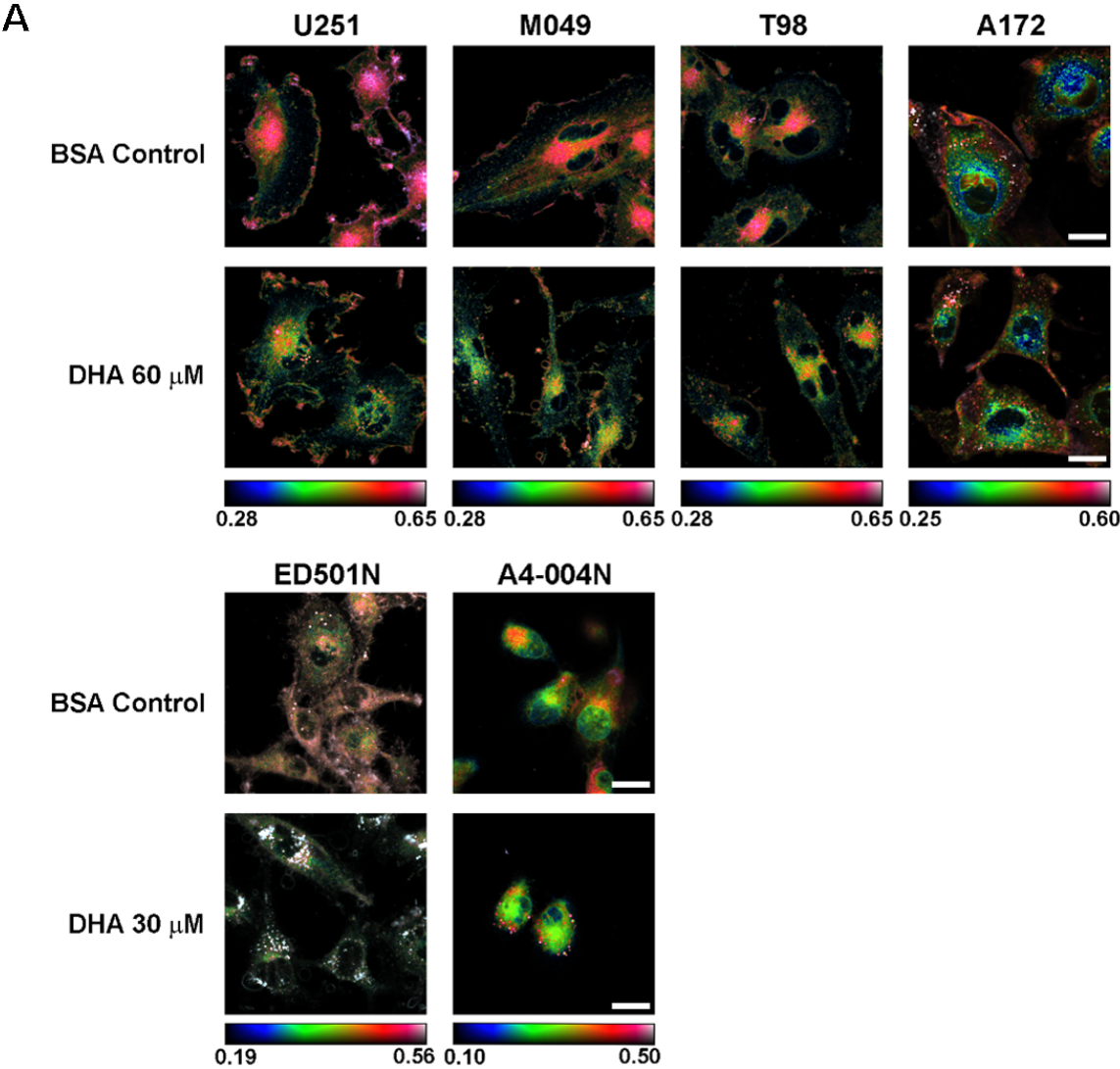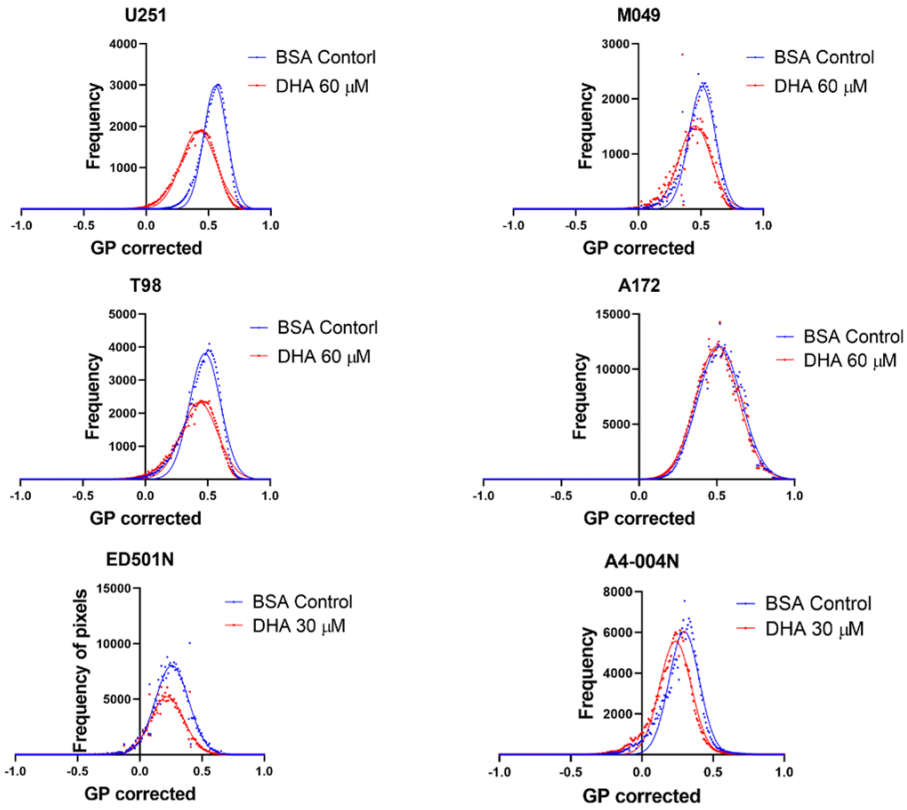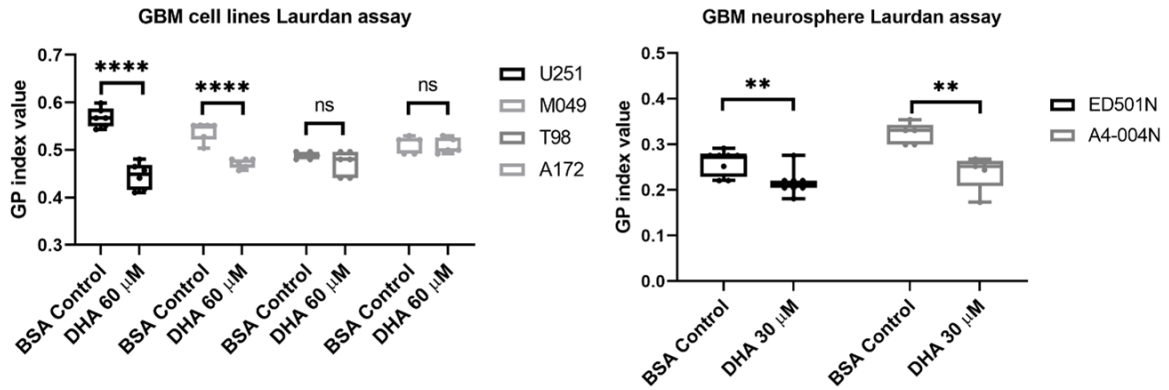
Figure S2.1 DHA decreases membrane lipid order in FABP7-expressing GBM cells.

Laurdan imaging analysis of membrane lipid order in 4 GBM cell lines (U251, M049, T98 and A172) and 2 patient-derived GBM neurosphere cultures (ED501N and A4-004N) treated with BSA (control) or 60 μM (GBM cell lines)/30 μM (GBM neurosphere cultures) DHA for 24 hours, respectively. (A) Representative merged pseudo-colored GP images are shown, with color range indicated by the color bar. Scale bars = 20 μm. (B) Histograms of FABP7-expressing GBM cells (U251, M049, ED501N and A4-004N cells) are shifted to the left (lower GP value) upon DHA treatment, whereas histograms of FABP7-negative GBM cells (T98 and A172 cells) show no shift upon DHA treatment. (C) Average GP index from several images similar to the ones shown in panel a (n=6-8). Statistical analysis was performed with multiple *t*-test the Holm-Sidak method, with alpha = 0.05. Center line, median; box limits, 25th and 75th percentiles; whiskers, minimum to maximum with all points shown. ** indicates $p < 0.01$, **** indicates $p < 0.001$, and ns indicates $p > 0.05$. GP, generalized polarization.
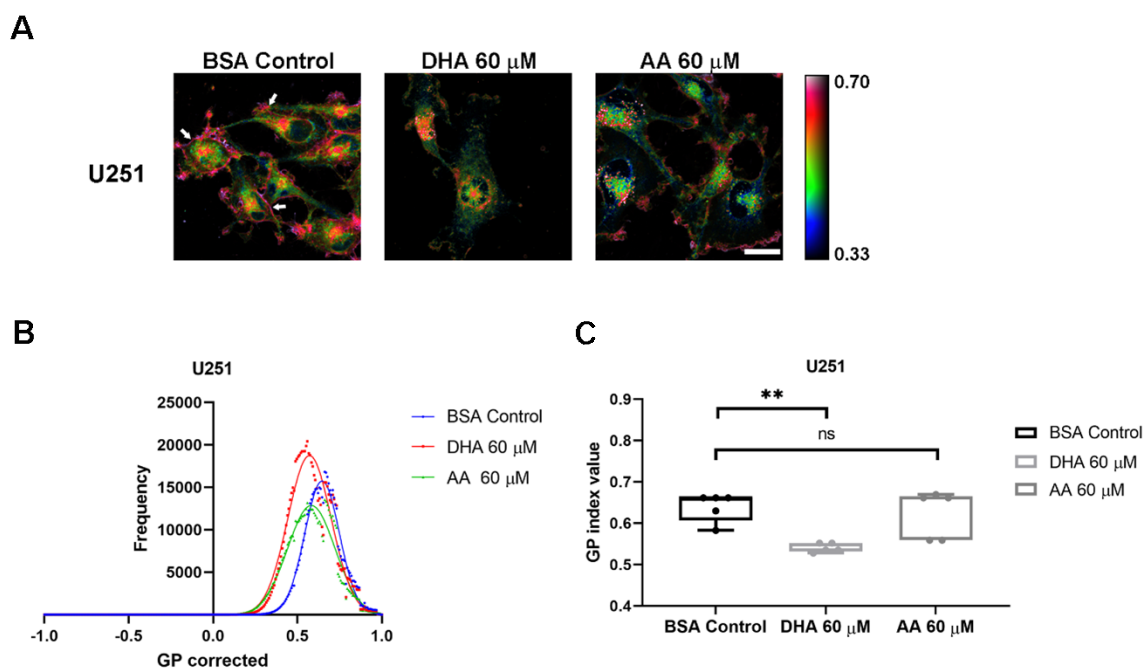
Figure S2.2 AA has no effect on membrane lipid order in GBM cells.

Laurdan imaging analysis of membrane lipid order in U251 cells cultured in BSA (control) or medium supplemented with different fatty acids (60 μM DHA/AA) for 24 hours. (A) Representative merged pseudo-colored GP images are shown, with color range indicated by the color bar. Scale bar = 20 μm. (B) Histograms of U251 cells are shifted to the left (lower GP value) in cells cultured in DHA-supplemented medium but show no shift in cells cultured in AA. (C) Average GP index from several images similar to those shown in panel A (n=5). Statistical analysis was performed with one-way ANOVA and Dunnett multiple comparisons test. Center line, median; box limits, 25th and 75th percentiles; whiskers, minimum to maximum with all points shown. ** indicates $p < 0.01$, and ns indicates $p > 0.05$. GP, generalized polarization.
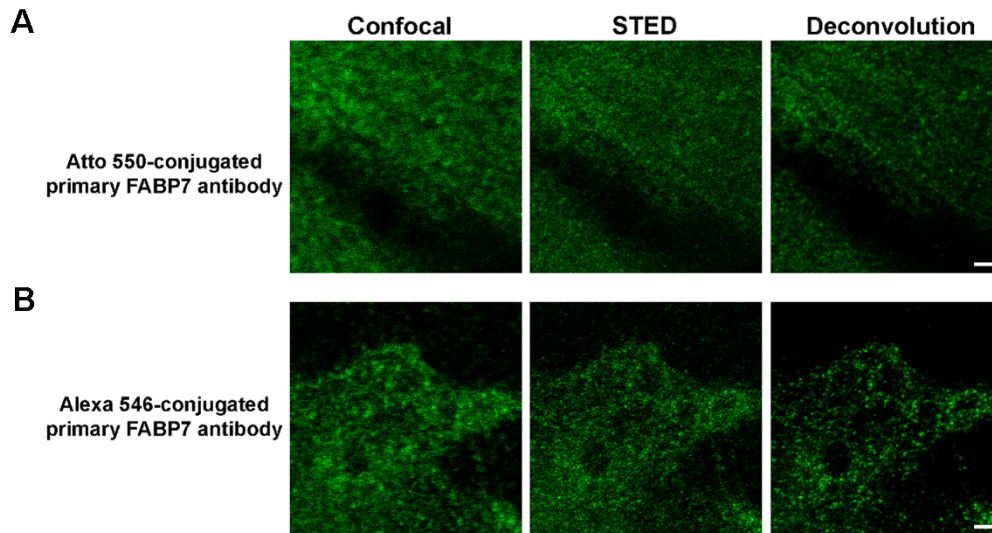
Figure S2.3 STED images reveal the distribution of FABP7 membrane nanoscale domains in GBM cells.

U251 GBM cells were labelled with either Atto 550-conjugated primary anti-FABP7 antibody (A) or Alexa 546-conjugated primary anti-FABP7 antibody (B). Images were acquired using a Leica confocal microscope, a super-resolution STED microscope and STED microscope with deconvolution (Lightning). Images are maximum intensity projections of Z-stacks. Scale bars = 1 μm.
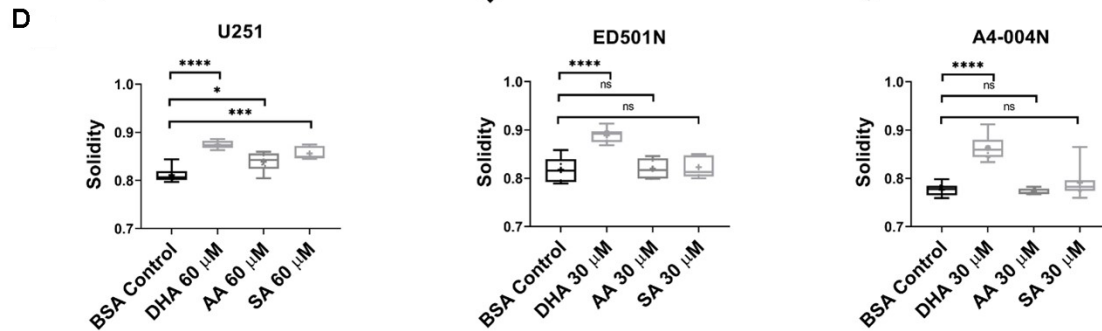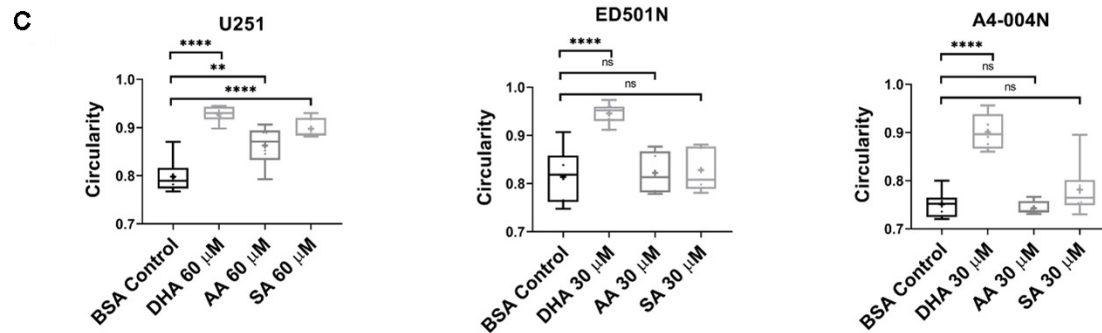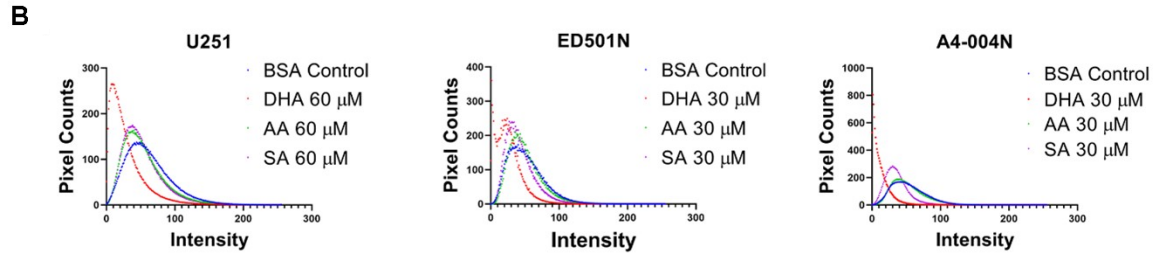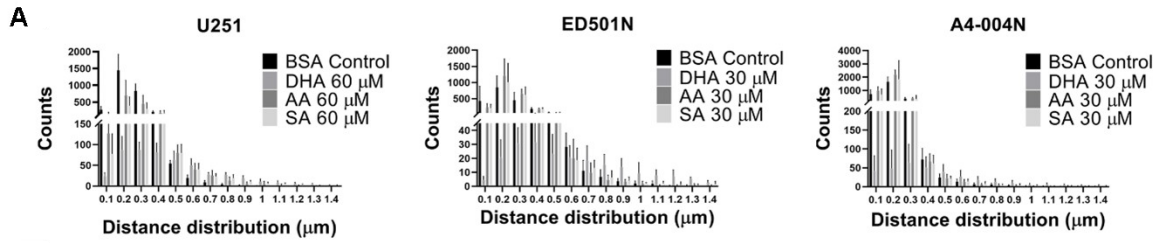
Figure S2.4 DHA disrupts FABP7 membrane nanoscale domains in GBM cells.

Nearest neighbour distance analysis (NND) was performed to determine the distance of an individual FABP7 nanoscale domain to its five nearest neighbors. (A) The NDD distribution curve is shifted to the right (increased inter-domain distance) upon DHA supplementation for all three GBM cell lines tested. Error bars represent standard deviation. (B) Quantitative intensity distribution shows that the FABP7 nanoscale domain intensity curve shifts to the left (reduced intensity counts) upon DHA treatment for all three GBM cell lines tested. Particle shape analysis shows that DHA-treated FABP7 nanoscale domains are more circular (C) and have a significantly higher solidity (D) compared to either BSA control or cells cultured in medium supplemented with AA or SA ($p < 0.0001$, n=7 for all three GBM cell lines tested). Each data point in (C) and (D) represents the average circularity or solidity value, respectively, of all the particles in one image. Statistical analysis of (C) and (D) was performed with one-way ANOVA and Dunnett multiple comparisons test. Center line, median; box limits, 25th and 75th percentiles; whiskers, min to max with all data points shown; mean values are labelled as "+". * indicates $p < 0.05$, ** indicates $p < 0.01$, *** indicates $p < 0.001$, **** indicates $p < 0.0001$, and ns indicates $p > 0.05$.
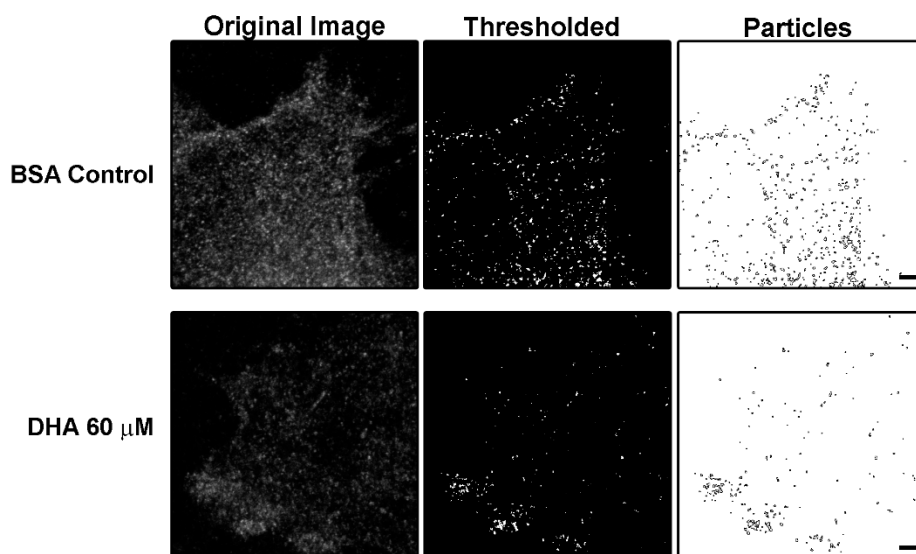
Figure S2.5 Particle analysis of U251 Cells BSA (control) and DHA-supplemented.

U251 cells were cultured in BSA (control) or medium supplemented with 60 μM DHA. Images were exported as 16-bit images to Photoshop and thresholded with threshold level 2. The thresholded images were then imported into ImageJ for particle analysis. Particles are defined as areas with more than two pixels. Scale bars = 1 μm.
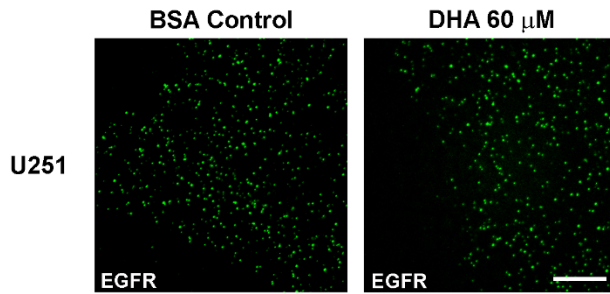
Figure S2.6 DHA treatment has no effect on EGFR membrane nanodomains distribution in U251 cells.

U251 GBM cells were immunostained with anti-EGFR antibody, then labelled with Alexa 555 secondary antibody. Images were acquired using a STED microscope with deconvolution (Lightning). Images are maximum intensity projections of Z-stacks. Scale bar = 5 μm.

A

U251, ED501N, A4-004N — Pixel Counts vs Intensity (Non-migratory / Migratory)

B

U251, ED501N, A4-004N — Counts vs Distance distribution (µm) (Non-migratory / Migratory)

C

U251, ED501N, A4-004N — Circularity (Non-migratory vs Migratory), **** , **** , ****

D

U251, ED501N, A4-004N — Solidity (Non-migratory vs Migratory), **** , *** , ****
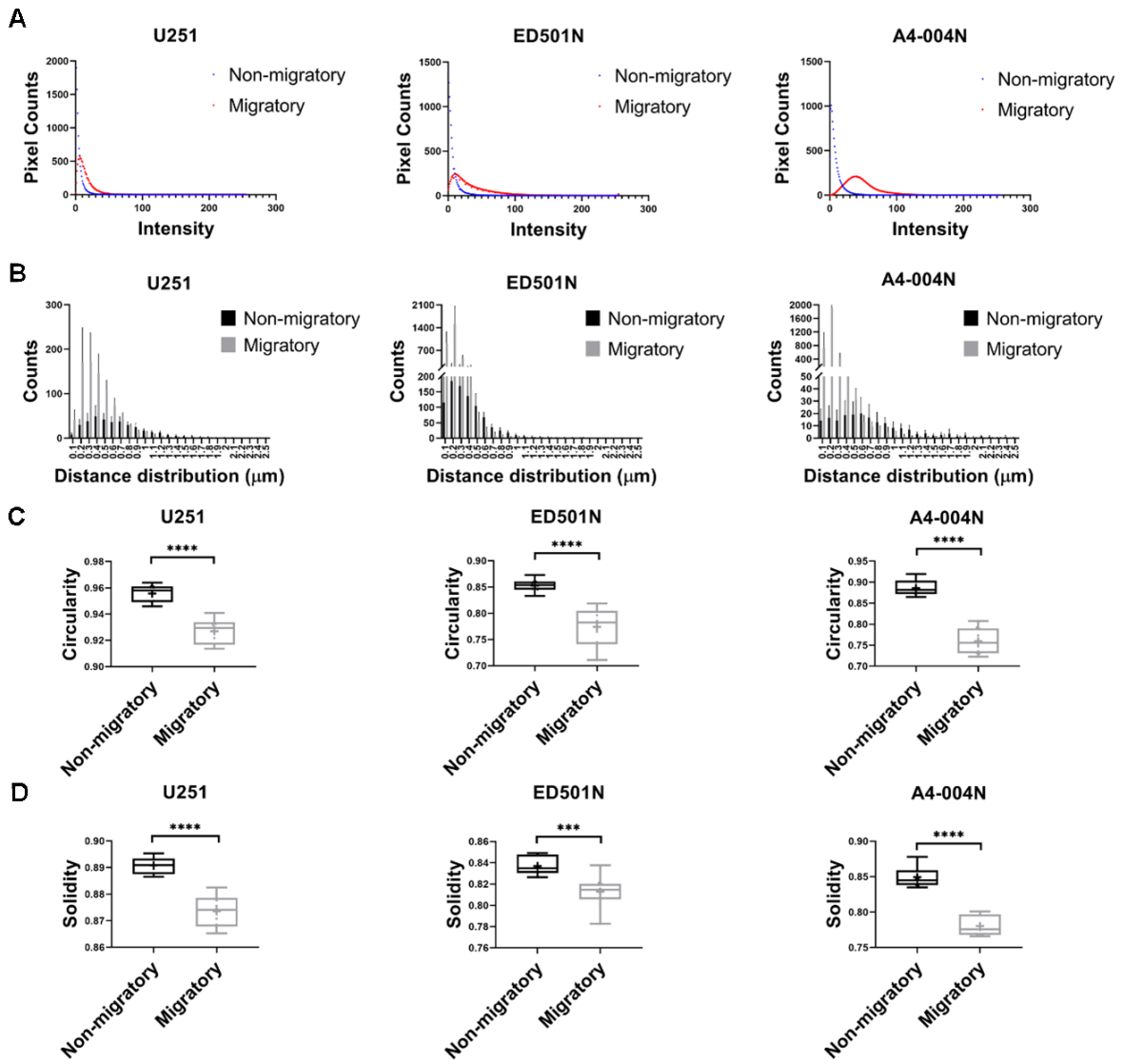
Figure S2.7 FABP7 membrane nanoscale domains are differentially distributed in migratory and non-migratory GBM cells.

(A) Quantitative intensity distribution of FABP7 nanoscale domain intensity curves show a shift to the left (reduced intensity counts) in non-migratory cells compared to migratory cells in all three GBM cell lines tested. (B) Nearest neighbour distance analysis (NND) was performed to determine the distance between individual FABP7 nanoscale domains and their five nearest neighbors. Results show that the NND distribution curves are shifted to the right (increased inter-domain distance) in non-migratory cells compared to migratory cells. Error bars represent standard deviation. Particle shape analysis shows that FABP7 nanoscale domains in migratory cells are significantly less circular (C) and have a significantly lower solidity (D) than control area cells ($p < 0.0001$, n=10) in all three GBM cell lines tested. Each data point in (C) and (D) represents the average circularity or solidity value, respectively, of all the particles in one image. Statistical analysis was performed with two-tailed unpaired t-test. Center line, median; box limits, 25th and 75th percentiles; whiskers, min to max with all data points shown; mean values are labelled as "+". *** indicates $p < 0.001$, **** indicates $p < 0.0001$.
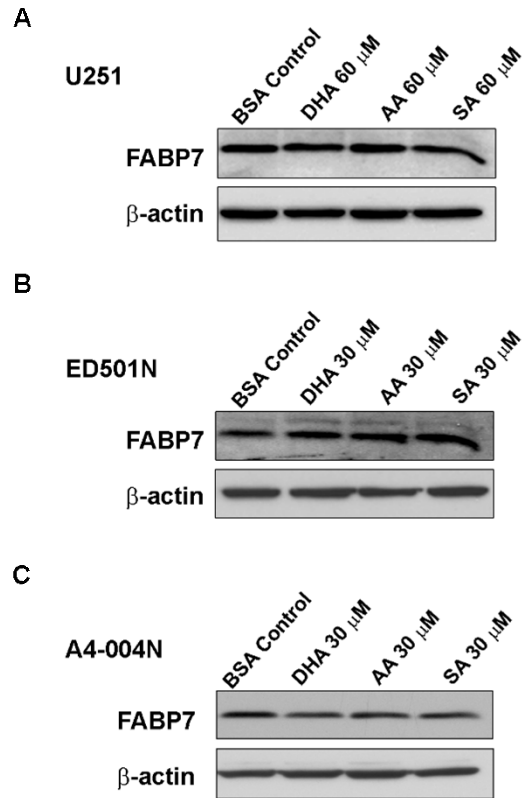
Figure S2.8 FABP7 levels in GBM cells are not altered by fatty acid supplementation.

U251 (A), ED501N (B) and A4-004N (C) were cultured in control medium (BSA), or in medium supplemented with DHA, AA or SA 60 μM (U251) or 30 μM (ED501N and A4-004N) for 24 hours.

Figure S2.9 FABP7 localizes to mitochondria in U251 cells.

U251 cells fixed with 4% PFA were co-stained with Atto 550-conjugated primary anti-FABP7 antibody and MitoTracker® Deep Red. Arrows point to mitochondria. Scale bar = 20 μm.

Chapter 3.

FABP7 Facilitates Uptake of Docosahexaenoic Acid in Glioblastoma Neural Stem-like Cells

3.1 Introduction

Glioblastoma (grade IV astrocytoma) is the most common primary brain cancer in adults (Ostrom et al., 2019; Wen and Kesari, 2008). It is a highly aggressive and deadly cancer, with a median survival time of ~15 months despite multimodality therapy (Buckner, 2003; Stupp et al., 2009). Resistance to treatment is due in part to the invasion of surrounding brain parenchyma by GBM cells, suggesting that targeting the infiltrative properties of GBM cells might be an effective therapeutic strategy (Vehlow and Cordes, 2013). In addition to their infiltrative nature, GBMs are highly heterogeneous tumors at both the cellular and molecular levels, adding an additional level of complexity to the effective targeting of these tumors (Aum et al., 2014; Bonavia et al., 2011). Multi-lineage differentiation from GBM neural stem-like cells forms the basis of GBM heterogeneity (Lathia et al., 2015; Yi et al., 2016), with GBM neural stem-like cells displaying resistance to radiation and chemotherapy, thereby repopulating the tumor (Eramo et al., 2006; Pallini et al., 2008). GBM neural stem-like cells exhibit distinct metabolic profiles compared to non-stem cell populations, with reduced glycolysis and higher lipid metabolism (Strickland and Stoll, 2017; Vlashi et al., 2011; Yasumoto et al., 2016). Dysregulation of lipid metabolism has also been associated with maintenance of GBM stemness and poor survival (Garnier et al., 2019; Strickland and Stoll, 2017). Important mediators of lipid metabolism, such as brain fatty acid binding protein (B-FABP or FABP7) (De Rosa et al., 2012), fatty acid transporter CD36 (Hale et al., 2014), acyl-CoA-binding protein (ACBP) (Duman et al., 2019), and lipid elongation enzyme ELOVL2 (Gimple et al., 2019) have all been reported to be highly expressed in GBM neural stem-like cells, highlighting the importance of lipid metabolism.

The human adult brain is highly enriched in lipids, especially long chain polyunsaturated fatty acids (PUFAs) (Bazinet and Laye, 2014; Lacombe et al., 2018). The two main types of PUFAs in the brain are ω-6 arachidonic acid (AA) and ω-3 docosahexaenoic acid (DHA) (Bazinet and Laye, 2014). DHA and AA are believed to have opposing roles in cancer (Azrad et al., 2013). AA is the precursor of ω-6 series eicosanoids such as prostaglandin E_2 (PGE_2), which stimulate inflammation, cancer growth and invasion (Qiu et al., 2017; Rand et al., 2017; Ricciotti and FitzGerald, 2011). In contrast, DHA is the precursor of neuroprotectins and resolvins, which resolve inflammation and inhibit cancer growth (Serhan and Levy, 2018; Sulciner et al., 2018; Zhang et al., 2017). In healthy adult brain, there is a tightly controlled balance between ω-6 and ω-3 PUFAs, with DHA levels exceeding AA levels in both total lipids and total phospholipids (Owada, 2008). In human GBM tumor tissue, AA levels remain similar to that of healthy brain tissue; however, DHA levels are decreased by 50%, resulting in a significantly lower DHA:AA ratio (Marszalek et al., 2010; Martin et al., 1996). DHA supplementation in GBM cells inhibits cell proliferation (Harvey et al., 2015; Leonardi et al., 2005) and migration (Mita et al., 2010; Ruan et al., 2019), and induces apoptosis (Harvey et al., 2015; Kim et al., 2018b; Ruan et al., 2019). Furthermore, DHA sensitizes GBM cells to ionizing radiation (Antal et al., 2014), suggesting that DHA supplementation may benefit GBM patients.

Brain fatty acid-binding protein (B-FABP or FABP7) is normally expressed in neural stem cells during development (Feng et al., 1994; Kurtz et al., 1994), and is also expressed in GBM stem-like cells (De Rosa et al., 2012; Morihiro et al., 2013). FABP7, whose preferred ligands are PUFAs (Balendiran et al., 2000), is preferentially found at

the infiltrative edges of GBM tumors (De Rosa et al., 2012; Mita et al., 2007) and its expression correlates with increased GBM cell migration (Liang et al., 2005). DHA treatment has previously been shown to increase DHA content in the total lipids of U87 GBM cells (Harvey et al., 2015). Furthermore, C6 glioma cells injected directly into rat brain have elevated ω-3 PUFA levels and an increased ω-3:ω-6 ratio when rats are fed a DHA-rich diet compared to control diet (Nasrollahzadeh et al., 2008). Based on our previous work, DHA inhibits GBM cell migration in a FABP7-dependent manner (Mita et al., 2010). However, these results were obtained with well-established cell lines believed to represent the more 'differentiated' aspect of GBM tumors. As resistance to treatment and poor prognosis has been linked to the neural stem-like tumor cell populations (a.k.a. brain tumor-initiating cells) in GBM tumors (Chen et al., 2012; Eramo et al., 2006; Osuka and Van Meir, 2017; Pallini et al., 2008), it is important to know whether DHA treatment will have similar effects on GBM neural stem-like cells.

Here, we examine the fatty acid composition of patient-derived GBM cells cultured in either regular medium (contains fetal calf serum and promotes a generally more differentiated phenotype) or neurosphere medium (contains B-27 supplement and growth factors and promotes a more neural stem cell-like phenotype) (Lee et al., 2006; Lenting et al., 2017). We compare the effects of DHA treatment and FABP7 expression on DHA uptake and cell migration in these two types of GBM cells. We also investigate the role of FABP7, which is highly expressed in GBM stem-like cells (Morihiro et al., 2013), in the uptake of DHA in lipids and phospholipids. Our results indicate that DHA treatment increases the DHA content in total lipids and phospholipids of GBM neural stem-like cells,

with FABP7 expression facilitating DHA uptake. We also report a correlation between increased DHA uptake and decreased cell migration in GBM neural stem-like cells.

3.2 Materials and methods

3.2.1 Primary GBM neurosphere cultures

GBM primary cultures (A4-004, A4-007, A4-011 and A4-012) were prepared by enzymatic digestion of GBM biopsies obtained from patients who were consented prior to surgery under Health Research Ethics Board of Alberta Cancer Committee approval (HREBA.CC-14-0070). GBM cells were plated in either DMEM supplemented with 10% fetal calf serum (FCS) (for the generation of adherent cultures with a more differentiated phenotype) or DMEM/F12 medium supplemented with 0.5× B-27 (Life Technologies, Carlsbad, CA, USA), 20 ng/mL epidermal growth factor (EGF), and 10 ng/mL fibroblast growth factor (FGF) (for the generation of neurosphere cultures with a neural stem cell-like phenotype). ED501 neurosphere cultures and U251 GBM cells have been previously described (Xu et al., 2021).

3.2.2 Establishment of stable FABP7-depleted cell lines

Lentivirus shRNA packaging plasmids and control plasmids were purchased from Sigma. The two lentivirus FABP7 shRNA constructs used for our experiments were obtained from the University of Alberta RNAi Core Facility. FABP7 shRNA constructs sequences and virus production have been described previously (Xu et al., 2021). The MISSION pLKO.1 plasmid (SHC002; Sigma-Aldrich, St. Louis, MO, USA) served as the control vector. A4-004N, U251 and ED501N cells were infected with lentivirus overnight and the medium changed. Infected GBM cells were selected in 1 µg/mL puromycin.

3.2.3 Western blotting

For western blot analysis, we loaded 40 μg of whole cell lysates per lane. Proteins from whole cell lysates were separated by SDS-polyacrylamide gel electrophoresis and transferred to nitrocellulose membranes. Membranes were then immunoblotted with rabbit polyclonal anti-FABP7 (prepared in-house; 1:1000) (Xu et al., 2021) and mouse anti-GAPDH (1:1000; Thermo Fisher Scientific, Waltham, MA, USA) antibodies, followed by horseradish peroxidase-conjugated secondary antibodies (1:50,000; Invitrogen, Thermo Fisher Scientific, Waltham, MA, USA) using ECL Western Detection Reagent (GE Healthcare Life Sciences, Chicago, IL, USA).

3.2.4 Fatty acid preparation and treatment

Fatty acids (DHA and AA) (Sigma-Aldrich, St. Louis, MO, USA) were dissolved in ethanol, then complexed to BSA (Roche) over a steady stream of nitrogen gas and stored at -80°C under reducing conditions. Both GBM neurosphere and GBM adherent cells were cultured at 37°C in a humidified 5% CO_2 atmosphere. For fatty acid treatment, A4-004 neurosphere and adherent cells at 60–70% confluency were cultured in medium (neurosphere medium for A4-004N and serum-free DMEM for A4-004Adh) with 30 μM BSA (vehicle control), 30 μM DHA, or 30 μM AA for 24 hours. Cells were then collected for lipid extraction and fatty acid analysis. Experiments were repeated three times.

3.2.5 Lipid extraction and gas chromatography

Total lipids were extracted with chloroform/methanol (2:1 vol/vol) using a modification of the Folch procedure (Layne et al., 1996). Thin layer chromatography on silica G plates was used to isolate total phospholipids. Samples were scraped and methylated at 110°C with a mixture (1:1) of BF_3/methanol reagent (Sigma) and hexane. Fatty acid methyl esters were separated and identified by gas liquid chromatography (Agilent Model7890A, Agilent Technologies) using a 100 m CP-Sil 88 fused capillary column (100 m ×0.25mm, Agilent Technologies, Santa Clara, CA, USA) and STD 502 (NuChek, Elysian, MN, USA) (Cruz-Hernandez et al., 2013). Fatty acids with a 14 to 24 carbon chain length were quantified and are presented as % of total fatty acids.

3.2.6 Semi-quantitative RT-PCR

RNA was purified from paired patient-derived GBM neurosphere (A4-004N, A4-007N, A4-011N and A4-012N) and adherent cells (A4-004Adh, A4-007Adh, A4-011Adh and A4-012Adh) using the RNeasy Plus Kit (Qiagen, Hilden, Germany), and cDNA was generated using Superscript II reverse transcriptase (Life Technologies). The following primers were used for semi-quantitative RT-PCR analysis: FABP7 (Forward 5'-TGGAGGCTTTCTGTGCTAC-3'; Reverse 5'-TAGGATAGCACTGAGACTTG-3'), SOX-2 (Forward 5'-ACACTGCCCCTCTCACACA-3'; Reverse 5'-CATTTTTTTCGTCGCTT-GGAG-30), Nestin (Forward 5'-GGAGAAACAGGGCCTACAG-3'; Reverse 5'-GCAGAGAGAGAGGAGCATC-3') and β-actin (Forward 5'-CTGGCACCACACCT-TCTAC-3'; Reverse 5'-CATACTCCTGCTTGCTGATC-3').

3.2.7 Lipid droplet analysis

GBM neural stem-like cells (A4-004N and ED501N) were cultured on coverslips in neurosphere medium followed by treatment with BSA (vehicle control) or 30 µM DHA for 24 hours. U251 cells were cultured in serum-free DMEM supplemented with BSA or 60 µM DHA for 24 hours. Cells were fixed with 4% paraformaldehyde for 5 min at room temperature and stained with 1 µg/mL Nile Red for 15 min. Coverslips were mounted with Mowiol 4-88 mounting medium containing DAPI and images were acquired using a Zeiss confocal microscope. ImageJ software was used for quantitative analysis. We used particle analysis to identify the number of nuclei (indicative of number of cells) in each image. The images were thresholded so that particles >20 μm^2 were identified as nuclei. The Nile Red channel was thresholded to minimize background signal and identify regions of interest (ROIs). Nile Red total intensity was calculated based on the number of pixels under each intensity (0–255) in the ROIs of each image. The average Nile Red intensity per cell was calculated based on total Nile Red intensity divided by the number of cells in each image.

3.2.8 Transwell assay

Directional cell migration was measured using the Transwell cell migration assay. Fifty thousand cells in neurosphere medium were seeded in the top chambers of 24-well cell culture Transwell inserts (Falcon Cell Culture Inserts, Corning, Glendale, AZ, USA). Cells were allowed to migrate through an 8-µm polyethylene terephthalate (PET) membrane towards a chemoattractant (DMEM + 10% fetal calf serum) in the bottom chamber for 20 hours. Fatty acids were added to culture medium for 24 hours before

132

carrying out the migration assay. Cell fixation, immunostaining and cell counts have been previously described (Brun et al., 2018). Three independent experiments were carried out for each cell line tested.

3.2.9 Statistical analysis

Assessment of the significance of differences between groups was by one-way ANOVA followed by post-hoc Tukey's test (three groups comparison) and student's unpaired t-test (two groups comparison). Microsoft Excel (Microsoft, Redmond, WA, USA) and Prism 8 (GraphPad Software, San Diego, CA, USA) were used for statistical analysis of data. A p-value < 0.05 was considered statistically significant.

3.3 Results

3.3.1 Fatty acid profiles of total lipids extracted from GBM neural stem-like versus adherent cells

GBM tumor tissues have elevated levels of proteins involved in fatty acid metabolism compared to normal brain (Saurty-Seerunghen et al., 2019). Many of these proteins (FABP7, FASN and ELOVL2) are upregulated in GBM patient-derived tumor stem cell cultures compared to more-differentiated adherent cells cultured in serum-containing medium (Gimple et al., 2019; Morihiro et al., 2013; Yasumoto et al., 2016). Expression of PUFA metabolism genes in GBM neural stem-like cells suggests that it may be possible to alter the PUFA content of these cells through manipulation of the lipid microenvironment. As our previous results indicate that an increased DHA:AA ratio inhibits GBM cell migration (Mita et al., 2010), we compared the fatty acid profiles of GBM neural stem-like cells versus GBM adherent cells, and the effect of DHA and AA supplementation on their respective fatty acid profiles.

We established GBM cultures from patients using "neurosphere" medium (promotes growth of neural stem-like cells) and "FCS-containing" medium (promotes growth of GBM cells with a more differentiated adherent phenotype) (Lee et al., 2006). We first examined the expression of FABP7, an established GBM neural stem-like cell marker (Morihiro et al., 2013), in our paired GBM cultures using semi-quantitative RT-PCR. While all eight cultures expressed FABP7, levels were generally higher in the neural stem-like cell cultures compared to adherent cultures (**Figure 3.1**). Similar trends were observed when we examined the expression of the well characterized GBM neural stem

cell markers, Nestin and SOX-2 (**Figure 3.1**). These results are consistent with a previous report showing higher expression of FABP7 in neurosphere cultures compared to adherent cultures, and correlation of FABP7 with Nestin and SOX-2 (Morihiro et al., 2013). As the biggest difference in FABP7 levels was observed in A4-004, we used A4-004N and A4-004Adh cultures for our fatty acid profiling study.

Total lipids were extracted from A4-004N and A4-004Adh cells cultured in their respective media and fatty acid composition was analysed by gas chromatography (**Table S3.1**). Differences in fatty acid composition were observed for all classes of fatty acids (saturated fatty acids (SFAs), monounsaturated fatty acids (MUFAs), and polyunsaturated ω-6 and ω-3 PUFAs)) (**Table S3.1 and Figure 3.2A**). The most prevalent ω-3 PUFA in A4-004Adh was DHA (1% of total fatty acids), while DHA was virtually undetectable in A4-004N (**Figure 3.2C**). In A4-004N, the most abundant ω-3 PUFA was C18:3ω-3 (alpha-linolenic acid (ALA)) (1.79% of total fatty acids) (**Table S3.1**). The most prevalent forms of ω-6 PUFA were C20:2ω-6 (3.25% of total fatty acids in A4-004N vs 0.95% in A4-004Adh) and C20:4ω-6 (AA) (1.01% in A4-004N vs 3.01% in A4-004Adh) (**Figure 3.2D**). The DHA:AA ratio was much lower in A4-004N compared to A4-004Adh cells (0.14 vs. 0.84), whereas the ω-3: ω-6 ratio showed no difference in A4-004N compared to A4-004Adh cells (0.42 vs. 0.41) (**Figure 3.2E**).

Next, we examined the effect of AA or DHA treatment on the fatty acid composition of A4-004N and A4-004Adh total lipids (**Table S3.2**). Cells were cultured in their respective "neurosphere" versus "adherent" media, supplemented with BSA (control), 30 μM AA or 30 μM DHA for 24 hours before they were harvested for lipid extraction. To ensure that BSA itself would not affect our results, we also compared the fatty acid

composition of A4-004N and A4-004Adh lipids in BSA (vehicle control) and untreated cells. No significant differences were noted between untreated and BSA-treated cells (**Table S3.3**).

AA treatment increased AA levels, along with its downstream mediators, adrenic acid (ADA, C22:4ω-6) and docosapentaenoic acid (DPA, C22:5ω-6) in both A4-004N and A4-004Adh cells (**Table S3.2**). The DHA:AA ratio was decreased ~7-fold and 3-fold upon AA treatment in A4-004N and A4-004Adh, respectively (**Figure 3.3C**), whereas the ω-3:ω-6 ratio was decreased ~3-fold and 2-fold upon AA treatment in A4-004N and A4-004Adh, respectively (**Figure 3.3D**).

Strikingly, DHA treatment increased DHA content by more than 100-fold (an increase from 0.1% of fatty acids to 11.2% of fatty acids) in A4-004N total lipids compared to 8-fold (1.01% to 8.09%) in A4-004Adh (**Figure 3.3A**). This increase in DHA resulted in an ~130-fold increase in the DHA:AA ratio in A4-004N (from 0.07 to 9.65) compared to ~9-fold in A4-004Adh cells (**Figure 3.3C**). The overall increase in the ω-3:ω-6 ratio was ~6-fold and ~4-fold in A4-004N and A4-004Adh DHA-treated cells, respectively (**Figure 3.3D**). These results indicate efficient uptake of both AA and DHA in neural stem cell-like cultures.
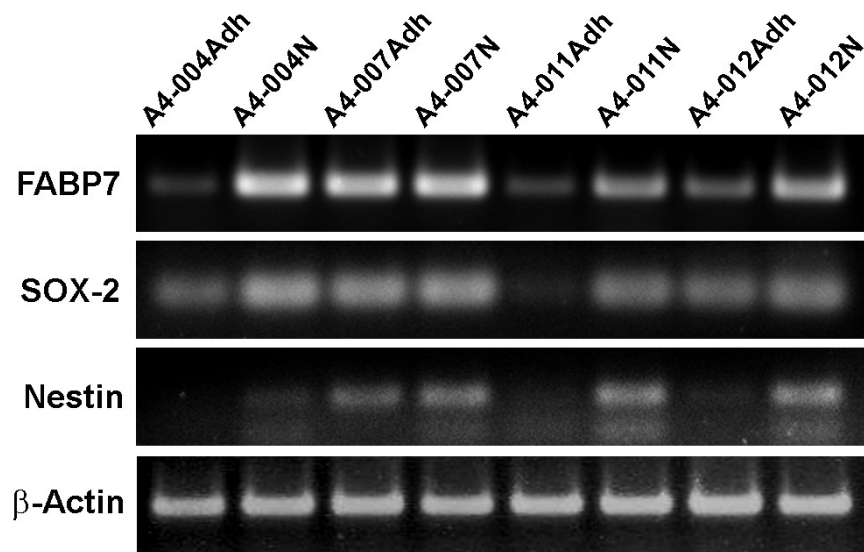
Figure 3.1 Preferential expression of FABP7 in neurosphere cultures.

Semi-quantitative RT-PCR analysis of FABP7, SOX-2, and Nestin (NES) in paired patient-derived GBM adherent and neurosphere cultures. β-Actin was used as the loading control.

3.3.2 Fatty acid profiles of phospholipids from GBM neural stem-like versus adherent cells

Phospholipids are a major component of cell membranes. PUFA supplementation affects membrane phospholipid composition and fatty acid recycling (Fuentes et al., 2018a; Lands, 1958). In turn, PUFAs in cell membranes affect their properties, including fluidity and distribution of membrane-bound proteins (Corsetto et al., 2011; Fuentes et al., 2018b; Levental et al., 2020; Xu et al., 2021). We therefore examined the fatty acid composition of phospholipids from A4-004N and A4-004Adh cells **(Table S3.4 and Figure 3.2)**. Trends similar to those observed in total lipids were seen in phospholipids, such as increased MUFAs (42.8% vs. 39.2%) and decreased PUFAs (9.9% vs. 14.4%) in A4-004N compared to A4-004Adh cells **(Table S3.4 and Figure 3.2A)**. There was less ω-6 PUFA incorporated into the phospholipids from A4-004N (7.1%) compared to A4-004Adh cells (9.9%). Similarly, less ω-3 PUFAs were incorporated in the phospholipids from A4-004N (2.9%) compared to A4-004Adh cells (4.6%) (**Figure 3.2B**). Levels of ω-3 PUFAs were similar in total lipids and phospholipids of both A4-004N and A4-004Adh cells, whereas ω-6 PUFAs were more abundant in phospholipids compared to total lipids in A4-004Adh cells, suggesting preferential incorporation of ω-6 PUFAs in membrane phospholipids of adherent cultures (**Figure 3.2B**).

Similar to that observed for total lipids, AA was the most abundant ω-6 PUFA in A4-004Adh phospholipids (3.8%), whereas C20:2ω-6 was the most abundant ω-6 PUFA in A4-004N total phospholipids (3.9%) (**Table S3.4 and Figure 3.2D**). Similar to total lipids, ALA (1.6%) was also abundant in A4-004N phospholipids (**Table S3.4**). Increased levels of DHA in both A4-004N and A4-004Adh total phospholipids (0.2% and 1.8%,

respectively) compared to total lipids (undetectable and 1%, respectively) were noted, suggesting preferential incorporation of DHA in phospholipids when cells are grown in their standard culture media (**Figure 3.2C**). Similar to total lipids, the DHA:AA ratio was lower in A4-004N compared to A4-004Adh phospholipids (0.2 vs. 0.5). The overall ω-3:ω-6 ratio in A4-004N phospholipids was similar to that observed in A4-004Adh (0.4 vs.0.5) (**Table S3.4 and Figure 3.2E**).

AA treatment resulted in ~6X and ~2X increases in the AA content of phospholipids extracted from A4-004N and A4-004Adh cells, respectively, whereas DHA treatment increased the DHA content of phospholipids by ~18X and ~3.8X in A4-004N and A4-004Adh cells, respectively (**Table S3.5**). Similar to what was observed in total lipids, AA treatment resulted in ~14-fold and ~5-fold increases in the levels of the AA downstream product, ADA, in A4-004N and A4-004Adh phospholipids, respectively. In DHA-treated cells, the DHA:AA ratio increased by ~21-fold in A4-004N phospholipids, resulting in DHA:AA ratio of 4.9 (**Figure 3.3G**). In comparison, there was a ~3.8-fold increase in the ratio of DHA:AA in the phospholipids of DHA-treated A4-004Adh cells compared to BSA control cells, resulting in a DHA:AA ratio of 1.8 (**Figure 3.3G**). The overall increase in the phospholipid ω-3:ω-6 ratio was ~3-fold and ~2-fold in A4-004N and A4-004Adh DHA-treated cells, respectively (**Figure 3.3H**). Thus, while highly significant, the incorporation of DHA into A4-004N and A4-004Adh phospholipids was not as strikingly different as that observed for total lipids, suggesting that DHA levels may be relatively more stable in phospholipids compared to total lipids in GBM cells.
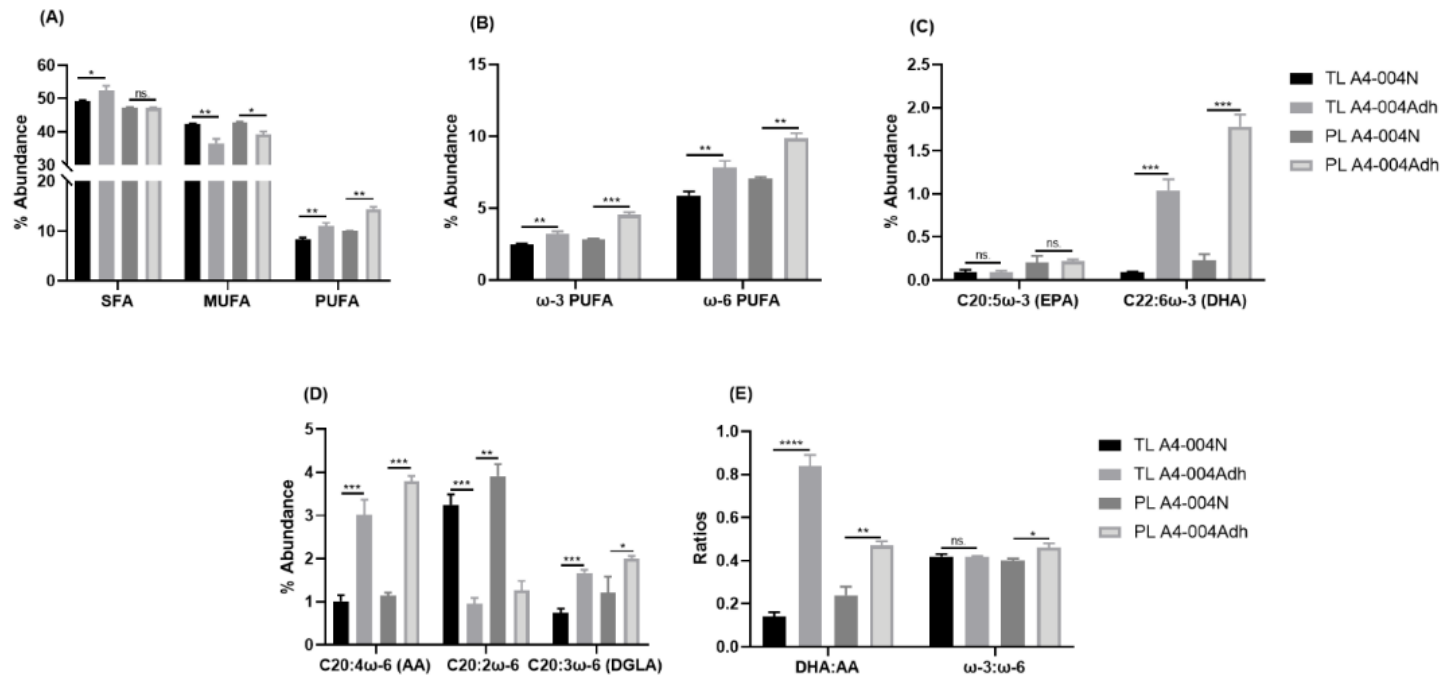
Figure 3.2 Fatty acid composition of total lipids and total phospholipids extracted from A4-004N and A4-004Adh cells.

Total lipids (TL) were extracted and total phospholipids (PL) separated from A4-004N and A4-004Adh and fatty acid composition measured by gas chromatography. (A) Percent abundance of saturated fatty acids (SFA), monounsaturated fatty acids (MUFA) and polyunsaturated fatty acids (PUFA) in total lipids and total phospholipids of A4-004N and A4-004Adh

cells. (B) Percent abundance of ω-3 PUFA and ω-6 fatty acids PUFA in total lipids and total phospholipids of A4-004N and A4-004Adh cells. (C) Percent abundance of C20:5ω-3 (EPA) and C22:6ω-3 (DHA) fatty acids in total lipids and total phospholipids of A4-004N and A4-004Adh cells. (D) Percent abundance of C20:4ω-6 (AA), C20:2ω-6 and C20:3ω-6 (DGLA) fatty acids in total lipids and total phospholipids of A4-004N and A4-004Adh cells. (E) DHA:AA ratio, and ω-3:ω-6 ratios in total lipids and total phospholipids of A4-004N and A4-004Adh cells. See **Tables S3.1** and **S3.4** for comprehensive lists of fatty acids in total lipids and phospholipids, respectively. N = 3. * indicates $p < 0.05$, ** indicates $p < 0.01$, *** indicates $p < 0.001$, and **** indicates $p < 0.0001$. Abbreviations: DHA, docosahexaenoic acid; AA, arachidonic acid.
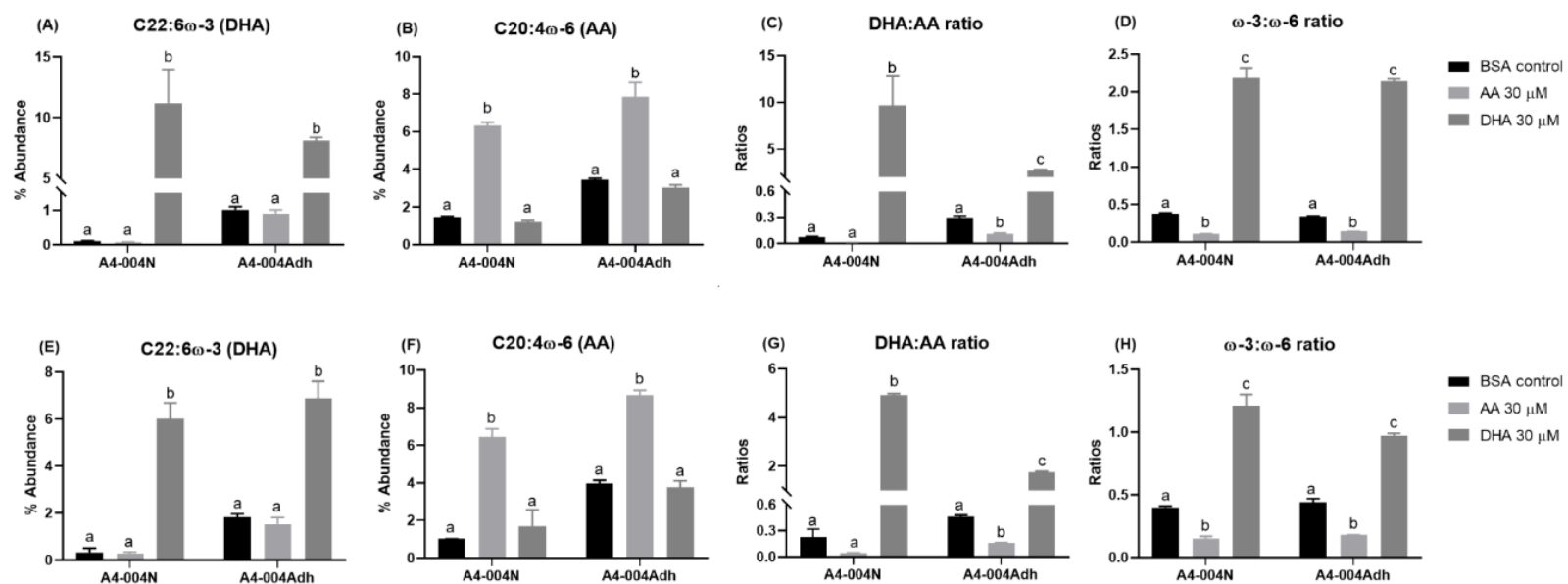
Figure 3.3 Effects of PUFA treatment on AA- and DHA-incorporation in total lipids and total phospholipids from A4-004N and A4-004Adh cells.

A4-004N and A4-004Adh culture media were supplemented with BSA (control), 30 µM AA, or 30 µM DHA. Percent abundance of DHA (A, E), percent abundance of AA (B, F), DHA:AA ratio (C, G) and ω-3:ω-6 ratio (D, H) in total lipids (A-D) and total phospholipids (E- H) of A4-004N and A4-004Adh cells. N = 3. Different letters indicate that groups are significantly different. See **Tables S3.2** and **S3.5** for comprehensive lists of fatty acids in total lipids and phospholipids, respectively.

3.3.3 FABP7 facilitates DHA uptake in GBM neural stem-like cells

FABPs play an important role in lipid-mediated biological processes through the regulation of fatty acid uptake, storage, and trafficking fatty acids to different locations in the cell (Amiri et al., 2018; Furuhashi and Hotamisligil, 2008). PUFAs, especially DHA and AA, are preferred ligands for FABP7, with ω-3 DHA having a 4-fold higher binding affinity for FABP7 compared to ω-6 AA based on Isothermal Titration Calorimetry and Lipidex 1000 (Balendiran et al., 2000; Liu et al., 2010).

To gain insight into the role of FABP7 in the uptake of ω-3 DHA or ω-6 AA in GBM neural stem-like cells, we investigated the effect of FABP7 knockdown on DHA and AA incorporation in the total lipids and phospholipids of GBM neural stem-like cells. FABP7 was knocked-down in A4-004N cells using lentiviral shRNA constructs (shFABP7-1 and shFABP7-2) (**Figure 3.4**). In A4-004N shControl cells, AA and DHA treatment increased the intracellular levels of AA and DHA, respectively, in both total lipid and total phospholipid fractions, as described earlier for non-transfected A4-004N cells (**Figure 3.5**). Upon FABP7 depletion, however, DHA uptake into total lipids was significantly reduced in DHA-treated A4-004N cells (6.4% in A4-004 shFABP7-1 cells and 6.6% A4-004N shFABP7-2 cells, compared to 12.9% in A4-004N shControl cells) (**Figure 3.5A**). Reduced DHA incorporation also resulted in a decreased DHA:AA ratio and ω-3:ω-6 ratio in total lipids of FABP7-depleted A4-004N cells compared to A4-004N shControl cells (**Figure 3.5D**). Notably, reduced DHA incorporation was not observed in total phospholipids of FABP7-depleted cells (**Figure 3.5E**), nor were the DHA:AA and ω-3:ω-6 ratios affected by FABP7 depletion (**Figure 3.5G-H**). Interestingly, even though AA is also a ligand for FABP7, FABP7 depletion had no significant effect on the uptake of AA

in either total lipids (**Figure 3.5B**) or total phospholipids (**Figure 3.5F**). In agreement with these data, neither the DHA:AA ratio nor the ω-3:ω-6 ratio was affected by FABP7 depletion in AA-treated A4-004N cells (**Figure 3.5G-H**). Our combined FABP7 results suggest the presence of a compensatory mechanism for AA uptake in GBM neural stem-like cells when FABP7 is depleted, and a specialized role for FABP7 in the uptake of DHA in total lipids of A4-004N cells.

FABPs are responsible for both the uptake and trafficking of their fatty acid ligands within cells. FABP7 has previously been shown to increase the formation of lipid droplets, an organelle responsible for lipid storage (Hoang-Minh et al., 2018; Islam et al., 2019). As our data indicate that FABP7 expression increases the uptake of DHA into total lipids, but not phospholipids, we examined whether FABP7 delivers DHA to lipid droplets. We observed increased accumulation of lipid droplets when A4-004N shControl cells were cultured in medium supplemented with 30 µM DHA (**Figure 3.6**). Intriguingly, upon FABP7 depletion, lipid droplet accumulation was significantly reduced, suggesting that DHA may be preferentially stored in lipid droplets in FABP7-expressing cells (**Figure 3.6A**). Quantitative analyses revealed a >2-fold decrease in the average intensity of Nile Red staining per cell upon FABP7 depletion in DHA-treated A4-004N cells (**Figure 3.6B**). Similar results were observed in U251 cells and ED501N cells, both of which also express FABP7 (**Figure S3.1**) (Xu et al., 2021).
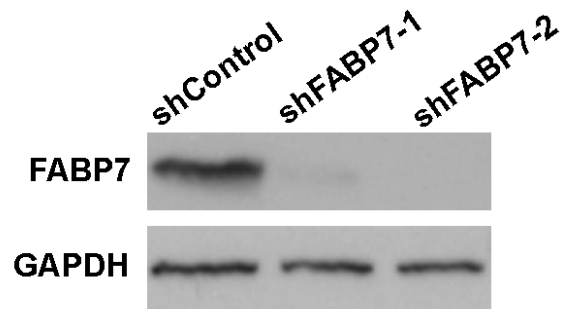
Figure 3.4 FABP7 levels in lentivirus-infected A4-004N cells.

Western blot analysis of FABP7 in total lysates prepared from A4-004N cells transfected with shControl, shFABP7-1 and FABP7-2 lentiviral constructs. GAPDH was used as the loading control.
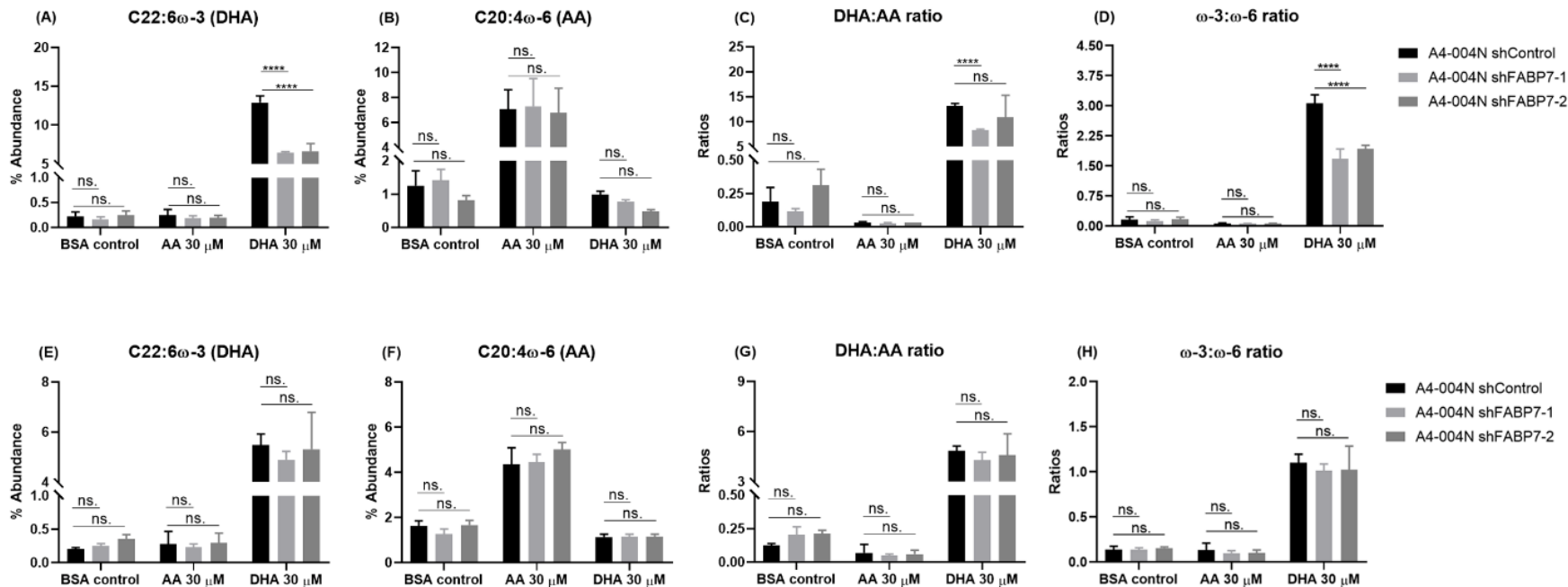
Figure 3.5 Effects of PUFA treatment on the incorporation of AA and DHA into total lipids and total phospholipids from A4-004N control and shFABP7 knockdown cells.

A4-004N shControl, shFABP7-1, and shFABP7-2 were cultured in medium supplemented with BSA (control), 30 μM AA, or 30 μM DHA. Percent abundance of DHA, AA, DHA:AA ratio and ω-3:ω-6 ratio in total lipids (A, B, C and D) and total phospholipids (E, F, G and H) of A4-004N shControl and shFABP7 cells. ** indicates $p < 0.01$, *** indicates $p < 0.001$, and **** indicates $p < 0.0001$. n.s. indicates not significant.
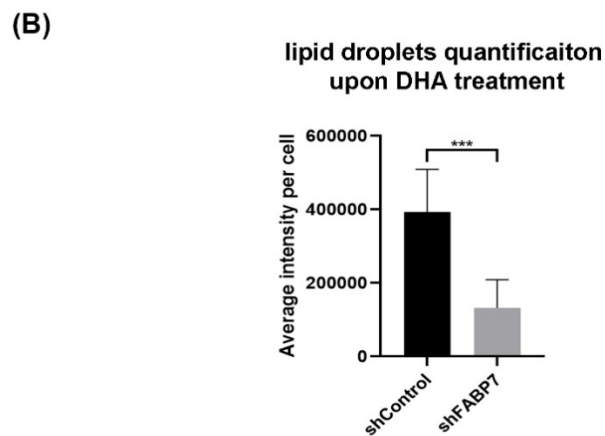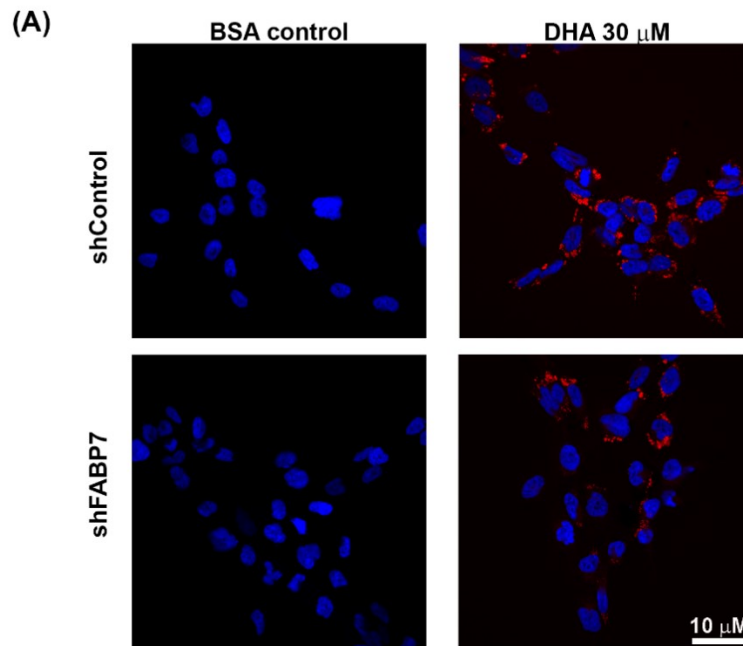
Figure 3.6 Effect of DHA treatment on lipid droplet formation in A4-004N shControl and A4-004N shFABP7 cells.

(A) A4-004N shControl and shFABP7 cells were cultured in medium supplemented with BSA control or 30 µM DHA. Cells were stained with Nile Red and images captured by confocal microscopy. DAPI was used to stain the nucleus. (B) Quantification of lipid droplets in A4-004N shControl and shFABP7 cells cultured in DHA-supplemented

medium. The average intensity of Nile Red staining per cell was measured using raw images (n = 8, 15-30 cells/image) taken by confocal microscopy. *** indicates $p < 0.001$.

3.3.4 DHA-mediated inhibition of GBM neural stem-like cell migration is dependent on FABP7 expression

We have previously reported that AA promotes, whereas DHA inhibits U87 GBM cell migration in an FABP7-dependent manner (Mita et al., 2010). We therefore used the Transwell migration assay to examine the effect of DHA and FABP7 expression on GBM neural stem-like cell migration. A4-004N shControl cells and A4-004N shFABP7 cells were cultured in neurosphere medium supplemented with 30 µM DHA or BSA control for 24 hours before carrying out the Transwell assay. As previously shown for adherent GBM cells, migration rates of FABP7-depleted A4-004N cells were significantly reduced compared to A4-004N shControl cells (**Figures 3.7A and 3.7B**). DHA treatment resulted in a >60% decrease in the migration of A4-004N shControl cells compared to BSA control ($p < 0.05$). In contrast, the migration of A4-004N shFABP7 cells was not affected by DHA treatment. Our combined results indicate that although DHA uptake is observed in both shControl and shFABP7 cells, it is only when FABP7 is present that uptake of DHA leads to the inhibition of GBM neural stem-like cell migration.

(A)

(B)
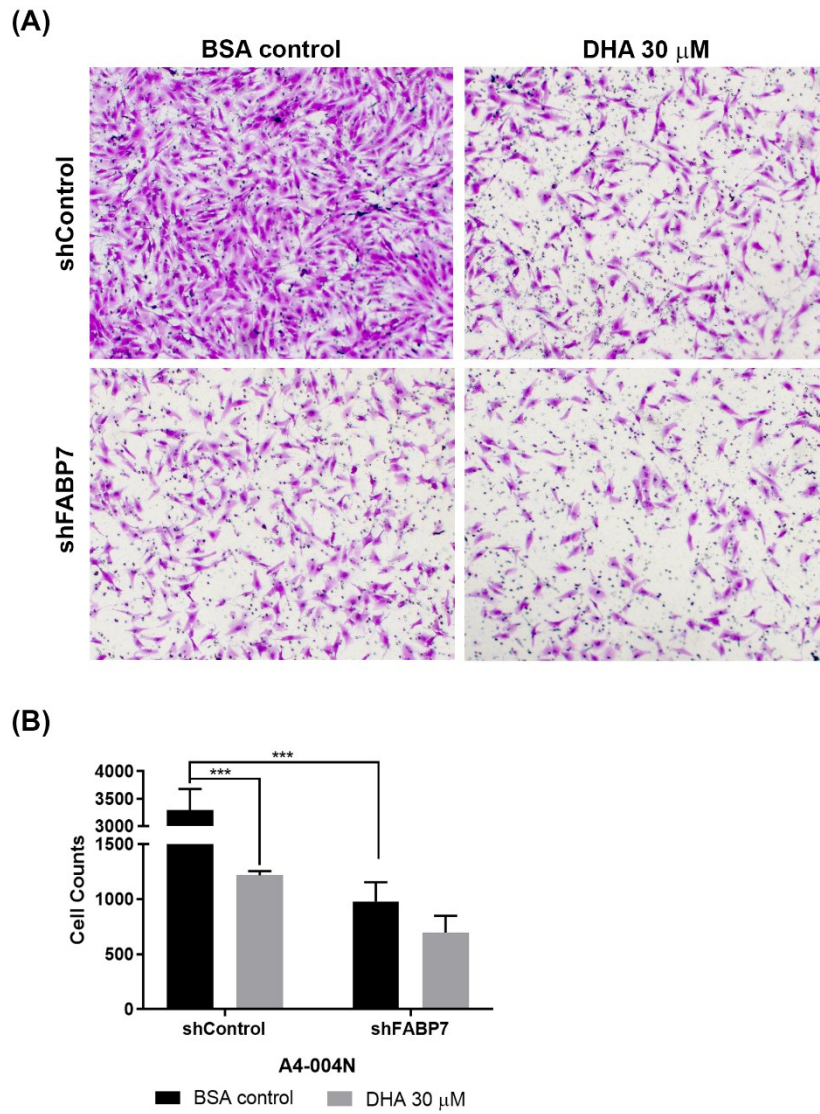
Figure 3.7 Effects of DHA treatment on the migration of A4-004N shControl and A4-004N shFABP7 cells.

(A) Representative Transwell images of A4-004N shControl and A4-004N shFABP7 cells cultured in medium supplemented with bovine serum albumin (BSA control) or 30 µM DHA. (B) Quantification of migrating cells described in (A). Differences were assessed for significance using the two-tailed unpaired *t*-test. N = 3; *** indicates $p < 0.005$.

3.4 Discussion

GBM tumors share key features with the development of the central nervous system (CNS) (Jung et al., 2019). First, GBM tumors have subpopulations of neural stem-like cells that express neural stem cell markers, such as Nestin, CD133 and FABP7. Second, migration and infiltration of GBM cells share morphologically and structurally similar features to those associated with long-distance migration during neurogenesis in developing brain. Third, the DHA:AA ratio in GBM tissue is similar to that seen in the fetal brain when neural cells are undergoing long distance migrations (Marszalek et al., 2010; Martin et al., 1996). Notably, FABP7 is essential for both the maintenance of radial glial progenitor cells (Arai et al., 2005) and neuronal cell migration during brain development (Feng et al., 1994; Kurtz et al., 1994). In standard GBM adherent cell cultures, overexpression of FABP7 increases, whereas knockdown of FABP7 decreases GBM cell migration and infiltration (De Rosa et al., 2012; Mita et al., 2007). Moreover, FABP7 is highly expressed in GBM neural stem-like cells (Morihiro et al., 2013) and its elevated levels are associated with poor clinical outcome (Hoang-Minh et al., 2018). In combination, these data suggest that FABP7 may be able to hijack the brain's normal developmental processes for the maintenance of GBM stemness and tumor infiltration in brain parenchyma.

The brain is highly enriched in long chain PUFAs, especially FABP7's preferred ligands, ω-3 DHA and ω-6 AA, which make up 8% and 6% of the dry weight of adult human brain, respectively (Elsherbiny et al., 2013; Owada, 2008). FABP7 is found in both the cytoplasm and nucleus, as well as at the plasma membrane where it is involved in the uptake of PUFAs (Mita et al., 2010; Xu et al., 2021). FABP7 plays different roles in the

cell depending on which ligand it is bound to (Elsherbiny et al., 2013; Kagawa et al., 2019; Mita et al., 2010). DHA has previously been shown to inhibit the migration of FABP7-expressing GBM cells (Mita et al., 2010; Ruan et al., 2019), as well as sensitize GBM cells to chemotherapy and radiation *in vitro* (Antal et al., 2014; Harvey et al., 2015; Manda et al., 2011; Wang et al., 2011). It is already known that dietary DHA can affect the fatty acid composition of lipids in brain tissue (diNicolantonio, 2020; Elsherbiny et al., 2015; Lauritzen et al., 2016), opening the door to the possibility that GBM patient outcome could be improved by increasing the DHA content in the tumor microenvironment.

Neural stem-like cells are key players in GBM cellular heterogeneity and therapy resistance (Osuka and Van Meir, 2017; Prager et al., 2020). Gene expression profiling has revealed significant differences between neural stem-like GBM cells cultured under neurosphere conditions and adherent GBM cells cultured in serum-containing medium, with the neural stem-like cells more closely mirroring the original tumor (Kim et al., 2018a; Lee et al., 2006; Lenting et al., 2017). Furthermore, compared to their matched serum-differentiated counterparts, GBM neurosphere cultures are enriched in enzymes involved in the PUFA synthesis cascade such as ELOVL2 and FASD2 (Gimple et al., 2019). Cyclooxygenase 2 (COX-2), which metabolizes AA to its downstream bioactive metabolites (e.g. prostaglandins), is preferentially activated in GBM neural stem-like cells compared to adherent cells (Wu et al., 2017). We have previously shown that COX-2 is upregulated in FABP7-expressing GBM cells cultured in AA-rich medium (Mita et al., 2010). Interestingly, when patient-derived GBM tumors are sorted into fast- versus slow-cycling (neural stem-like) cells, the latter not only preferentially express FABP7 but have elevated levels of PUFA metabolism intermediates (Hoang-Minh et al., 2018). Thus, there

is an emerging link between stemness, FABP7 expression and increased PUFA metabolism in GBM.

PUFA metabolism is gaining recognition as an important contributor to GBM tumorigenic properties. However, little is known about the uptake and trafficking of PUFAs in GBM neural stem-like cells. To date, the effect of DHA on GBM fatty acid composition has only been investigated using established GBM cell lines cultured under adherent (differentiation-promoting) conditions (Harvey et al., 2015). By comparing the fatty acid composition of patient-derived GBM neural stem-like cells with that of their adherent counterparts, we found that DHA treatment effectively increases the DHA content in both total lipids and total phospholipids of GBM neural stem-like cells, but especially in total lipids. Our results further indicate that FABP7 plays an important role in the efficient uptake of DHA in total lipids but not phospholipids. This preferential link between DHA, FABP7 and total lipids is particularly interesting in light of our recent finding that DHA treatment disrupts FABP7 nanodomains clustered on the surface of GBM neural stem-like cells and promotes FABP7 localization to mitochondria (Xu et al., 2021). Our previous work also shows that DHA treatment in FABP7-expressing GBM cells promotes the nuclear localization of FABP7 and induction of PPAR activity (Mita et al., 2010). Thus, FABP7's main role in DHA-supplemented GBM cells may be to facilitate the uptake, intracellular transport and utilization of DHA for functions that are unrelated or not directly related to phospholipids.

Along with the decrease in DHA uptake in total lipids observed in FABP7-depleted GBM neural stem like cells, we also found that FABP7 depletion decreased the formation of lipid droplets in GBM neural stem-like cells cultured in DHA-supplemented medium. Associations between FABP7 expression and lipid droplet formation have been

previously reported. For example, FABP7 expression is associated with elevated numbers of lipid droplets in both astrocytes and GBM cells (Hoang-Minh et al., 2018; Islam et al., 2019). Furthermore, up-regulation of FABP7 expression in U87 adherent GBM cells cultured under hypoxic conditions was accompanied by increased fatty acid uptake and increased formation of lipid droplets (Bensaad et al., 2014). Long believed to simply serve as storage sites for fats, lipid droplets are now known to be hubs that coordinate a wide range of lipid-related functions ranging from delivery of fatty acids to mitochondria, regulation of membrane dynamics, and timed release of bioactive lipids that regulate inflammation (Bozza et al., 2011; Petan et al., 2018). DHA has already been implicated in the remodeling of lipid droplets in microglia, with a demonstrated effect on the inhibition of neuro-inflammation (Tremblay et al., 2016). Based on these combined data, one may therefore postulate that FABP7 expression in GBM neural stem-like cells has the potential of inducing an anti-tumorigenic response when cells are cultured in a DHA-rich microenvironment that promotes the formation of DHA-rich lipid droplets.

Consistent with the idea that DHA has anti-tumorigenic properties in FABP7-expressing GBM neural stem-like cells, we found that DHA inhibited the migration of FABP7-expressing GBM neural stem-like cells but had negligible effects on their FABP7-depleted counterparts. These results are consistent with our previous findings using the established adherent U87 GBM cell line (Mita et al., 2010), and indicate that the migratory properties of FABP7-expressing GBM cells are dependent on the ratio of DHA:AA in the tumor microenvironment. Together, our findings suggest that infiltrative FABP7-expressing GBM neural stem-like cells will be selectively targeted by DHA treatment. Thus, while expression of FABP7 may promote GBM growth in an AA-rich tumor microenvironment, in a DHA-rich microenvironment, FABP7 may inhibit tumor infiltration

as the result of increased DHA uptake and utilization. We thus propose that FABP7 is the Achilles' heel of GBM neural stem-like cells, with the potential of inhibiting the migration/infiltration of these cells in a DHA-rich microenvironment. DHA-rich diets have already been shown to inhibit breast cancer xenograft tumor growth and metastasis (Newell et al., 2019; Yun et al., 2016), delay neuroblastoma cancer progression in immunodeficient mice (Barnes et al., 2012), as well as increase the *in vitro* and *in vivo* efficacy of chemotherapy drugs used for the treatment of colon cancer (Calviello et al., 2005; Jordan and Stein, 2003; Rani et al., 2014; Vasudevan et al., 2014). It will be important to investigate whether DHA supplementation can increase DHA levels in both the GBM microenvironment and GBM tissue, thereby paving the way to improved GBM patient outcome, by inhibiting the infiltration of FABP7-expressing GBM neural stem-like cells into brain parenchyma.

3.5 Acknowledgements

3.6 Conflicts of interest

The authors declare no conflict of interest.

3.7 References

Amiri, M., Yousefnia, S., Seyed Forootan, F., Peymani, M., Ghaedi, K., Nasr Esfahani, M.H., 2018. Diverse roles of fatty acid binding proteins (FABPs) in development and pathogenesis of cancers. Gene 676, 171-183.

Antal, O., Hackler, L., Jr., Shen, J., Man, I., Hideghety, K., Kitajka, K., Puskas, L.G., 2014. Combination of unsaturated fatty acids and ionizing radiation on human glioma cells: cellular, biochemical and gene expression analysis. Lipids Health Dis 13, 142.

Arai, Y., Funatsu, N., Numayama-Tsuruta, K., Nomura, T., Nakamura, S., Osumi, N., 2005. Role of Fabp7, a downstream gene of Pax6, in the maintenance of neuroepithelial cells during early embryonic development of the rat cortex. J Neurosci 25, 9752-9761.

Aum, D.J., Kim, D.H., Beaumont, T.L., Leuthardt, E.C., Dunn, G.P., Kim, A.H., 2014. Molecular and cellular heterogeneity: the hallmark of glioblastoma. Neurosurg Focus 37, E11.

Azrad, M., Turgeon, C., Demark-Wahnefried, W., 2013. Current evidence linking polyunsaturated Fatty acids with cancer risk and progression. Front Oncol 3, 224.

Balendiran, G.K., Schnutgen, F., Scapin, G., Borchers, T., Xhong, N., Lim, K., Godbout, R., Spener, F., Sacchettini, J.C., 2000. Crystal structure and thermodynamic analysis of human brain fatty acid-binding protein. J Biol Chem 275, 27045-27054.

Barnes, C.M., Prox, D., Christison-Lagay, E.A., Le, H.D., Short, S., Cassiola, F., Panigrahy, D., Chaponis, D., Butterfield, C., Nehra, D., Fallon, E.M., Kieran, M., Folkman, J., Puder, M., 2012. Inhibition of neuroblastoma cell proliferation with omega-3 fatty acids and treatment of a murine model of human neuroblastoma using a diet enriched with omega-3 fatty acids in combination with sunitinib. Pediatr Res 71, 168-178.

Bazinet, R.P., Laye, S., 2014. Polyunsaturated fatty acids and their metabolites in brain function and disease. Nat Rev Neurosci 15, 771-785.

Bensaad, K., Favaro, E., Lewis, C.A., Peck, B., Lord, S., Collins, J.M., Pinnick, K.E., Wigfield, S., Buffa, F.M., Li, J.L., Zhang, Q., Wakelam, M.J.O., Karpe, F., Schulze, A., Harris, A.L., 2014. Fatty acid uptake and lipid storage induced by HIF-1alpha contribute to cell growth and survival after hypoxia-reoxygenation. Cell reports 9, 349-365.

Bonavia, R., Inda, M.M., Cavenee, W.K., Furnari, F.B., 2011. Heterogeneity maintenance in glioblastoma: a social network. Cancer Res 71, 4055-4060.

Bozza, P.T., Bakker-Abreu, I., Navarro-Xavier, R.A., Bandeira-Melo, C., 2011. Lipid body function in eicosanoid synthesis: an update. Prostaglandins Leukot Essent Fatty Acids 85, 205-213.

Brun, M., Jain, S., Monckton, E.A., Godbout, R., 2018. Nuclear Factor I Represses the Notch Effector HEY1 in Glioblastoma. Neoplasia 20, 1023-1037.

Buckner, J.C., 2003. Factors influencing survival in high-grade gliomas. Semin Oncol 30, 10-14.

Calviello, G., Di Nicuolo, F., Serini, S., Piccioni, E., Boninsegna, A., Maggiano, N., Ranelletti, F.O., Palozza, P., 2005. Docosahexaenoic acid enhances the susceptibility of human colorectal cancer cells to 5-fluorouracil. Cancer Chemother Pharmacol 55, 12-20.

Chen, J., Li, Y., Yu, T.S., McKay, R.M., Burns, D.K., Kernie, S.G., Parada, L.F., 2012. A restricted cell population propagates glioblastoma growth after chemotherapy. Nature 488, 522-526.

Corsetto, P.A., Montorfano, G., Zava, S., Jovenitti, I.E., Cremona, A., Berra, B., Rizzo, A.M., 2011. Effects of n-3 PUFAs on breast cancer cells through their incorporation in plasma membrane. Lipids Health Dis 10, 73.

Cruz-Hernandez, C., Goeuriot, S., Giuffrida, F., Thakkar, S.K., Destaillats, F., 2013. Direct quantification of fatty acids in human milk by gas chromatography. J Chromatogr A 1284, 174-179.

De Rosa, A., Pellegatta, S., Rossi, M., Tunici, P., Magnoni, L., Speranza, M.C., Malusa, F., Miragliotta, V., Mori, E., Finocchiaro, G., Bakker, A., 2012. A Radial Glia Gene Marker, Fatty Acid Binding Protein 7 (FABP7), Is Involved in Proliferation and Invasion of Glioblastoma Cells. PLoS One 7, e52113.

diNicolantonio, J.J.O.K., James H., 2020. The Importance of Marine Omega-3s for Brain Development and the Prevention and Treatment of Behavior, Mood, and Other Brain Disorders. Nutrients 12, 2333.

Duman, C., Yaqubi, K., Hoffmann, A., Acikgoz, A.A., Korshunov, A., Bendszus, M., Herold-Mende, C., Liu, H.K., Alfonso, J., 2019. Acyl-CoA-Binding Protein Drives Glioblastoma Tumorigenesis by Sustaining Fatty Acid Oxidation. Cell Metab 30, 274-289 e275.

Elsherbiny, M.E., Emara, M., Godbout, R., 2013. Interaction of brain fatty acid-binding protein with the polyunsaturated fatty acid environment as a potential determinant of poor prognosis in malignant glioma. Prog Lipid Res 52, 562-570.

Elsherbiny, M.E., Goruk, S., Monckton, E.A., Richard, C., Brun, M., Emara, M., Field, C.J., Godbout, R., 2015. Long-Term Effect of Docosahexaenoic Acid Feeding on Lipid Composition and Brain Fatty Acid-Binding Protein Expression in Rats. Nutrients 7, 8802-8817.

Eramo, A., Ricci-Vitiani, L., Zeuner, A., Pallini, R., Lotti, F., Sette, G., Pilozzi, E., Larocca, L.M., Peschle, C., De Maria, R., 2006. Chemotherapy resistance of glioblastoma stem cells. Cell Death Differ 13, 1238-1241.

Feng, L., Hatten, M.E., Heintz, N., 1994. Brain lipid-binding protein (BLBP): a novel signaling system in the developing mammalian CNS. Neuron 12, 895-908.

Fuentes, N.R., Kim, E., Fan, Y.Y., Chapkin, R.S., 2018a. Omega-3 fatty acids, membrane remodeling and cancer prevention. Mol Aspects Med 64, 79-91.

Fuentes, N.R., Mlih, M., Barhoumi, R., Fan, Y.Y., Hardin, P., Steele, T.J., Behmer, S., Prior, I.A., Karpac, J., Chapkin, R.S., 2018b. Long-Chain n-3 Fatty Acids Attenuate Oncogenic KRas-Driven Proliferation by Altering Plasma Membrane Nanoscale Proteolipid Composition. Cancer Res 78, 3899-3912.

Furuhashi, M., Hotamisligil, G.S., 2008. Fatty acid-binding proteins: role in metabolic diseases and potential as drug targets. Nat Rev Drug Discov 7, 489-503.

Garnier, D., Renoult, O., Alves-Guerra, M.C., Paris, F., Pecqueur, C., 2019. Glioblastoma Stem-Like Cells, Metabolic Strategy to Kill a Challenging Target. Front Oncol 9, 118.

Gimple, R.C., Kidwell, R.L., Kim, L.J.Y., Sun, T., Gromovsky, A.D., Wu, Q., Wolf, M., Lv, D., Bhargava, S., Jiang, L., Prager, B.C., Wang, X., Ye, Q., Zhu, Z., Zhang, G., Dong, Z., Zhao, L., Lee, D., Bi, J., Sloan, A.E., Mischel, P.S., Brown, J.M., Cang, H., Huan, T., Mack, S.C., Xie, Q., Rich, J.N., 2019. Glioma Stem Cell-Specific Superenhancer Promotes Polyunsaturated Fatty-Acid Synthesis to Support EGFR Signaling. Cancer Discov 9, 1248-1267.

Hale, J.S., Otvos, B., Sinyuk, M., Alvarado, A.G., Hitomi, M., Stoltz, K., Wu, Q., Flavahan, W., Levison, B., Johansen, M.L., Schmitt, D., Neltner, J.M., Huang, P., Ren, B., Sloan, A.E., Silverstein, R.L., Gladson, C.L., DiDonato, J.A., Brown, J.M., McIntyre, T., Hazen, S.L., Horbinski, C., Rich, J.N., Lathia, J.D., 2014. Cancer stem cell-specific scavenger receptor CD36 drives glioblastoma progression. Stem Cells 32, 1746-1758.

Harvey, K.A., Xu, Z., Saaddatzadeh, M.R., Wang, H., Pollok, K., Cohen-Gadol, A.A., Siddiqui, R.A., 2015. Enhanced anticancer properties of lomustine in conjunction with docosahexaenoic acid in glioblastoma cell lines. J Neurosurg 122, 547-556.

Hoang-Minh, L.B., Siebzehnrubl, F.A., Yang, C., Suzuki-Hatano, S., Dajac, K., Loche, T., Andrews, N., Schmoll Massari, M., Patel, J., Amin, K., Vuong, A., Jimenez-Pascual, A., Kubilis, P., Garrett, T.J., Moneypenny, C., Pacak, C.A., Huang, J., Sayour, E.J., Mitchell, D.A., Sarkisian, M.R., Reynolds, B.A., Deleyrolle, L.P., 2018. Infiltrative and drug-resistant slow-cycling cells support metabolic heterogeneity in glioblastoma. EMBO J 37.

Islam, A., Kagawa, Y., Miyazaki, H., Shil, S.K., Umaru, B.A., Yasumoto, Y., Yamamoto, Y., Owada, Y., 2019. FABP7 Protects Astrocytes Against ROS Toxicity via Lipid Droplet Formation. Mol Neurobiol 56, 5763-5779.

Jordan, A., Stein, J., 2003. Effect of an omega-3 fatty acid containing lipid emulsion alone and in combination with 5-fluorouracil (5-FU) on growth of the colon cancer cell line Caco-2. Eur J Nutr 42, 324-331.

Jung, E., Alfonso, J., Osswald, M., Monyer, H., Wick, W., Winkler, F., 2019. Emerging intersections between neuroscience and glioma biology. Nat Neurosci 22, 1951-1960.

Kagawa, Y., Umaru, B.A., Ariful, I., Shil, S.K., Miyazaki, H., Yamamoto, Y., Ogata, M., Owada, Y., 2019. Role of FABP7 in tumor cell signaling. Advances in biological regulation 71, 206-218.

Kim, E.J., Jin, X., Kim, O.R., Ham, S.W., Park, S.H., Kim, H., 2018a. Glioma stem cells and their non-stem differentiated glioma cells exhibit differences in mitochondrial structure and function. Oncol Rep 39, 411-416.

Kim, S., Jing, K., Shin, S., Jeong, S., Han, S.H., Oh, H., Yoo, Y.S., Han, J., Jeon, Y.J., Heo, J.Y., Kweon, G.R., Park, S.K., Park, J.I., Wu, T., Lim, K., 2018b. omega3-polyunsaturated fatty acids induce cell death through apoptosis and autophagy in glioblastoma cells: In vitro and in vivo. Oncol Rep 39, 239-246.

Kurtz, A., Zimmer, A., Schnutgen, F., Bruning, G., Spener, F., Muller, T., 1994. The expression pattern of a novel gene encoding brain-fatty acid binding protein correlates with neuronal and glial cell development. Development 120, 2637-2649.

Lacombe, R.J.S., Chouinard-Watkins, R., Bazinet, R.P., 2018. Brain docosahexaenoic acid uptake and metabolism. Mol Aspects Med 64, 109-134.

Lands, W.E., 1958. Metabolism of glycerolipides; a comparison of lecithin and triglyceride synthesis. J Biol Chem 231, 883-888.

Lathia, J.D., Mack, S.C., Mulkearns-Hubert, E.E., Valentim, C.L., Rich, J.N., 2015. Cancer stem cells in glioblastoma. Genes Dev 29, 1203-1217.

Lauritzen, L., Brambilla, P., Mazzocchi, A., Harslof, L.B., Ciappolino, V., Agostoni, C., 2016. DHA Effects in Brain Development and Function. Nutrients 8.

Layne, K.S., Goh, Y.K., Jumpsen, J.A., Ryan, E.A., Chow, P., Clandinin, M.T., 1996. Normal subjects consuming physiological levels of 18:3(n-3) and 20:5(n-3) from flaxseed or fish oils have characteristic differences in plasma lipid and lipoprotein fatty acid levels. J Nutr 126, 2130-2140.

Lee, J., Kotliarova, S., Kotliarov, Y., Li, A., Su, Q., Donin, N.M., Pastorino, S., Purow, B.W., Christopher, N., Zhang, W., Park, J.K., Fine, H.A., 2006. Tumor stem cells derived from glioblastomas cultured in bFGF and EGF more closely mirror the phenotype and genotype of primary tumors than do serum-cultured cell lines. Cancer Cell 9, 391-403.

Lenting, K., Verhaak, R., Ter Laan, M., Wesseling, P., Leenders, W., 2017. Glioma: experimental models and reality. Acta Neuropathol 133, 263-282.

Leonardi, F., Attorri, L., Di Benedetto, R., Di Biase, A., Sanchez, M., Nardini, M., Salvati, S., 2005. Effect of arachidonic, eicosapentaenoic and docosahexaenoic acids on the oxidative status of C6 glioma cells. Free radical research 39, 865-874.

Levental, K.R., Malmberg, E., Symons, J.L., Fan, Y.Y., Chapkin, R.S., Ernst, R., Levental, I., 2020. Lipidomic and biophysical homeostasis of mammalian membranes counteracts dietary lipid perturbations to maintain cellular fitness. Nat Commun 11, 1339.

Liang, Y., Diehn, M., Watson, N., Bollen, A.W., Aldape, K.D., Nicholas, M.K., Lamborn, K.R., Berger, M.S., Botstein, D., Brown, P.O., Israel, M.A., 2005. Gene expression profiling reveals molecularly and clinically distinct subtypes of glioblastoma multiforme. Proc Natl Acad Sci U S A 102, 5814-5819.

Liu, R.Z., Mita, R., Beaulieu, M., Gao, Z., Godbout, R., 2010. Fatty acid binding proteins in brain development and disease. The International journal of developmental biology 54, 1229-1239.

Manda, K., Kriesen, S., Hildebrandt, G., Fietkau, R., Klautke, G., 2011. Omega-3 fatty acid supplementation in cancer therapy : does eicosapentanoic acid influence the radiosensitivity of tumor cells? Strahlenther Onkol 187, 127-134.

Marszalek, R., Pisklak, M., Jankowski, W., Lukaszkiewicz, J., Horsztynski, D., Wawer, I., 2010. NMR and gas chromatography studies of lyophilized human brain tumors. Acta Pol Pharm 67, 129-136.

Martin, D.D., Robbins, M.E., Spector, A.A., Wen, B.C., Hussey, D.H., 1996. The fatty acid composition of human gliomas differs from that found in nonmalignant brain tissue. Lipids 31, 1283-1288.

Mita, R., Beaulieu, M.J., Field, C., Godbout, R., 2010. Brain fatty acid-binding protein and omega-3/omega-6 fatty acids: mechanistic insight into malignant glioma cell migration. J Biol Chem 285, 37005-37015.

Mita, R., Coles, J.E., Glubrecht, D.D., Sung, R., Sun, X., Godbout, R., 2007. B-FABP-expressing radial glial cells: the malignant glioma cell of origin? Neoplasia 9, 734-744.

Morihiro, Y., Yasumoto, Y., Vaidyan, L.K., Sadahiro, H., Uchida, T., Inamura, A., Sharifi, K., Ideguchi, M., Nomura, S., Tokuda, N., Kashiwabara, S., Ishii, A., Ikeda, E., Owada, Y., Suzuki, M., 2013. Fatty acid binding protein 7 as a marker of glioma stem cells. Pathol Int 63, 546-553.

Nasrollahzadeh, J., Siassi, F., Doosti, M., Eshraghian, M.R., Shokri, F., Modarressi, M.H., Mohammadi-Asl, J., Abdi, K., Nikmanesh, A., Karimian, S.M., 2008. The influence of feeding linoleic, gamma-linolenic and docosahexaenoic acid rich oils on rat brain tumor fatty acids composition and fatty acid binding protein 7 mRNA expression. Lipids Health Dis 7, 45.

Newell, M., Goruk, S., Mazurak, V., Postovit, L., Field, C.J., 2019. Role of docosahexaenoic acid in enhancement of docetaxel action in patient-derived breast cancer xenografts. Breast Cancer Res Treat 177, 357-367.

Ostrom, Q.T., Cioffi, G., Gittleman, H., Patil, N., Waite, K., Kruchko, C., Barnholtz-Sloan, J.S., 2019. CBTRUS Statistical Report: Primary Brain and Other Central Nervous System Tumors Diagnosed in the United States in 2012-2016. Neuro Oncol 21, v1-v100.

Osuka, S., Van Meir, E.G., 2017. Overcoming therapeutic resistance in glioblastoma: the way forward. J Clin Invest 127, 415-426.

Owada, Y., 2008. Fatty acid binding protein: localization and functional significance in the brain. Tohoku J Exp Med 214, 213-220.

Pallini, R., Ricci-Vitiani, L., Banna, G.L., Signore, M., Lombardi, D., Todaro, M., Stassi, G., Martini, M., Maira, G., Larocca, L.M., De Maria, R., 2008. Cancer stem cell analysis

and clinical outcome in patients with glioblastoma multiforme. Clin Cancer Res 14, 8205-8212.

Petan, T., Jarc, E., Jusovic, M., 2018. Lipid Droplets in Cancer: Guardians of Fat in a Stressful World. Molecules 23.

Prager, B.C., Bhargava, S., Mahadev, V., Hubert, C.G., Rich, J.N., 2020. Glioblastoma Stem Cells: Driving Resilience through Chaos. Trends Cancer 6, 223-235.

Qiu, J., Shi, Z., Jiang, J., 2017. Cyclooxygenase-2 in glioblastoma multiforme. Drug Discov Today 22, 148-156.

Rand, A.A., Barnych, B., Morisseau, C., Cajka, T., Lee, K.S.S., Panigrahy, D., Hammock, B.D., 2017. Cyclooxygenase-derived proangiogenic metabolites of epoxyeicosatrienoic acids. Proc Natl Acad Sci U S A 114, 4370-4375.

Rani, I., Vaiphei, K., Agnihotri, N., 2014. Supplementation of fish oil augments efficacy and attenuates toxicity of 5-fluorouracil in 1,2-dimethylhydrazine dihydrochloride/dextran sulfate sodium-induced colon carcinogenesis. Cancer Chemother Pharmacol 74, 309-322.

Ricciotti, E., FitzGerald, G.A., 2011. Prostaglandins and inflammation. Arterioscler Thromb Vasc Biol 31, 986-1000.

Ruan, M., Liu, J., Ren, X., Li, C., Zhao, A.Z., Li, L., Yang, H., Dai, Y., Wang, Y., 2019. Whole transcriptome sequencing analyses of DHA treated glioblastoma cells. J Neurol Sci 396, 247-253.

Saurty-Seerunghen, M.S., Bellenger, L., El-Habr, E.A., Delaunay, V., Garnier, D., Chneiweiss, H., Antoniewski, C., Morvan-Dubois, G., Junier, M.P., 2019. Capture at the single cell level of metabolic modules distinguishing aggressive and indolent glioblastoma cells. Acta Neuropathol Commun 7, 155.

Serhan, C.N., Levy, B.D., 2018. Resolvins in inflammation: emergence of the pro-resolving superfamily of mediators. J Clin Invest 128, 2657-2669.

Strickland, M., Stoll, E.A., 2017. Metabolic Reprogramming in Glioma. Front Cell Dev Biol 5, 43.

Stupp, R., Hegi, M.E., Mason, W.P., van den Bent, M.J., Taphoorn, M.J., Janzer, R.C., Ludwin, S.K., Allgeier, A., Fisher, B., Belanger, K., Hau, P., Brandes, A.A., Gijtenbeek, J., Marosi, C., Vecht, C.J., Mokhtari, K., Wesseling, P., Villa, S., Eisenhauer, E., Gorlia, T., Weller, M., Lacombe, D., Cairncross, J.G., Mirimanoff, R.O., European Organisation for, R., Treatment of Cancer Brain, T., Radiation Oncology, G., National Cancer Institute of Canada Clinical Trials, G., 2009. Effects of radiotherapy with concomitant and adjuvant temozolomide versus radiotherapy alone on survival in glioblastoma in a randomised phase III study: 5-year analysis of the EORTC-NCIC trial. Lancet Oncol 10, 459-466.

Sulciner, M.L., Serhan, C.N., Gilligan, M.M., Mudge, D.K., Chang, J., Gartung, A., Lehner, K.A., Bielenberg, D.R., Schmidt, B., Dalli, J., Greene, E.R., Gus-Brautbar, Y., Piwowarski, J., Mammoto, T., Zurakowski, D., Perretti, M., Sukhatme, V.P., Kaipainen, A., Kieran,

M.W., Huang, S., Panigrahy, D., 2018. Resolvins suppress tumor growth and enhance cancer therapy. J Exp Med 215, 115-140.

Tremblay, M.E., Zhang, I., Bisht, K., Savage, J.C., Lecours, C., Parent, M., Titorenko, V., Maysinger, D., 2016. Remodeling of lipid bodies by docosahexaenoic acid in activated microglial cells. J Neuroinflammation 13, 116.

Vasudevan, A., Yu, Y., Banerjee, S., Woods, J., Farhana, L., Rajendra, S.G., Patel, A., Dyson, G., Levi, E., Maddipati, K.R., Majumdar, A.P., Nangia-Makker, P., 2014. Omega-3 fatty acid is a potential preventive agent for recurrent colon cancer. Cancer Prev Res (Phila) 7, 1138-1148.

Vehlow, A., Cordes, N., 2013. Invasion as target for therapy of glioblastoma multiforme. Biochim Biophys Acta 1836, 236-244.

Vlashi, E., Lagadec, C., Vergnes, L., Matsutani, T., Masui, K., Poulou, M., Popescu, R., Della Donna, L., Evers, P., Dekmezian, C., Reue, K., Christofk, H., Mischel, P.S., Pajonk, F., 2011. Metabolic state of glioma stem cells and nontumorigenic cells. Proc Natl Acad Sci U S A 108, 16062-16067.

Wang, F., Bhat, K., Doucette, M., Zhou, S., Gu, Y., Law, B., Liu, X., Wong, E.T., Kang, J.X., Hsieh, T.C., Qian, S.Y., Wu, E., 2011. Docosahexaenoic acid (DHA) sensitizes brain tumor cells to etoposide-induced apoptosis. Curr Mol Med 11, 503-511.

Wen, P.Y., Kesari, S., 2008. Malignant gliomas in adults. N Engl J Med 359, 492-507.

Wu, M., Guan, J., Li, C., Gunter, S., Nusrat, L., Ng, S., Dhand, K., Morshead, C., Kim, A., Das, S., 2017. Aberrantly activated Cox-2 and Wnt signaling interact to maintain cancer stem cells in glioblastoma. Oncotarget 8, 82217-82230.

Xu, X., Wang, Y., Choi, W.S., Sun, X., Godbout, R., 2021. Super resolution microscopy reveals DHA-dependent alterations in glioblastoma membrane remodelling and cell migration. Nanoscale 13, 9706-9722.

Yasumoto, Y., Miyazaki, H., Vaidyan, L.K., Kagawa, Y., Ebrahimi, M., Yamamoto, Y., Ogata, M., Katsuyama, Y., Sadahiro, H., Suzuki, M., Owada, Y., 2016. Inhibition of Fatty Acid Synthase Decreases Expression of Stemness Markers in Glioma Stem Cells. PLoS One 11, e0147717.

Yi, Y., Hsieh, I.Y., Huang, X., Li, J., Zhao, W., 2016. Glioblastoma Stem-Like Cells: Characteristics, Microenvironment, and Therapy. Front Pharmacol 7, 477.

Yun, E.J., Song, K.S., Shin, S., Kim, S., Heo, J.Y., Kweon, G.R., Wu, T., Park, J.I., Lim, K., 2016. Docosahexaenoic acid suppresses breast cancer cell metastasis by targeting matrix-metalloproteinases. Oncotarget 7, 49961-49971.

Zhang, Q., Zhu, B., Li, Y., 2017. Resolution of Cancer-Promoting Inflammation: A New Approach for Anticancer Therapy. Front Immunol 8, 71.

3.8 Supplementary figures
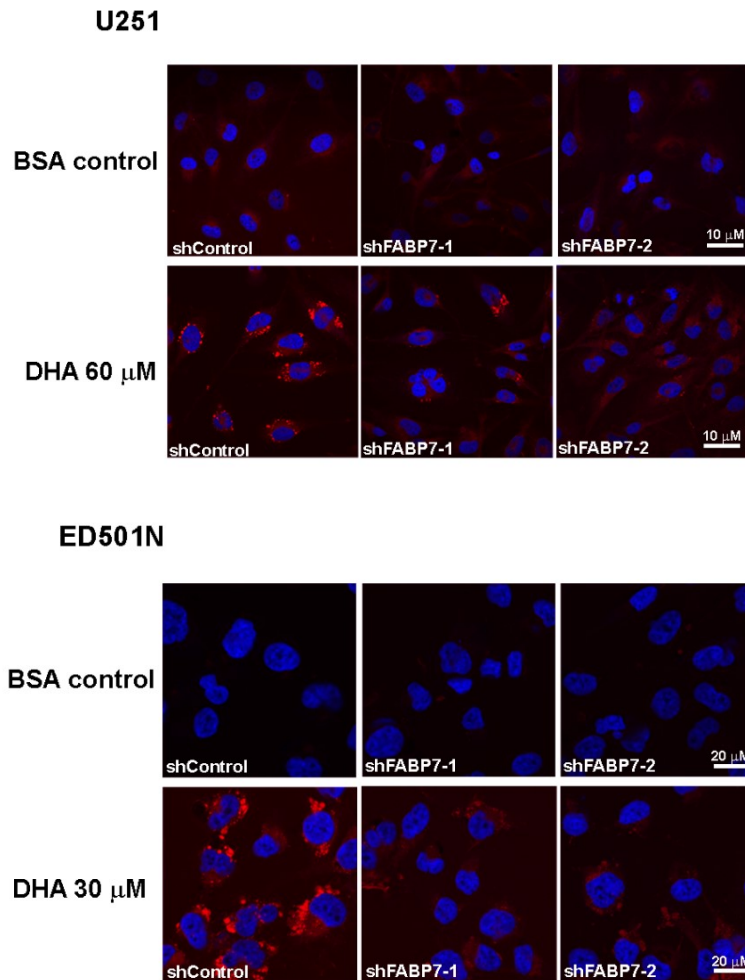
U251

ED501N

Figure S3.1 Effect of DHA treatment and FABP7-knockdown on lipid droplet formation in U251 and ED501N cells.

Stable knockdown of FABP7 in U251 GBM adherent cells and ED501 GBM neural stem-like cells was confirmed as previously described [49]. Cells were cultured in medium supplemented with BSA (control), 60 µM DHA (U251 cells), or 30 µM DHA (ED501N cells). After 24 hours, cells were fixed and stained with Nile Red. Representative confocal images are shown. DAPI was used to stain the nucleus.

Table S3.1 Fatty acid composition of total lipids extracted from A4-004N and A4-004Adh cells.

Fatty Acids	A4-004N (N = 3)		A4-004Adh (N = 3)		
	% Abundance of fatty acids in total lipids				
	Mean	±SD	Mean	±SD	p-value
C14:0	2.14	±0.10	1.71	±0.07	$p = 0.53$
C15:0	0.13	±0.02	0.52	±0.03	$p = 0.0001$
C16:0 (PA)	25.75	±0.59	29.22	±1.08	$p = 0.008$
C17:0	0.89	±0.06	0.67	±0.06	$p = 0.01$
C18:0 (SA)	15.74	±0.11	17.87	±1.15	$p = 0.03$
C20:0	0.21	±0.04	0.39	±0.07	$p = 0.01$
C24:0	4.37	±0.40	0.63	±0.13	$p = 0.0001$
Total SFA	49.24	±0.27	52.39	±1.48	$p = 0.02$
C16:1ω-9	7.88	±0.16	6.14	±0.50	$p = 0.004$
C18:1ω-9 (OA)	27.45	±0.48	21.94	±0.66	$p = 0.0003$
C18:1ω-7	5.65	±0.09	7.37	±0.25	$p = 0.0004$
C24:1ω-9	1.42	±0.51	1.15	±0.17	$p = 0.44$
Total MUFA	42.40	±0.09	36.59	±1.26	$p = 0.001$
C18:2ω-6 (LA)	0.18	±0.03	0.72	±0.09	$p = 0.0005$
C20:2ω-6	3.25	±0.24	0.95	±0.14	$p = 0.0001$
C20:3ω-6 (DGLA)	0.74	±0.10	1.67	±0.07	$p = 0.0002$
C20:4ω-6 (AA)	1.01	±0.14	3.01	±0.36	$p = 0.0008$
C22:4ω-6 (ADA)	0.60	±0.01	1.24	±0.13	$p = 0.001$
C22:5ω-6 (ω-6 DPA)	0.10	±0.03	0.22	±0.03	$p = 0.006$
Total ω-6	5.88	±0.29	7.82	±0.47	$p = 0.004$
C18:3ω-3 (ALA)	1.79	±0.09	0.95	±0.08	$p = 0.0003$
C20:4ω-3	0.06	±0.02	0.16	±0.01	$p = 0.001$
C20:5ω-3 (EPA)	0.09	±0.03	0.09	±0.02	$p = 0.88$
C22:5ω-3 (ω-3 DPA)	0.47	±0.04	0.96	±0.11	$p = 0.002$
C22:6ω-3 (DHA)	0.09	±0.01	1.04	±0.13	$p = 0.0002$
Total ω-3	2.49	±0.05	3.20	±0.19	$p = 0.003$
Total PUFA	8.36	±0.34	11.02	±0.65	$p = 0.003$
C22:6ω-3:C20:4ω-6	0.14	±0.02	0.84	±0.05	$p < 0.0001$
ω-3 PUFA:ω-6 PUFA	0.42	±0.01	0.41	±0.00	$p = 0.13$

Data are presented as mean ± standard deviation (SD). p-value of <0.05 was considered statistically significant.

Table S3.2 Fatty acid composition of total lipids extracted from A4-004N and A4-004Adh cells cultured in media supplemented with BSA (control), 30 µM AA or 30 µM DHA.

Fatty Acids	A4-004N							A4-004Adh						
	BSA Control (N = 3)		AA 30 µM (N = 3)		DHA 30 µM (N = 3)			BSA Control (N = 3)		AA 30 µM (N = 3)		DHA 30 µM (N = 3)		
	% Abundance of fatty acids in total lipids													
	Average	±SD	Average	±SD	Average	±SD	ANOVA	Average	±SD	Average	±SD	Average	±SD	ANOVA
C14:0	2.21a	±0.08	2.65b	±0.05	2.18a	±0.03	$p = 0.0001$	1.89a	±0.02	1.73ab	±0.07	1.68b	±0.11	$p = 0.036$
C15:0	0.16	±0.02	0.14	±0.02	0.12	±0.03	$p = 0.14$	0.55a	±0.01	0.48b	±0.02	0.50b	±0.02	$p = 0.0066$
C16:0 (PA)	25.54a	±0.24	25.53a	±0.40	24.23b	±0.42	$p = 0.0065$	29.38a	±0.46	30.52b	±0.36	29.61ab	±0.41	$p = 0.033$
C17:0	0.81a	±0.06	0.83a	±0.04	0.55b	±0.07	$p = 0.0012$	0.60	±0.12	0.64	±0.04	0.70	±0.04	$p = 0.38$
C18:0 (SA)	16.39a	±0.46	17.74b	±0.48	17.47ab	±0.54	$p = 0.034$	17.30a	±0.40	18.45b	±0.07	17.91ab	±0.29	$p = 0.027$
C20:0	0.29	±0.05	0.24	±0.03	0.24	±0.03	$p = 0.17$	0.36a	±0.03	0.29b	±0.02	0.29b	±0.01	$p = 0.014$
C24:0	3.91a	±0.44	2.52b	±0.29	2.72b	±0.06	$p = 0.0082$	0.77a	±0.03	0.34b	±0.06	0.39b	±0.06	$p = 0.0001$
Total SFA	49.30	±0.71	49.65	±0.45	47.79	±1.27	$p = 0.10$	50.85	±0.98	52.22	±0.22	51.08	±0.73	$p = 0.23$
C16:1ω-9	7.43a	±0.14	5.75b	±0.05	5.46b	±0.49	$p = 0.0004$	5.76a	±0.25	3.74b	±0.19	4.10b	±0.23	$p < 0.0001$
C18:1ω-9 (OA)	27.27a	±0.37	20.67b	±0.24	23.39c	±0.52	$p < 0.0001$	22.31a	±0.47	15.64b	±0.54	18.70c	±0.56	$p < 0.0001$
C18:1ω-7	5.85a	±0.03	4.33b	±0.13	3.98b	±0.41	$p = 0.0002$	7.25a	±0.16	5.81b	±0.13	5.76b	±0.19	$p < 0.0001$
C24:1ω-9	1.25	±0.16	0.98	±0.10	0.95	±0.13	$p = 0.058$	1.47a	±0.05	0.78b	±0.22	1.05b	±0.02	$p = 0.0018$
Total MUFA	41.80a	±0.62	31.73b	±0.46	34.22c	±0.73	$p < 0.0001$	36.79a	±0.90	25.97b	±0.98	29.60c	±0.95	$p < 0.0001$
C18:2ω-6 (LA)	0.34a	±0.01	0.16b	±0.03	0.79c	±0.20	$p < 0.0001$	1.20a	±0.14	0.68b	±0.07	1.81c	±0.08	$p < 0.0001$
C20:2ω-6	2.72a	±0.22	1.75b	±0.20	1.83b	±0.28	$p = 0.0042$	0.82a	±0.15	0.35b	±0.05	0.39b	±0.05	$p = 0.0017$
C20:3ω-6 (DGLA)	0.94	±0.09	1.06	±0.07	1.07	±0.11	$p = 0.22$	2.20a	±0.11	1.54b	±0.05	2.05a	±0.09	$p = 0.0002$
C20:4ω-6 (AA)	1.47a	±0.04	6.31b	±0.19	1.18a	±0.09	$p < 0.0001$	3.43a	±0.09	7.87b	±0.75	3.01a	±0.16	$p < 0.0001$
C22:4ω-6 (ADA)	0.87a	±0.06	6.77b	±0.12	0.58c	±0.07	$p < 0.0001$	1.40a	±0.03	6.81b	±0.79	1.12a	±0.08	$p < 0.0001$
C22:5ω-6 (ω-6 DPA)	0.10a	±0.01	0.76b	±0.07	0.11a	±0.03	$p < 0.0001$	0.19a	±0.01	1.04b	±0.09	0.24a	±0.04	$p < 0.0001$
Total ω-6	6.45a	±0.29	16.80b	±0.07	5.66c	±0.09	$p < 0.0001$	9.24a	±0.35	18.30b	±1.55	8.63a	±0.20	$p < 0.0001$
C18:3ω-3 (ALA)	1.68a	±0.04	1.19b	±0.06	1.13b	±0.12	$p = 0.0003$	0.91a	±0.04	0.60b	±0.08	0.63b	±0.03	$p = 0.0006$
C20:4ω-3	0.08	±0.02	0.05	±0.01	0.04	±0.01	$p = 0.12$	0.19a	±0.02	0.11b	±0.03	0.10b	±0.02	$p = 0.014$
C20:5ω-3 (EPA)	0.07a	±0.01	0.07a	±0.01	0.41b	±0.08	$p = 0.0001$	0.09a	±0.01	0.07a	±0.01	0.45b	±0.03	$p < 0.0001$
C22:5ω-3 (ω-3 DPA)	0.52a	±0.06	0.42a	±0.03	1.21b	±0.18	$p = 0.0003$	0.92a	±0.05	0.86a	±0.10	1.42b	±0.09	$p = 0.0003$
C22:6ω-3 (DHA)	0.10a	±0.02	0.07a	±0.01	11.20b	±2.76	$p = 0.0002$	1.01a	±0.09	0.90a	±0.11	8.09b	±0.29	$p < 0.0001$
Total ω-3	2.45a	±0.06	1.81a	±0.06	13.99b	±2.91	$p = 0.0002$	3.12a	±0.07	2.54a	±0.15	10.69b	±0.41	$p < 0.0001$
Total PUFA	8.90a	±0.35	18.62b	±0.01	18.00b	±0.54	$p < 0.0001$	12.36a	±0.37	20.84b	±1.69	19.31b	±0.58	$p = 0.0001$
C22:6ω-3:C20:4ω-6	0.07a	±0.01	0.01a	±0.00	9.65b	±3.13	$p = 0.0009$	0.30a	±0.02	0.11b	±0.01	2.69c	±0.12	$p < 0.0001$
ω-3 PUFA:ω-6 PUFA	0.38a	±0.01	0.11b	±0.00	2.18c	±0.14	$p < 0.0001$	0.34a	±0.01	0.14b	±0.00	1.24c	±0.03	$p < 0.0001$

Different letters indicate that groups are significantly different. Differences were assessed for significance using one-way analysis of variance followed by post-hoc Tukey's test. *p*-value of <0.05 was considered statistically significant.

Table S3.3 Fatty acid composition of total lipids and total phospholipids extracted from A4-004N and A4-004Adh cells cultured under normal culture conditions (not treated (NT); from Tables S3.1 and S3.4) and in media supplemented with 30 µM BSA (from Tables S3.2 and S3.5).

Fatty Acids	A4-004N total lipid					A4-004Adh total lipid					A4-004N total phospholipid					A4-004Adh total phospholipid				
	NT		BSA			NT		BSA			NT		BSA			NT		BSA		
	Mean	±SD	Average	±SD	t-test	Mean	±SD	Average	±SD	t-test	Mean	±SD	Average	±SD	t-test	Mean	±SD	Average	±SD	t-test
C14:0	2.14	±0.10	2.21	±0.08	0.39	1.71	±0.07	1.89	±0.02	0.43	1.92	±0.15	1.56	±0.56	0.34	1.47	±0.10	1.48	±0.17	0.92
C15:0	0.13	±0.02	0.16	±0.02	0.21	0.52	±0.03	0.55	±0.01	0.35	0.21	±0.14	0.20	±0.09	0.93	0.47	±0.04	0.46	±0.07	0.88
C16:0 (PA)	25.75	±0.59	25.54	±0.24	0.59	29.22	±1.08	29.38	±0.46	0.83	24.59	±0.04	24.50	±0.54	0.84	26.23	±0.88	26.18	±0.97	0.95
C17:0	0.89	±0.06	0.81	±0.06	0.17	0.67	±0.06	0.60	±0.12	0.43	0.72	±0.11	0.70	±0.19	0.89	0.58	±0.06	0.57	±0.08	0.91
C18:0 (SA)	15.74	±0.11	16.39	±0.46	0.08	17.87	±1.15	17.30	±0.40	0.47	14.86	±0.58	14.53	±0.54	0.62	16.40	±0.55	16.24	±0.85	0.81
C20:0	0.21	±0.04	0.29	±0.05	0.08	0.39	±0.07	0.36	±0.03	0.55	0.50	±0.05	0.56	±0.14	0.55	0.43	±0.11	0.55	±0.11	0.32
C24:0	4.37	±0.40	3.91	±0.44	0.26	0.63	±0.13	0.77	±0.03	0.14	4.43	±0.15	3.92	±0.57	0.35	0.82	±0.22	0.78	±0.15	0.85
Total SFA	49.24	±0.27	49.30	±0.71	0.89	52.39	±1.48	50.85	±0.98	0.21	47.23	±0.13	46.17	±0.21	0.03	47.20	±0.10	46.27	±2.10	0.59
C16:1ω-9	7.88	±0.16	7.43	±0.14	0.02	6.14	±0.50	5.76	±0.25	0.31	8.22	±0.15	8.00	±0.06	0.17	7.46	±0.39	7.33	±0.38	0.73
C18:1ω-9 (OA)	27.45	±0.48	27.27	±0.37	0.64	21.94	±0.66	22.31	±0.47	0.48	27.29	±0.22	28.14	±0.36	0.10	23.66	±0.41	23.56	±0.46	0.82
C18:1ω-7	5.65	±0.09	5.85	±0.03	0.02	7.37	±0.25	7.25	±0.16	0.53	6.18	±0.10	6.26	±0.20	0.59	6.96	±0.19	6.93	±0.40	0.92
C24:1ω-9	1.42	±0.51	1.25	±0.16	0.62	1.15	±0.17	1.47	±0.05	0.04	1.35	±0.29	1.40	±0.04	0.78	1.11	±0.33	1.23	±0.17	0.69
Total MUFA	42.40	±0.09	41.80	±0.62	0.18	36.59	±1.26	36.79	±0.90	0.84	42.85	±0.22	43.88	±0.20	0.04	39.18	±0.92	39.05	±1.41	0.90
C18:2ω-6 (LA)	0.18	±0.03	0.34	±0.01	0.00	0.72	±0.09	1.20	±0.14	0.01	0.39	±0.30	0.33	±0.08	0.81	0.97	±0.08	1.00	±0.26	0.84
C20:2ω-6	3.25	±0.24	2.72	±0.22	0.05	0.95	±0.14	0.82	±0.15	0.32	3.91	±0.28	3.99	±0.09	0.77	1.27	±0.21	1.27	±0.27	0.99
C20:3ω-6 (DGLA)	0.74	±0.10	0.94	±0.09	0.06	1.67	±0.07	2.20	±0.11	0.00	1.21	±0.37	1.02	±0.07	0.55	2.00	±0.06	1.97	±0.20	0.81
C20:4ω-6 (AA)	1.01	±0.14	1.47	±0.04	0.01	3.01	±0.36	3.43	±0.09	0.11	1.14	±0.07	1.01	±0.02	0.13	3.80	±0.12	3.96	±0.18	0.33
C22:4ω-6 (ADA)	0.60	±0.01	0.87	±0.06	0.00	1.24	±0.13	1.40	±0.03	0.10	0.56	±0.02	0.49	±0.02	0.07	1.36	±0.05	1.42	±0.14	0.51
C22:5ω-6 (ω-6 DPA)	0.10	±0.03	0.10	±0.01	0.84	0.22	±0.03	0.19	±0.01	0.12	0.24	±0.04	0.34	±0.23	0.62	0.45	±0.08	0.54	±0.29	0.61
Total ω-6	5.88	±0.29	6.45	±0.29	0.07	7.82	±0.47	9.24	±0.35	0.01	7.07	±0.10	7.04	±0.21	0.88	9.86	±0.36	10.18	±0.24	0.37
C18:3ω-3 (ALA)	1.79	±0.09	1.68	±0.04	0.12	0.95	±0.08	0.91	±0.04	0.45	1.65	±0.27	2.01	±0.11	0.10	1.15	±0.10	0.98	±0.21	0.28
C20:4ω-3	0.06	±0.02	0.08	±0.02	0.36	0.16	±0.01	0.19	±0.02	0.13	0.16	±0.07	0.19	±0.09	0.37	0.36	±0.07	0.38	±0.09	0.72
C20:5ω-3 (EPA)	0.09	±0.03	0.07	±0.01	0.54	0.09	±0.02	0.09	±0.01	0.73	0.20	±0.08	0.14	±0.00	0.18	0.22	±0.02	0.26	±0.14	0.61
C22:5ω-3 (ω-3 DPA)	0.47	±0.04	0.52	±0.06	0.23	0.96	±0.11	0.92	±0.05	0.62	0.51	±0.01	0.34	±0.02	0.01	1.04	±0.08	1.08	±0.14	0.69
C22:6ω-3 (DHA)	0.09	±0.01	0.10	±0.02	0.40	1.04	±0.13	1.01	±0.09	0.78	0.23	±0.07	0.33	±0.18	0.72	1.78	±0.14	1.81	±0.15	0.85
Total ω-3	2.49	±0.05	2.45	±0.06	0.45	3.20	±0.19	3.12	±0.07	0.52	2.86	±0.01	2.85	±0.10	0.95	4.55	±0.17	4.51	±0.45	0.90
Total PUFA	8.36	±0.34	8.90	±0.35	0.13	11.02	±0.65	12.36	±0.37	0.04	9.93	±0.09	9.84	±0.25	0.68	14.41	±0.47	14.69	±0.69	0.62
C22:6ω-3:C20:4ω-6	0.14	±0.02	0.07	±0.01	0.01	0.84	±0.05	0.30	±0.02	0.00	0.24	±0.04	0.23	±0.09	0.84	0.47	±0.02	0.46	±0.02	0.60
ω-3 PUFA:ω-6 PUFA	0.42	±0.01	0.38	±0.01	0.01	0.41	±0.00	0.34	±0.01	0.00	0.40	±0.01	0.40	±0.01	0.41	0.46	±0.02	0.44	±0.03	0.46

Data are presented as mean ± standard deviation (SD). p-value of <0.05 was considered statistically significant. N = 3.

Table S3.4 Fatty acid composition of total phospholipids from A4-004N and A4-004Adh cells.

Fatty Acids	A4-004N (N = 3)		A4-004Adh (N = 3)		
	% Abundance of fatty acids in total phospholipids				
	Mean	±SD	Mean	±SD	*p*-value
C14:0	1.92	±0.15	1.47	±0.10	*p = 0.011*
C15:0	0.21	±0.14	0.47	±0.04	*p = 0.038*
C16:0 (PA)	24.59	±0.04	26.23	±0.88	*p = 0.09*
C17:0	0.72	±0.11	0.58	±0.06	*p = 0.12*
C18:0 (SA)	14.86	±0.58	16.40	±0.55	*p = 0.057*
C20:0	0.50	±0.05	0.43	±0.11	*p = 0.38*
C24:0	4.43	±0.15	0.82	±0.22	*p = 0.0003*
Total SFA	47.23	±0.13	47.20	±0.10	*p = 0.84*
C16:1ω-9	8.22	±0.15	7.46	±0.39	*p = 0.08*
C18:1ω-9 (OA)	27.29	±0.22	23.66	±0.41	*p = 0.0015*
C18:1ω-7	6.18	±0.10	6.96	±0.19	*p = 0.0035*
C24:1ω-9	1.35	±0.29	1.11	±0.33	*p = 0.40*
Total MUFA	42.85	±0.22	39.18	±0.92	*p = 0.013*
C18:2ω-6 (LA)	0.39	±0.30	0.97	±0.08	*p = 0.032*
C20:2ω-6	3.91	±0.28	1.27	±0.21	*p = 0.0012*
C20:3ω-6 (DGLA)	1.21	±0.37	2.00	±0.06	*p = 0.021*
C20:4ω-6 (AA)	1.14	±0.07	3.80	±0.12	*p = 0.0001*
C22:4ω-6 (ADA)	0.56	±0.02	1.36	±0.05	*p = 0.0002*
C22:5ω-6 (ω-6 DPA)	0.24	±0.04	0.45	±0.08	*p = 0.049*
Total ω-6	7.07	±0.10	9.86	±0.36	*p = 0.002*
C18:3ω-3 (ALA)	1.65	±0.27	1.15	±0.10	*p = 0.041*
C20:4ω-3	0.16	±0.07	0.36	±0.07	*p = 0.020*
C20:5ω-3 (EPA)	0.20	±0.08	0.22	±0.02	*p = 0.028*
C22:5ω-3 (ω-3 DPA)	0.51	±0.01	1.04	±0.08	*p = 0.003*
C22:6ω-3 (DHA)	0.23	±0.07	1.78	±0.14	*p = 0.0008*
Total ω-3	2.86	±0.01	4.55	±0.17	*p = 0.0009*
Total PUFA	9.93	±0.09	14.41	±0.47	*p = 0.0010*
C22:6ω-3:C20:4ω-6	0.24	±0.04	0.47	±0.02	*p = 0.0035*
ω-3 PUFA:ω-6 PUFA	0.40	±0.01	0.46	±0.02	*p = 0.025*

Data are presented as mean ± standard deviation (SD). *p*-value of <0.05 was considered statistically significant.

Table S3.5 Fatty acid composition of total phospholipids from A4-004N and A4-004Adh cells cultured in media supplemented with BSA (control), 30 µM AA or 30 µM DHA.

Fatty Acids	A4-004N							A4-004Adh						
	BSA Control (N = 3)		AA 30 µM (N = 3)		DHA 30 µM (N = 3)			BSA Control (N = 3)		AA 30 µM (N = 3)		DHA 30 µM (N = 3)		
	% Abundance of fatty acids in total phospholipids													
	Average	±SD	Average	±SD	Average	±SD	ANOVA	Average	±SD	Average	±SD	Average	±SD	ANOVA
C14:0	1.56	±0.56	2.08	±0.54	1.89	±0.36	$p = 0.47$	1.48	±0.17	1.68	±0.20	1.63	±0.16	$p = 0.49$
C15:0	0.20	±0.09	0.18	±0.09	0.22	±0.10	$p = 0.85$	0.46	±0.07	0.46	±0.06	0.49	±0.05	$p = 0.85$
C16:0 (PA)	24.50	±0.54	24.06	±0.15	25.01	±0.23	$p = 0.15$	26.18a	±0.97	29.56b	±0.20	28.20ab	±0.85	$p = 0.030$
C17:0	0.70	±0.19	0.58	±0.17	0.49	±0.13	$p = 0.33$	0.57	±0.08	0.66	±0.07	0.73	±0.07	$p = 0.17$
C18:0 (SA)	14.53	±0.54	18.29	±2.10	19.20	±1.55	$p = 0.064$	16.24a	±0.85	17.26ab	±0.36	18.44b	±0.49	$p = 0.017$
C20:0	0.56	±0.14	0.35	±0.04	0.48	±0.01	$p = 0.20$	0.55	±0.11	0.42	±0.02	0.37	±0.00	$p = 0.061$
C24:0	3.92	±0.57	2.78	±0.19	2.52	±0.30	$p = 0.070$	0.78a	±0.15	0.42b	±0.04	0.45b	±0.02	$p = 0.017$
Total SFA	46.17a	±0.21	47.41b	±0.10	49.14c	±0.31	$p = 0.0021$	46.27	±2.10	50.81	±0.15	50.04	±1.36	$p = 0.062$
C16:1ω-9	8.00a	±0.06	5.41b	±0.89	5.56b	±0.71	$p = 0.022$	7.33	±0.38	4.22	±0.26	4.53	±0.40	$p = 0.0004$
C18:1ω-9 (OA)	28.14a	±0.36	21.62b	±1.57	23.72ab	±1.39	$p = 0.028$	23.56a	±0.46	15.99b	±0.80	18.84c	±0.63	$p = 0.0002$
C18:1ω-7	6.26a	±0.20	4.95b	±0.08	4.61c	±0.04	$p < 0.0001$	6.93a	±0.40	5.33b	±0.19	5.21b	±0.14	$p = 0.0010$
C24:1ω-9	1.40	±0.04	1.18	±0.32	1.01	±0.30	$p = 0.24$	1.23	±0.17	1.22	±0.28	1.08	±0.15	$p = 0.69$
Total MUFA	43.88a	±0.20	33.46b	±2.04	35.32b	±2.02	$p = 0.016$	39.05a	±1.41	26.76b	±1.03	29.67b	±1.29	$p = 0.0003$
C18:2ω-6 (LA)	0.33a	±0.08	0.24a	±0.02	1.08b	±0.02	$p = 0.0007$	1.00a	±0.26	0.91a	±0.10	2.17b	±0.27	$p = 0.0016$
C20:2ω-6	3.99a	±0.09	2.39b	±0.03	2.44b	±0.02	$p = 0.0001$	1.27a	±0.27	0.42b	±0.14	0.42b	±0.07	$p = 0.0028$
C20:3ω-6 (DGLA)	1.02	±0.07	1.34	±0.13	1.31	±0.06	$p = 0.059$	1.97ab	±0.20	1.77a	±0.11	2.13b	±0.04	$p = 0.035$
C20:4ω-6 (AA)	1.01a	±0.02	6.44b	±0.44	1.70a	±0.87	$p = 0.0020$	3.96a	±0.18	8.65b	±0.28	3.76a	±0.35	$p < 0.0001$
C22:4ω-6 (ADA)	0.49a	±0.02	6.64b	±0.92	0.77a	±0.31	$p = 0.0001$	1.42a	±0.14	6.71b	±0.22	1.22a	±0.18	$p < 0.0001$
C22:5ω-6 (ω-6 DPA)	0.34a	±0.23	1.03b	±0.28	0.45a	±0.14	$p = 0.019$	0.54a	±0.29	1.32b	±0.07	0.47a	±0.15	$p = 0.0032$
Total ω-6	7.04a	±0.21	17.26b	±1.32	7.02a	±0.50	$p = 0.0017$	10.18a	±0.24	19.77b	±0.62	10.17a	±0.45	$p < 0.0001$
C18:3ω-3 (ALA)	2.01a	±0.11	1.23b	±0.17	1.13b	±0.10	$p = 0.0003$	0.98	±0.21	0.89	±0.03	0.93	±0.17	$p = 0.81$
C20:4ω-3	0.19	±0.09	0.13	±0.01	0.10	±0.003	$p = 0.29$	0.38a	±0.09	0.18b	±0.03	0.20ab	±0.08	$p = 0.045$
C20:5ω-3 (EPA)	0.14a	±0.00	0.11a	±0.06	0.41b	±0.06	$p = 0.0026$	0.26a	±0.14	0.16a	±0.06	0.62b	±0.09	$p = 0.0044$
C22:5ω-3 (ω-3 DPA)	0.34a	±0.02	0.84b	±0.05	0.90b	±0.11	$p = 0.0036$	1.08	±0.14	0.97	±0.10	1.22	±0.11	$p = 0.095$
C22:6ω-3 (DHA)	0.33a	±0.18	0.27a	±0.07	6.01b	±0.68	$p < 0.0001$	1.81a	±0.15	1.52a	±0.29	6.88b	±0.73	$p < 0.0001$
Total ω-3	2.85a	±0.10	2.53a	±0.13	8.53b	±0.86	$p < 0.0001$	4.51a	±0.45	3.71a	±0.42	9.85b	±0.64	$p < 0.0001$
Total PUFA	9.84a	±0.25	19.80b	±1.19	15.54b	±1.71	$p = 0.0086$	14.69a	±0.69	23.48b	±1.01	20.02c	±1.08	$p = 0.0006$
C22:6ω-3:C20:4ω-6	0.23a	±0.09	0.04a	±0.01	4.92b	±0.06	$p < 0.0001$	0.46a	±0.02	0.16b	±0.00	1.76c	±0.03	$p < 0.0001$
ω-3 PUFA:ω-6 PUFA	0.40a	±0.01	0.15b	±0.02	1.21c	±0.09	$p = 0.0005$	0.44a	±0.03	0.18b	±0.00	0.97c	±0.02	$p < 0.0001$

Different letters indicate that groups are significantly different. Differences were assessed for significance using one-way analysis of variance followed by post-hoc Tukey's test. *p*-value of <0.05 was considered statistically significant.

Chapter 4.

Role of FABP7 in GBM neural stem-like cell lipid metabolism

4.1 Introduction

GBM neural stem-like cells (GSCs) exhibit distinct metabolic profiles compared to their differentiated progeny. It has recently been reported that GSCs are less glycolytic (e.g., consuming lower levels of glucose) while maintaining higher ATP levels (Strickland and Stoll, 2017). Dysregulation of lipid metabolism is associated with maintenance of GBM stemness and poor GBM patient survival (Garnier et al., 2019; Strickland and Stoll, 2017). Genes involved in different lipid metabolism pathways are up-regulated in GBM neural stem-like cells, such as *FASN*, *ELOVL2*, *FABP7* and *ACBP*, highlighting the importance of lipid synthesis, transport and metabolism in GBM (De Rosa et al., 2012; Duman et al., 2019; Saurty-Seerunghen et al., 2019). A recent single cell RNA-sequencing analysis from GBM surgical resections demonstrates specific enrichment of lipid metabolism enzymes, such as ELOVL2 and carnitine palmitoyltransferase 1, isoform c (CPT1c) and acyl-CoA synthetase bubblegum family, member 1 (ACSBG1) in GBM tumours with high tumourigenic potential (Saurty-Seerunghen et al., 2019).

Fatty acids pass easily through the blood brain barrier (Hamilton and Brunaldi, 2007). Emerging evidence shows that fatty acids serve not only as materials for lipid membrane synthesis but also as substrates for energy production (Strickland and Stoll, 2017). In a 2017 study, Lin *et al.* reported that human primary GBM cells cultured under serum-free conditions oxidize fatty acids to maintain both respiratory and proliferative activities (Lin et al., 2017). Etomoxir, an inhibitor of CPT1 involved in the rate-limiting step of fatty acid β-oxidation, inhibits GBM energy production and cellular proliferation in GBM cells (Lin et al., 2017). This study also demonstrated that the serum-free conditions under which GBM stem-like cells are cultured can better recapitulate GBM tumour metabolic

status than the traditional serum-containing medium used to culture GBM cells. In 2018, another study defined and classified GBM neural stem-like cells as slow-cycling cells which preferentially utilize mitochondrial oxidative phosphorylation for their functions, particularly under glucose-deprivation conditions (Hoang-Minh et al., 2018). Slow-cycling cells highly express FABP7, display elevated lipid metabolism levels, show increased lipid droplet formation, as well as enhanced tumour invasion and chemoresistance, suggesting their important role in tumour recurrence. This study further showed that FABP7 expression attenuates the effect of glycolysis inhibition on GBM tumour growth in mice(Hoang-Minh et al., 2018). These recent findings further suggest an important role for FABP7 in regulating GBM mitochondrial fatty acid β-oxidation processes, especially in GBM neural stem-like cells.

In human brain, long chain fatty acids are converted into fatty acid acyl-CoA by long-chain acyl-CoA synthetase, such as ACSL6 and ACSBG1, for further plasma membrane fatty acid recycling, mitochondrial fatty acid β-oxidation or phospholipid synthesis (Lacombe et al., 2018). Recently, an *Acsl6*-deficient mouse model study showed that ACSL6 promotes brain DHA enrichment (Fernandez et al., 2018). The *in vivo* role of ACSBG1 in brain fatty acid β-oxidation remains unknown (Fernandez and Ellis, 2020). Long chain fatty acid acyl-CoA transport from the cytosol into the mitochondrial matrix is dependent on CPT1 family members, which are found in the outer mitochondrial membrane. Long chain fatty acid acyl-CoA transport is the rate-limiting step in fatty acid β-oxidation. The CPT1a and CPT1b isoforms are specific to liver and muscle fatty acid β-oxidation, respectively, whereas CPT1c is specifically expressed in brain, as

well as some types of cancer (e.g. neuroblastoma, glioblastoma, breast cancer and lung cancer) (Price et al., 2002; Reilly and Mak, 2012; Zaugg et al., 2011).

Fatty acid recycling pathways (called Lands' cycle) by phospholipase A_2 (PLA_2) proteins are essential for fatty acid hydrolysis from phospholipids in plasma membrane. Elevated levels of PLA_2, such as $cPLA_2$ and $iPLA_2$, facilitate the phospholipid membrane turnover of brain-enriched AA and DHA, respectively (Bazinet and Laye, 2014). Understanding the relationship between PUFA membrane recycling, FABP7 expression and presence of FABP7 PUFA ligands DHA and AA in GBM will provide mechanistic insight into FABP7-mediated plasma membrane remodelling in GBM.

Osswald *et al.* reported that GBM cells extend ultra-long membrane protrusions, called microtubes, that serve as multicellular communicating channels in GBM (Broekman et al., 2018; Osswald et al., 2015). Microtubes have been reported in both 2D neurosphere cultures and 3D organoid cultures using GBM-patient derived GSCs, as well as in xenograft GBM tumours, and patient GBM tissue (Linkous et al., 2019; Osswald et al., 2015). Microtubes create tumour-tumour connections as well as tumour-astrocyte connections (Formicola et al., 2019), and play an important role in GBM tumour progression and resistance to therapy based on experimental models (Linkous et al., 2019; Weil et al., 2017). It is hypothesized that when tumour tissue is damaged by chemotherapy/radiotherapy or surgically removed, microtubes facilitate the shuttling of tumour cells to less-damaged sites (e.g. by transporting molecules involved in the propagation of calcium flux), resulting in GBM tumour recurrence (Broekman et al., 2018; Osswald et al., 2015; Weil et al., 2017). Many organelles have been identified within microtubes, such as mitochondria and lysosomes (Formicola et al., 2019; Pinto et al.,

172

2021). Other communication channels, called tunnelling nanotubes, have also been described in GBM neurosphere cultures generated from the highly infiltrative regions of GBM tumours (Pinto et al., 2021; Valdebenito et al., 2020). These authors found a correlation between GBM stem cell markers, increased levels of oxidative phosphorylation and elevated transfer of mitochondria through tunnelling nanotubes. FABP7 is a well-known GBM stem cell marker that is highly expressed in the infiltrative regions of GBM tumours (Morihiro et al., 2013). We have found that FABP7 localizes to mitochondria in several GBM neurosphere cultures. One of the objectives of Chapter 4 was therefore to investigate FABP7 in GBM neurosphere microtubes.

4.2 Materials and methods

4.2.1 Quantitative RT-PCR

RNA was purified from patient-derived GBM neurosphere cultures (A4-004N, A4-007N, A4-011N and A4-012N) and their paired adherent culture counterparts (A4-004Adh, A4-007Adh, A4-011Adh and A4-012Adh) using the RNeasy Plus Kit (Qiagen) following the manufacturer's protocol. cDNA was transcribed using Superscript II reverse transcriptase (Invitrogen) and oligodT. The following primers were used for quantitative RT-PCR (RT-qPCR) analysis: *CPT1c variant 1* (Forward 5′-TCTTCAGTGCCATCCAGCTT -3'; Reverse 5′- ACAAACACGAGGCAAACAGC -3'), *CPT1c variants 2/3/4* (Forward 5′-GCTTTCAGCTGGGCTACTCA -3'; Reverse 5′-ACGACATGGCAGTCGACATT -3'), *ACSBG1* (Forward 5′-ACGCAATTCTGGAGCTGGAT -3'; Reverse 5′- GAGCTCGAGAGCATGGTTCA -3'), *ACSL6* (Forward 5′- CTGGGGCTATCCGCTACATC -3'; Reverse 5′-ACTTAATGACCACCCCGCAC -3'), *GAPDH* (Forward 5′- ACCAGGGAGGGCTGCAGT -3'; Reverse 5′- CAGTTCGGAGCCCACACG -3'). RT-qPCR analyses was carried out with BrightGreen® qPCR master mix (ABM Scientific). All samples were assayed in triplicate, and data were normalized for gene expression using *GAPDH* as an internal control.

4.2.2 Western blot analysis

Whole cell lysates were prepared as previously described (Liu et al., 2020a). Whole cell lysates (50 μg per lane) were analysed by sodium dodecyl sulfate-polyacrylamide gel electrophoresis (SDS-PAGE) followed by electroblotting onto

nitrocellulose membranes. For lambda-phosphatase treatment, 10 µg of nuclear lysates were incubated with either water (negative control) or 400 units of lambda-phosphatase for 1 h at 30°C in the supplied reaction buffer, supplemented with 1 mM MnCl$_2$. Membranes were immunoblotted with rabbit anti-cPLA2 (1:1000, abcam 135825), mouse anti-group VI iPLA (1:1000, Santa Cruz sc-14463), rabbit anti-phospho-p38-MAPK (Thr180/Tyr182) (1:1000, cell signalling #9211), or mouse anti-β-Actin (Thermo Fisher Scientific; 1:1000) antibodies, followed by anti-rabbit or anti-mouse secondary antibodies (Invitrogen,1:50000).

4.2.3 GBM xenograft mouse brain tissue immunohistochemistry and immunofluorescence analysis

Animal experiments were reviewed and approved by the Cross Cancer Institute Animal Care Committee under protocol AC19249. All animal experiments were in accordance with the Canadian Council on Animal Care guidelines. Immunodeficient 8-week-old male NOD.Cg-PrkdcscidIl2rg (NSG) mice were injected with patient-derived A4-007N neurosphere cells (Giannini et al., 2005). Mice were fully anesthetized and positioned on a stereotaxic apparatus. Local anesthetic bupivacaine was injected at the surgical site before intracranial tumour injection. Approximately 5 X 10^4 cells (in 5 µL) were injected into the right frontal cortex at a depth of 2 mm (1.5 mm lateral, 1 mm anterior from the bregma). The skin overlying the injection site was stapled and mice allowed to recover for 7 days after GBM cell injection, then weighed twice weekly. Mice were euthanized upon reaching 20% weight loss.

Mouse brains were dissected, processed and immunostained as previously described for human GBM tissue (Mita et al., 2007). Tissue sections were immunostained with rabbit anti-FABP7 (prepared in-house; 1:1000), followed by EnVision+ System anti-rabbit HRP-labeled polymer (DakoCytomation, Carpinteria, CA, USA). For co-immunofluorescence analysis, GBM xenograft tissue sections were immunostained with anti-human mitochondria primary antibody (Sigma-Aldrich, 1:800, MAB1273) and rabbit anti-FABP7 primary antibody, followed by anti-mouse Alexa 647 secondary antibody (1:400, Invitrogen) and anti-rabbit Alexa 555 secondary antibody (1:400, Invitrogen). Images were acquired with a Zeiss LSM 710 confocal microscope using a 40x/1.3 oil-immersion objective.

4.2.4 Primary GBM neurosphere cultures and FABP7 depletion

The generation of patient-derived GBM cultures under adherent and neurosphere culture conditions has been described in Chapters 2 and 3. For FABP7 depletion, lentivirus shRNA packaging plasmids and control plasmids were purchased from Sigma. The two lentivirus FABP7 shRNA constructs used for our experiments were obtained from the University of Alberta RNAi Core Facility. FABP7 shRNA sequences, control shRNA sequence and virus production procedures are described in Chapter 2 (Xu et al., 2021). The MISSION pLKO. (Sigma-Aldrich, SHC002) served as the control vector. U251 GBM and A4-004N cells were infected with lentivirus overnight and the medium changed. Infected GBM cells were selected in 1 µg/mL puromycin.

4.2.5 ATP assay

U251 and A4-004N cells were grown in 12-well plates (25 000 cells/well) for three days. Cells were then trypsinized, resuspended in DMEM, and counted. ATP levels of intact cells (in triplicate) were measured using the ATP Determination Kit (Invitrogen, Thermo Fisher) following the manufacturer's instructions. ATP levels for each sample were normalized to cell numbers obtained using a Coulter Counter.

4.2.6 Immunofluorescence analysis of GBM cells

For co-immunofluorescence analysis of $cPLA_2$ and cell membrane dye wheat germ agglutinin (WGA) Texas Red™ in U87 GBM cells, the WGA dye was diluted to 5 µg/mL using Hank's balanced salt solution (HBSS). GBM cells were incubated in WGA dye for 15 minutes at 37°C. Labelled cells were washed two times with HBSS, then fixed with 4% paraformaldehyde (PFA) for 10 minutes at room temperature, followed by immunostaining with rabbit anti-$cPLA_2$ antibody (Abcam, 1:400, 135825), and anti-rabbit Alexa 488 secondary antibody (Invitrogen,1:400). Images were acquired with a Zeiss LSM 710 confocal microscope using a 40x/1.3 oil-immersion objective.

A4-007N were cultured on high-performance plates (Greiner Bio-One 96-well microplate, µclear), then co-(immuno)stained with mouse anti-FABP7 antibody (Santa Cruz, 1:400, sc-374588) and lipid droplets marker (rabbit anti-ADRP antibody, Proteintech,1:400, 15294-1-AP), or mitochondria marker (Thermo Fisher, 200 nM/mL, Mitotracker™ Deep Red FM), or peroxisome marker (rabbit anti-Acox1 antibody, Sigma, 1:400, HPA021192), followed by (where appropriate) anti-mouse Alexa 555 secondary antibody (1:400, Invitrogen) and anti-rabbit Alexa 647 secondary antibody (1:400,

Invitrogen). Images were acquired with a Zeiss LSM 710 confocal microscope using a 40x/NA1.3 oil lens. Co-localization analysis (Pearson's coefficient and M1 & M2 coefficient) of FABP7 signal was calculated using colocalization analysis Plugin of ImageJ software (version 1.53e, National Institutes of Health, USA).

To quantitate overlapping FABP7 and mitochondria signals upon treatment with different fatty acids, raw images were acquired by confocal microscopy (5 images were acquired in each of three independent experiments, with an average of 3 neurospheres in each image; total of 15 neurospheres). Both FABP7 and Mitotracker™ Deep Red signal intensities were calculated for every single pixel. The Mitotracker™ Deep Red signal intensity calculation using ImageJ software was as described in our recent publication (Xu et al., 2021). For microtube analysis, A4-007N shcontrol cells and shFABP7 cells were cultured in 60 mm dishes for 7-10 days until microtube connections/long processes had formed. Images were acquired with a MH bright field light microscope using a 10x lens. Neurosphere size, processes length and numbers were quantified using ImageJ software (version 1.53e, National Institutes of Health, USA).

4.2.7 GBM lipid metabolism gene expression based on RNA-sequencing data analysis

Upper quantile normalized fragments per kilobase million (FPKM) reads of 27 different cancers were obtained from open-source Genomic Data Commons (GDC) Data Portal. The read data within each cancer type were then merged according to the gene names. Within each cancer type, the mean expression levels of each gene across different patients were calculated and used as the representation of the gene expression

levels in the cancer type. The gene expression levels of the 27 different cancers were merged into one file and plotted with plots package in R.

4.2.8 Statistical analysis

Assessment of the significance of differences between groups was by student's unpaired *t*-test (two groups comparison). Microsoft Excel (Microsoft, Redmond, WA, USA) and Prism 8 (GraphPad Software, San Diego, CA, USA) were used for statistical analysis of data. A *p*-value < 0.05 was considered statistically significant.

4.3 Results

4.3.1 Mitochondria lipid metabolism genes are highly expressed in GBM neurosphere cultures

Single cell RNA-sequencing data indicate that elevated expression of lipid metabolism genes correlates with a high tumourigenic potential (Saurty-Seerunghen et al., 2019). Here, we use RNA sequencing data from Genomic Data Commons (GDC) database to compare fatty acid metabolism genes expression profiles between GBM and 26 other cancer types. We focused on the expression profiles of genes involved in mitochondrial fatty acid β-oxidation pathways. Our results indicate that the long chain fatty acid mitochondrial transporting gene '*carnitine palmitoyltransferase I isoform c*' (*CPT1C*) and '*acyl-CoA synthetase long-chain family, member 6*' *(ACSL6)* and *acyl-CoA synthetase bubblegum family, member 1*' (*ACSBG1*), which are key rate-limiting steps in mitochondrial fatty acid β-oxidation, are up-regulated in GBM tumour tissues compared to other cancer types (**Figure 4.1A**).

We carried out quantitative RT-PCR to compare the expression levels of the mitochondrial fatty acid β-oxidation genes, *CPT1c*, *ACSL6* and *ACSBG1*, as well as *FABP7* in 10 GBM cell lines cultured in standard serum-containing medium and 8 GBM patient-derived neurosphere cultures. Our results show that FABP7-positive GBM cell lines and neurosphere cultures have generally higher levels of *CPT1c*, *ACSL6* and *ACSBG1* mRNA compared to FABP7-negative GBM cell lines (**Figure 4.1B**). The cell line that showed the most dramatic increase in the levels of *CPT1c*, *ACSL6* and *ACSBG1* was A4-007N (**Figure 4.1B**).

To further assess the effect of culture medium on the expression of mitochondrial fatty acid β-oxidation genes, we examined levels of *CPT1c, ACSL6* and *ACSBG1* mRNA in patient-derived GBM neurosphere cultures and their paired counterparts cultured in standard serum-containing medium. We found significantly higher levels of fatty acid β-oxidation in neurosphere cultures compared to their adherent counterparts (**Figure 4.1C**).

A

182

B

CPT1c

ACSL6

ACSBG1

FABP7

C

CPT1c

ACSL6

ACSBG1

FABP7

183
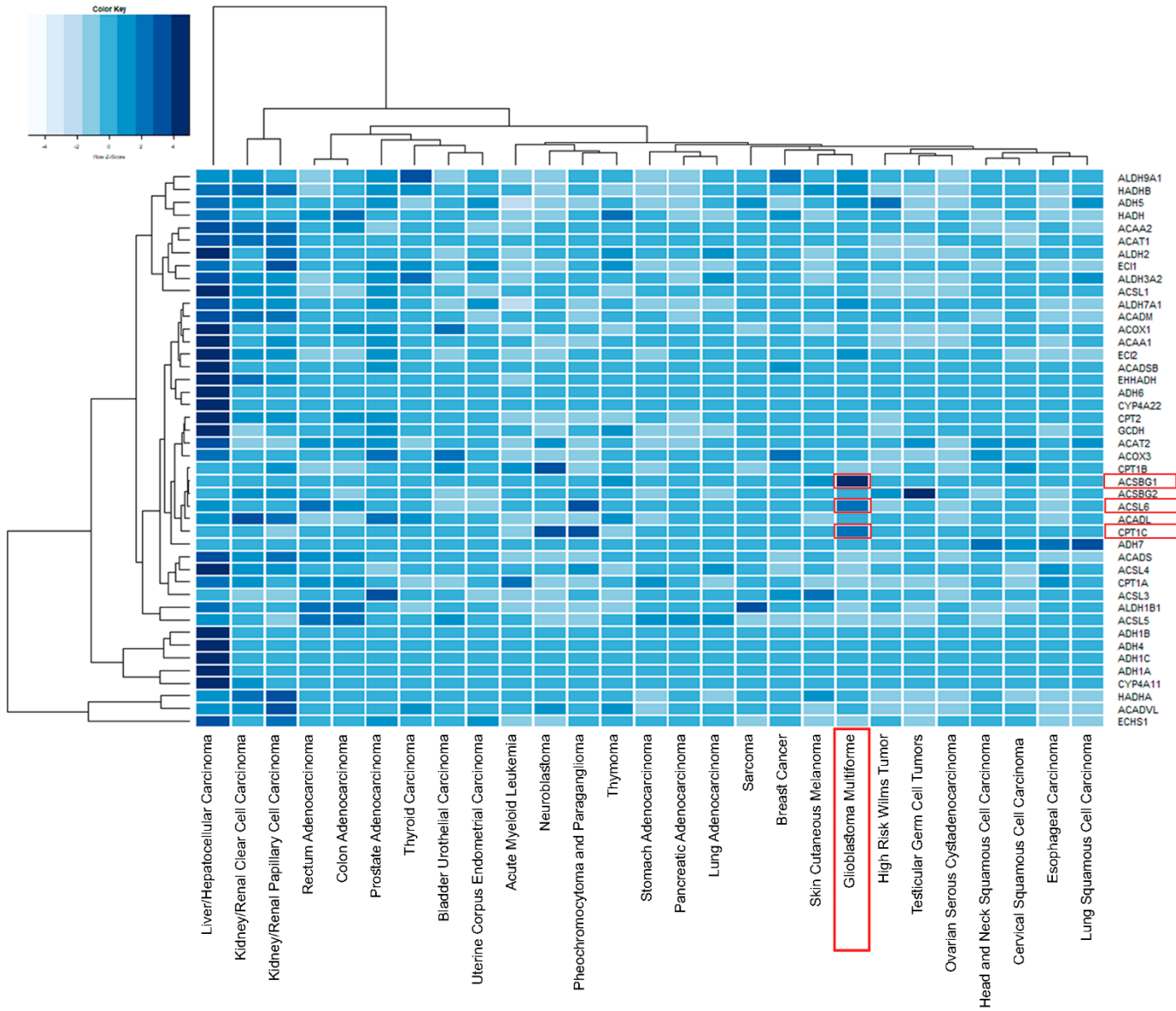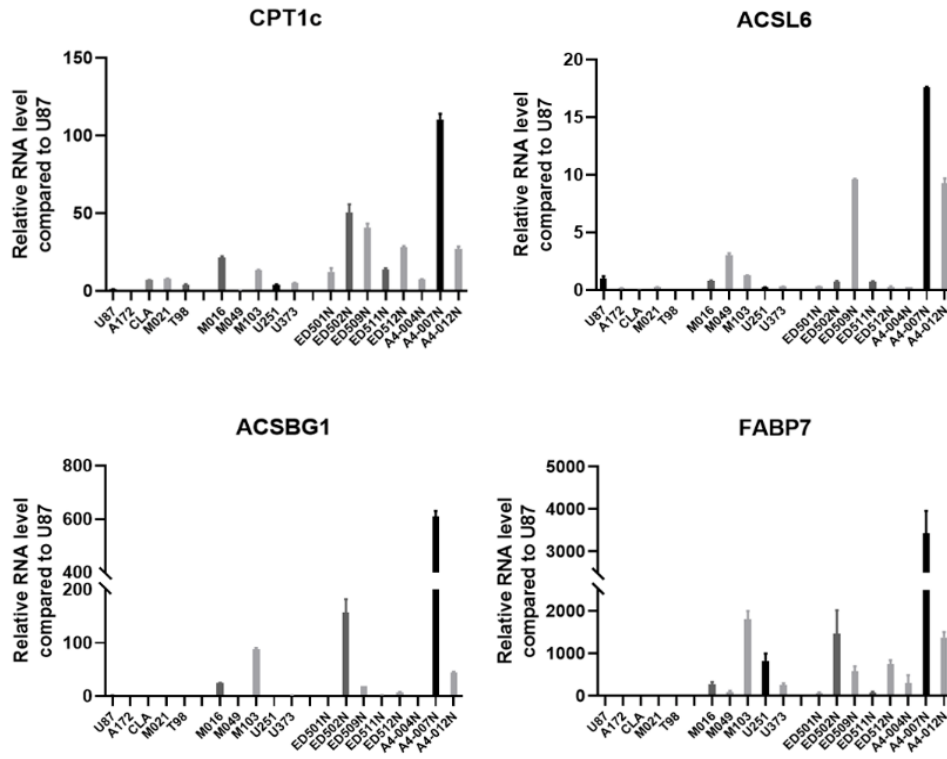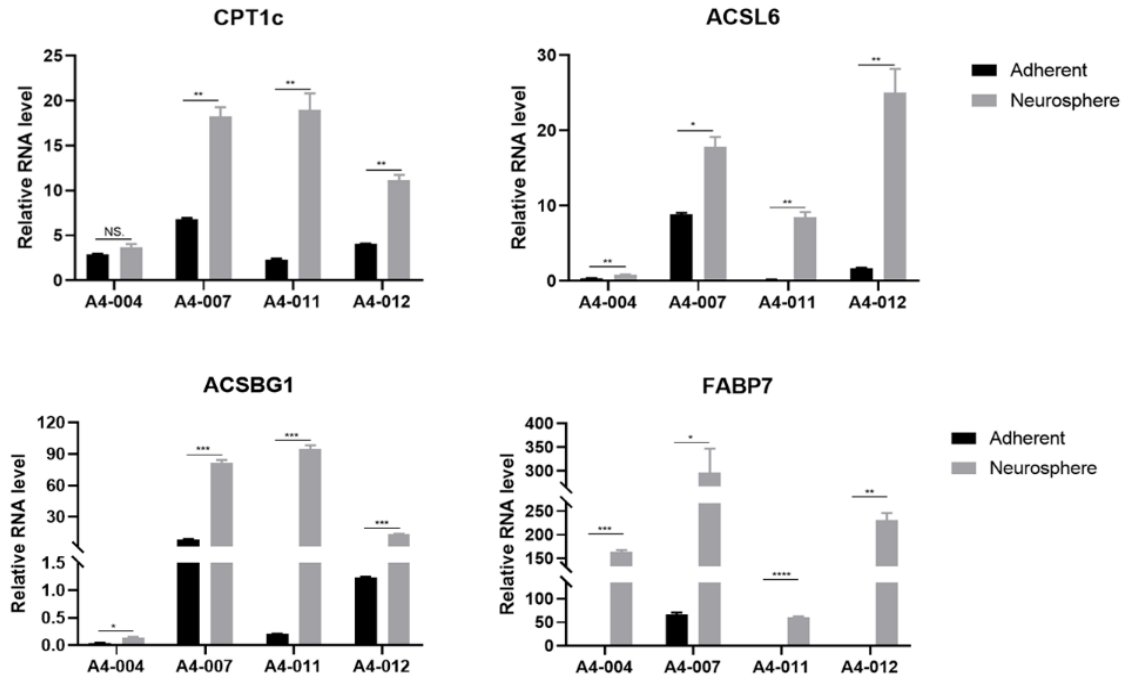
Figure 4.1 GBM tissue and neurosphere cultures highly express mitochondrial fatty acid β-oxidation genes.

(A) RNA-sequencing data from 27 different cancers obtained from the open source GDC Data Portal. Mitochondrial fatty acid β-oxidation gene expression levels were compared across the different cancer types. Our results show that the fatty acid mitochondrial transport gene *CPT1c,* long-chain fatty-acyl-CoA biosynthesis genes, *ACSL6* and *ACSBG1* are particularly up-regulated in GBM tumour tissues compared to other cancer types. (B) RT-qPCR shows that *CPT1c*, *ACSL6*, ACSBG*1* and *FABP7* mRNA levels in 5 *FABP7*-negative cell lines are generally lower than in 5 *FABP7*-positive GBM cells and 8 GBM patient-derived neurosphere. (C) RT-qPCR shows that GBM neurosphere cultures generally have higher levels of *CPT1c*, *ACSL6*, *ACSBG1* and *FABP7* mRNA than GBM adherent cultures. Statistical analysis of 4 pairs of GBM adherent and neurosphere culture RT-qPCR was performed using the two-tailed unpaired *t*-test. Error bars represent standard deviation (SD). N=3. * indicates $p < 0.05$, ** indicates $p < 0.01$, *** indicates $p < 0.001$, and **** indicates $p < 0.0001$. n.s., not significant.

4.3.2 Effect of FABP7 on mitochondrial fatty acid β-oxidation gene expression

As FABP7 has been linked to GBM mitochondrial oxidative phosphorylation activity, we depleted FABP7 in an endogenously FABP7-expressing cell line (U251 GBM cells) and a GBM neurosphere culture (A4-004N cells). FABP7 knockdown efficiency in U251 and A4-004N cells is shown in **Figure 4.2A**. RT-qPCR was used to investigate the effect of FABP7 on the expression of *CPT1c*, *ACSL6* and *ACSBG1*. *CPT1c* and *ACSL6* were both down-regulated upon FABP7 depletion, while *ACSBG1* was up-regulated (**Figure 4.2A**).

GBM neural stem-like cells which naturally express elevated levels of FABP7, show increased lipid metabolism under glucose-deprived conditions. This is indicative of increased mitochondrial oxidative phosphorylation in glucose-deprived neural stem-like cells (Hoang-Minh et al., 2018). To directly investigate the effect of FABP7 on ATP production, we used lentivirus constructs to deplete FABP7 in U251 and A4-004N cells and measured ATP production in these cells using the ATP Determination kit. Our results indicate that ATP production in FABP7-depleted cells is reduced by about 30-40% compared to FABP7-shcontrol cells (**Figure 4.2B**).

A
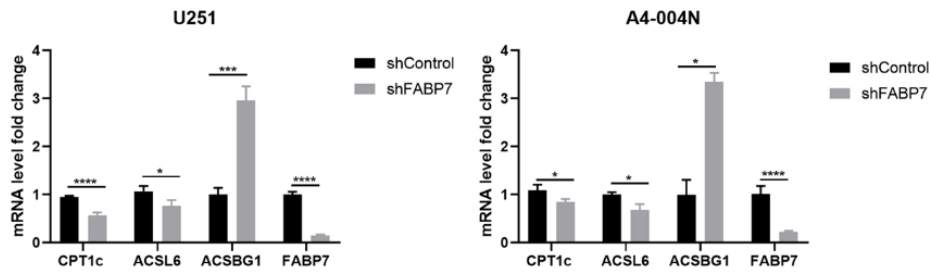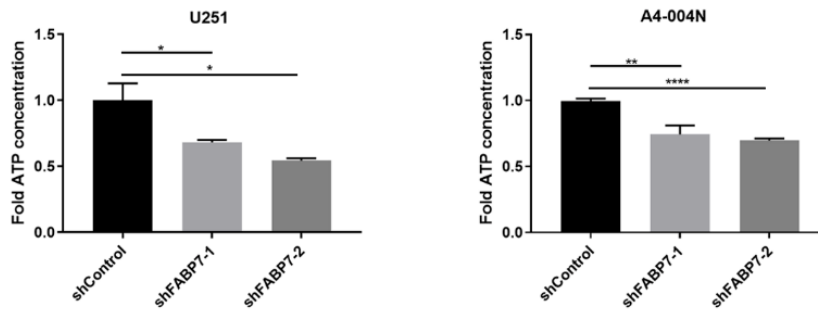
U251

A4-004N

Figure 4.2 FABP7 down-regulates mitochondrial fatty acid β-oxidation gene expression and ATP production in GBM cells.

(A) U251 and A4-004N cells were infected with lentivirus control shRNA or FABP7 shRNA constructs. Cells were FABP7-depleted by >80%. *CPT1c* and *ACSL6* mRNA levels were down-regulated, whereas *ACSBG1* were up-regulated in FABP7-depleted GBM cells. (B) ATP production was reduced by 30-40% in FABP7-depleted U251 and A4-004N cells compared to control cells. ATP levels are based on cell numbers. Statistical analyses were carried out using the two-tailed unpaired *t*-test. N=3. Error bars represent standard deviation (SD). * indicates $p < 0.05$, ** indicates $p < 0.01$, *** indicates $p < 0.001$, and **** indicates $p < 0.0001$. n.s., not significant.

186

4.3.3 FABP7 upregulates phospholipase expression

When long chain fatty acids are converted into fatty acid acyl-CoA by ACSL6 and ACSBG1, they can be used for a number of purposes, including plasma membrane phospholipid recycling which is essential for the maintenance of high levels of AA and DHA in brain phospholipid membranes (Bazinet and Laye, 2014). In turn, esterified AA and DHA in phospholipid membranes can be hydrolyzed by PLA_2, as part of the Lands' cycle mentioned in the introduction to this chapter. Calcium-dependent cytosolic PLA_2 ($cPLA_2$), a phospholipase highly expressed in GBM tissues, is responsible for triggering the release of esterified AA from membrane phospholipids (Clark et al., 1995). $iPLA_2$ has been previously reported to be responsible for the selective hydrolysis of DHA from the sn-2 position in phospholipids (Rosa and Rapoport, 2009). We therefore investigated the effect of FABP7 and its fatty acid ligands AA and DHA, on the expression levels of $cPLA_2$ and $iPLA_2$ in GBM cells.

The establishment of stable U87 control (U87C) and U87-FABP7 expressing (U87B) cell lines has been described in a previous publication (Mita et al., 2007). U87C and U87B cells were treated with BSA (control), 60 µM AA or 60 µM DHA for 24 hours. Western blot analysis revealed the presence of a slower-migrating band unique to U87B cells. This band was observed in U87B control cells as well as U87B cells cultured in AA- and DHA-supplemented media (**Figure 4.3A**). Our results also show that U87B cells have higher levels of $iPLA_2$ than U87C cells, with DHA supplementation in U87B cells decreasing levels of $iPLA_2$ (**Figure 4.3A**). The latter suggests that DHA supplementation in U87B cells decreases the release of DHA from phospholipid membranes.

We next examined whether the upper $cPLA_2$ band observed in U87B cells represents a phosphorylated product of cPLA2. Treatment of lysates with lambda phosphatase indicates that the upper $cPLA_2$ band may indeed represent a phosphorylated form of $cPLA_2$ (**Figure 4.3B**). $cPLA_2$ has previously been shown to be activated by phosphorylation of serine residues (Pavicevic et al., 2008) When $cPLA_2$ is activated, it is translocated from the cytosol to the membrane where its substrate, phospholipid, is located (Klapisz et al., 1999). We therefore examined the localization of $cPLA_2$ in U87C and U87B cells by immunofluorescence analysis using the WGA-Texas Red membrane marker. We observed dramatically increased localization of $cPLA_2$ to membranes in U87B compared to U87C cells (**Figure 4.3C**).
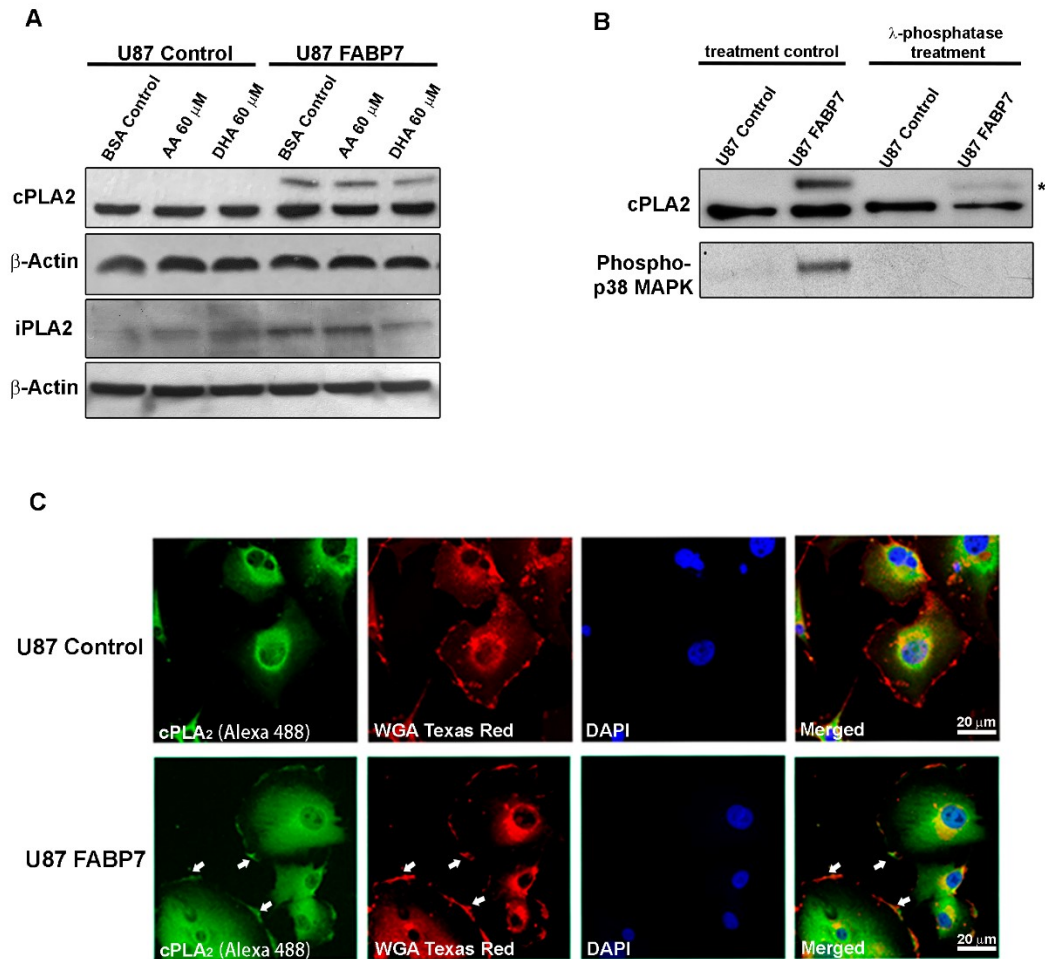
Figure 4.3 FABP7 regulates plasma membrane phospholipase expression and localization.

(A) Western blot analysis of cPLA2 and iPLA2 in U87B and U87C cells treated with BSA control, 60 μM AA or 60 μM DHA. cPLA2 in U87B cells shows an extra upper band compared to U87C cells, with no change in this upper band observed upon AA or DHA supplementation. iPLA2 is induced by FABP7 expression, with DHA supplementation decreasing iPLA2 protein levels in U87B cells. β-actin was used as the loading control. (B) Treatment of cell lysates with lambda phosphatase indicates that the upper cPLA2

band may represent the phosphorylated form of cPLA$_2$ (shown by asterisk). Phospho-p38 MAPK served as a positive control for the lambda phosphatase assay. (C) U87C and U87B cells were co-stained with an antibody to cPLA$_2$ and WGA Texas Red (membrane marker). Significant co-localization of cPLA2 and WGA Texas Red was observed in U87B but not in U87C cells (shown by arrows). Scale bar = 20 μm. N=3.

4.3.4 FABP7 localizes to A4-007N mitochondria

In Chapter 2, we showed that FABP7 localizes to GBM mitochondria in U251, ED501N and A4-004N cells. Here, we use the highly-infiltrative A4-007N cell line, which expresses abundant FABP7, to further investigate the subcellular localization of FABP7. A4-007N cells form neurospheres which gradually adhere to plastic and form interconnections between clumps of neurospheres (**Figure 4.4A**). As mentioned earlier, A4-007N expresses elevated levels of FABP7 and mitochondrial fatty acid β-oxidation genes *CPT1c*, *ACSL6* and *ACSBG1*.

In addition to mitochondria, peroxisomes and lipid droplets are the main organelles involved in lipid metabolism, with roles in long chain fatty acid metabolism and lipid storage, respectively (Lodhi and Semenkovich, 2014; Olzmann and Carvalho, 2019). We therefore carried out co-(immuno)staining of A4-007N cells with FABP7 antibody and organelle-specific markers (ADRP antibody for lipid droplets, ACOX-1 antibody for peroxisomes and Mitotracker^{TM} Deep Red for mitochondria) (**Figure 4.4B**). Co-localization of organelle markers with the FABP7 signal was determined using Pearson's correlation and ImageJ software. The best correlation was observed between FABP7 and

Mitotracker^{TM} Deep Red (r=0.752), followed by the peroxisome marker ACOX-1 (r=0.598). The correlation coefficient for FABP7 and ADRP was lowest (r=0.377) (**Figure 4.4C**).

Next, we cultured A4-007N in BSA (control), 30 µM AA, or 30 µM DHA and quantified the correlation between FABP7 and mitochondria signals (**Figure 4.4D**). We observed a 2-fold increase in mitochondrial-localized FABP7 signal intensity upon DHA treatment (**Figure 4.4E**). An increase in mitochondria/FABP7 co-localization was also observed in AA-supplemented medium, but was of considerably lower magnitude, in the range of 15% increase. We then used Mander's M1 and M2 colocalization coefficients to further analyse the correlation between FABP7 and mitochondrial signals. M1 represents the FABP7 signal that localizes with the mitochondria signal, whereas M2 represents the mitochondrial signal that overlaps with the FABP7 signal. In BSA (control) culture conditions, the M2 coefficient showed 49.5% mitochondria/FABP7 colocalization whereas the M1 coefficient showed 26.6% FABP7/mitochondria colocalization. Both M1 and M2 were significantly increased upon DHA treatment, with M1 and M2 coefficients of 39.2% and 77.4%, respectively (**Figure 4.4E**). No increases in M1 and M2 coefficients were observed in AA-supplemented culture conditions. The higher colocalization coefficient observed for M2 compared to M1 suggests that FABP7 localizes to sites other than mitochondria. Part of this difference could be accounted for by FABP7 colocalization to peroxisomes, as shown in **Figure 4.4B and 4.4C**. Together, our results indicate that FABP7 predominantly localizes to mitochondria in A4-007N neurosphere cultures, and that DHA significantly increases FABP7 localization to mitochondria.

A

B

Lipid droplets

DAPI | FABP7(Alexa 555) | ADRP(Alexa 647) | Merged | 40 μm

Mitochondria

DAPI | FABP7(Alexa 555) | Mitotracker(Deep Red) | Merged | 40 μm

Peroxisome

DAPI | FABP7(Alexa 555) | ACOX-1(Alexa 647) | Merged | 40 μm

C

Colocalization with FABP7

Pearson's correlation coefficient
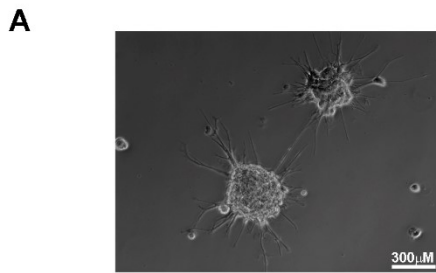
Lipid droplets
Mitochondria
Peroxisome

192
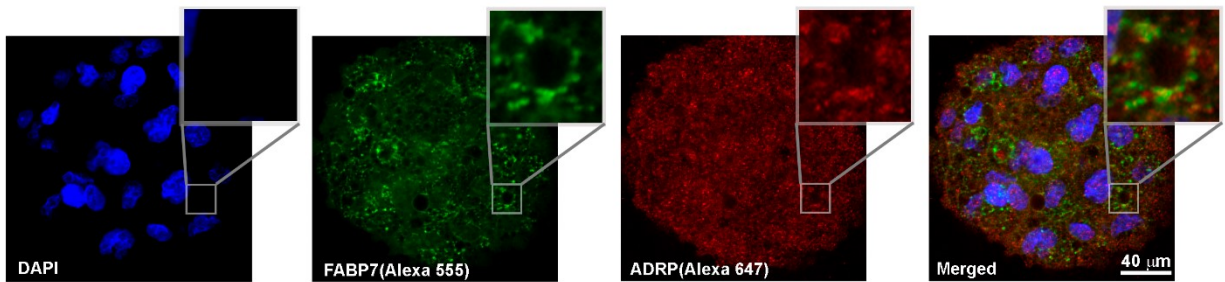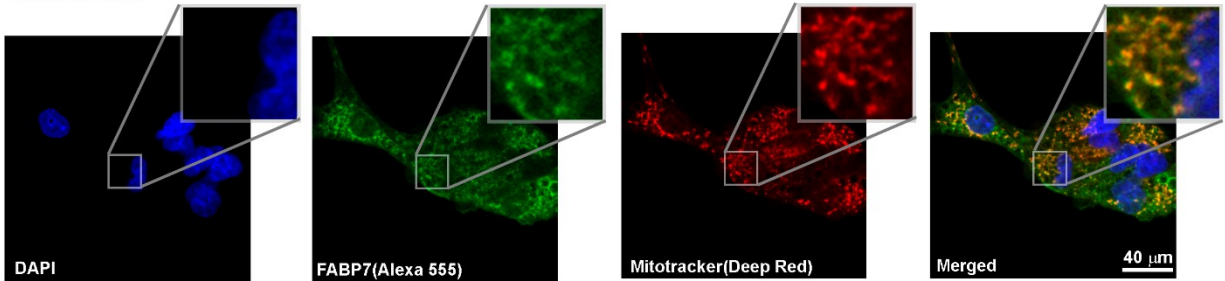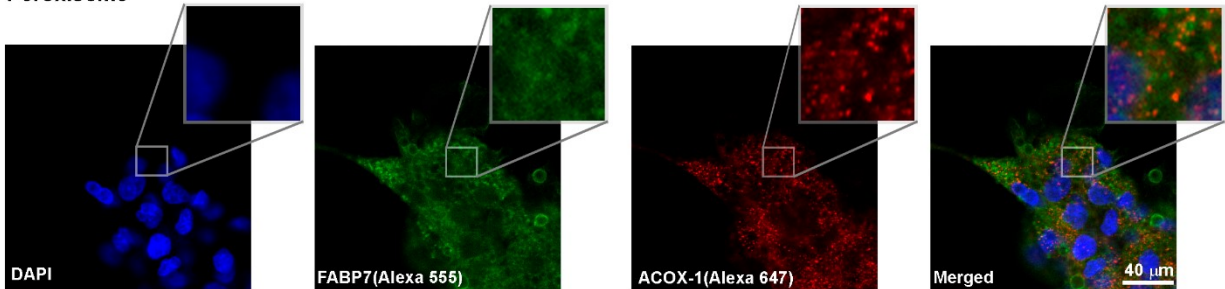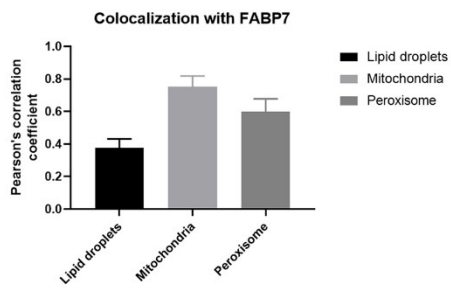
D

BSA control
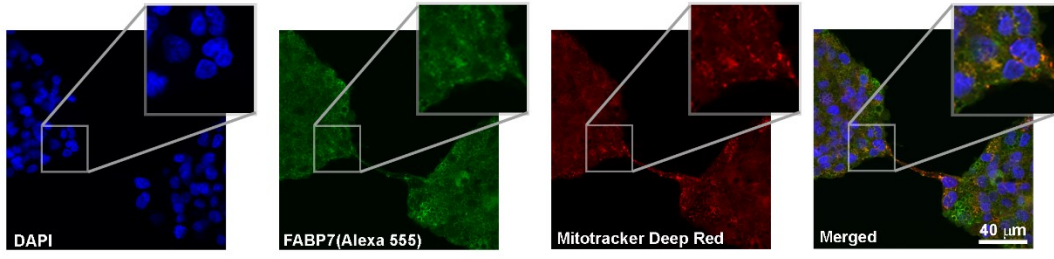
AA 30 μM
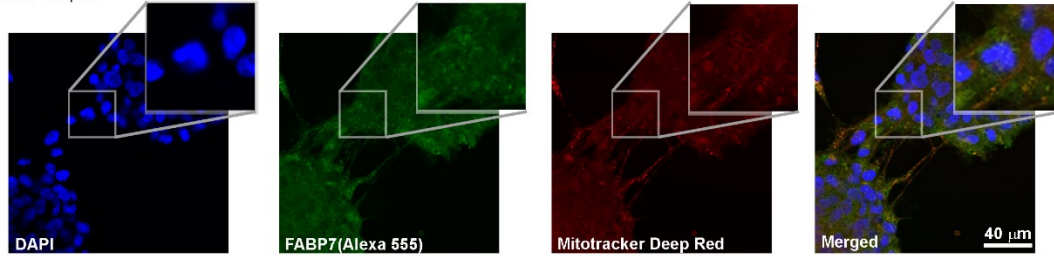
DHA 30 μM
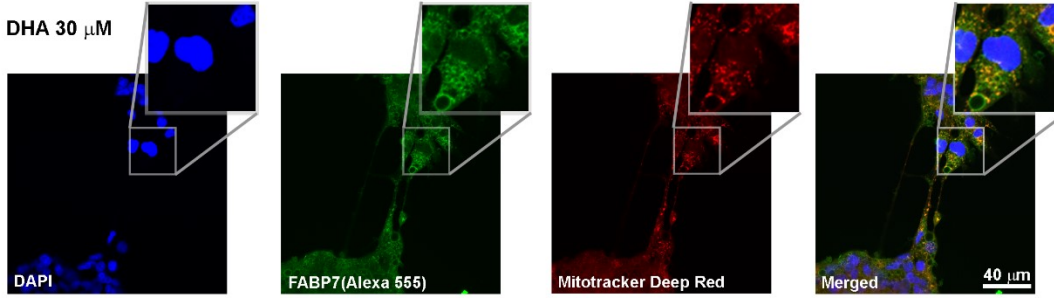
E
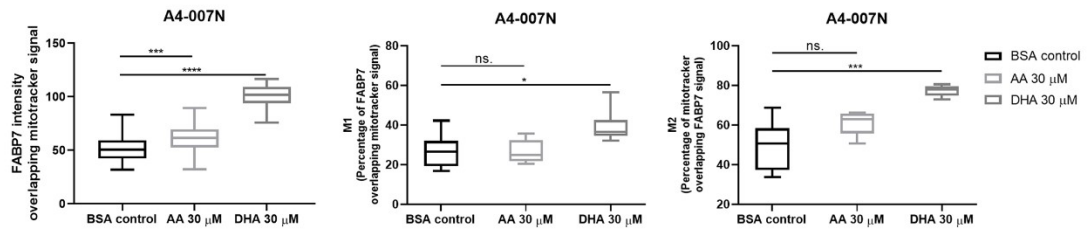
Figure 4.4 FABP7 localizes to A4-007N mitochondria.

(A) A4-007N GBM cells form neurospheres with extended microtubes. Scale bar = 300 µm. A4-007N cells were co-(immuno)stained with FABP7 antibody and lipid droplet marker (ADRP antibody), mitochondria marker (Mitotracker™ Deep Red) or peroxisome marker (ACOX-1 antibody). Representative images are shown in (B), and the panels on the top-right corner show magnified images. Scale bar = 40 µm. (C) Pearson correlation coefficients for FABP7 and organelle markers colocalization analysis. The best correlation coefficient was observed for FABP7 and Mitotracker™ Deep Red (r=0.752). (D) A4-007N cells were cultured in medium supplemented with BSA (control), 30 µM AA, or 30 µM DHA, and then co-stained with FABP7 and Mitotracker™ Deep Red. Representative images are shown, and the panels on the top-right corner show magnified images. Scale bar = 40 µm. (E) Quantification of mitochondrial and FABP7 average signal intensities in A4-007N cells under BSA (control), 30 µM AA or 30 µM DHA culture conditions (left panel). Mander's correlation coefficients (M1 and M2) for FABP7 and mitochondria colocalization are shown in the middle and right panels. Both quantitative intensity analysis and colocalization analysis indicate that DHA supplementation increases FABP7 localization to mitochondria in A4-007N cells. Statistical analysis of signal intensities and M1 and M2 coefficients was using the two-tailed unpaired *t*-test. N=3, with 6 representative images analyzed for each condition. Error bars represent standard deviation (SD). Center line, median; box limits, 25th and 75th percentiles; whiskers, minimum to maximum. * indicates $p < 0.05$, ** indicates $p < 0.01$, *** indicates $p < 0.001$, and **** indicates $p < 0.0001$. n.s., not significant.

4.3.5 FABP7 localizes to GBM mitochondria in microtubes

GBM cells extend long membrane protrusions, called microtubes, which serve an intercellular connection channels. When we stained A4-007N with Mitotracker™ Deep Red and FABP7 antibody, we observed abundant mitochondria with high levels of FABP7 throughout the microtubes (**Figure 4.5A**). These results suggest intercellular transport of FABP7-carrying mitochondria via microtubes.

We further investigated FABP7 expression in microtubes using an *in vivo* model. A4-007N cells were intracranially injected into NSG mice to establish GBM xenograft tumours. A4-007N formed highly infiltrative tumours in NSG mouse brain, with FABP7 expressed in both the tumour core and infiltrative regions (**Figure 4.5B**). Interestingly, the infiltrative regions of the tumours expressed high levels of nuclear FABP7, with abundant FABP7 found in microtubes (see arrows). In contrast, FABP7 was predominantly found in the cytoplasm of tumour cells in the core region. We also co-stained xenograft tumour tissue with anti-FABP7 antibody and Mitotracker™ Deep Red, and obtained similar results to those observed *in vitro*, with co-localization of FABP7 and mitochondria in microtubes (**Figure 4.5C**).
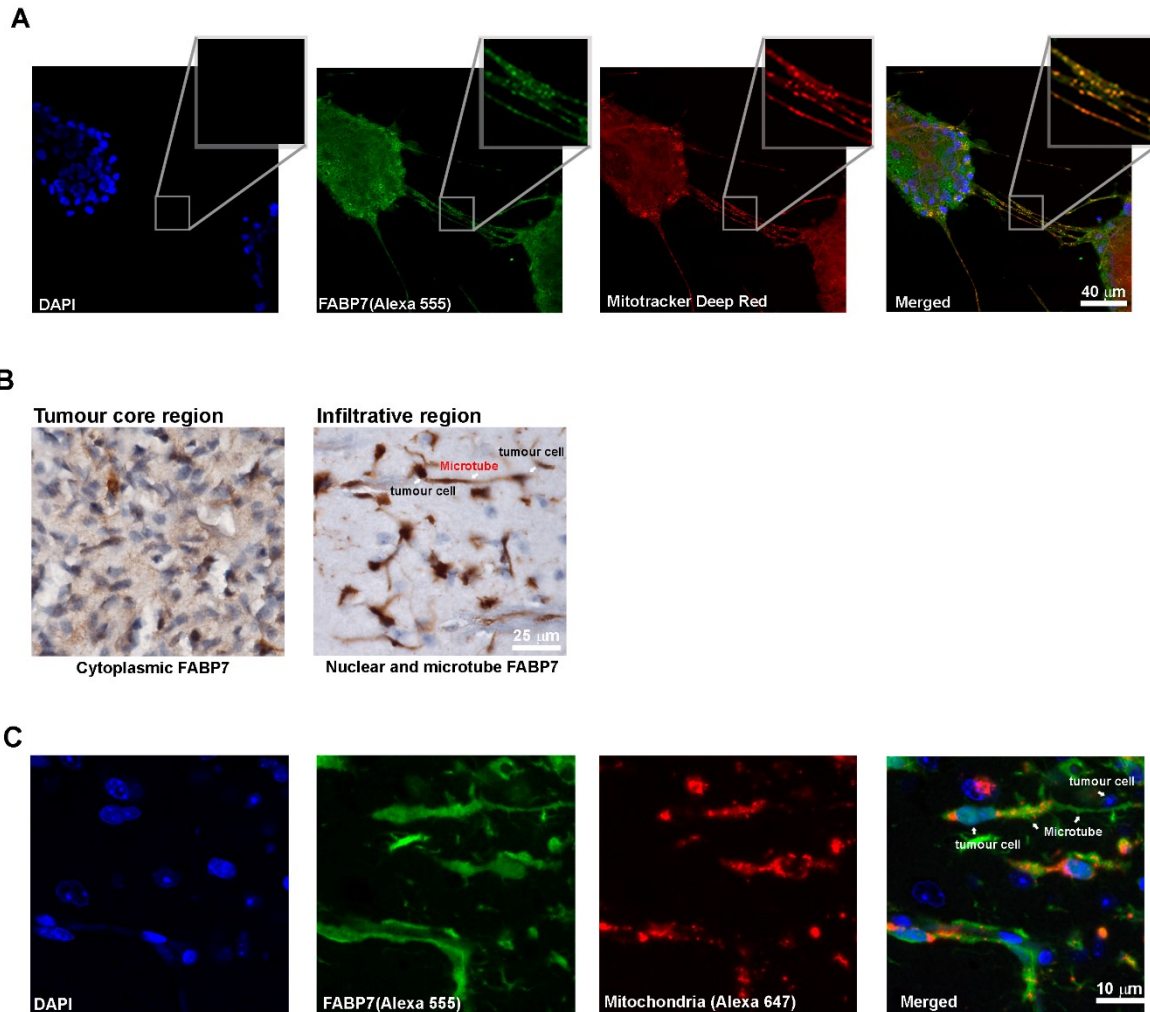
Figure 4.5 FABP7 localizes to mitochondria in microtubes.

(A) Co-staining of A4-007N cultures with FABP7 antibody and Mitotracker™ Deep Red revealed abundant FABP7 in the microtube mitochondria. Representative images are shown, and the panels on the top-right corner show magnified images. N=3. Scale bar = 40 μm. (B) A4-007N xenograft tumour tissue was immunostained with anti-FABP7 antibody, followed by EnVision+ System anti-rabbit HRP-labeled polymer. Tumour cells in the core region expressed primarily cytoplasmic FABP7, whereas tumour cells in

infiltrative regions primarily expressed FABP7 in the nucleus as well as microtubes (shown by arrows). Scale bar = 25 μm (C) A4-007N xenograft tumour tissue was co-immunostained with FABP7 antibody and anti-human mitochondria antibody (detected with Alexa 488 anti-rabbit secondary antibody and Alexa 647 anti-mouse secondary antibody, respectively) FABP7 was found in both the nuclei and microtube mitochondria of tumour cells located in the infiltrative regions (shown by arrows). Scale bar = 10 μm. Brain tissues from three A4-007N xenograft mice were analysed, with representative images shown.

4.3.6 FABP7 depletion inhibits A4-007N microtube formation

GBM microtubes are believed to contribute to tumour invasion/migration, by acting as channels for intercellular nutrient exchange or shuttling of tumour cells to tumour cell-free regions, contributing to GBM tumour recurrence. Although we have shown that FABP7 plays an important role in GBM neural stem-like cell migration *in vitro*, the importance of FABP7 in GBM microtube formation is not known. To address this question, we depleted FABP7 in A4-007N cells using lentiviral vectors. We then used bright field images to quantitate the effect of FABP7 depletion on microtube formation. We observed dramatic changes in the appearance of A4-007N neurospheres in cells that were infected with lentiviral vectors carrying two different FABP7 shRNAs compared to cells infected with a control lentiviral vector (**Figure 4.6A**). Not only was microtube formation greatly reduced, but neurosphere size was reduced as well, suggesting reduced growth of A4-007N cells (**Figure 4.6B**).
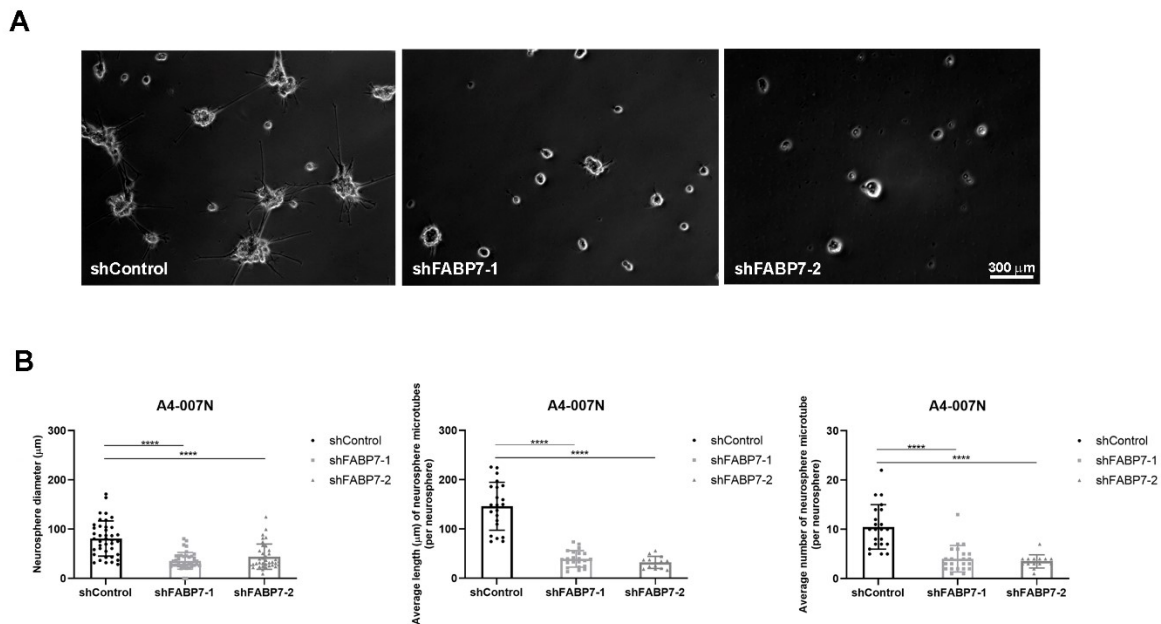
Figure 4.6 FABP7 depletion inhibits GBM microtube formation.

(A) FABP7 depletion reduces microtube formation in A4-007N cells. Representative images of lentivirus-infected A4-007N cells (shControl and shFABP7) were obtained using a digital imaging microscope 7-10 days after cell seeding. Scale bar = 300 µm. (B) Quantification analysis shows that neurosphere size, the length and the number of microtubes, are all reduced in FABP7-depleted A4-007N cells. Neurosphere images (neurosphere size, microtube length and number) were analyzed with ImageJ software after setting the measurement scale (e.g., microtubes defined as protrusions/processes connecting 2 independent neurospheres with length >5 µm). Statistical analysis of quantitative data was performed using the two-tailed unpaired t-test. N=3, with 6 representative images analyzed for each condition in each independent experiment. Error bars represent standard deviation (SD). * indicates $p < 0.05$, ** indicates $p < 0.01$, *** indicates $p < 0.001$, and **** indicates $p < 0.0001$. n.s., not significant.

4.4 Discussion

Human GBM cells have been reported to oxidize fatty acids to maintain mitochondrial oxidative phosphorylation activity, particularly under the serum-free conditions used to culture GBM neural stem-like cells (Lin et al., 2017). Here we show that the following three fatty acid β-oxidation genes are preferentially up-regulated in GBM: *CPT1c*, *ACSL6* and *ACSBG1*. All three genes are involved in key steps in the long chain fatty acid β-oxidation pathway in mitochondria, either in long chain fatty acid mitochondrial transport or synthesis of long-chain fatty acid acyl-CoA. Expression of these genes also correlates with a high tumourigenic potential in GBM (Saurty-Seerunghen et al., 2019).

CPT1c is expressed in neurons (Price et al., 2002) and a number of cancer types, including breast cancer, lung cancer and glioblastoma (Price et al., 2002; Wakamiya et al., 2014). Cancer cells expressing CPT1c show increased fatty acid β-oxidation, ATP production and resistance to glucose deprivation (Zaugg et al., 2011). Although CPT1c is widely expressed in GBM tumour tissues, its specific role in GBM has yet to be defined. We show that GBM stem-like cells express higher levels of *CPT1c* compared to their differentiated counterparts *in vitro*, suggesting a need for increased long chain fatty acid β-oxidation in GBM neural stem-like cells. In support of an upstream role for FABP7 in fatty acid metabolism, FABP7 depletion not only reduces *CPT1c* mRNA levels in GBM neural stem-like cells, but also decreases ATP production and lipid droplet formation. FABP7 has recently been shown to interact with ATP-citrate lyase (ACLY) in astrocytes, an enzyme that converts citrate into acetyl-CoA (Kagawa et al., 2020). Acetyl-CoA is a key intermediate that quickly enters the tricarboxylic acid (TCA) cycle for energy production, and acetyl-CoA can be produced by both glycolysis and fatty acid β-oxidation

in cancer cells (Koundouros and Poulogiannis, 2020). In GBM cells, the uptake of exogenous fatty acids has previously been shown to result in accumulation of lipid droplets in an FABP3/7 dependent manner (Bensaad et al., 2014). The subsequent increase in fatty acid mitochondrial β-oxidation and acetyl-CoA production resulting from lipid droplet accumulation could provide a valuable source of ATP for GBM tumour growth. Future work will address whether FABP7 is directly involved in long chain fatty acid β-oxidation and acetyl-CoA production.

Non-esterified DHA and AA can be converted to fatty acid acyl-CoAs by long chain fatty acid acyl-CoA synthetases, such as ACSL6 and ACSBG1. Human brain RNAseq data indicate that ACSL6 and ACSBG1 are the most abundant acyl-CoA synthetases in astrocytes (Fernandez and Ellis, 2020). Once converted into acyl-CoA derivatives, DHA and AA can then enter various metabolic pathways, including mitochondrial fatty acid β-oxidation, phospholipid synthesis or plasma membrane fatty acid recycling via Land's cycle (Lacombe et al., 2018). ACSL6 displays a high affinity for DHA and plays an essential role in the DHA-rich brain enrichment (Fernandez et al., 2018; Van Horn et al., 2005). Our data indicate that FABP7 depletion reduces *ACSL6* RNA levels, suggesting that FABP7-mediated DHA transport may be an important regulator of DHA enrichment via ACSL6 in GBM cells. ACSBG1 is another acyl-CoA synthetase which shows specificity for long chain fatty acid β-oxidation. The opposite effects observed on *ACSL6* and *ACSBG1* expression upon FABP7 depletion may reflect compensatory mechanisms to ensure GBM cell survival.

The brain is especially enriched in two PUFAs, DHA and AA. Upon entry into the brain, both DHA and AA are esterified to phospholipid membranes (Bazinet and Laye,

2014). We show that AA and DHA-specific phospholipases, cPLA$_2$ and iPLA$_2$, respectively, key to the removal of AA and DHA from membrane phospholipids, are activated upon FABP7 expression through either phosphorylation (cPLA$_2$) or up-regulation (iPLA$_2$). A recent breast cancer study demonstrated that cPLA$_2$ activation (i.e., phosphorylation and elevated activity) is directly correlated to increased levels of non-phospholipid-incorporated AA and its downstream eicosanoids, which enhance tumorigenicity (Koundouros et al., 2020). Thus, the cPLA$_2$ activation that we observed in FABP7-expressing GBM cells could lead to increased levels of AA and its downstream eicosanoid effectors in GBM as well, further promoting tumour growth.

In addition to cPLA$_2$ activation, we also observed increased iPLA$_2$ levels in FABP7-expressing U87 GBM cells (control BSA and AA-supplemented) compared to control U87 cells. Increased iPLA$_2$ can reduce plasma membrane phospholipid DHA content. However, removal of DHA from GBM plasma membrane phospholipids by iPLA$_2$ may not result in increased levels of DHA metabolites because the GBM microenvironment is AA-rich. Importantly, our Chapter 3 results indicate that FABP7 expression itself does not alter either the AA or DHA content in the phospholipids of GBM cells cultured in AA- and DHA-supplemented media. However, FABP7 expression can increase the uptake of AA and DHA from the microenvironment. Thus, while our results suggest increased removal of AA and DHA from the plasma membrane phospholipids of FABP7-expressing GBM cells, these results must be examined in the context of increased uptake of AA and DHA in FABP7 expressing cells. We postulate that in the GBM AA-rich microenvironment, FABP7 expression promotes formation of non-esterified AA, activation of AA-metabolizing enzymes and increased production of AA metabolites which enhance GBM

cell migration and tumour infiltration. By increasing the DHA content in the GBM microenvironment, it may be possible to increase the production of DHA metabolites which are generally anti-tumorigenic.

Hoang-Minh *et al.* reported that intracranial xenotransplantation of slow-cycling GBM cells (i.e., likely GBM neural stem-like cells) that highly express FABP7 generated a network of invasive cells with long processes that are consistent with GBM microtubes (Hoang-Minh et al., 2018). Subsequent experiments have revealed the importance of availability of long-chain fatty acyl-CoAs to mitochondria and fatty acid oxidation in promoting the aggressive properties of GBM neural stem-like cells (Duman et al., 2019). In Chapter 2, we first reported that FABP7 localizes to mitochondria in GBM cells cultured under neurosphere (serum-free) conditions. In this Chapter, we use highly infiltrative A4-007N to show that FABP7 is also found in mitochondria located in microtubes that connect cells located at long distances from each other. It is already known that mitochondria can travel quickly in microtubes (Osswald et al., 2015). Furthermore, it is well-established that ATP has limited diffusion capacity in the cytosol and particularly within long neuronal processes (Sheng and Cai, 2012). One may therefore postulate that at least one of the functions of mitochondria found within microtubes is related to energy production. In light of FABP7's role as a regulator of mitochondrial oxidative phosphorylation and lipid droplet formation in slow-cycling GBM cells (Hoang-Minh et al., 2018), we propose that FABP7 promotes fatty acid β-oxidation within GBM neural stem-like cell microtubes to provide sufficient energy for long-distance invasion/migration.

Another potential role for FABP7 in mitochondria may be through mitochondrial phospholipid remodelling. Cardiolipin is a mitochondria-specific phospholipid (~20% of

the total phospholipid content) (Daum, 1985). Several mitochondrial protein complexes that are essential for mitochondrial energy production, such as respiratory chain supercomplexes (Pfeiffer et al., 2003) and the ADP/ATP translocase (Claypool et al., 2008) require cardiolipin. Interestingly, with the exception of oleic acid (OA), brain cardiolipins are mostly made up of long-chain polyunsaturated fatty acids (i.e., AA and DHA) compared to other tissues (Oemer et al., 2020). Thus, we postulate that FABP7 may transport its fatty acid ligands to GBM mitochondrial cardiolipins, thereby facilitating mitochondrial oxidative phosphorylation and energy production necessary for tumour survival. Our future studies will involve using fluorescently-tagged FABP7 and fluorescently-tagged FABP7 ligands to investigate the dynamics of mitochondria phospholipid remodelling using super-resolution microscopy.

Metabolic reprogramming is becoming a recognized feature of GBM neural stem-like cells, with the latter using mitochondrial oxidative phosphorylation rather than glycolysis for their energy production. Key players in metabolic reprogramming such as FABP7 and FABP7-related fatty acid metabolic pathways and lipid metabolites may represent therapeutic targets for GBM. We thus propose that a better understanding of the role of FABP7 and its ligands DHA/AA in regulating GBM fatty acid metabolism (e.g., fatty acid β-oxidation, phospholipid remodelling, oxidative phosphorylation and energy production), particularly in GBM neural stem-like cells, will shed light on the development of new strategies for mitigating GBM migration/invasion.

Chapter 5.

Discussion and future directions

5.1 Discussion

5.1.1 GSCs at invasive niches, a main obstacle in curing GBM

To date, the standard approach to the treatment of newly diagnosed GBM includes surgery followed by concurrent radiotherapy with TMZ, and further adjuvant TMZ. In spite of decades of innovative therapies and clinical trials, GBM remains the most aggressive and incurable malignant disease with the short 5-year patient survival of 5% and a 14.6-month median survival time (Ostrom et al., 2020). Multiple factors contribute to GBM therapeutic resistance and early recurrence, such as a highly infiltrative nature and tumour heterogeneity, which attenuates the effectiveness of current therapies. The infiltration of GBM into surrounding brain parenchyma beyond the tumour margins (Watanabe et al., 1992), and the long-distance tumour migration via intra-tumoral connections (e.g., microtubes) (Osswald et al., 2015), makes complete GBM surgical resection virtually impossible (Young et al., 2015).

GBMs exhibit a diffuse invasion pattern, even in the early disease stage. The standard initial management for GBM is maximal safe surgical resection, which allows for accurate GBM histological and molecular diagnosis, as well as a reduction in tumour volume. Gross total resection is generally recommended, and the extent of resection is one of the important predicting factors for progression-free survival (Tan et al., 2020). Several fluorescent dyes (e.g., fluorescein sodium) have been developed to improve the identification of the tumour edge during surgery, with confirmed safety and feasibility. These dyes improve the visualization of the tumour margins during tumour resection (Schebesch et al., 2013; Shinoda et al., 2003). In addition to new approaches for improving surgical resection margin visualization, GBM radiotherapy protocol applies a 2-

cm margin beyond the gadolinium-enhanced tumour margin, which is supported by patterns of first relapse showing on MRI (Sherriff et al., 2013).

A characteristic feature of GBM is its highly heterogeneous nature, and GSCs are the main contributors to this heterogeneity (Jin et al., 2017). Different subsets of GSCs have been identified in different tumour regions, which is recognized as intra-tumoral spatial heterogeneity (Bastola et al., 2020). There are three major GBM microenvironment niches, including the necrotic niche, perivascular niche, and invasive niche (Prager et al., 2020). In addition to GSCs locating at the necrotic and perivascular niches, GSCs located at the infiltrating edge of tumours all facilitate the therapeutic resistance of GBM (Bastola et al., 2020).

It has been reported that cancer stem cells display higher invasive potential compared to non-cancer stem cells (Cheng et al., 2011; Inoue et al., 2010). FABP7 is an important regulator of GBM infiltrative/invasive properties. It is highly expressed in GSCs and is found in cells located at the GBM perivascular niche, invasive niche, and tumour migratory leading edge (De Rosa et al., 2012; Mita et al., 2007). During normal brain development, FABP7 is expressed in radial glial cells and promotes the formation of the radial glia fiber system along which neurons migrate (Feng et al., 1994; Kurtz et al., 1994). Studies have shown that depletion of FABP7 in GSCs can reduce GBM tumour growth and invasion both *ex vivo* and *in vivo* (De Rosa et al., 2012). Our early studies also revealed that FABP7 regulates DHA-mediated inhibitory effects in GBM cell migration (Mita et al., 2010). Furthermore, the work described in both Chapters 2 and 3 further documents the inhibitory effect of DHA on FABP7-expressing GSCs and demonstrates that the effect of FABP7/DHA on the inhibition of migration occurs through alteration of

GBM membrane properties and distinct GSC lipid metabolism. Therefore, understanding the mechanisms underlying GBM migration and infiltration, particularly in FABP7-enriched GSCs, will most likely shed light on developing new strategies to manage GBM therapeutic resistance and recurrence.

5.1.2 Membrane remodeling promotes GBM aggressiveness

Phospholipids are the main components of membrane lipids. Many early studies have revealed that the lipid composition of the fatty acid acyl chains affects membrane properties, such as membrane fluidity (Spector and Yorek, 1985), membrane protein clustering and subsequent signaling transduction (e.g., growth factor signaling pathways) (Arkhipov et al., 2013; Erazo-Oliveras et al., 2018). In cancer cells, including GBM, the membrane phospholipid composition is often dramatically distinct from that of normal cells (Fernandez and Ellis, 2020; Martin et al., 1996; Swinnen et al., 2019). A recent study clearly demonstrates that increased saturated lipid membrane incorporation can promote EGFR-mediated GBM aggressive growth (Bi et al., 2019). Even though the brain has limited capacity to synthesize PUFAs *de novo*, dietary PUFAs are able to cross the blood-brain-barrier and modulate brain phospholipid composition (Bazinet and Laye, 2014). In this thesis, I show that ω-3 PUFA DHA treatment alters the ω-3:ω-6 ratio of GBM neural stem-like cell phospholipids, increases membrane fluidity and reduces GBM migration in a FABP7-dependent manner.

In Chapter 2, we show that FABP7 expression results in increased membrane rigidity that contributes to FABP7-mediated GBM invasion/migration in GSCs in an AA-rich/DHA-poor environment. In different cancer models, increased membrane rigidity is

tightly correlated with the formation of protrusions/processes during tumour migration (Guerra et al., 2016; Schwan et al., 2011). As well, our data support a role for FABP7 in promoting GBM neurosphere microtube formation, as shown in Chapter 4. As increased aggressiveness in GBM cells has recently been shown to be tightly linked to increased incorporation of saturated fatty acids in membranes (Bi et al., 2019), we first hypothesized that FABP7-mediated GBM cell migration could also be driven by elevated saturated fatty acid content in plasma membrane phospholipids. Interestingly, however, FABP7 expression does not alter the overall levels of saturated fatty acids in GBM cells (**Figure 5.1**, data derived from Chapter 3).

A4-004N

Legend:
- A4-004N shControl
- A4-004N shFABP7-1
- A4-004N shFABP7-2
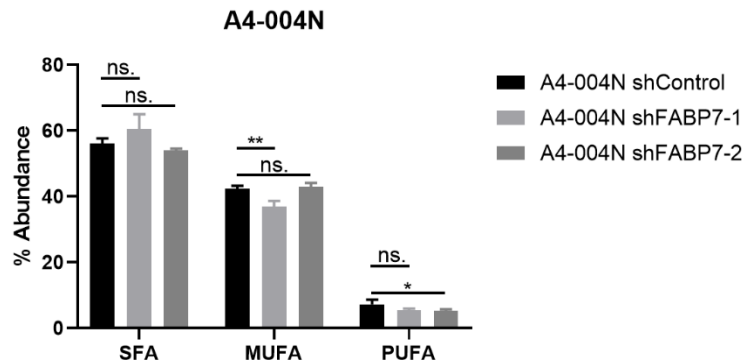
Figure 5.1 Effects of PUFA treatment on the incorporation of saturated fatty acids (SFA), monounsaturated fatty acids (MUFA) and polyunsaturated fatty acids (PUFA) into total phospholipids from A4-004N control and shFABP7 knockdown cells.

Percent abundance of SFA, MUFA and PUFA in total phospholipids are shown. * indicates $p < 0.05$, ** indicates $p < 0.01$. ns. indicates not significant.

Different mechanisms other than increased saturated fatty acid content could explain the observed FABP7-mediated increased GBM membrane rigidity. First, key structural components of liquid-ordered (Lo) domain, cholesterol and caveolin-1, are known regulators of plasma membrane fluidity (Abulrob et al., 2004; Murai et al., 2011). In this regard, FABP7 has been shown to regulate caveolin-1 function (Kagawa et al., 2015) and increase acetyl-CoA levels, a key intermediate for cholesterol biosynthesis in astrocyte models (Kagawa et al., 2020). Second, actin-cytoskeleton remodeling at the submembrane regions also contributes to higher membrane rigidity (Saarikangas et al., 2010). We have previously shown that FABP7 co-immunostains with cytoskeleton F-actin at the leading edge of GBM cells (Mita et al., 2007). These all suggest that FABP7-mediated alterations in GBM membrane fluidity could occur via different mechanisms.

Thus, understanding FABP7 and its direct effects on the formation of highly-ordered membranes, as well as the formation of GBM migratory protrusions and microtube formation, may lead to the identification of therapeutic targets that directly affect GBM migration and infiltration.

Even though both DHA and AA are long chain PUFAs, the differences in membrane fluidity (shown in Chapter 2) and membrane phospholipid composition (shown in Chapter 3) observed between AA- versus DHA-supplemented FABP7-expressing GBM cells is another interesting finding. Our results indicate that DHA treatment increased GBM membrane fluidity, but AA maintained GBM membrane rigidity (Chapter 2). The gas chromatography results described in Chapter 3 (**Figure 3**) showed that AA supplementation increased the AA content in GSC phospholipids by ~6.3-fold and decreased the ω-3:ω-6 PUFA ratio by ~2.5-fold; however, DHA supplementation increased the DHA content by ~18-fold and the ω-3:ω-6 PUFA ratio by ~8-fold. Although these differences between AA and DHA supplementation can be attributed to the virtual absence of DHA in neurosphere medium, it is clear that DHA supplementation can elevate plasma membrane DHA levels close to the AA levels observed upon AA supplementation.

We propose two possible mechanisms to explain the differences in AA and DHA effects on GBM cell membrane biophysical properties and migration. First, this could be due to the different properties of AA and DHA-containing phospholipids. For example, AA-containing phosphotidylethanolamine (PE) has been shown to be important for the function and formation of liquid ordered (Lo) domains (Pike et al., 2002; Rubio et al., 2018). In contrast, DHA incorporation in membranes disrupts Lo domain formation (Fuentes et

al., 2021; Teague et al., 2013). Our GC data only provide the total content of AA and DHA in phospholipids, without showing their nanoscale distribution and domain preference (i.e., Lo domain vs. Ld domain) upon phospholipid incorporation. This could be addressed by costaining Lo/Ld domain markers with fluorescence labelled DHA or AA. Second, the differences observed upon AA versus DHA supplementation could be related to the different effects of DHA and AA on actin-cytoskeleton remodeling. Several studies have revealed that AA supplementation increases F-actin subplasma membrane localization at the cell edges, or induces Rho-mediated cell motility pathways, in breast cancer and prostate cancer cells, respectively (Brown et al., 2014; Fiorio Pla et al., 2012). In contrast, DHA has been shown to inhibit the expression of actin-binding proteins (profilin 1 and cofilin-1) and reduce F-actin content, as well as reduce their localization to the leading edges of migratory lung cancer A549 cells and choriocarcinoma cells (Ali et al., 2016; Ali et al., 2019). Thus, our future directions will involve analysis of F-actin and actin-binding protein expression and studying their localization to the plasma membrane upon DHA/AA treatment in migratory FABP7-expressing GSCs.

5.1.3 Metabolic reprogramming in GBM neural stem-like cells

GBM cells at the infiltrative leading edge express GBM stem cell markers, such as L1 cell adhesion molecule (L1CAM), CD133, SOX-2 and Nestin, supporting the idea that these stem cells are indeed responsible for GBM invasion (Alonso et al., 2011; Ardebili et al., 2011; Cheng et al., 2011; Ishiwata et al., 2011). In addition to distinct molecular phenotypes, GSCs have a unique metabolic landscape, characterized by metabolic reprogramming and plasticity (Strickland and Stoll, 2017) so that the cells are less reliant

on glycolysis and more reliant on mitochondrial fatty acid β-oxidation (Duman et al., 2019; Hoang-Minh et al., 2018; Lin et al., 2017).

Several lipid metabolism genes show correlation with elevated mitochondrial oxidative phosphorylation (OXPHOS) in GSCs, such as FABP7 which contributes to the storage of long chain fatty acids in lipid droplets (Hoang-Minh et al., 2018) and acyl-CoA-binding protein (ACBP) which facilitates the transport of long-chain fatty acyl-CoAs to mitochondria (Duman et al., 2019). Hoang-Minh *et al.* showed that elevated OXPHOS activity in FABP7-expressing slow-cycling GBM populations (i.e., likely GBM neural stem-like cells) and the inhibition of FABP7 in GSCs prevents their migration and invasion using both *in vitro* assays and a xenograft orthotopic mouse model of GBM (Hoang-Minh et al., 2018). Lin *et al.* demonstrated that inhibition of carnitine acyltransferase I (CPT1), which is responsible for production of acylcarnitines from long-chain fatty acyl-CoA, using etomoxir, can decrease the oxygen consumption rate in GBM primary cultures (Lin et al., 2017). Duman *et al.* further showed that etomoxir reduces mitochondrial ATP production in GSC cultures and inhibits GBM tumour infiltration *in vivo* (Duman et al., 2019). These publications all support mitochondrial OXPHOS via fatty acid β-oxidation being a preferred energy source for GCSs. Thus, analyzing the transcriptional and metabolic features of GSCs located in GBM niches associated with infiltration, may provide novel strategies for GBM clinical management.

GBM tumours are characterized by infiltrative growth along white matter tracts and perivascular space (Cuddapah et al., 2014). Compared to the tumour core, we observed elevated levels of FABP7 along white matter tracts, surrounding blood vessels and at the leading edge of tumours in both GBM patient tissue (Mita et al., 2007) and A4-007N

orthotopic GBM xenograft tumours (data not shown). Recently, Bastola *et al.* used LC-MS/MS to compare proteins expressed at the GBM core versus infiltrative margin (Bastola et al., 2020). These authors found that FABP7 levels are increased ~10-fold in infiltrative margins compared to the tumour core. As mentioned earlier, FABP7 is important for forming the radial glia scaffold required for long-distance migration of neurons (Feng et al., 1994; Kurtz et al., 1994). Thus, thus we propose that GSCs have hijacked the FABP7-mediated neuronal cell migration mechanism for driving infiltration in GBM tumours.

Intriguingly, our data show that FABP7 is highly expressed in GBM microtubes, ultralong tubes that connect different parts of the tumour. FABP7 depletion prevents microtube formation in A4-007N cultures. These microtubes are reminiscent of the "microtube-like" radial glia fibers along which neurons migrate during brain development (Feng et al., 1994; Kurtz et al., 1994). Osswald *et al.* reported mitochondrial travelling within GBM microtubes, giving rise to the possibility that the mitochondria in microtubes serve as a regional source of energy for long-distance infiltration of GBM cells (Osswald et al., 2015). Here, we postulate that FABP7 along with its fatty acid ligands are involved in the fatty acid β-oxidation processes within these aggressive microtubes, such as elevated acylcarnitine production, mitochondrial OXPHOS and ATP production to support the migration/invasion of GBM.

5.2 Future Directions

5.2.1 Effect of FABP7 and its fatty acid ligands on plasma membrane remodeling

Plasma membranes are complex assemblies of lipids and proteins, and the dynamics and nanoscale distribution of these components have important implications for many cellular processes. Our current work has shown a correlation between membrane FABP7 nanoscale domain formation and increased GBM migratory properties, which can be disrupted upon FABP7-mediated DHA supplementation. However, our research to date has not generated mechanistic insight into how membrane FABP7 is involved in GBM plasma membrane remodeling, particularly the interaction with tumour migration-driven membrane proteins (e.g., Lo domain components and membrane-anchored cytoskeleton proteins). Future work will involve performing super-resolution STED microscopy with fluorescence-conjugated primary antibodies to investigate: (i) whether membrane-localized FABP7 interacts with known liquid-ordered (Lo) domain components, such as caveolin-1, EGFR and cholesterol (Maekawa et al., 2016), (ii) whether this interaction is affected by the presence of serum or different fatty acids (AA/DHA), and (iii) interaction between FABP7, GBM tumour processes/protrusions and membrane-anchored cytoskeleton proteins such as profilin 1 and cofilin-1. The above-stated experiments will be performed in non-permeabilized fixed GBM cells.

Further spatial and temporal nanoscale dynamics of lipid-protein and protein-protein interactions during GBM cell migration will be carried out using time-lapse live cell STED imaging (Eggeling et al., 2009). For these experiments, we will use fluorescence-labelled proteins (i.e., GFP-FABP7, GFP-caveolin1 and GFP-EGFR) and fluorescence-labelled lipids (e.g., Atto647-labelled phospholipid/cholesterol analogues) (Honigmann et

al., 2014a). Live-cell STED microscopy usually produces imaging data for structures that are moving more slowly than the required acquisition time. We will therefore use combined STED microscopy and fluorescence correlation spectroscopy (STED-FCS) for our experiments, as this will allow direct visualization of transient lipid-protein and protein-protein interactions at the nanoscale level (Honigmann et al., 2014a). We can also study the diffusion dynamics of FABP7 to further examine membrane-localized FABP7 at highly ordered-domains (a process called trapping diffusion) or the compartmentalized distribution of FABP7 along the actin cytoskeleton (a process called hop diffusion) by STED-FCS (Sezgin et al., 2019).

AA and DHA are highly hydrophobic molecules. Thus, by binding to FABPs for transport and conversion into fatty acid acyl-CoA, AA and DHA are solubilized within the aqueous intracellular environment and available for metabolic pathways (Bazinet and Laye, 2014). The cyclic integration and removal of fatty acids in plasma membranes is an essential process for fatty acid acyl-CoA metabolism and is governed by synergistic activity of specific phospholipases (PLAs) and lysophospholipid acyltransferases (LPLATs) (referred to as the Lands' cycle) (Lacombe et al., 2018). Both AA and DHA are esterified at the sn-2 position of membrane phospholipids and hydrolyzed by phospholipases $cPLA_2$ and $iPLA_2$, respectively, to release non-esterified-fatty acids from the plasma membrane. To explore the effects of FABP7 expression and AA/DHA supplementation on GBM plasma membrane phospholipid remodeling, we can perform enzymatic activity assays for $cPLA_2$ and $iPLA_2$ using the Cytosolic Phospholipase A_2 Assay Kit (abcam#133090) and the Calcium-independent Phospholipase A2 ELISA Kit

(MBS#7228069). These enzymatic assays could be used to further support our observation that FABP7 regulates $cPLA_2$ and $iPLA_2$ expression.

AA and DHA acyl-CoAs are reincorporated into membrane phospholipids by LPLATs. Lysophosphatidylethanolamine acyltransferase 2 (LPEAT2) is predominantly expressed in the brain, and has recently been reported to have high specificity and activity towards DHA acyl-CoA based on its membrane incorporation in mouse neuroblastoma cells (Eto et al., 2020). In turn, lysophosphatidylcholine acyltransferase 3 (LPCAT3) has been reported to facilitate the incorporation of AA into plasma membrane (Hashidate-Yoshida et al., 2015). Thus, the activity and expression levels of LPLATs can also be measured in GBM cells and GBM neural stem-like cultures upon FABP7 expression and AA or DHA supplementation, particularly for LPEAT2 and LPCAT3.

5.2.2 FABP7 and its fatty acid ligands effect on GBM energy production

In addition to plasma membrane, we are first to report a preferred localization of FABP7 to mitochondria in GSCs. Localization to mitochondria is increased upon DHA supplementation. We have not yet investigated the sub-mitochondrial localization of FABP7. The mitochondrial outer membrane is mainly responsible for critical transport functions (e.g., fatty acids and ions), whereas the mitochondrial inner membrane is where mitochondrial OXPHOS takes place (Kuhlbrandt, 2015). Fluorescence-labelled DHA (i.e., DHA-BODIPY), already shown to localize to the mitochondria of cardiomyocytes and lymphoma cells (Raza Shaikh and Brown, 2013; Teague et al., 2013), provides us with a real-time fatty acid imaging approach to study the subcellular location of DHA in GBM cells. Here, we hypothesize that DHA that is taken up by GBM cells can be transferred to

mitochondria for further β-oxidation and energy production. We will first perform STED microscopy or STED live-cell microscopy using DHA-BODIPY, fluorescence-conjugated primary antibodies/fluorescence-labelled protein for FABP7, mitochondrial outer membrane marker (i.e., Translocase of the outer mitochondrial membrane complex subunit 20, Tomm20) and/or mitochondrial inner membrane marker (i.e., Cytochrome C oxidase subunit 8A, COX8A) to determine the preferred sub-mitochondrial localization for FABP7 and DHA in GBM cells and GBM neural stem-like cultures.

The mitochondrial outer membrane is important for the exchange of metabolites and cations between the cytosol and mitochondria and contains transporter proteins and channel proteins (Gellerich et al., 2000). CPT1c is localized to the mitochondrial outer membrane, which is responsible for the rate-limiting step of mitochondrial fatty acid β-oxidation, converting fatty acid acyl-CoA to fatty acid acylcarnitine (Chen et al., 2017b). We have shown that CPT1c is highly expressed in GSCs. If we find that FABP7/DHA are located on the mitochondrial outer membrane, we will use fluorescence-conjugated primary antibodies to CPT1c and FABP7 to investigate whether FABP7 directly interacts with the CPT1c acylcarnitine transporter and whether the interaction is affected by DHA or AA supplementation. If we find co-localization of FABP7 with CPT1c, we will then extract acylcarnitines from our cells, followed by derivatization and LC-MS (Giesbertz et al., 2015; Meierhofer, 2019) to identify acylcarnitine species with the goal of quantifying production of DHA- or AA- acylcarnitines in FABP7-expressing/depleted GSCs. The existence of DHA- or AA acylcarnitines will provide direct evidence that DHA or AA undergoes β-oxidation.

The mitochondrial inner membrane is mainly loaded with proteins involved in electron transport and ATP synthesis. Cardiolipin is a mitochondrial-exclusive phospholipid located at the inner mitochondrial membrane, which is involved in the organization and proper function of respiratory chain supercomplexes and Complex V (ATP synthase). Lipidomic studies have shown that brain cardiolipin has a high percentage of AA and DHA (Kant et al., 2020). Cardiolipin has been reported to be a preferred phospholipid for DHA incorporation (Raza Shaikh and Brown, 2013). The Cardiolipin dye, 10-Nonyl acridine orange (NAO, Thermo Fisher, #A1372) (Garcia Fernandez et al., 2004), has recently been demonstrated to be photo-stable with STED microscopy (Wolf et al., 2019). If FABP7/DHA are located in the mitochondrial inner membrane, future experiments will involve STED live-cell microscopy and/or STED-FCS with fluorescence-labelled FABP7, fluorescence-labelled DHA (e.g., DHA-BODIPY), and cardiolipin NAO dye to study the sub-mitochondrial localization of FABP7/DHA, and their potential interaction with cardiolipin.

The mitochondrial inner membrane consists of cristae and boundary membranes. ATP is produced in mitochondria cristae. We have shown that FABP7-depleted GBM cells produce lower levels of ATP compared to control cells. As mitochondrial membrane potential ($\Delta\Psi$m) is the key driver for oxidative phosphorylation (OXPHOS) and ATP synthesis, we will co-stain fluorescence-labelled FABP7 and DHA-BODIPY with $\Delta\Psi$m-dependent dye tetramethylrhodamine ethyl ester (TMRE, Thermo Fisher, #T669) using STED live-cell microscopy and perform quantification analysis (Wolf et al., 2019). Results from these experiments may provide us with mechanistic insight into the effect of FABP7 and DHA on mitochondrial OXPHOS in GBM cells and GSCs. Further experiments can

include ATP-linked respiration measurement (using High-Resolution Respirometry; Oxygraph-2k) using the inhibitor of CPT, etomoxir, to specifically measure alterations in respiration and OXPHOS derived from fatty acid β-oxidation.

We also observed abundant FABP7 in A4-007N GBM microtubes, specifically in mitochondria. Osswald *et al.* showed that mitochondria are transported through GBM microtubes. So far, we have observed FABP7 in microtubes using fluorescence-labelling in fixed A4-007N; however, we still need to see whether FABP7 is bound to its ligands in microtubes. Fluorescence-labelled DHA (e.g., DHA-BODIPY) has been shown to have a similar distribution pattern as untagged DHA and can be used in both fixed cells and for live cell imaging (Teague et al., 2013). Future experiments will involve carrying out the immunostaining experiments described above in A4-007N GBM cells to determine whether FABP7 and its ligands can be transported across microtubes. A4-007N GBM live cell imaging will be performed with fluorescence-labelled FABP7, fluorescence-labelled DHA (e.g., DHA-BODIPY) and fluorescence-labelled mitochondria (CellLight Mitochondria-GFP, BacMam 2.0, Life Technologies) using STED microscopy to examine the importance of FABP7 and its ligands in mitochondria transfer via microtubes.

5.2.3 Quantification of FABP7 PUFA ligand metabolites

In additional to mitochondria energy production, DHA and AA can be metabolized into bioactive docosanoids/eicosanoids by COXs/LOXs/CYP450 families located in ER, which have been shown and notably highlighted for their anti-inflammatory/pro-inflammatory effects within the brain (Bannenberg and Serhan, 2010). DHA-derived lipid mediators are often referred to as specialized pro-resolving mediators (SPMs), such as

series DHA-derived resolvins (RvDs), protectin/neuroprotectin (PD/NPD) and maresins (MaRs) for their potent neural protective and anti-inflammatory effects (Lin et al., 2017). Thus, we will perform LC-MS to identify and quantify AA and DHA mediators upon AA and DHA supplementation in FABP7-expressing and FABP7-depleted GBM cells. Then we will further assess the effects of identified SPMs on GBM cell migration and aggressive properties of GSCs.

5.3 Significance

Glioblastoma is a devastating brain disease. The early stage GBM tumour infiltration, aggressive tumour growth and tumour recurrence leads to difficulties in clinical management. FABP7 is highly expressed in GBM neural stem-like cells, but its role in GBM aggressiveness is not yet clear. In our study, using leading-edge super-resolution STED microscopy, we discovered that FABP7 is located at the plasma membrane and mitochondria of GBM cells. Using GSCs as our pre-clinical model, we obtained evidence that FABP7 may affect GBM migration in a PUFA-dependent manner through several potential mechanisms. These include: (i) membrane lipid remodeling through altered membrane fluidity and membrane FABP7 nanoclustering, (ii) increased storage of PUFAs and utilization of PUFAs for energy production in mitochondria, and (iii) microtube formation allowing transport of FABP7 cargo to distantly located cells. Although not directly addressed in this thesis, FABP7 may also function through fatty acid-dependent activation of nuclear receptors such as PPARγ. Thus, understanding the FABP7/PUFA-mediated mechanisms in GBM will lead to novel therapeutic strategies for the clinical management of GBM. We are proposing that dietary intervention to elevate DHA levels in the GBM tumour microenvironment, along with the currently-used therapies, may contribute to longer survival time and better quality of life for GBM patients.

References

Abbott, R.D., Ross, G.W., White, L.R., Sanderson, W.T., Burchfiel, C.M., Kashon, M., Sharp, D.S., Masaki, K.H., Curb, J.D., Petrovitch, H., 2003. Environmental, life-style, and physical precursors of clinical Parkinson's disease: recent findings from the Honolulu-Asia Aging Study. J Neurol 250 Suppl 3, III30-39.

Abulrob, A., Giuseppin, S., Andrade, M.F., McDermid, A., Moreno, M., Stanimirovic, D., 2004. Interactions of EGFR and caveolin-1 in human glioblastoma cells: evidence that tyrosine phosphorylation regulates EGFR association with caveolae. Oncogene 23, 6967-6979.

Adamski, V., Schmitt, A.D., Fluh, C., Synowitz, M., Hattermann, K., Held-Feindt, J., 2017. Isolation and Characterization of Fast-Migrating Human Glioma Cells in the Progression of Malignant Gliomas. Oncol Res 25, 341-353.

Adida, A., Spener, F., 2006. Adipocyte-type fatty acid-binding protein as inter-compartmental shuttle for peroxisome proliferator activated receptor gamma agonists in cultured cell. Biochim Biophys Acta 1761, 172-181.

Alakbarzade, V., Hameed, A., Quek, D.Q., Chioza, B.A., Baple, E.L., Cazenave-Gassiot, A., Nguyen, L.N., Wenk, M.R., Ahmad, A.Q., Sreekantan-Nair, A., Weedon, M.N., Rich, P., Patton, M.A., Warner, T.T., Silver, D.L., Crosby, A.H., 2015. A partially inactivating mutation in the sodium-dependent lysophosphatidylcholine transporter MFSD2A causes a non-lethal microcephaly syndrome. Nat Genet 47, 814-817.

Alcantara Llaguno, S., Chen, J., Kwon, C.H., Jackson, E.L., Li, Y., Burns, D.K., Alvarez-Buylla, A., Parada, L.F., 2009. Malignant astrocytomas originate from neural stem/progenitor cells in a somatic tumor suppressor mouse model. Cancer Cell 15, 45-56.

Alcantara Llaguno, S., Sun, D., Pedraza, A.M., Vera, E., Wang, Z., Burns, D.K., Parada, L.F., 2019. Cell-of-origin susceptibility to glioblastoma formation declines with neural lineage restriction. Nat Neurosci 22, 545-555.

Alcantara Llaguno, S.R., Wang, Z., Sun, D., Chen, J., Xu, J., Kim, E., Hatanpaa, K.J., Raisanen, J.M., Burns, D.K., Johnson, J.E., Parada, L.F., 2015. Adult Lineage-Restricted CNS Progenitors Specify Distinct Glioblastoma Subtypes. Cancer Cell 28, 429-440.

Ali, M., Heyob, K., Jacob, N.K., Rogers, L.K., 2016. Alterative Expression and Localization of Profilin 1/VASPpS157 and Cofilin 1/VASPpS239 Regulates Metastatic Growth and Is Modified by DHA Supplementation. Mol Cancer Ther 15, 2220-2231.

Ali, M., Rogers, L.K., Heyob, K.M., Buhimschi, C.S., Buhimschi, I.A., 2019. Changes in Vasodilator-Stimulated Phosphoprotein Phosphorylation, Profilin-1, and Cofilin-1 in Accreta and Protection by DHA. Reprod Sci 26, 757-765.

Alonso, F., Henson, P.M., Leslie, C.C., 1986. A cytosolic phospholipase in human neutrophils that hydrolyzes arachidonoyl-containing phosphatidylcholine. Biochim Biophys Acta 878, 273-280.

Alonso, M.M., Diez-Valle, R., Manterola, L., Rubio, A., Liu, D., Cortes-Santiago, N., Urquiza, L., Jauregi, P., Lopez de Munain, A., Sampron, N., Aramburu, A., Tejada-Solis, S., Vicente, C., Odero, M.D., Bandres, E., Garcia-Foncillas, J., Idoate, M.A., Lang, F.F., Fueyo, J., Gomez-Manzano, C., 2011. Genetic and epigenetic modifications of Sox2 contribute to the invasive phenotype of malignant gliomas. PLoS One 6, e26740.

Amiri, M., Yousefnia, S., Seyed Forootan, F., Peymani, M., Ghaedi, K., Nasr Esfahani, M.H., 2018. Diverse roles of fatty acid binding proteins (FABPs) in development and pathogenesis of cancers. Gene 676, 171-183.

An, Z., Aksoy, O., Zheng, T., Fan, Q.W., Weiss, W.A., 2018. Epidermal growth factor receptor and EGFRvIII in glioblastoma: signaling pathways and targeted therapies. Oncogene 37, 1561-1575.

Angelov, B., Angelova, A., 2017. Nanoscale clustering of the neurotrophin receptor TrkB revealed by super-resolution STED microscopy. Nanoscale 9, 9797-9804.

Antal, O., Hackler, L., Jr., Shen, J., Man, I., Hideghety, K., Kitajka, K., Puskas, L.G., 2014. Combination of unsaturated fatty acids and ionizing radiation on human glioma cells: cellular, biochemical and gene expression analysis. Lipids Health Dis 13, 142.

Anthony, T.E., Mason, H.A., Gridley, T., Fishell, G., Heintz, N., 2005. Brain lipid-binding protein is a direct target of Notch signaling in radial glial cells. Genes Dev 19, 1028-1033.

Arai, Y., Funatsu, N., Numayama-Tsuruta, K., Nomura, T., Nakamura, S., Osumi, N., 2005. Role of Fabp7, a downstream gene of Pax6, in the maintenance of neuroepithelial cells during early embryonic development of the rat cortex. J Neurosci 25, 9752-9761.

Aranda, J.F., Reglero-Real, N., Kremer, L., Marcos-Ramiro, B., Ruiz-Saenz, A., Calvo, M., Enrich, C., Correas, I., Millan, J., Alonso, M.A., 2011. MYADM regulates Rac1 targeting to ordered membranes required for cell spreading and migration. Mol Biol Cell 22, 1252-1262.

Ardebili, S.Y., Zajc, I., Gole, B., Campos, B., Herold-Mende, C., Drmota, S., Lah, T.T., 2011. CD133/prominin1 is prognostic for GBM patient's survival, but inversely correlated with cysteine cathepsins' expression in glioblastoma derived spheroids. Radiol Oncol 45, 102-115.

Arkhipov, A., Shan, Y., Das, R., Endres, N.F., Eastwood, M.P., Wemmer, D.E., Kuriyan, J., Shaw, D.E., 2013. Architecture and membrane interactions of the EGF receptor. Cell 152, 557-569.

Arnold, C., Markovic, M., Blossey, K., Wallukat, G., Fischer, R., Dechend, R., Konkel, A., von Schacky, C., Luft, F.C., Muller, D.N., Rothe, M., Schunck, W.H., 2010. Arachidonic acid-metabolizing cytochrome P450 enzymes are targets of {omega}-3 fatty acids. J Biol Chem 285, 32720-32733.

Aum, D.J., Kim, D.H., Beaumont, T.L., Leuthardt, E.C., Dunn, G.P., Kim, A.H., 2014. Molecular and cellular heterogeneity: the hallmark of glioblastoma. Neurosurg Focus 37, E11.

Avallone, R., Vitale, G., Bertolotti, M., 2019. Omega-3 Fatty Acids and Neurodegenerative Diseases: New Evidence in Clinical Trials. Int J Mol Sci 20.

Azrad, M., Turgeon, C., Demark-Wahnefried, W., 2013. Current evidence linking polyunsaturated Fatty acids with cancer risk and progression. Front Oncol 3, 224.

Balendiran, G.K., Schnutgen, F., Scapin, G., Borchers, T., Xhong, N., Lim, K., Godbout, R., Spener, F., Sacchettini, J.C., 2000. Crystal structure and thermodynamic analysis of human brain fatty acid-binding protein. J Biol Chem 275, 27045-27054.

Bannenberg, G., Serhan, C.N., 2010. Specialized pro-resolving lipid mediators in the inflammatory response: An update. Biochim Biophys Acta 1801, 1260-1273.

Bao, S., Wu, Q., McLendon, R.E., Hao, Y., Shi, Q., Hjelmeland, A.B., Dewhirst, M.W., Bigner, D.D., Rich, J.N., 2006. Glioma stem cells promote radioresistance by preferential activation of the DNA damage response. Nature 444, 756-760.

Barnes, C.M., Prox, D., Christison-Lagay, E.A., Le, H.D., Short, S., Cassiola, F., Panigrahy, D., Chaponis, D., Butterfield, C., Nehra, D., Fallon, E.M., Kieran, M., Folkman, J., Puder, M., 2012. Inhibition of neuroblastoma cell proliferation with omega-3 fatty acids and treatment of a murine model of human neuroblastoma using a diet enriched with omega-3 fatty acids in combination with sunitinib. Pediatr Res 71, 168-178.

Bastola, S., Pavlyukov, M.S., Yamashita, D., Ghosh, S., Cho, H., Kagaya, N., Zhang, Z., Minata, M., Lee, Y., Sadahiro, H., Yamaguchi, S., Komarova, S., Yang, E., Markert, J., Nabors, L.B., Bhat, K., Lee, J., Chen, Q., Crossman, D.K., Shin-Ya, K., Nam, D.H., Nakano, I., 2020. Glioma-initiating cells at tumor edge gain signals from tumor core cells to promote their malignancy. Nat Commun 11, 4660.

Bazinet, R.P., Laye, S., 2014. Polyunsaturated fatty acids and their metabolites in brain function and disease. Nat Rev Neurosci 15, 771-785.

Behnan, J., Finocchiaro, G., Hanna, G., 2019. The landscape of the mesenchymal signature in brain tumours. Brain 142, 847-866.

Bensaad, K., Favaro, E., Lewis, C.A., Peck, B., Lord, S., Collins, J.M., Pinnick, K.E., Wigfield, S., Buffa, F.M., Li, J.L., Zhang, Q., Wakelam, M.J.O., Karpe, F., Schulze, A.,

Harris, A.L., 2014. Fatty acid uptake and lipid storage induced by HIF-1alpha contribute to cell growth and survival after hypoxia-reoxygenation. Cell Rep 9, 349-365.

Berezovsky, A.D., Poisson, L.M., Cherba, D., Webb, C.P., Transou, A.D., Lemke, N.W., Hong, X., Hasselbach, L.A., Irtenkauf, S.M., Mikkelsen, T., deCarvalho, A.C., 2014. Sox2 promotes malignancy in glioblastoma by regulating plasticity and astrocytic differentiation. Neoplasia 16, 193-206, 206 e119-125.

Bernardi, A., Jacques-Silva, M.C., Delgado-Canedo, A., Lenz, G., Battastini, A.M., 2006. Nonsteroidal anti-inflammatory drugs inhibit the growth of C6 and U138-MG glioma cell lines. Eur J Pharmacol 532, 214-222.

Bhave, S.R., Dadey, D.Y., Karvas, R.M., Ferraro, D.J., Kotipatruni, R.P., Jaboin, J.J., Hallahan, A.N., Dewees, T.A., Linkous, A.G., Hallahan, D.E., Thotala, D., 2013. Autotaxin Inhibition with PF-8380 Enhances the Radiosensitivity of Human and Murine Glioblastoma Cell Lines. Front Oncol 3, 236.

Bi, J., Ichu, T.A., Zanca, C., Yang, H., Zhang, W., Gu, Y., Chowdhry, S., Reed, A., Ikegami, S., Turner, K.M., Zhang, W., Villa, G.R., Wu, S., Quehenberger, O., Yong, W.H., Kornblum, H.I., Rich, J.N., Cloughesy, T.F., Cavenee, W.K., Furnari, F.B., Cravatt, B.F., Mischel, P.S., 2019. Oncogene Amplification in Growth Factor Signaling Pathways Renders Cancers Dependent on Membrane Lipid Remodeling. Cell Metab 30, 525-538 e528.

Bird, J.K., Calder, P.C., Eggersdorfer, M., 2018. The Role of n-3 Long Chain Polyunsaturated Fatty Acids in Cardiovascular Disease Prevention, and Interactions with Statins. Nutrients 10.

Bleau, A.M., Hambardzumyan, D., Ozawa, T., Fomchenko, E.I., Huse, J.T., Brennan, C.W., Holland, E.C., 2009. PTEN/PI3K/Akt pathway regulates the side population phenotype and ABCG2 activity in glioma tumor stem-like cells. Cell Stem Cell 4, 226-235.

Bonavia, R., Inda, M.M., Cavenee, W.K., Furnari, F.B., 2011. Heterogeneity maintenance in glioblastoma: a social network. Cancer Res 71, 4055-4060.

Bond, A.M., Ming, G.L., Song, H., 2015. Adult Mammalian Neural Stem Cells and Neurogenesis: Five Decades Later. Cell Stem Cell 17, 385-395.

Bonny, M., Hui, X., Schweizer, J., Kaestner, L., Zeug, A., Kruse, K., Lipp, P., 2016. C2-domain mediated nano-cluster formation increases calcium signaling efficiency. Sci Rep 6, 36028.

Bosetti, F., 2007. Arachidonic acid metabolism in brain physiology and pathology: lessons from genetically altered mouse models. J Neurochem 102, 577-586.

Boyd, P.S., Struve, N., Bach, M., Eberle, J.P., Gote, M., Schock, F., Cremer, C., Kriegs, M., Hausmann, M., 2016. Clustered localization of EGFRvIII in glioblastoma cells as detected by high precision localization microscopy. Nanoscale 8, 20037-20047.

Bozza, P.T., Bakker-Abreu, I., Navarro-Xavier, R.A., Bandeira-Melo, C., 2011. Lipid body function in eicosanoid synthesis: an update. Prostaglandins Leukot Essent Fatty Acids 85, 205-213.

Brabletz, T., Jung, A., Spaderna, S., Hlubek, F., Kirchner, T., 2005. Opinion: migrating cancer stem cells - an integrated concept of malignant tumour progression. Nat Rev Cancer 5, 744-749.

Bralten, L.B., Kloosterhof, N.K., Balvers, R., Sacchetti, A., Lapre, L., Lamfers, M., Leenstra, S., de Jonge, H., Kros, J.M., Jansen, E.E., Struys, E.A., Jakobs, C., Salomons, G.S., Diks, S.H., Peppelenbosch, M., Kremer, A., Hoogenraad, C.C., Smitt, P.A., French, P.J., 2011. IDH1 R132H decreases proliferation of glioma cell lines in vitro and in vivo. Ann Neurol 69, 455-463.

Brenna, J.T., 2002. Efficiency of conversion of alpha-linolenic acid to long chain n-3 fatty acids in man. Curr Opin Clin Nutr Metab Care 5, 127-132.

Brennan, C.W., Verhaak, R.G., McKenna, A., Campos, B., Noushmehr, H., Salama, S.R., Zheng, S., Chakravarty, D., Sanborn, J.Z., Berman, S.H., Beroukhim, R., Bernard, B., Wu, C.J., Genovese, G., Shmulevich, I., Barnholtz-Sloan, J., Zou, L., Vegesna, R., Shukla, S.A., Ciriello, G., Yung, W.K., Zhang, W., Sougnez, C., Mikkelsen, T., Aldape, K., Bigner, D.D., Van Meir, E.G., Prados, M., Sloan, A., Black, K.L., Eschbacher, J., Finocchiaro, G., Friedman, W., Andrews, D.W., Guha, A., Iacocca, M., O'Neill, B.P., Foltz, G., Myers, J., Weisenberger, D.J., Penny, R., Kucherlapati, R., Perou, C.M., Hayes, D.N., Gibbs, R., Marra, M., Mills, G.B., Lander, E., Spellman, P., Wilson, R., Sander, C., Weinstein, J., Meyerson, M., Gabriel, S., Laird, P.W., Haussler, D., Getz, G., Chin, L., Network, T.R., 2013. The somatic genomic landscape of glioblastoma. Cell 155, 462-477.

Broekman, M.L., Maas, S.L.N., Abels, E.R., Mempel, T.R., Krichevsky, A.M., Breakefield, X.O., 2018. Multidimensional communication in the microenvirons of glioblastoma. Nat Rev Neurol 14, 482-495.

Brown, M., Roulson, J.A., Hart, C.A., Tawadros, T., Clarke, N.W., 2014. Arachidonic acid induction of Rho-mediated transendothelial migration in prostate cancer. Br J Cancer 110, 2099-2108.

Brun, M., Jain, S., Monckton, E.A., Godbout, R., 2018. Nuclear Factor I Represses the Notch Effector HEY1 in Glioblastoma. Neoplasia 20, 1023-1037.

Buckner, J.C., 2003. Factors influencing survival in high-grade gliomas. Semin Oncol 30, 10-14.

Calviello, G., Di Nicuolo, F., Serini, S., Piccioni, E., Boninsegna, A., Maggiano, N., Ranelletti, F.O., Palozza, P., 2005. Docosahexaenoic acid enhances the susceptibility of human colorectal cancer cells to 5-fluorouracil. Cancer Chemother Pharmacol 55, 12-20.

Chen, C.T., Green, J.T., Orr, S.K., Bazinet, R.P., 2008. Regulation of brain polyunsaturated fatty acid uptake and turnover. Prostaglandins Leukot Essent Fatty Acids 79, 85-91.

Chen, J., Li, Y., Yu, T.S., McKay, R.M., Burns, D.K., Kernie, S.G., Parada, L.F., 2012. A restricted cell population propagates glioblastoma growth after chemotherapy. Nature 488, 522-526.

Chen, R., Smith-Cohn, M., Cohen, A.L., Colman, H., 2017a. Glioma Subclassifications and Their Clinical Significance. Neurotherapeutics 14, 284-297.

Chen, Y., Wang, Y., Huang, Y., Zeng, H., Hu, B., Guan, L., Zhang, H., Yu, A.M., Johnson, C.H., Gonzalez, F.J., Huang, M., Bi, H., 2017b. PPARα regulates tumor cell proliferation and senescence via a novel target gene carnitine palmitoyltransferase 1C. Carcinogenesis 38, 474-483.

Cheng, L., Wu, Q., Guryanova, O.A., Huang, Z., Huang, Q., Rich, J.N., Bao, S., 2011. Elevated invasive potential of glioblastoma stem cells. Biochem Biophys Res Commun 406, 643-648.

Cheng, Y.Y., Huang, Y.F., Lin, H.H., Chang, W.W., Lyu, P.C., 2019. The ligand-mediated affinity of brain-type fatty acid-binding protein for membranes determines the directionality of lipophilic cargo transport. Biochim Biophys Acta Mol Cell Biol Lipids 1864, 158506.

Chichili, G.R., Rodgers, W., 2009. Cytoskeleton-membrane interactions in membrane raft structure. Cell Mol Life Sci 66, 2319-2328.

Chinot, O.L., Wick, W., Mason, W., Henriksson, R., Saran, F., Nishikawa, R., Carpentier, A.F., Hoang-Xuan, K., Kavan, P., Cernea, D., Brandes, A.A., Hilton, M., Abrey, L., Cloughesy, T., 2014. Bevacizumab plus radiotherapy-temozolomide for newly diagnosed glioblastoma. N Engl J Med 370, 709-722.

Chiu, W.T., Shen, S.C., Chow, J.M., Lin, C.W., Shia, L.T., Chen, Y.C., 2010. Contribution of reactive oxygen species to migration/invasion of human glioblastoma cells U87 via ERK-dependent COX-2/PGE(2) activation. Neurobiol Dis 37, 118-129.

Chmurzynska, A., 2006. The multigene family of fatty acid-binding proteins (FABPs): function, structure and polymorphism. J Appl Genet 47, 39-48.

Chow, L.M., Endersby, R., Zhu, X., Rankin, S., Qu, C., Zhang, J., Broniscer, A., Ellison, D.W., Baker, S.J., 2011. Cooperativity within and among Pten, p53, and Rb pathways induces high-grade astrocytoma in adult brain. Cancer Cell 19, 305-316.

Chuang, S.S., Helvig, C., Taimi, M., Ramshaw, H.A., Collop, A.H., Amad, M., White, J.A., Petkovich, M., Jones, G., Korczak, B., 2004. CYP2U1, a novel human thymus- and brain-specific cytochrome P450, catalyzes omega- and (omega-1)-hydroxylation of fatty acids. J Biol Chem 279, 6305-6314.

Clark, J.D., Schievella, A.R., Nalefski, E.A., Lin, L.L., 1995. Cytosolic phospholipase A2. J Lipid Mediat Cell Signal 12, 83-117.

Claypool, S.M., Oktay, Y., Boontheung, P., Loo, J.A., Koehler, C.M., 2008. Cardiolipin defines the interactome of the major ADP/ATP carrier protein of the mitochondrial inner membrane. J Cell Biol 182, 937-950.

Coe, N.R., Bernlohr, D.A., 1998. Physiological properties and functions of intracellular fatty acid-binding proteins. Biochim Biophys Acta 1391, 287-306.

Cordero, A., Kanojia, D., Miska, J., Panek, W.K., Xiao, A., Han, Y., Bonamici, N., Zhou, W., Xiao, T., Wu, M., Ahmed, A.U., Lesniak, M.S., 2019. FABP7 is a key metabolic regulator in HER2+ breast cancer brain metastasis. Oncogene 38, 6445-6460.

Corsetto, P.A., Montorfano, G., Zava, S., Jovenitti, I.E., Cremona, A., Berra, B., Rizzo, A.M., 2011. Effects of n-3 PUFAs on breast cancer cells through their incorporation in plasma membrane. Lipids Health Dis 10, 73.

Cruz-Hernandez, C., Goeuriot, S., Giuffrida, F., Thakkar, S.K., Destaillats, F., 2013. Direct quantification of fatty acids in human milk by gas chromatography. J Chromatogr A 1284, 174-179.

Cuddapah, V.A., Robel, S., Watkins, S., Sontheimer, H., 2014. A neurocentric perspective on glioma invasion. Nat Rev Neurosci 15, 455-465.

Czapski, G.A., Czubowicz, K., Strosznajder, J.B., Strosznajder, R.P., 2016. The Lipoxygenases: Their Regulation and Implication in Alzheimer's Disease. Neurochem Res 41, 243-257.

Daugherty, S.E., Moore, S.C., Pfeiffer, R.M., Inskip, P.D., Park, Y., Hollenbeck, A., Rajaraman, P., 2011. Nonsteroidal anti-inflammatory drugs and glioma in the NIH-AARP Diet and Health Study cohort. Cancer Prev Res (Phila) 4, 2027-2034.

Daum, G., 1985. Lipids of mitochondria. Biochim Biophys Acta 822, 1-42.

Davis, M.E., 2016. Glioblastoma: Overview of Disease and Treatment. Clin J Oncol Nurs 20, S2-8.

De Leon, M., Welcher, A.A., Nahin, R.H., Liu, Y., Ruda, M.A., Shooter, E.M., Molina, C.A., 1996. Fatty acid binding protein is induced in neurons of the dorsal root ganglia after peripheral nerve injury. J Neurosci Res 44, 283-292.

De Rosa, A., Pellegatta, S., Rossi, M., Tunici, P., Magnoni, L., Speranza, M.C., Malusa, F., Miragliotta, V., Mori, E., Finocchiaro, G., Bakker, A., 2012. A Radial Glia Gene Marker, Fatty Acid Binding Protein 7 (FABP7), Is Involved in Proliferation and Invasion of Glioblastoma Cells. PLoS One 7, e52113.

Demar, J.C., Jr., Ma, K., Chang, L., Bell, J.M., Rapoport, S.I., 2005. alpha-Linolenic acid does not contribute appreciably to docosahexaenoic acid within brain phospholipids of adult rats fed a diet enriched in docosahexaenoic acid. J Neurochem 94, 1063-1076.

Denkins, Y., Kempf, D., Ferniz, M., Nileshwar, S., Marchetti, D., 2005. Role of omega-3 polyunsaturated fatty acids on cyclooxygenase-2 metabolism in brain-metastatic melanoma. J Lipid Res 46, 1278-1284.

Dennis, E.A., Cao, J., Hsu, Y.H., Magrioti, V., Kokotos, G., 2011. Phospholipase A2 enzymes: physical structure, biological function, disease implication, chemical inhibition, and therapeutic intervention. Chem Rev 111, 6130-6185.

diNicolantonio, J.J.O.K., James H., 2020. The Importance of Marine Omega-3s for Brain Development and the Prevention and Treatment of Behavior, Mood, and Other Brain Disorders. Nutrients 12, 2333.

Doetsch, F., Caille, I., Lim, D.A., Garcia-Verdugo, J.M., Alvarez-Buylla, A., 1999. Subventricular zone astrocytes are neural stem cells in the adult mammalian brain. Cell 97, 703-716.

Dudek, J., 2017. Role of Cardiolipin in Mitochondrial Signaling Pathways. Front Cell Dev Biol 5, 90.

Duman, C., Yaqubi, K., Hoffmann, A., Acikgoz, A.A., Korshunov, A., Bendszus, M., Herold-Mende, C., Liu, H.K., Alfonso, J., 2019. Acyl-CoA-Binding Protein Drives Glioblastoma Tumorigenesis by Sustaining Fatty Acid Oxidation. Cell Metab 30, 274-289 e275.

Dyszy, F., Pinto, A.P., Araujo, A.P., Costa-Filho, A.J., 2013. Probing the interaction of brain fatty acid binding protein (B-FABP) with model membranes. PLoS One 8, e60198.

Eggeling, C., Ringemann, C., Medda, R., Schwarzmann, G., Sandhoff, K., Polyakova, S., Belov, V.N., Hein, B., von Middendorff, C., Schonle, A., Hell, S.W., 2009. Direct observation of the nanoscale dynamics of membrane lipids in a living cell. Nature 457, 1159-1162.

Elsherbiny, M.E., Emara, M., Godbout, R., 2013. Interaction of brain fatty acid-binding protein with the polyunsaturated fatty acid environment as a potential determinant of poor prognosis in malignant glioma. Prog Lipid Res 52, 562-570.

Elsherbiny, M.E., Goruk, S., Monckton, E.A., Richard, C., Brun, M., Emara, M., Field, C.J., Godbout, R., 2015. Long-Term Effect of Docosahexaenoic Acid Feeding on Lipid

Composition and Brain Fatty Acid-Binding Protein Expression in Rats. Nutrients 7, 8802-8817.

Eramo, A., Ricci-Vitiani, L., Zeuner, A., Pallini, R., Lotti, F., Sette, G., Pilozzi, E., Larocca, L.M., Peschle, C., De Maria, R., 2006. Chemotherapy resistance of glioblastoma stem cells. Cell Death Differ 13, 1238-1241.

Erazo-Oliveras, A., Fuentes, N.R., Wright, R.C., Chapkin, R.S., 2018. Functional link between plasma membrane spatiotemporal dynamics, cancer biology, and dietary membrane-altering agents. Cancer Metastasis Rev 37, 519-544.

Eto, M., Shindou, H., Yamamoto, S., Tamura-Nakano, M., Shimizu, T., 2020. Lysophosphatidylethanolamine acyltransferase 2 (LPEAT2) incorporates DHA into phospholipids and has possible functions for fatty acid-induced cell death. Biochemical and Biophysical Research Communications 526, 246-252.

Evers, P., Lee, P.P., DeMarco, J., Agazaryan, N., Sayre, J.W., Selch, M., Pajonk, F., 2010. Irradiation of the potential cancer stem cell niches in the adult brain improves progression-free survival of patients with malignant glioma. BMC Cancer 10, 384.

Fadhlullah, S.F.B., Halim, N.B.A., Yeo, J.Y.T., Ho, R.L.Y., Um, P., Ang, B.T., Tang, C., Ng, W.H., Virshup, D.M., Ho, I.A.W., 2019. Pathogenic mutations in neurofibromin identifies a leucine-rich domain regulating glioma cell invasiveness. Oncogene 38, 5367-5380.

Falomir-Lockhart, L.J., Franchini, G.R., Guerbi, M.X., Storch, J., Corsico, B., 2011. Interaction of enterocyte FABPs with phospholipid membranes: clues for specific physiological roles. Biochim Biophys Acta 1811, 452-459.

Farooqui, A.A., Yang, H.C., Rosenberger, T.A., Horrocks, L.A., 1997. Phospholipase A2 and its role in brain tissue. J Neurochem 69, 889-901.

Feng, L., Hatten, M.E., Heintz, N., 1994. Brain lipid-binding protein (BLBP): a novel signaling system in the developing mammalian CNS. Neuron 12, 895-908.

Feng, L., Heintz, N., 1995. Differentiating neurons activate transcription of the brain lipid-binding protein gene in radial glia through a novel regulatory element. Development 121, 1719-1730.

Fer, M., Dreano, Y., Lucas, D., Corcos, L., Salaun, J.P., Berthou, F., Amet, Y., 2008. Metabolism of eicosapentaenoic and docosahexaenoic acids by recombinant human cytochromes P450. Arch Biochem Biophys 471, 116-125.

Fernandez, R.F., Ellis, J.M., 2020. Acyl-CoA synthetases as regulators of brain phospholipid acyl-chain diversity. Prostaglandins Leukot Essent Fatty Acids 161, 102175.

Fernandez, R.F., Kim, S.Q., Zhao, Y., Foguth, R.M., Weera, M.M., Counihan, J.L., Nomura, D.K., Chester, J.A., Cannon, J.R., Ellis, J.M., 2018. Acyl-CoA synthetase 6 enriches the neuroprotective omega-3 fatty acid DHA in the brain. Proc Natl Acad Sci U S A 115, 12525-12530.

Ferreira, M.T., Gomes, R.N., Panagopoulos, A.T., de Almeida, F.G., Veiga, J.C.E., Colquhoun, A., 2018. Opposing roles of PGD2 in GBM. Prostaglandins Other Lipid Mediat 134, 66-76.

Fiorio Pla, A., Ong, H.L., Cheng, K.T., Brossa, A., Bussolati, B., Lockwich, T., Paria, B., Munaron, L., Ambudkar, I.S., 2012. TRPV4 mediates tumor-derived endothelial cell migration via arachidonic acid-activated actin remodeling. Oncogene 31, 200-212.

Formicola, B., D'Aloia, A., Dal Magro, R., Stucchi, S., Rigolio, R., Ceriani, M., Re, F., 2019. Differential Exchange of Multifunctional Liposomes Between Glioblastoma Cells and Healthy Astrocytes via Tunneling Nanotubes. Front Bioeng Biotechnol 7, 403.

Forsyth, P.A., Posner, J.B., 1993. Headaches in patients with brain tumors: a study of 111 patients. Neurology 43, 1678-1683.

Fuentes, N.R., Kim, E., Fan, Y.Y., Chapkin, R.S., 2018a. Omega-3 fatty acids, membrane remodeling and cancer prevention. Mol Aspects Med 64, 79-91.

Fuentes, N.R., Mlih, M., Barhoumi, R., Fan, Y.Y., Hardin, P., Steele, T.J., Behmer, S., Prior, I.A., Karpac, J., Chapkin, R.S., 2018b. Long-Chain n-3 Fatty Acids Attenuate Oncogenic KRas-Driven Proliferation by Altering Plasma Membrane Nanoscale Proteolipid Composition. Cancer Res 78, 3899-3912.

Fuentes, N.R., Mlih, M., Wang, X., Webster, G., Cortes-Acosta, S., Salinas, M.L., Corbin, I.R., Karpac, J., Chapkin, R.S., 2021. Membrane therapy using DHA suppresses epidermal growth factor receptor signaling by disrupting nanocluster formation. J Lipid Res, 100026.

Fujino, T., Yamamoto, T., 1992. Cloning and functional expression of a novel long-chain acyl-CoA synthetase expressed in brain. J Biochem 111, 197-203.

Furuhashi, M., Hotamisligil, G.S., 2008. Fatty acid-binding proteins: role in metabolic diseases and potential as drug targets. Nat Rev Drug Discov 7, 489-503.

Gage, F.H., 2000. Mammalian neural stem cells. Science 287, 1433-1438.

Gaist, D., Garcia-Rodriguez, L.A., Sorensen, H.T., Hallas, J., Friis, S., 2013. Use of low-dose aspirin and non-aspirin nonsteroidal anti-inflammatory drugs and risk of glioma: a case-control study. Br J Cancer 108, 1189-1194.

Garcia-Parajo, M.F., Cambi, A., Torreno-Pina, J.A., Thompson, N., Jacobson, K., 2014. Nanoclustering as a dominant feature of plasma membrane organization. J Cell Sci 127, 4995-5005.

Garcia Fernandez, M.I., Ceccarelli, D., Muscatello, U., 2004. Use of the fluorescent dye 10-N-nonyl acridine orange in quantitative and location assays of cardiolipin: a study on different experimental models. Analytical Biochemistry 328, 174-180.

Garcia, M.C., Ray, D.M., Lackford, B., Rubino, M., Olden, K., Roberts, J.D., 2009. Arachidonic acid stimulates cell adhesion through a novel p38 MAPK-RhoA signaling pathway that involves heat shock protein 27. J Biol Chem 284, 20936-20945.

Garnier, D., Renoult, O., Alves-Guerra, M.C., Paris, F., Pecqueur, C., 2019. Glioblastoma Stem-Like Cells, Metabolic Strategy to Kill a Challenging Target. Front Oncol 9, 118.

Gellerich, F.N., Trumbeckaite, S., Opalka, J.R., Seppet, E., Rasmussen, H.N., Neuhoff, C., Zierz, S., 2000. Function of the mitochondrial outer membrane as a diffusion barrier in health and diseases. Biochemical Society transactions 28, 164-169.

Gerster, H., 1998. Can adults adequately convert alpha-linolenic acid (18:3n-3) to eicosapentaenoic acid (20:5n-3) and docosahexaenoic acid (22:6n-3)? Int J Vitam Nutr Res 68, 159-173.

Giannini, C., Sarkaria, J.N., Saito, A., Uhm, J.H., Galanis, E., Carlson, B.L., Schroeder, M.A., James, C.D., 2005. Patient tumor EGFR and PDGFRA gene amplifications retained in an invasive intracranial xenograft model of glioblastoma multiforme. Neuro Oncol 7, 164-176.

Giesbertz, P., Ecker, J., Haag, A., Spanier, B., Daniel, H., 2015. An LC-MS/MS method to quantify acylcarnitine species including isomeric and odd-numbered forms in plasma and tissues. J Lipid Res 56, 2029-2039.

Gilbert, M.R., Dignam, J.J., Armstrong, T.S., Wefel, J.S., Blumenthal, D.T., Vogelbaum, M.A., Colman, H., Chakravarti, A., Pugh, S., Won, M., Jeraj, R., Brown, P.D., Jaeckle, K.A., Schiff, D., Stieber, V.W., Brachman, D.G., Werner-Wasik, M., Tremont-Lukats, I.W., Sulman, E.P., Aldape, K.D., Curran, W.J., Jr., Mehta, M.P., 2014. A randomized trial of bevacizumab for newly diagnosed glioblastoma. N Engl J Med 370, 699-708.

Gilbert, M.R., Wang, M., Aldape, K.D., Stupp, R., Hegi, M.E., Jaeckle, K.A., Armstrong, T.S., Wefel, J.S., Won, M., Blumenthal, D.T., Mahajan, A., Schultz, C.J., Erridge, S., Baumert, B., Hopkins, K.I., Tzuk-Shina, T., Brown, P.D., Chakravarti, A., Curran, W.J., Jr., Mehta, M.P., 2013. Dose-dense temozolomide for newly diagnosed glioblastoma: a randomized phase III clinical trial. J Clin Oncol 31, 4085-4091.

Gimple, R.C., Kidwell, R.L., Kim, L.J.Y., Sun, T., Gromovsky, A.D., Wu, Q., Wolf, M., Lv, D., Bhargava, S., Jiang, L., Prager, B.C., Wang, X., Ye, Q., Zhu, Z., Zhang, G., Dong, Z., Zhao, L., Lee, D., Bi, J., Sloan, A.E., Mischel, P.S., Brown, J.M., Cang, H., Huan, T., Mack,

S.C., Xie, Q., Rich, J.N., 2019. Glioma Stem Cell-Specific Superenhancer Promotes Polyunsaturated Fatty-Acid Synthesis to Support EGFR Signaling. Cancer Discov 9, 1248-1267.

Glantz, M.J., Cole, B.F., Forsyth, P.A., Recht, L.D., Wen, P.Y., Chamberlain, M.C., Grossman, S.A., Cairncross, J.G., 2000. Practice parameter: anticonvulsant prophylaxis in patients with newly diagnosed brain tumors. Report of the Quality Standards Subcommittee of the American Academy of Neurology. Neurology 54, 1886-1893.

Golfetto, O., Hinde, E., Gratton, E., 2013. Laurdan fluorescence lifetime discriminates cholesterol content from changes in fluidity in living cell membranes. Biophys J 104, 1238-1247.

Gomez-Llobregat, J., Buceta, J., Reigada, R., 2013. Interplay of cytoskeletal activity and lipid phase stability in dynamic protein recruitment and clustering. Sci Rep 3, 2608.

Green, P., Yavin, E., 1993. Elongation, desaturation, and esterification of essential fatty acids by fetal rat brain in vivo. J Lipid Res 34, 2099-2107.

Griffiths, B., Lewis, C.A., Bensaad, K., Ros, S., Zhang, Q., Ferber, E.C., Konisti, S., Peck, B., Miess, H., East, P., Wakelam, M., Harris, A.L., Schulze, A., 2013. Sterol regulatory element binding protein-dependent regulation of lipid synthesis supports cell survival and tumor growth. Cancer Metab 1, 3.

Guemez-Gamboa, A., Nguyen, L.N., Yang, H., Zaki, M.S., Kara, M., Ben-Omran, T., Akizu, N., Rosti, R.O., Rosti, B., Scott, E., Schroth, J., Copeland, B., Vaux, K.K., Cazenave-Gassiot, A., Quek, D.Q., Wong, B.H., Tan, B.C., Wenk, M.R., Gunel, M., Gabriel, S., Chi, N.C., Silver, D.L., Gleeson, J.G., 2015. Inactivating mutations in MFSD2A, required for omega-3 fatty acid transport in brain, cause a lethal microcephaly syndrome. Nat Genet 47, 809-813.

Guerra, F.S., Sampaio, L.d.S., Konig, S., Bonamino, M., Rossi, M.I.D., Costa, M.L., Fernandes, P., Mermelstein, C., 2016. Membrane cholesterol depletion reduces breast tumor cell migration by a mechanism that involves non-canonical Wnt signaling and IL-10 secretion. Translational Medicine Communications 1, 3.

Guo, A.M., Sheng, J., Scicli, G.M., Arbab, A.S., Lehman, N.L., Edwards, P.A., Falck, J.R., Roman, R.J., Scicli, A.G., 2008. Expression of CYP4A1 in U251 human glioma cell induces hyperproliferative phenotype in vitro and rapidly growing tumors in vivo. J Pharmacol Exp Ther 327, 10-19.

Guo, D., Prins, R.M., Dang, J., Kuga, D., Iwanami, A., Soto, H., Lin, K.Y., Huang, T.T., Akhavan, D., Hock, M.B., Zhu, S., Kofman, A.A., Bensinger, S.J., Yong, W.H., Vinters, H.V., Horvath, S., Watson, A.D., Kuhn, J.G., Robins, H.I., Mehta, M.P., Wen, P.Y., DeAngelis, L.M., Prados, M.D., Mellinghoff, I.K., Cloughesy, T.F., Mischel, P.S., 2009. EGFR signaling through an Akt-SREBP-1-dependent, rapamycin-resistant pathway sensitizes glioblastomas to antilipogenic therapy. Sci Signal 2, ra82.

Hainfellner, J., Louis, D.N., Perry, A., Wesseling, P., 2014. Letter in response to David N. Louis et al, International Society of Neuropathology-Haarlem Consensus Guidelines for Nervous System Tumor Classification and Grading, Brain Pathology, doi: 10.1111/bpa.12171. Brain Pathol 24, 671-672.

Hale, J.S., Otvos, B., Sinyuk, M., Alvarado, A.G., Hitomi, M., Stoltz, K., Wu, Q., Flavahan, W., Levison, B., Johansen, M.L., Schmitt, D., Neltner, J.M., Huang, P., Ren, B., Sloan, A.E., Silverstein, R.L., Gladson, C.L., DiDonato, J.A., Brown, J.M., McIntyre, T., Hazen, S.L., Horbinski, C., Rich, J.N., Lathia, J.D., 2014. Cancer stem cell-specific scavenger receptor CD36 drives glioblastoma progression. Stem Cells 32, 1746-1758.

Hambardzumyan, D., Bergers, G., 2015. Glioblastoma: Defining Tumor Niches. Trends Cancer 1, 252-265.

Hamilton, J.A., Brunaldi, K., 2007. A model for fatty acid transport into the brain. J Mol Neurosci 33, 12-17.

Han, S., Liu, Y., Cai, S.J., Qian, M., Ding, J., Larion, M., Gilbert, M.R., Yang, C., 2020. IDH mutation in glioma: molecular mechanisms and potential therapeutic targets. Br J Cancer 122, 1580-1589.

Hanada, K., Nishijima, M., Akamatsu, Y., Pagano, R.E., 1995. Both sphingolipids and cholesterol participate in the detergent insolubility of alkaline phosphatase, a glycosylphosphatidylinositol-anchored protein, in mammalian membranes. J Biol Chem 270, 6254-6260.

Hanna, V.S., Hafez, E.A.A., 2018. Synopsis of arachidonic acid metabolism: A review. J Adv Res 11, 23-32.

Harvey, K.A., Xu, Z., Saaddatzadeh, M.R., Wang, H., Pollok, K., Cohen-Gadol, A.A., Siddiqui, R.A., 2015. Enhanced anticancer properties of lomustine in conjunction with docosahexaenoic acid in glioblastoma cell lines. J Neurosurg 122, 547-556.

Hashidate-Yoshida, T., Harayama, T., Hishikawa, D., Morimoto, R., Hamano, F., Tokuoka, S.M., Eto, M., Tamura-Nakano, M., Yanobu-Takanashi, R., Mukumoto, Y., Kiyonari, H., Okamura, T., Kita, Y., Shindou, H., Shimizu, T., 2015. Fatty acid remodeling by LPCAT3 enriches arachidonate in phospholipid membranes and regulates triglyceride transport. Elife 4.

Hegi, M.E., Diserens, A.C., Gorlia, T., Hamou, M.F., de Tribolet, N., Weller, M., Kros, J.M., Hainfellner, J.A., Mason, W., Mariani, L., Bromberg, J.E., Hau, P., Mirimanoff, R.O., Cairncross, J.G., Janzer, R.C., Stupp, R., 2005. MGMT gene silencing and benefit from temozolomide in glioblastoma. N Engl J Med 352, 997-1003.

Hernandez, M., Burillo, S.L., Crespo, M.S., Nieto, M.L., 1998. Secretory phospholipase A2 activates the cascade of mitogen-activated protein kinases and cytosolic phospholipase A2 in the human astrocytoma cell line 1321N1. J Biol Chem 273, 606-612.

Hewett, S.J., Bell, S.C., Hewett, J.A., 2006. Contributions of cyclooxygenase-2 to neuroplasticity and neuropathology of the central nervous system. Pharmacol Ther 112, 335-357.

Hickey, R.W., Adelson, P.D., Johnnides, M.J., Davis, D.S., Yu, Z., Rose, M.E., Chang, Y.F., Graham, S.H., 2007. Cyclooxygenase-2 activity following traumatic brain injury in the developing rat. Pediatr Res 62, 271-276.

Hoang-Minh, L.B., Siebzehnrubl, F.A., Yang, C., Suzuki-Hatano, S., Dajac, K., Loche, T., Andrews, N., Schmoll Massari, M., Patel, J., Amin, K., Vuong, A., Jimenez-Pascual, A., Kubilis, P., Garrett, T.J., Moneypenny, C., Pacak, C.A., Huang, J., Sayour, E.J., Mitchell, D.A., Sarkisian, M.R., Reynolds, B.A., Deleyrolle, L.P., 2018. Infiltrative and drug-resistant slow-cycling cells support metabolic heterogeneity in glioblastoma. EMBO J 37.

Hoelzinger, D.B., Nakada, M., Demuth, T., Rosensteel, T., Reavie, L.B., Berens, M.E., 2008. Autotaxin: a secreted autocrine/paracrine factor that promotes glioma invasion. J Neurooncol 86, 297-309.

Hofmanova, J., Slavik, J., Ovesna, P., Tylichova, Z., Vondracek, J., Strakova, N., Vaculova, A.H., Ciganek, M., Kozubik, A., Knopfova, L., Smarda, J., Machala, M., 2017. Dietary fatty acids specifically modulate phospholipid pattern in colon cells with distinct differentiation capacities. Eur J Nutr 56, 1493-1508.

Holland, E.C., Celestino, J., Dai, C., Schaefer, L., Sawaya, R.E., Fuller, G.N., 2000. Combined activation of Ras and Akt in neural progenitors induces glioblastoma formation in mice. Nat Genet 25, 55-57.

Honigmann, A., Mueller, V., Ta, H., Schoenle, A., Sezgin, E., Hell, S.W., Eggeling, C., 2014a. Scanning STED-FCS reveals spatiotemporal heterogeneity of lipid interaction in the plasma membrane of living cells. Nat Commun 5, 5412.

Honigmann, A., Sadeghi, S., Keller, J., Hell, S.W., Eggeling, C., Vink, R., 2014b. A lipid bound actin meshwork organizes liquid phase separation in model membranes. Elife 3, e01671.

Hsu, K.T., Storch, J., 1996. Fatty acid transfer from liver and intestinal fatty acid-binding proteins to membranes occurs by different mechanisms. J Biol Chem 271, 13317-13323.

Huang, T.L., Zandi, P.P., Tucker, K.L., Fitzpatrick, A.L., Kuller, L.H., Fried, L.P., Burke, G.L., Carlson, M.C., 2005. Benefits of fatty fish on dementia risk are stronger for those without APOE epsilon4. Neurology 65, 1409-1414.

Hurley, J.H., Dean, A.M., Koshland, D.E., Jr., Stroud, R.M., 1991. Catalytic mechanism of NADP(+)-dependent isocitrate dehydrogenase: implications from the structures of magnesium-isocitrate and NADP+ complexes. Biochemistry 30, 8671-8678.

Huse, J.T., Holland, E.C., 2009. Genetically engineered mouse models of brain cancer and the promise of preclinical testing. Brain Pathol 19, 132-143.

Iliff, J.J., Jia, J., Nelson, J., Goyagi, T., Klaus, J., Alkayed, N.J., 2010. Epoxyeicosanoid signaling in CNS function and disease. Prostaglandins Other Lipid Mediat 91, 68-84.

Inoue, A., Takahashi, H., Harada, H., Kohno, S., Ohue, S., Kobayashi, K., Yano, H., Tanaka, J., Ohnishi, T., 2010. Cancer stem-like cells of glioblastoma characteristically express MMP-13 and display highly invasive activity. Int J Oncol 37, 1121-1131.

Ishiwata, T., Teduka, K., Yamamoto, T., Kawahara, K., Matsuda, Y., Naito, Z., 2011. Neuroepithelial stem cell marker nestin regulates the migration, invasion and growth of human gliomas. Oncol Rep 26, 91-99.

Islam, A., Kagawa, Y., Miyazaki, H., Shil, S.K., Umaru, B.A., Yasumoto, Y., Yamamoto, Y., Owada, Y., 2019. FABP7 Protects Astrocytes Against ROS Toxicity via Lipid Droplet Formation. Mol Neurobiol 56, 5763-5779.

Janakiram, N.B., Mohammed, A., Rao, C.V., 2011. Role of lipoxins, resolvins, and other bioactive lipids in colon and pancreatic cancer. Cancer Metastasis Rev 30, 507-523.

Jiang, J., Qiu, J., Li, Q., Shi, Z., 2017. Prostaglandin E2 Signaling: Alternative Target for Glioblastoma? Trends Cancer 3, 75-78.

Jiang, J.G., Ning, Y.G., Chen, C., Ma, D., Liu, Z.J., Yang, S., Zhou, J., Xiao, X., Zhang, X.A., Edin, M.L., Card, J.W., Wang, J., Zeldin, D.C., Wang, D.W., 2007. Cytochrome p450 epoxygenase promotes human cancer metastasis. Cancer Res 67, 6665-6674.

Jin, X., Kim, L.J.Y., Wu, Q., Wallace, L.C., Prager, B.C., Sanvoranart, T., Gimple, R.C., Wang, X., Mack, S.C., Miller, T.E., Huang, P., Valentim, C.L., Zhou, Q.G., Barnholtz-Sloan, J.S., Bao, S., Sloan, A.E., Rich, J.N., 2017. Targeting glioma stem cells through combined BMI1 and EZH2 inhibition. Nat Med 23, 1352-1361.

Joki, T., Heese, O., Nikas, D.C., Bello, L., Zhang, J., Kraeft, S.K., Seyfried, N.T., Abe, T., Chen, L.B., Carroll, R.S., Black, P.M., 2000. Expression of cyclooxygenase 2 (COX-2) in human glioma and in vitro inhibition by a specific COX-2 inhibitor, NS-398. Cancer Res 60, 4926-4931.

Jordan, A., Stein, J., 2003. Effect of an omega-3 fatty acid containing lipid emulsion alone and in combination with 5-fluorouracil (5-FU) on growth of the colon cancer cell line Caco-2. Eur J Nutr 42, 324-331.

Jung, E., Alfonso, J., Osswald, M., Monyer, H., Wick, W., Winkler, F., 2019. Emerging intersections between neuroscience and glioma biology. Nat Neurosci 22, 1951-1960.

K., M.I., F., C.T., Y., W.P., W., T.J., L.., C.J., 2019. A phase 1, open-label, perioperative study of ivosidenib (AG-120) and vorasidenib (AG-881) in recurrent IDH1 mutant, low-grade glioma: Updated results. Neuro-Oncol 21.

K., M.I., M., P.-P., B., P.K., F., C.T., A., B.H.A.M.E., Y., W.P., 2018. Phase 1 study of AG-881, an inhibitor of mutant IDH1/IDH2, in patients with advanced IDH-mutant solid tumors, including glioma. J Clin Oncol 36.

Kagawa, Y., Umaru, B.A., Ariful, I., Shil, S.K., Miyazaki, H., Yamamoto, Y., Ogata, M., Owada, Y., 2019. Role of FABP7 in tumor cell signaling. Advances in biological regulation 71, 206-218.

Kagawa, Y., Umaru, B.A., Shima, H., Ito, R., Zama, R., Islam, A., Kanno, S.I., Yasui, A., Sato, S., Jozaki, K., Shil, S.K., Miyazaki, H., Kobayashi, S., Yamamoto, Y., Kogo, H., Shimamoto-Mitsuyama, C., Sugawara, A., Sugino, N., Kanamori, M., Tominaga, T., Yoshikawa, T., Fukunaga, K., Igarashi, K., Owada, Y., 2020. FABP7 Regulates Acetyl-CoA Metabolism Through the Interaction with ACLY in the Nucleus of Astrocytes. Mol Neurobiol 57, 4891-4910.

Kagawa, Y., Yasumoto, Y., Sharifi, K., Ebrahimi, M., Islam, A., Miyazaki, H., Yamamoto, Y., Sawada, T., Kishi, H., Kobayashi, S., Maekawa, M., Yoshikawa, T., Takaki, E., Nakai, A., Kogo, H., Fujimoto, T., Owada, Y., 2015. Fatty acid-binding protein 7 regulates function of caveolae in astrocytes through expression of caveolin-1. Glia 63, 780-794.

Kaiser, H.J., Lingwood, D., Levental, I., Sampaio, J.L., Kalvodova, L., Rajendran, L., Simons, K., 2009. Order of lipid phases in model and plasma membranes. Proc Natl Acad Sci U S A 106, 16645-16650.

Kalmijn, S., Launer, L.J., Ott, A., Witteman, J.C., Hofman, A., Breteler, M.M., 1997. Dietary fat intake and the risk of incident dementia in the Rotterdam Study. Ann Neurol 42, 776-782.

Kaloshi, G., Mokhtari, K., Carpentier, C., Taillibert, S., Lejeune, J., Marie, Y., Delattre, J.Y., Godbout, R., Sanson, M., 2007. FABP7 expression in glioblastomas: relation to prognosis, invasion and EGFR status. J Neurooncol 84, 245-248.

Kambach, D.M., Halim, A.S., Cauer, A.G., Sun, Q., Tristan, C.A., Celiku, O., Kesarwala, A.H., Shankavaram, U., Batchelor, E., Stommel, J.M., 2017. Disabled cell density sensing leads to dysregulated cholesterol synthesis in glioblastoma. Oncotarget 8, 14860-14875.

Kamp, F., Zakim, D., Zhang, F., Noy, N., Hamilton, J.A., 1995. Fatty acid flip-flop in phospholipid bilayers is extremely fast. Biochemistry 34, 11928-11937.

Kant, S., Kesarwani, P., Prabhu, A., Graham, S.F., Buelow, K.L., Nakano, I., Chinnaiyan, P., 2020. Enhanced fatty acid oxidation provides glioblastoma cells metabolic plasticity to accommodate to its dynamic nutrient microenvironment. Cell Death Dis 11, 253.

Karsenty, J., Helal, O., de la Porte, P.L., Beauclair-Deprez, P., Martin-Elyazidi, C., Planells, R., Storch, J., Gastaldi, M., 2009. I-FABP expression alters the intracellular distribution of the BODIPY C16 fatty acid analog. Mol Cell Biochem 326, 97-104.

Keime-Guibert, F., Chinot, O., Taillandier, L., Cartalat-Carel, S., Frenay, M., Kantor, G., Guillamo, J.S., Jadaud, E., Colin, P., Bondiau, P.Y., Menei, P., Loiseau, H., Bernier, V., Honnorat, J., Barrie, M., Mokhtari, K., Mazeron, J.J., Bissery, A., Delattre, J.Y., Association of French-Speaking, N.-O., 2007. Radiotherapy for glioblastoma in the elderly. N Engl J Med 356, 1527-1535.

Keller, S., Schmidt, M.H.H., 2017. EGFR and EGFRvIII Promote Angiogenesis and Cell Invasion in Glioblastoma: Combination Therapies for an Effective Treatment. Int J Mol Sci 18.

Kim, E.J., Jin, X., Kim, O.R., Ham, S.W., Park, S.H., Kim, H., 2018a. Glioma stem cells and their non-stem differentiated glioma cells exhibit differences in mitochondrial structure and function. Oncol Rep 39, 411-416.

Kim, H.W., Rao, J.S., Rapoport, S.I., Igarashi, M., 2011. Regulation of rat brain polyunsaturated fatty acid (PUFA) metabolism during graded dietary n-3 PUFA deprivation. Prostaglandins Leukot Essent Fatty Acids 85, 361-368.

Kim, S., Jing, K., Shin, S., Jeong, S., Han, S.H., Oh, H., Yoo, Y.S., Han, J., Jeon, Y.J., Heo, J.Y., Kweon, G.R., Park, S.K., Park, J.I., Wu, T., Lim, K., 2018b. omega3-polyunsaturated fatty acids induce cell death through apoptosis and autophagy in glioblastoma cells: In vitro and in vivo. Oncol Rep 39, 239-246.

Kishi, Y., Okudaira, S., Tanaka, M., Hama, K., Shida, D., Kitayama, J., Yamori, T., Aoki, J., Fujimaki, T., Arai, H., 2006. Autotaxin is overexpressed in glioblastoma multiforme and contributes to cell motility of glioblastoma by converting lysophosphatidylcholine to lysophosphatidic acid. J Biol Chem 281, 17492-17500.

Klapisz, E., Ziari, M., Wendum, D., Koumanov, K., Brachet-Ducos, C., Olivier, J.L., Bereziat, G., Trugnan, G., Masliah, J., 1999. N-terminal and C-terminal plasma membrane anchoring modulate differently agonist-induced activation of cytosolic phospholipase A2. Eur J Biochem 265, 957-966.

Klotzsch, E., Schutz, G.J., 2013. A critical survey of methods to detect plasma membrane rafts. Philos Trans R Soc Lond B Biol Sci 368, 20120033.

Komori, T., Sasaki, H., Yoshida, K., 2016. [Revised WHO Classification of Tumours of the Central Nervous System:Summary of the Revision and Perspective]. No Shinkei Geka 44, 625-635.

Konkel, A., Schunck, W.H., 2011. Role of cytochrome P450 enzymes in the bioactivation of polyunsaturated fatty acids. Biochim Biophys Acta 1814, 210-222.

Kornberg, A., Pricer, W.E., Jr., 1953. Enzymatic synthesis of the coenzyme A derivatives of long chain fatty acids. J Biol Chem 204, 329-343.

Koundouros, N., Karali, E., Tripp, A., Valle, A., Inglese, P., Perry, N.J.S., Magee, D.J., Anjomani Virmouni, S., Elder, G.A., Tyson, A.L., Doria, M.L., van Weverwijk, A., Soares, R.F., Isacke, C.M., Nicholson, J.K., Glen, R.C., Takats, Z., Poulogiannis, G., 2020. Metabolic Fingerprinting Links Oncogenic PIK3CA with Enhanced Arachidonic Acid-Derived Eicosanoids. Cell 181, 1596-1611 e1527.

Koundouros, N., Poulogiannis, G., 2020. Reprogramming of fatty acid metabolism in cancer. Br J Cancer 122, 4-22.

Kuhlbrandt, W., 2015. Structure and function of mitochondrial membrane protein complexes. BMC Biol 13, 89.

Kuhn, H., Thiele, B.J., 1999. The diversity of the lipoxygenase family. Many sequence data but little information on biological significance. FEBS Lett 449, 7-11.

Kurtz, A., Zimmer, A., Schnutgen, F., Bruning, G., Spener, F., Muller, T., 1994. The expression pattern of a novel gene encoding brain-fatty acid binding protein correlates with neuronal and glial cell development. Development 120, 2637-2649.

Kwong, S.C., Jamil, A.H.A., Rhodes, A., Taib, N.A., Chung, I., 2019. Metabolic role of fatty acid binding protein 7 in mediating triple-negative breast cancer cell death via PPAR-alpha signaling. J Lipid Res 60, 1807-1817.

Lacombe, R.J.S., Chouinard-Watkins, R., Bazinet, R.P., 2018. Brain docosahexaenoic acid uptake and metabolism. Mol Aspects Med 64, 109-134.

Lalier, L., Cartron, P.F., Pedelaborde, F., Olivier, C., Loussouarn, D., Martin, S.A., Meflah, K., Menanteau, J., Vallette, F.M., 2007. Increase in PGE2 biosynthesis induces a Bax dependent apoptosis correlated to patients' survival in glioblastoma multiforme. Oncogene 26, 4999-5009.

Lands, W.E., 1958. Metabolism of glycerolipides; a comparison of lecithin and triglyceride synthesis. J Biol Chem 231, 883-888.

Larsson, S.C., Kumlin, M., Ingelman-Sundberg, M., Wolk, A., 2004. Dietary long-chain n-3 fatty acids for the prevention of cancer: a review of potential mechanisms. Am J Clin Nutr 79, 935-945.

Lathia, J.D., Mack, S.C., Mulkearns-Hubert, E.E., Valentim, C.L., Rich, J.N., 2015. Cancer stem cells in glioblastoma. Genes Dev 29, 1203-1217.

Lauritzen, L., Brambilla, P., Mazzocchi, A., Harslof, L.B., Ciappolino, V., Agostoni, C., 2016. DHA Effects in Brain Development and Function. Nutrients 8.

Laye, S., Nadjar, A., Joffre, C., Bazinet, R.P., 2018. Anti-Inflammatory Effects of Omega-3 Fatty Acids in the Brain: Physiological Mechanisms and Relevance to Pharmacology. Pharmacol Rev 70, 12-38.

Layne, K.S., Goh, Y.K., Jumpsen, J.A., Ryan, E.A., Chow, P., Clandinin, M.T., 1996. Normal subjects consuming physiological levels of 18:3(n-3) and 20:5(n-3) from flaxseed or fish oils have characteristic differences in plasma lipid and lipoprotein fatty acid levels. J Nutr 126, 2130-2140.

Lee, J., Kotliarova, S., Kotliarov, Y., Li, A., Su, Q., Donin, N.M., Pastorino, S., Purow, B.W., Christopher, N., Zhang, W., Park, J.K., Fine, H.A., 2006. Tumor stem cells derived from glioblastomas cultured in bFGF and EGF more closely mirror the phenotype and genotype of primary tumors than do serum-cultured cell lines. Cancer Cell 9, 391-403.

Lee, J.H., Lee, J.E., Kahng, J.Y., Kim, S.H., Park, J.S., Yoon, S.J., Um, J.Y., Kim, W.K., Lee, J.K., Park, J., Kim, E.H., Lee, J.H., Lee, J.H., Chung, W.S., Ju, Y.S., Park, S.H., Chang, J.H., Kang, S.G., Lee, J.H., 2018. Human glioblastoma arises from subventricular zone cells with low-level driver mutations. Nature 560, 243-247.

Lee, K.H., Seong, H.J., Kim, G., Jeong, G.H., Kim, J.Y., Park, H., Jung, E., Kronbichler, A., Eisenhut, M., Stubbs, B., Solmi, M., Koyanagi, A., Hong, S.H., Dragioti, E., de Rezende, L.F.M., Jacob, L., Keum, N., van der Vliet, H.J., Cho, E., Veronese, N., Grosso, G., Ogino, S., Song, M., Radua, J., Jung, S.J., Thompson, T., Jackson, S.E., Smith, L., Yang, L., Oh, H., Choi, E.K., Shin, J.I., Giovannucci, E.L., Gamerith, G., 2020. Consumption of Fish and omega-3 Fatty Acids and Cancer Risk: An Umbrella Review of Meta-Analyses of Observational Studies. Adv Nutr 11, 1134-1149.

Lei, X., Chen, X., Quan, Y., Tao, Y., Li, J., 2020. Targeting CYP2J2 to Enhance the Anti-Glioma Efficacy of Cannabinoid Receptor 2 Stimulation by Inhibiting the Pro-Angiogenesis Function of M2 Microglia. Front Oncol 10, 574277.

Lenting, K., Verhaak, R., Ter Laan, M., Wesseling, P., Leenders, W., 2017. Glioma: experimental models and reality. Acta Neuropathol 133, 263-282.

Leonardi, F., Attorri, L., Di Benedetto, R., Di Biase, A., Sanchez, M., Nardini, M., Salvati, S., 2005. Effect of arachidonic, eicosapentaenoic and docosahexaenoic acids on the oxidative status of C6 glioma cells. Free radical research 39, 865-874.

Levental, K.R., Malmberg, E., Symons, J.L., Fan, Y.Y., Chapkin, R.S., Ernst, R., Levental, I., 2020. Lipidomic and biophysical homeostasis of mammalian membranes counteracts dietary lipid perturbations to maintain cellular fitness. Nat Commun 11, 1339.

Li, C., Wu, X., Liu, S., Shen, D., Zhu, J., Liu, K., 2020. Role of Resolvins in the Inflammatory Resolution of Neurological Diseases. Front Pharmacol 11, 612.

Li, J., Liang, R., Song, C., Xiang, Y., Liu, Y., 2018. Prognostic significance of epidermal growth factor receptor expression in glioma patients. Onco Targets Ther 11, 731-742.

Li, Z., Bao, S., Wu, Q., Wang, H., Eyler, C., Sathornsumetee, S., Shi, Q., Cao, Y., Lathia, J., McLendon, R.E., Hjelmeland, A.B., Rich, J.N., 2009. Hypoxia-inducible factors regulate tumorigenic capacity of glioma stem cells. Cancer Cell 15, 501-513.

Lian, W., Wang, R., Xing, B., Yao, Y., 2017. Fish intake and the risk of brain tumor: a meta-analysis with systematic review. Nutr J 16, 1.

Liang, C.C., Park, A.Y., Guan, J.L., 2007. In vitro scratch assay: a convenient and inexpensive method for analysis of cell migration in vitro. Nat Protoc 2, 329-333.

Liang, Y., Bollen, A.W., Aldape, K.D., Gupta, N., 2006. Nuclear FABP7 immunoreactivity is preferentially expressed in infiltrative glioma and is associated with poor prognosis in EGFR-overexpressing glioblastoma. BMC Cancer 6, 97.

Liang, Y., Diehn, M., Watson, N., Bollen, A.W., Aldape, K.D., Nicholas, M.K., Lamborn, K.R., Berger, M.S., Botstein, D., Brown, P.O., Israel, M.A., 2005. Gene expression profiling reveals molecularly and clinically distinct subtypes of glioblastoma multiforme. Proc Natl Acad Sci U S A 102, 5814-5819.

Lim, J.Y., Oh, J.H., Jung, J.R., Kim, S.M., Ryu, C.H., Kim, H.T., Jeun, S.S., 2010. MK886-induced apoptosis depends on the 5-LO expression level in human malignant glioma cells. J Neurooncol 97, 339-346.

Lin, H., Patel, S., Affleck, V.S., Wilson, I., Turnbull, D.M., Joshi, A.R., Maxwell, R., Stoll, E.A., 2017. Fatty acid oxidation is required for the respiration and proliferation of malignant glioma cells. Neuro Oncol 19, 43-54.

Lingwood, D., Simons, K., 2010. Lipid rafts as a membrane-organizing principle. Science 327, 46-50.

Linkous, A., Balamatsias, D., Snuderl, M., Edwards, L., Miyaguchi, K., Milner, T., Reich, B., Cohen-Gould, L., Storaska, A., Nakayama, Y., Schenkein, E., Singhania, R., Cirigliano, S., Magdeldin, T., Lin, Y., Nanjangud, G., Chadalavada, K., Pisapia, D., Liston, C., Fine, H.A., 2019. Modeling Patient-Derived Glioblastoma with Cerebral Organoids. Cell Rep 26, 3203-3211 e3205.

Liu, C., Sage, J.C., Miller, M.R., Verhaak, R.G., Hippenmeyer, S., Vogel, H., Foreman, O., Bronson, R.T., Nishiyama, A., Luo, L., Zong, H., 2011. Mosaic analysis with double markers reveals tumor cell of origin in glioma. Cell 146, 209-221.

Liu, R.Z., Choi, W.S., Jain, S., Dinakaran, D., Xu, X., Han, W.H., Yang, X.H., Glubrecht, D.D., Moore, R.B., Lemieux, H., Godbout, R., 2020a. The FABP12/PPARgamma pathway promotes metastatic transformation by inducing epithelial-to-mesenchymal transition and lipid-derived energy production in prostate cancer cells. Mol Oncol.

Liu, R.Z., Choi, W.S., Jain, S., Dinakaran, D., Xu, X., Han, W.H., Yang, X.H., Glubrecht, D.D., Moore, R.B., Lemieux, H., Godbout, R., 2020b. The FABP12/PPARgamma pathway

promotes metastatic transformation by inducing epithelial-to-mesenchymal transition and lipid-derived energy production in prostate cancer cells. Mol Oncol 14, 3100-3120.

Liu, R.Z., Graham, K., Glubrecht, D.D., Lai, R., Mackey, J.R., Godbout, R., 2012. A fatty acid-binding protein 7/RXRbeta pathway enhances survival and proliferation in triple-negative breast cancer. J Pathol 228, 310-321.

Liu, R.Z., Mita, R., Beaulieu, M., Gao, Z., Godbout, R., 2010. Fatty acid binding proteins in brain development and disease. Int J Dev Biol 54, 1229-1239.

Lodhi, I.J., Semenkovich, C.F., 2014. Peroxisomes: a nexus for lipid metabolism and cellular signaling. Cell Metab 19, 380-392.

Louis, D.N., Ohgaki, H., Wiestler, O.D., Cavenee, W.K., Burger, P.C., Jouvet, A., Scheithauer, B.W., Kleihues, P., 2007. The 2007 WHO classification of tumours of the central nervous system. Acta Neuropathol 114, 97-109.

Louis, D.N., Perry, A., Reifenberger, G., von Deimling, A., Figarella-Branger, D., Cavenee, W.K., Ohgaki, H., Wiestler, O.D., Kleihues, P., Ellison, D.W., 2016. The 2016 World Health Organization Classification of Tumors of the Central Nervous System: a summary. Acta Neuropathol 131, 803-820.

Lukiw, W.J., Cui, J.G., Marcheselli, V.L., Bodker, M., Botkjaer, A., Gotlinger, K., Serhan, C.N., Bazan, N.G., 2005. A role for docosahexaenoic acid-derived neuroprotectin D1 in neural cell survival and Alzheimer disease. J Clin Invest 115, 2774-2783.

Maekawa, M., Yang, Y., Fairn, G.D., 2016. Perfringolysin O Theta Toxin as a Tool to Monitor the Distribution and Inhomogeneity of Cholesterol in Cellular Membranes. Toxins (Basel) 8, 67.

Malmstrom, A., Gronberg, B.H., Marosi, C., Stupp, R., Frappaz, D., Schultz, H., Abacioglu, U., Tavelin, B., Lhermitte, B., Hegi, M.E., Rosell, J., Henriksson, R., Nordic Clinical Brain Tumour Study, G., 2012. Temozolomide versus standard 6-week radiotherapy versus hypofractionated radiotherapy in patients older than 60 years with glioblastoma: the Nordic randomised, phase 3 trial. Lancet Oncol 13, 916-926.

Manda, K., Kriesen, S., Hildebrandt, G., Fietkau, R., Klautke, G., 2011. Omega-3 fatty acid supplementation in cancer therapy : does eicosapentanoic acid influence the radiosensitivity of tumor cells? Strahlenther Onkol 187, 127-134.

Mao, Y., 2016. Nearest Neighbor Distances Calculation with ImageJ.

Marszalek, R., Pisklak, M., Jankowski, W., Lukaszkiewicz, J., Horsztynski, D., Wawer, I., 2010. NMR and gas chromatography studies of lyophilized human brain tumors. Acta Pol Pharm 67, 129-136.

Martin, D.D., Robbins, M.E., Spector, A.A., Wen, B.C., Hussey, D.H., 1996. The fatty acid composition of human gliomas differs from that found in nonmalignant brain tissue. Lipids 31, 1283-1288.

Martin, S., Cosset, E.C., Terrand, J., Maglott, A., Takeda, K., Dontenwill, M., 2009. Caveolin-1 regulates glioblastoma aggressiveness through the control of alpha(5)beta(1) integrin expression and modulates glioblastoma responsiveness to SJ749, an alpha(5)beta(1) integrin antagonist. Biochim Biophys Acta 1793, 354-367.

Matsuo, M., Yoshida, N., Zaitsu, M., Ishii, K., Hamasaki, Y., 2004. Inhibition of human glioma cell growth by a PHS-2 inhibitor, NS398, and a prostaglandin E receptor subtype EP1-selective antagonist, SC51089. J Neurooncol 66, 285-292.

Mattila, P.K., Batista, F.D., Treanor, B., 2016. Dynamics of the actin cytoskeleton mediates receptor cross talk: An emerging concept in tuning receptor signaling. J Cell Biol 212, 267-280.

Maxwell, K.N., Zhou, Y., Hancock, J.F., 2018. Rac1 Nanoscale Organization on the Plasma Membrane Is Driven by Lipid Binding Specificity Encoded in the Membrane Anchor. Mol Cell Biol 38.

Mazzocchi-Jones, D., 2015. Impaired corticostriatal LTP and depotentiation following iPLA2 inhibition is restored following acute application of DHA. Brain Res Bull 111, 69-75.

Meierhofer, D., 2019. Acylcarnitine profiling by low-resolution LC-MS. PLoS One 14, e0221342.

Minghetti, L., 2004. Cyclooxygenase-2 (COX-2) in inflammatory and degenerative brain diseases. J Neuropathol Exp Neurol 63, 901-910.

Mita, R., Beaulieu, M.J., Field, C., Godbout, R., 2010. Brain fatty acid-binding protein and omega-3/omega-6 fatty acids: mechanistic insight into malignant glioma cell migration. J Biol Chem 285, 37005-37015.

Mita, R., Coles, J.E., Glubrecht, D.D., Sung, R., Sun, X., Godbout, R., 2007. B-FABP-expressing radial glial cells: the malignant glioma cell of origin? Neoplasia 9, 734-744.

Moghadasian, M.H., 2008. Advances in dietary enrichment with n-3 fatty acids. Crit Rev Food Sci Nutr 48, 402-410.

Montecillo-Aguado, M., Tirado-Rodriguez, B., Tong, Z., Vega, O.M., Morales-Martinez, M., Abkenari, S., Pedraza-Chaverri, J., Huerta-Yepez, S., 2020. Importance of the Role of omega-3 and omega-6 Polyunsaturated Fatty Acids in the Progression of Brain Cancer. Brain Sci 10.

Morihiro, Y., Yasumoto, Y., Vaidyan, L.K., Sadahiro, H., Uchida, T., Inamura, A., Sharifi, K., Ideguchi, M., Nomura, S., Tokuda, N., Kashiwabara, S., Ishii, A., Ikeda, E., Owada,

Y., Suzuki, M., 2013. Fatty acid binding protein 7 as a marker of glioma stem cells. Pathol Int 63, 546-553.

Moro, K., Nagahashi, M., Ramanathan, R., Takabe, K., Wakai, T., 2016. Resolvins and omega three polyunsaturated fatty acids: Clinical implications in inflammatory diseases and cancer. World J Clin Cases 4, 155-164.

Morrison, S.J., Kimble, J., 2006. Asymmetric and symmetric stem-cell divisions in development and cancer. Nature 441, 1068-1074.

Mouchlis, V.D., Chen, Y., McCammon, J.A., Dennis, E.A., 2018. Membrane Allostery and Unique Hydrophobic Sites Promote Enzyme Substrate Specificity. J Am Chem Soc 140, 3285-3291.

Murai, T., 2012. The role of lipid rafts in cancer cell adhesion and migration. Int J Cell Biol 2012, 763283.

Murai, T., Maruyama, Y., Mio, K., Nishiyama, H., Suga, M., Sato, C., 2011. Low cholesterol triggers membrane microdomain-dependent CD44 shedding and suppresses tumor cell migration. J Biol Chem 286, 1999-2007.

Murai, T., Miyazaki, Y., Nishinakamura, H., Sugahara, K.N., Miyauchi, T., Sako, Y., Yanagida, T., Miyasaka, M., 2004. Engagement of CD44 promotes Rac activation and CD44 cleavage during tumor cell migration. J Biol Chem 279, 4541-4550.

Murphy, E.J., Owada, Y., Kitanaka, N., Kondo, H., Glatz, J.F., 2005. Brain arachidonic acid incorporation is decreased in heart fatty acid binding protein gene-ablated mice. Biochemistry 44, 6350-6360.

Nan, X., Tamguney, T.M., Collisson, E.A., Lin, L.J., Pitt, C., Galeas, J., Lewis, S., Gray, J.W., McCormick, F., Chu, S., 2015. Ras-GTP dimers activate the Mitogen-Activated Protein Kinase (MAPK) pathway. Proc Natl Acad Sci U S A 112, 7996-8001.

Nasrollahzadeh, J., Siassi, F., Doosti, M., Eshraghian, M.R., Shokri, F., Modarressi, M.H., Mohammadi-Asl, J., Abdi, K., Nikmanesh, A., Karimian, S.M., 2008. The influence of feeding linoleic, gamma-linolenic and docosahexaenoic acid rich oils on rat brain tumor fatty acids composition and fatty acid binding protein 7 mRNA expression. Lipids Health Dis 7, 45.

Nathoo, N., Barnett, G.H., Golubic, M., 2004. The eicosanoid cascade: possible role in gliomas and meningiomas. J Clin Pathol 57, 6-13.

Nathoo, N., Prayson, R.A., Bondar, J., Vargo, L., Arrigain, S., Mascha, E.J., Suh, J.H., Barnett, G.H., Golubic, M., 2006. Increased expression of 5-lipoxygenase in high-grade astrocytomas. Neurosurgery 58, 347-354; discussion 347-354.

Newell, M., Goruk, S., Mazurak, V., Postovit, L., Field, C.J., 2019. Role of docosahexaenoic acid in enhancement of docetaxel action in patient-derived breast cancer xenografts. Breast Cancer Res Treat 177, 357-367.

Neyns, B., Sadones, J., Joosens, E., Bouttens, F., Verbeke, L., Baurain, J.F., D'Hondt, L., Strauven, T., Chaskis, C., In't Veld, P., Michotte, A., De Greve, J., 2009. Stratified phase II trial of cetuximab in patients with recurrent high-grade glioma. Ann Oncol 20, 1596-1603.

Ng, Y., Barhoumi, R., Tjalkens, R.B., Fan, Y.Y., Kolar, S., Wang, N., Lupton, J.R., Chapkin, R.S., 2005. The role of docosahexaenoic acid in mediating mitochondrial membrane lipid oxidation and apoptosis in colonocytes. Carcinogenesis 26, 1914-1921.

Nguyen, L.N., Ma, D., Shui, G., Wong, P., Cazenave-Gassiot, A., Zhang, X., Wenk, M.R., Goh, E.L., Silver, D.L., 2014. Mfsd2a is a transporter for the essential omega-3 fatty acid docosahexaenoic acid. Nature 509, 503-506.

Nishikawa, R., Ji, X.D., Harmon, R.C., Lazar, C.S., Gill, G.N., Cavenee, W.K., Huang, H.J., 1994. A mutant epidermal growth factor receptor common in human glioma confers enhanced tumorigenicity. Proc Natl Acad Sci U S A 91, 7727-7731.

Nobusawa, S., Watanabe, T., Kleihues, P., Ohgaki, H., 2009. IDH1 mutations as molecular signature and predictive factor of secondary glioblastomas. Clin Cancer Res 15, 6002-6007.

Nourallah, B., Digpal, R., Jena, R., Watts, C., 2017. Irradiating the Subventricular Zone in Glioblastoma Patients: Is there a Case for a Clinical Trial? Clin Oncol (R Coll Radiol) 29, 26-33.

Oemer, G., Koch, J., Wohlfarter, Y., Alam, M.T., Lackner, K., Sailer, S., Neumann, L., Lindner, H.H., Watschinger, K., Haltmeier, M., Werner, E.R., Zschocke, J., Keller, M.A., 2020. Phospholipid Acyl Chain Diversity Controls the Tissue-Specific Assembly of Mitochondrial Cardiolipins. Cell Rep 30, 4281-4291 e4284.

Ohgaki, H., Kleihues, P., 2013. The definition of primary and secondary glioblastoma. Clin Cancer Res 19, 764-772.

Olzmann, J.A., Carvalho, P., 2019. Dynamics and functions of lipid droplets. Nat Rev Mol Cell Biol 20, 137-155.

Ong, W.Y., Farooqui, T., Farooqui, A.A., 2010. Involvement of cytosolic phospholipase A(2), calcium independent phospholipase A(2) and plasmalogen selective phospholipase A(2) in neurodegenerative and neuropsychiatric conditions. Curr Med Chem 17, 2746-2763.

Osswald, M., Jung, E., Sahm, F., Solecki, G., Venkataramani, V., Blaes, J., Weil, S., Horstmann, H., Wiestler, B., Syed, M., Huang, L., Ratliff, M., Karimian Jazi, K., Kurz, F.T.,

Schmenger, T., Lemke, D., Gommel, M., Pauli, M., Liao, Y., Haring, P., Pusch, S., Herl, V., Steinhauser, C., Krunic, D., Jarahian, M., Miletic, H., Berghoff, A.S., Griesbeck, O., Kalamakis, G., Garaschuk, O., Preusser, M., Weiss, S., Liu, H., Heiland, S., Platten, M., Huber, P.E., Kuner, T., von Deimling, A., Wick, W., Winkler, F., 2015. Brain tumour cells interconnect to a functional and resistant network. Nature 528, 93-98.

Ostrom, Q.T., Cioffi, G., Gittleman, H., Patil, N., Waite, K., Kruchko, C., Barnholtz-Sloan, J.S., 2019. CBTRUS Statistical Report: Primary Brain and Other Central Nervous System Tumors Diagnosed in the United States in 2012-2016. Neuro Oncol 21, v1-v100.

Ostrom, Q.T., Patil, N., Cioffi, G., Waite, K., Kruchko, C., Barnholtz-Sloan, J.S., 2020. CBTRUS Statistical Report: Primary Brain and Other Central Nervous System Tumors Diagnosed in the United States in 2013-2017. Neuro Oncol 22, iv1-iv96.

Osuka, S., Van Meir, E.G., 2017. Overcoming therapeutic resistance in glioblastoma: the way forward. J Clin Invest 127, 415-426.

Owada, Y., 2008. Fatty acid binding protein: localization and functional significance in the brain. Tohoku J Exp Med 214, 213-220.

Owada, Y., Abdelwahab, S.A., Kitanaka, N., Sakagami, H., Takano, H., Sugitani, Y., Sugawara, M., Kawashima, H., Kiso, Y., Mobarakeh, J.I., Yanai, K., Kaneko, K., Sasaki, H., Kato, H., Saino-Saito, S., Matsumoto, N., Akaike, N., Noda, T., Kondo, H., 2006. Altered emotional behavioral responses in mice lacking brain-type fatty acid-binding protein gene. Eur J Neurosci 24, 175-187.

Owada, Y., Yoshimoto, T., Kondo, H., 1996. Spatio-temporally differential expression of genes for three members of fatty acid binding proteins in developing and mature rat brains. J Chem Neuroanat 12, 113-122.

Owen, D.M., Rentero, C., Magenau, A., Abu-Siniyeh, A., Gaus, K., 2011. Quantitative imaging of membrane lipid order in cells and organisms. Nat Protoc 7, 24-35.

Pallini, R., Ricci-Vitiani, L., Banna, G.L., Signore, M., Lombardi, D., Todaro, M., Stassi, G., Martini, M., Maira, G., Larocca, L.M., De Maria, R., 2008. Cancer stem cell analysis and clinical outcome in patients with glioblastoma multiforme. Clin Cancer Res 14, 8205-8212.

Palumbo, P., Lombardi, F., Augello, F.R., Giusti, I., Dolo, V., Leocata, P., Cifone, M.G., Cinque, B., 2020. Biological effects of selective COX-2 inhibitor NS398 on human glioblastoma cell lines. Cancer Cell Int 20, 167.

Pan, H., Wu, N., Huang, Y., Li, Q., Liu, C., Liang, M., Zhou, W., Liu, X., Wang, S., 2015a. Aldehyde dehydrogenase 1 expression correlates with the invasion of breast cancer. Diagn Pathol 10, 66.

Pan, Y., Morris, E.R., Scanlon, M.J., Marriott, P.J., Porter, C.J.H., Nicolazzo, J.A., 2018. Dietary docosahexaenoic acid supplementation enhances expression of fatty acid-binding protein 5 at the blood-brain barrier and brain docosahexaenoic acid levels. J Neurochem 146, 186-197.

Pan, Y., Scanlon, M.J., Owada, Y., Yamamoto, Y., Porter, C.J., Nicolazzo, J.A., 2015b. Fatty Acid-Binding Protein 5 Facilitates the Blood-Brain Barrier Transport of Docosahexaenoic Acid. Mol Pharm 12, 4375-4385.

Pan, Y., Short, J.L., Choy, K.H., Zeng, A.X., Marriott, P.J., Owada, Y., Scanlon, M.J., Porter, C.J., Nicolazzo, J.A., 2016. Fatty Acid-Binding Protein 5 at the Blood-Brain Barrier Regulates Endogenous Brain Docosahexaenoic Acid Levels and Cognitive Function. J Neurosci 36, 11755-11767.

Parsons, D.W., Jones, S., Zhang, X., Lin, J.C., Leary, R.J., Angenendt, P., Mankoo, P., Carter, H., Siu, I.M., Gallia, G.L., Olivi, A., McLendon, R., Rasheed, B.A., Keir, S., Nikolskaya, T., Nikolsky, Y., Busam, D.A., Tekleab, H., Diaz, L.A., Jr., Hartigan, J., Smith, D.R., Strausberg, R.L., Marie, S.K., Shinjo, S.M., Yan, H., Riggins, G.J., Bigner, D.D., Karchin, R., Papadopoulos, N., Parmigiani, G., Vogelstein, B., Velculescu, V.E., Kinzler, K.W., 2008. An integrated genomic analysis of human glioblastoma multiforme. Science 321, 1807-1812.

Pastrana, E., Silva-Vargas, V., Doetsch, F., 2011. Eyes wide open: a critical review of sphere-formation as an assay for stem cells. Cell Stem Cell 8, 486-498.

Patel, A.P., Tirosh, I., Trombetta, J.J., Shalek, A.K., Gillespie, S.M., Wakimoto, H., Cahill, D.P., Nahed, B.V., Curry, W.T., Martuza, R.L., Louis, D.N., Rozenblatt-Rosen, O., Suva, M.L., Regev, A., Bernstein, B.E., 2014. Single-cell RNA-seq highlights intratumoral heterogeneity in primary glioblastoma. Science 344, 1396-1401.

Pavicevic, Z., Leslie, C.C., Malik, K.U., 2008. cPLA2 phosphorylation at serine-515 and serine-505 is required for arachidonic acid release in vascular smooth muscle cells. J Lipid Res 49, 724-737.

Perry, J.R., Laperriere, N., O'Callaghan, C.J., Brandes, A.A., Menten, J., Phillips, C., Fay, M., Nishikawa, R., Cairncross, J.G., Roa, W., Osoba, D., Rossiter, J.P., Sahgal, A., Hirte, H., Laigle-Donadey, F., Franceschi, E., Chinot, O., Golfinopoulos, V., Fariselli, L., Wick, A., Feuvret, L., Back, M., Tills, M., Winch, C., Baumert, B.G., Wick, W., Ding, K., Mason, W.P., Trial, I., 2017. Short-Course Radiation plus Temozolomide in Elderly Patients with Glioblastoma. N Engl J Med 376, 1027-1037.

Petan, T., Jarc, E., Jusovic, M., 2018. Lipid Droplets in Cancer: Guardians of Fat in a Stressful World. Molecules 23.

Pfeiffer, K., Gohil, V., Stuart, R.A., Hunte, C., Brandt, U., Greenberg, M.L., Schagger, H., 2003. Cardiolipin stabilizes respiratory chain supercomplexes. J Biol Chem 278, 52873-52880.

Phillips, A.C., Boghaert, E.R., Vaidya, K.S., Mitten, M.J., Norvell, S., Falls, H.D., DeVries, P.J., Cheng, D., Meulbroek, J.A., Buchanan, F.G., McKay, L.M., Goodwin, N.C., Reilly, E.B., 2016. ABT-414, an Antibody-Drug Conjugate Targeting a Tumor-Selective EGFR Epitope. Mol Cancer Ther 15, 661-669.

Phillips, H.S., Kharbanda, S., Chen, R., Forrest, W.F., Soriano, R.H., Wu, T.D., Misra, A., Nigro, J.M., Colman, H., Soroceanu, L., Williams, P.M., Modrusan, Z., Feuerstein, B.G., Aldape, K., 2006. Molecular subclasses of high-grade glioma predict prognosis, delineate a pattern of disease progression, and resemble stages in neurogenesis. Cancer Cell 9, 157-173.

Phillis, J.W., Horrocks, L.A., Farooqui, A.A., 2006. Cyclooxygenases, lipoxygenases, and epoxygenases in CNS: their role and involvement in neurological disorders. Brain Res Rev 52, 201-243.

Pike, L.J., 2006. Rafts defined: a report on the Keystone Symposium on Lipid Rafts and Cell Function. J Lipid Res 47, 1597-1598.

Pike, L.J., Han, X., Chung, K.N., Gross, R.W., 2002. Lipid rafts are enriched in arachidonic acid and plasmenylethanolamine and their composition is independent of caveolin-1 expression: a quantitative electrospray ionization/mass spectrometric analysis. Biochemistry 41, 2075-2088.

Pinto, G., Saenz-de-Santa-Maria, I., Chastagner, P., Perthame, E., Delmas, C., Toulas, C., Moyal-Jonathan-Cohen, E., Brou, C., Zurzolo, C., 2021. Patient-derived glioblastoma stem cells transfer mitochondria through tunneling nanotubes in tumor organoids. Biochem J 478, 21-39.

Prager, B.C., Bhargava, S., Mahadev, V., Hubert, C.G., Rich, J.N., 2020. Glioblastoma Stem Cells: Driving Resilience through Chaos. Trends Cancer 6, 223-235.

Prahl, L.S., Bangasser, P.F., Stopfer, L.E., Hemmat, M., White, F.M., Rosenfeld, S.S., Odde, D.J., 2018. Microtubule-Based Control of Motor-Clutch System Mechanics in Glioma Cell Migration. Cell Rep 25, 2591-2604 e2598.

Price, N., van der Leij, F., Jackson, V., Corstorphine, C., Thomson, R., Sorensen, A., Zammit, V., 2002. A novel brain-expressed protein related to carnitine palmitoyltransferase I. Genomics 80, 433-442.

Qiang, L., Wu, T., Zhang, H.W., Lu, N., Hu, R., Wang, Y.J., Zhao, L., Chen, F.H., Wang, X.T., You, Q.D., Guo, Q.L., 2012. HIF-1alpha is critical for hypoxia-mediated maintenance of glioblastoma stem cells by activating Notch signaling pathway. Cell Death Differ 19, 284-294.

Qiu, J., Shi, Z., Jiang, J., 2017. Cyclooxygenase-2 in glioblastoma multiforme. Drug Discov Today 22, 148-156.

Rahman, M., Reyner, K., Deleyrolle, L., Millette, S., Azari, H., Day, B.W., Stringer, B.W., Boyd, A.W., Johns, T.G., Blot, V., Duggal, R., Reynolds, B.A., 2015. Neurosphere and adherent culture conditions are equivalent for malignant glioma stem cell lines. Anat Cell Biol 48, 25-35.

Rand, A.A., Barnych, B., Morisseau, C., Cajka, T., Lee, K.S.S., Panigrahy, D., Hammock, B.D., 2017. Cyclooxygenase-derived proangiogenic metabolites of epoxyeicosatrienoic acids. Proc Natl Acad Sci U S A 114, 4370-4375.

Rani, I., Vaiphei, K., Agnihotri, N., 2014. Supplementation of fish oil augments efficacy and attenuates toxicity of 5-fluorouracil in 1,2-dimethylhydrazine dihydrochloride/dextran sulfate sodium-induced colon carcinogenesis. Cancer Chemother Pharmacol 74, 309-322.

Rapoport, S.I., Ramadan, E., Basselin, M., 2011. Docosahexaenoic acid (DHA) incorporation into the brain from plasma, as an in vivo biomarker of brain DHA metabolism and neurotransmission. Prostaglandins Other Lipid Mediat 96, 109-113.

Rapoport, S.I., Rao, J.S., Igarashi, M., 2007. Brain metabolism of nutritionally essential polyunsaturated fatty acids depends on both the diet and the liver. Prostaglandins Leukot Essent Fatty Acids 77, 251-261.

Raza Shaikh, S., Brown, D.A., 2013. Models of plasma membrane organization can be applied to mitochondrial membranes to target human health and disease with polyunsaturated fatty acids. Prostaglandins Leukot Essent Fatty Acids 88, 21-25.

Reifenberger, G., Wirsching, H.G., Knobbe-Thomsen, C.B., Weller, M., 2017. Advances in the molecular genetics of gliomas - implications for classification and therapy. Nat Rev Clin Oncol 14, 434-452.

Reilly, P.T., Mak, T.W., 2012. Molecular pathways: tumor cells Co-opt the brain-specific metabolism gene CPT1C to promote survival. Clin Cancer Res 18, 5850-5855.

Remorino, A., De Beco, S., Cayrac, F., Di Federico, F., Cornilleau, G., Gautreau, A., Parrini, M.C., Masson, J.B., Dahan, M., Coppey, M., 2017. Gradients of Rac1 Nanoclusters Support Spatial Patterns of Rac1 Signaling. Cell Rep 21, 1922-1935.

Reynolds, B.A., Weiss, S., 1992. Generation of neurons and astrocytes from isolated cells of the adult mammalian central nervous system. Science 255, 1707-1710.

Ricciotti, E., FitzGerald, G.A., 2011. Prostaglandins and inflammation. Arterioscler Thromb Vasc Biol 31, 986-1000.

Richter, K.N., Revelo, N.H., Seitz, K.J., Helm, M.S., Sarkar, D., Saleeb, R.S., D'Este, E., Eberle, J., Wagner, E., Vogl, C., Lazaro, D.F., Richter, F., Coy-Vergara, J., Coceano, G., Boyden, E.S., Duncan, R.R., Hell, S.W., Lauterbach, M.A., Lehnart, S.E., Moser, T., Outeiro, T.F., Rehling, P., Schwappach, B., Testa, I., Zapiec, B., Rizzoli, S.O., 2018.

Glyoxal as an alternative fixative to formaldehyde in immunostaining and super-resolution microscopy. EMBO J 37, 139-159.

Robinson, P.J., Noronha, J., DeGeorge, J.J., Freed, L.M., Nariai, T., Rapoport, S.I., 1992. A quantitative method for measuring regional in vivo fatty-acid incorporation into and turnover within brain phospholipids: review and critical analysis. Brain Res Brain Res Rev 17, 187-214.

Rohle, D., Popovici-Muller, J., Palaskas, N., Turcan, S., Grommes, C., Campos, C., Tsoi, J., Clark, O., Oldrini, B., Komisopoulou, E., Kunii, K., Pedraza, A., Schalm, S., Silverman, L., Miller, A., Wang, F., Yang, H., Chen, Y., Kernytsky, A., Rosenblum, M.K., Liu, W., Biller, S.A., Su, S.M., Brennan, C.W., Chan, T.A., Graeber, T.G., Yen, K.E., Mellinghoff, I.K., 2013. An inhibitor of mutant IDH1 delays growth and promotes differentiation of glioma cells. Science 340, 626-630.

Rosa, A.O., Rapoport, S.I., 2009. Intracellular- and extracellular-derived Ca(2+) influence phospholipase A(2)-mediated fatty acid release from brain phospholipids. Biochim Biophys Acta 1791, 697-705.

Rosenberger, T.A., Villacreses, N.E., Contreras, M.A., Bonventre, J.V., Rapoport, S.I., 2003. Brain lipid metabolism in the cPLA2 knockout mouse. J Lipid Res 44, 109-117.

Rosenberger, T.A., Villacreses, N.E., Hovda, J.T., Bosetti, F., Weerasinghe, G., Wine, R.N., Harry, G.J., Rapoport, S.I., 2004. Rat brain arachidonic acid metabolism is increased by a 6-day intracerebral ventricular infusion of bacterial lipopolysaccharide. J Neurochem 88, 1168-1178.

Ruan, M., Liu, J., Ren, X., Li, C., Zhao, A.Z., Li, L., Yang, H., Dai, Y., Wang, Y., 2019. Whole transcriptome sequencing analyses of DHA treated glioblastoma cells. J Neurol Sci 396, 247-253.

Rubio, J.M., Astudillo, A.M., Casas, J., Balboa, M.A., Balsinde, J., 2018. Regulation of Phagocytosis in Macrophages by Membrane Ethanolamine Plasmalogens. Front Immunol 9, 1723.

Rysman, E., Brusselmans, K., Scheys, K., Timmermans, L., Derua, R., Munck, S., Van Veldhoven, P.P., Waltregny, D., Daniels, V.W., Machiels, J., Vanderhoydonc, F., Smans, K., Waelkens, E., Verhoeven, G., Swinnen, J.V., 2010. De novo lipogenesis protects cancer cells from free radicals and chemotherapeutics by promoting membrane lipid saturation. Cancer Res 70, 8117-8126.

Saarikangas, J., Zhao, H., Lappalainen, P., 2010. Regulation of the actin cytoskeleton-plasma membrane interplay by phosphoinositides. Physiological reviews 90, 259-289.

Saha, A., Shree Padhi, S., Roy, S., Banerjee, B., 2014. Method of detecting new cancer stem cell-like enrichment in development front assay (DFA). J Stem Cells 9, 235-242.

Saha, S., Lee, I.H., Polley, A., Groves, J.T., Rao, M., Mayor, S., 2015. Diffusion of GPI-anchored proteins is influenced by the activity of dynamic cortical actin. Mol Biol Cell 26, 4033-4045.

Saleem, H., Kulsoom Abdul, U., Kucukosmanoglu, A., Houweling, M., Cornelissen, F.M.G., Heiland, D.H., Hegi, M.E., Kouwenhoven, M.C.M., Bailey, D., Wurdinger, T., Westerman, B.A., 2019. The TICking clock of EGFR therapy resistance in glioblastoma: Target Independence or target Compensation. Drug Resist Updat 43, 29-37.

Sampson, J.H., Choi, B.D., Sanchez-Perez, L., Suryadevara, C.M., Snyder, D.J., Flores, C.T., Schmittling, R.J., Nair, S.K., Reap, E.A., Norberg, P.K., Herndon, J.E., 2nd, Kuan, C.T., Morgan, R.A., Rosenberg, S.A., Johnson, L.A., 2014. EGFRvIII mCAR-modified T-cell therapy cures mice with established intracerebral glioma and generates host immunity against tumor-antigen loss. Clin Cancer Res 20, 972-984.

Saurty-Seerunghen, M.S., Bellenger, L., El-Habr, E.A., Delaunay, V., Garnier, D., Chneiweiss, H., Antoniewski, C., Morvan-Dubois, G., Junier, M.P., 2019. Capture at the single cell level of metabolic modules distinguishing aggressive and indolent glioblastoma cells. Acta Neuropathol Commun 7, 155.

Schebesch, K.M., Proescholdt, M., Hohne, J., Hohenberger, C., Hansen, E., Riemenschneider, M.J., Ullrich, W., Doenitz, C., Schlaier, J., Lange, M., Brawanski, A., 2013. Sodium fluorescein-guided resection under the YELLOW 560 nm surgical microscope filter in malignant brain tumor surgery--a feasibility study. Acta Neurochir (Wien) 155, 693-699.

Schley, P.D., Brindley, D.N., Field, C.J., 2007. (n-3) PUFA alter raft lipid composition and decrease epidermal growth factor receptor levels in lipid rafts of human breast cancer cells. J Nutr 137, 548-553.

Schonfeld, P., Reiser, G., 2013. Why does brain metabolism not favor burning of fatty acids to provide energy? Reflections on disadvantages of the use of free fatty acids as fuel for brain. J Cereb Blood Flow Metab 33, 1493-1499.

Schonfeld, P., Reiser, G., 2017. Brain energy metabolism spurns fatty acids as fuel due to their inherent mitotoxicity and potential capacity to unleash neurodegeneration. Neurochem Int 109, 68-77.

Schroeder, R., London, E., Brown, D., 1994. Interactions between saturated acyl chains confer detergent resistance on lipids and glycosylphosphatidylinositol (GPI)-anchored proteins: GPI-anchored proteins in liposomes and cells show similar behavior. Proc Natl Acad Sci U S A 91, 12130-12134.

Schuck, S., Honsho, M., Ekroos, K., Shevchenko, A., Simons, K., 2003. Resistance of cell membranes to different detergents. Proc Natl Acad Sci U S A 100, 5795-5800.

Schumacher, T., Bunse, L., Pusch, S., Sahm, F., Wiestler, B., Quandt, J., Menn, O., Osswald, M., Oezen, I., Ott, M., Keil, M., Balss, J., Rauschenbach, K., Grabowska, A.K., Vogler, I., Diekmann, J., Trautwein, N., Eichmuller, S.B., Okun, J., Stevanovic, S., Riemer, A.B., Sahin, U., Friese, M.A., Beckhove, P., von Deimling, A., Wick, W., Platten, M., 2014. A vaccine targeting mutant IDH1 induces antitumour immunity. Nature 512, 324-327.

Schwan, C., Nolke, T., Kruppke, A.S., Schubert, D.M., Lang, A.E., Aktories, K., 2011. Cholesterol- and sphingolipid-rich microdomains are essential for microtubule-based membrane protrusions induced by Clostridium difficile transferase (CDT). J Biol Chem 286, 29356-29365.

Semenza, G.L., 2013. HIF-1 mediates metabolic responses to intratumoral hypoxia and oncogenic mutations. J Clin Invest 123, 3664-3671.

Sengupta, P., Jovanovic-Talisman, T., Skoko, D., Renz, M., Veatch, S.L., Lippincott-Schwartz, J., 2011. Probing protein heterogeneity in the plasma membrane using PALM and pair correlation analysis. Nat Methods 8, 969-975.

Serhan, C.N., 2014. Pro-resolving lipid mediators are leads for resolution physiology. Nature 510, 92-101.

Serhan, C.N., Levy, B.D., 2018. Resolvins in inflammation: emergence of the pro-resolving superfamily of mediators. J Clin Invest 128, 2657-2669.

Serhan, C.N., Petasis, N.A., 2011. Resolvins and protectins in inflammation resolution. Chem Rev 111, 5922-5943.

Sezgin, E., 2017. Super-resolution optical microscopy for studying membrane structure and dynamics. J Phys Condens Matter 29, 273001.

Sezgin, E., Levental, I., Mayor, S., Eggeling, C., 2017. The mystery of membrane organization: composition, regulation and roles of lipid rafts. Nat Rev Mol Cell Biol 18, 361-374.

Sezgin, E., Schneider, F., Galiani, S., Urbančič, I., Waithe, D., Lagerholm, B.C., Eggeling, C., 2019. Measuring nanoscale diffusion dynamics in cellular membranes with super-resolution STED–FCS. Nature Protocols 14, 1054-1083.

Shan, K., Feng, N., Cui, J., Wang, S., Qu, H., Fu, G., Li, J., Chen, H., Wang, X., Wang, R., Qi, Y., Gu, Z., Chen, Y.Q., 2020. Resolvin D1 and D2 inhibit tumour growth and inflammation via modulating macrophage polarization. J Cell Mol Med 24, 8045-8056.

Sheng, Z.H., Cai, Q., 2012. Mitochondrial transport in neurons: impact on synaptic homeostasis and neurodegeneration. Nat Rev Neurosci 13, 77-93.

Sherriff, J., Tamangani, J., Senthil, L., Cruickshank, G., Spooner, D., Jones, B., Brookes, C., Sanghera, P., 2013. Patterns of relapse in glioblastoma multiforme following concomitant chemoradiotherapy with temozolomide. Br J Radiol 86, 20120414.

Shinoda, J., Yano, H., Yoshimura, S., Okumura, A., Kaku, Y., Iwama, T., Sakai, N., 2003. Fluorescence-guided resection of glioblastoma multiforme by using high-dose fluorescein sodium. Technical note. J Neurosurg 99, 597-603.

Shono, T., Tofilon, P.J., Bruner, J.M., Owolabi, O., Lang, F.F., 2001. Cyclooxygenase-2 expression in human gliomas: prognostic significance and molecular correlations. Cancer Res 61, 4375-4381.

Shukla, G., Alexander, G.S., Bakas, S., Nikam, R., Talekar, K., Palmer, J.D., Shi, W., 2017. Advanced magnetic resonance imaging in glioblastoma: a review. Chin Clin Oncol 6, 40.

Simons, K., Ikonen, E., 1997. Functional rafts in cell membranes. Nature 387, 569-572.

Simons, K., Vaz, W.L., 2004. Model systems, lipid rafts, and cell membranes. Annu Rev Biophys Biomol Struct 33, 269-295.

Simopoulos, A.P., 1999. Essential fatty acids in health and chronic disease. Am J Clin Nutr 70, 560S-569S.

Singer, A.G., Ghomashchi, F., Le Calvez, C., Bollinger, J., Bezzine, S., Rouault, M., Sadilek, M., Nguyen, E., Lazdunski, M., Lambeau, G., Gelb, M.H., 2002. Interfacial kinetic and binding properties of the complete set of human and mouse groups I, II, V, X, and XII secreted phospholipases A2. J Biol Chem 277, 48535-48549.

Singh, H., Lu, R., Rodriguez, P.F., Wu, Y., Bopassa, J.C., Stefani, E., Toro, L., 2012. Visualization and quantification of cardiac mitochondrial protein clusters with STED microscopy. Mitochondrion 12, 230-236.

Singh, S.K., Hawkins, C., Clarke, I.D., Squire, J.A., Bayani, J., Hide, T., Henkelman, R.M., Cusimano, M.D., Dirks, P.B., 2004. Identification of human brain tumour initiating cells. Nature 432, 396-401.

Sivak-Sears, N.R., Schwartzbaum, J.A., Miike, R., Moghadassi, M., Wrensch, M., 2004. Case-control study of use of nonsteroidal antiinflammatory drugs and glioblastoma multiforme. Am J Epidemiol 159, 1131-1139.

Slipicevic, A., Jorgensen, K., Skrede, M., Rosnes, A.K., Troen, G., Davidson, B., Florenes, V.A., 2008. The fatty acid binding protein 7 (FABP7) is involved in proliferation and invasion of melanoma cells. BMC Cancer 8, 276.

Son, M.J., Woolard, K., Nam, D.H., Lee, J., Fine, H.A., 2009. SSEA-1 is an enrichment marker for tumor-initiating cells in human glioblastoma. Cell Stem Cell 4, 440-452.

Soupene, E., Kuypers, F.A., 2008. Mammalian long-chain acyl-CoA synthetases. Exp Biol Med (Maywood) 233, 507-521.

Souza, F.D.C., Ferreira, M.T., Colquhoun, A., 2020. Influence of Lipoxygenase Inhibition on Glioblastoma Cell Biology. Int J Mol Sci 21.

Spector, A.A., Kim, H.Y., 2015. Cytochrome P450 epoxygenase pathway of polyunsaturated fatty acid metabolism. Biochim Biophys Acta 1851, 356-365.

Spector, A.A., Yorek, M.A., 1985. Membrane lipid composition and cellular function. J Lipid Res 26, 1015-1035.

Stillwell, W., Shaikh, S.R., Zerouga, M., Siddiqui, R., Wassall, S.R., 2005. Docosahexaenoic acid affects cell signaling by altering lipid rafts. Reprod Nutr Dev 45, 559-579.

Stillwell, W., Wassall, S.R., 2003. Docosahexaenoic acid: membrane properties of a unique fatty acid. Chem Phys Lipids 126, 1-27.

Storch, J., Corsico, B., 2008. The emerging functions and mechanisms of mammalian fatty acid-binding proteins. Annu Rev Nutr 28, 73-95.

Strickland, M., Stoll, E.A., 2017. Metabolic Reprogramming in Glioma. Front Cell Dev Biol 5, 43.

Strokin, M., Sergeeva, M., Reiser, G., 2003. Docosahexaenoic acid and arachidonic acid release in rat brain astrocytes is mediated by two separate isoforms of phospholipase A2 and is differently regulated by cyclic AMP and Ca2+. Br J Pharmacol 139, 1014-1022.

Strokin, M., Sergeeva, M., Reiser, G., 2004. Role of Ca2+-independent phospholipase A2 and n-3 polyunsaturated fatty acid docosahexaenoic acid in prostanoid production in brain: perspectives for protection in neuroinflammation. Int J Dev Neurosci 22, 551-557.

Strokin, M., Sergeeva, M., Reiser, G., 2007. Prostaglandin synthesis in rat brain astrocytes is under the control of the n-3 docosahexaenoic acid, released by group VIB calcium-independent phospholipase A2. J Neurochem 102, 1771-1782.

Stupp, R., Hegi, M.E., Mason, W.P., van den Bent, M.J., Taphoorn, M.J., Janzer, R.C., Ludwin, S.K., Allgeier, A., Fisher, B., Belanger, K., Hau, P., Brandes, A.A., Gijtenbeek, J., Marosi, C., Vecht, C.J., Mokhtari, K., Wesseling, P., Villa, S., Eisenhauer, E., Gorlia, T., Weller, M., Lacombe, D., Cairncross, J.G., Mirimanoff, R.O., European Organisation for, R., Treatment of Cancer Brain, T., Radiation Oncology, G., National Cancer Institute of Canada Clinical Trials, G., 2009. Effects of radiotherapy with concomitant and adjuvant temozolomide versus radiotherapy alone on survival in glioblastoma in a randomised phase III study: 5-year analysis of the EORTC-NCIC trial. Lancet Oncol 10, 459-466.

Stupp, R., Mason, W.P., van den Bent, M.J., Weller, M., Fisher, B., Taphoorn, M.J., Belanger, K., Brandes, A.A., Marosi, C., Bogdahn, U., Curschmann, J., Janzer, R.C., Ludwin, S.K., Gorlia, T., Allgeier, A., Lacombe, D., Cairncross, J.G., Eisenhauer, E., Mirimanoff, R.O., European Organisation for, R., Treatment of Cancer Brain, T., Radiotherapy, G., National Cancer Institute of Canada Clinical Trials, G., 2005. Radiotherapy plus concomitant and adjuvant temozolomide for glioblastoma. N Engl J Med 352, 987-996.

Sturm, D., Witt, H., Hovestadt, V., Khuong-Quang, D.A., Jones, D.T., Konermann, C., Pfaff, E., Tonjes, M., Sill, M., Bender, S., Kool, M., Zapatka, M., Becker, N., Zucknick, M., Hielscher, T., Liu, X.Y., Fontebasso, A.M., Ryzhova, M., Albrecht, S., Jacob, K., Wolter, M., Ebinger, M., Schuhmann, M.U., van Meter, T., Fruhwald, M.C., Hauch, H., Pekrun, A., Radlwimmer, B., Niehues, T., von Komorowski, G., Durken, M., Kulozik, A.E., Madden, J., Donson, A., Foreman, N.K., Drissi, R., Fouladi, M., Scheurlen, W., von Deimling, A., Monoranu, C., Roggendorf, W., Herold-Mende, C., Unterberg, A., Kramm, C.M., Felsberg, J., Hartmann, C., Wiestler, B., Wick, W., Milde, T., Witt, O., Lindroth, A.M., Schwartzentruber, J., Faury, D., Fleming, A., Zakrzewska, M., Liberski, P.P., Zakrzewski, K., Hauser, P., Garami, M., Klekner, A., Bognar, L., Morrissy, S., Cavalli, F., Taylor, M.D., van Sluis, P., Koster, J., Versteeg, R., Volckmann, R., Mikkelsen, T., Aldape, K., Reifenberger, G., Collins, V.P., Majewski, J., Korshunov, A., Lichter, P., Plass, C., Jabado, N., Pfister, S.M., 2012. Hotspot mutations in H3F3A and IDH1 define distinct epigenetic and biological subgroups of glioblastoma. Cancer Cell 22, 425-437.

Sulciner, M.L., Serhan, C.N., Gilligan, M.M., Mudge, D.K., Chang, J., Gartung, A., Lehner, K.A., Bielenberg, D.R., Schmidt, B., Dalli, J., Greene, E.R., Gus-Brautbar, Y., Piwowarski, J., Mammoto, T., Zurakowski, D., Perretti, M., Sukhatme, V.P., Kaipainen, A., Kieran, M.W., Huang, S., Panigrahy, D., 2018. Resolvins suppress tumor growth and enhance cancer therapy. J Exp Med 215, 115-140.

Sun, G.Y., Shelat, P.B., Jensen, M.B., He, Y., Sun, A.Y., Simonyi, A., 2010. Phospholipases A2 and inflammatory responses in the central nervous system. Neuromolecular Med 12, 133-148.

Svennerholm, L., 1968. Distribution and fatty acid composition of phosphoglycerides in normal human brain. J Lipid Res 9, 570-579.

Swinnen, J.V., Dehairs, J., Talebi, A., 2019. Membrane Lipid Remodeling Takes Center Stage in Growth Factor Receptor-Driven Cancer Development. Cell Metab 30, 407-408.

Taha, A.Y., Cheon, Y., Ma, K., Rapoport, S.I., Rao, J.S., 2013. Altered fatty acid concentrations in prefrontal cortex of schizophrenic patients. J Psychiatr Res 47, 636-643.

Tajuddin, N., Moon, K.H., Marshall, S.A., Nixon, K., Neafsey, E.J., Kim, H.Y., Collins, M.A., 2014. Neuroinflammation and neurodegeneration in adult rat brain from binge ethanol exposure: abrogation by docosahexaenoic acid. PLoS One 9, e101223.

Tan, A.C., Ashley, D.M., Lopez, G.Y., Malinzak, M., Friedman, H.S., Khasraw, M., 2020. Management of glioblastoma: State of the art and future directions. CA Cancer J Clin 70, 299-312.

Tassoni, D., Kaur, G., Weisinger, R.S., Sinclair, A.J., 2008. The role of eicosanoids in the brain. Asia Pac J Clin Nutr 17 Suppl 1, 220-228.

Teague, H., Ross, R., Harris, M., Mitchell, D.C., Shaikh, S.R., 2013. DHA-fluorescent probe is sensitive to membrane order and reveals molecular adaptation of DHA in ordered lipid microdomains. The Journal of nutritional biochemistry 24, 188-195.

Thumser, A.E., Storch, J., 2007. Characterization of a BODIPY-labeled fluorescent fatty acid analogue. Binding to fatty acid-binding proteins, intracellular localization, and metabolism. Mol Cell Biochem 299, 67-73.

Tolle, A., Krause, H., Miller, K., Jung, K., Stephan, C., 2011. Importance of braintype fatty acid binding protein for cell-biological processes in human renal carcinoma cells. Oncol Rep 25, 1307-1312.

Tremblay, M.E., Zhang, I., Bisht, K., Savage, J.C., Lecours, C., Parent, M., Titorenko, V., Maysinger, D., 2016. Remodeling of lipid bodies by docosahexaenoic acid in activated microglial cells. J Neuroinflammation 13, 116.

Tripathi, S., Kushwaha, R., Mishra, J., Gupta, M.K., Kumar, H., Sanyal, S., Singh, D., Sanyal, S., Sahasrabuddhe, A.A., Kamthan, M., Mudiam, M.K., Bandyopadhyay, S., 2017. Docosahexaenoic acid up-regulates both PI3K/AKT-dependent FABP7-PPARgamma interaction and MKP3 that enhance GFAP in developing rat brain astrocytes. J Neurochem 140, 96-113.

Turkalp, Z., Karamchandani, J., Das, S., 2014. IDH mutation in glioma: new insights and promises for the future. JAMA Neurol 71, 1319-1325.

Uchida, N., Buck, D.W., He, D., Reitsma, M.J., Masek, M., Phan, T.V., Tsukamoto, A.S., Gage, F.H., Weissman, I.L., 2000. Direct isolation of human central nervous system stem cells. Proc Natl Acad Sci U S A 97, 14720-14725.

Unruh, D., Zewde, M., Buss, A., Drumm, M.R., Tran, A.N., Scholtens, D.M., Horbinski, C., 2019. Methylation and transcription patterns are distinct in IDH mutant gliomas compared to other IDH mutant cancers. Sci Rep 9, 8946.

Valdebenito, S., Audia, A., Bhat, K.P.L., Okafo, G., Eugenin, E.A., 2020. Tunneling Nanotubes Mediate Adaptation of Glioblastoma Cells to Temozolomide and Ionizing Radiation Treatment. iScience 23, 101450.

van den Bent, M., Eoli, M., Sepulveda, J.M., Smits, M., Walenkamp, A., Frenel, J.S., Franceschi, E., Clement, P.M., Chinot, O., de Vos, F., Whenham, N., Sanghera, P., Weller, M., Dubbink, H.J., French, P., Looman, J., Dey, J., Krause, S., Ansell, P., Nuyens,

S., Spruyt, M., Brilhante, J., Coens, C., Gorlia, T., Golfinopoulos, V., 2020. INTELLANCE 2/EORTC 1410 randomized phase II study of Depatux-M alone and with temozolomide vs temozolomide or lomustine in recurrent EGFR amplified glioblastoma. Neuro Oncol.

van den Bent, M.J., 2010. Interobserver variation of the histopathological diagnosis in clinical trials on glioma: a clinician's perspective. Acta Neuropathol 120, 297-304.

Van Horn, C.G., Caviglia, J.M., Li, L.O., Wang, S., Granger, D.A., Coleman, R.A., 2005. Characterization of recombinant long-chain rat acyl-CoA synthetase isoforms 3 and 6: identification of a novel variant of isoform 6. Biochemistry 44, 1635-1642.

van Meer, G., Voelker, D.R., Feigenson, G.W., 2008. Membrane lipids: where they are and how they behave. Nat Rev Mol Cell Biol 9, 112-124.

Vasquez, A.M., Mouchlis, V.D., Dennis, E.A., 2018. Review of four major distinct types of human phospholipase A2. Adv Biol Regul 67, 212-218.

Vasudevan, A., Yu, Y., Banerjee, S., Woods, J., Farhana, L., Rajendra, S.G., Patel, A., Dyson, G., Levi, E., Maddipati, K.R., Majumdar, A.P., Nangia-Makker, P., 2014. Omega-3 fatty acid is a potential preventive agent for recurrent colon cancer. Cancer Prev Res (Phila) 7, 1138-1148.

Vehlow, A., Cordes, N., 2013. Invasion as target for therapy of glioblastoma multiforme. Biochim Biophys Acta 1836, 236-244.

Verhaak, R.G., Hoadley, K.A., Purdom, E., Wang, V., Qi, Y., Wilkerson, M.D., Miller, C.R., Ding, L., Golub, T., Mesirov, J.P., Alexe, G., Lawrence, M., O'Kelly, M., Tamayo, P., Weir, B.A., Gabriel, S., Winckler, W., Gupta, S., Jakkula, L., Feiler, H.S., Hodgson, J.G., James, C.D., Sarkaria, J.N., Brennan, C., Kahn, A., Spellman, P.T., Wilson, R.K., Speed, T.P., Gray, J.W., Meyerson, M., Getz, G., Perou, C.M., Hayes, D.N., Cancer Genome Atlas Research, N., 2010. Integrated genomic analysis identifies clinically relevant subtypes of glioblastoma characterized by abnormalities in PDGFRA, IDH1, EGFR, and NF1. Cancer Cell 17, 98-110.

Vicidomini, G., Bianchini, P., Diaspro, A., 2018. STED super-resolved microscopy. Nat Methods 15, 173-182.

Vlashi, E., Lagadec, C., Vergnes, L., Matsutani, T., Masui, K., Poulou, M., Popescu, R., Della Donna, L., Evers, P., Dekmezian, C., Reue, K., Christofk, H., Mischel, P.S., Pajonk, F., 2011. Metabolic state of glioma stem cells and nontumorigenic cells. Proc Natl Acad Sci U S A 108, 16062-16067.

Wakamiya, T., Suzuki, S.O., Hamasaki, H., Honda, H., Mizoguchi, M., Yoshimoto, K., Iwaki, T., 2014. Elevated expression of fatty acid synthase and nuclear localization of carnitine palmitoyltransferase 1C are common among human gliomas. Neuropathology 34, 465-474.

Wang, D., Dubois, R.N., 2010. Eicosanoids and cancer. Nat Rev Cancer 10, 181-193.

Wang, F., Bhat, K., Doucette, M., Zhou, S., Gu, Y., Law, B., Liu, X., Wong, E.T., Kang, J.X., Hsieh, T.C., Qian, S.Y., Wu, E., 2011. Docosahexaenoic acid (DHA) sensitizes brain tumor cells to etoposide-induced apoptosis. Curr Mol Med 11, 503-511.

Wang, L., Wang, Z., Li, J., Zhang, W., Ren, F., Yue, W., 2015a. NFATc1 activation promotes the invasion of U251 human glioblastoma multiforme cells through COX-2. Int J Mol Med 35, 1333-1340.

Wang, Q., Hu, B., Hu, X., Kim, H., Squatrito, M., Scarpace, L., deCarvalho, A.C., Lyu, S., Li, P., Li, Y., Barthel, F., Cho, H.J., Lin, Y.H., Satani, N., Martinez-Ledesma, E., Zheng, S., Chang, E., Sauve, C.G., Olar, A., Lan, Z.D., Finocchiaro, G., Phillips, J.J., Berger, M.S., Gabrusiewicz, K.R., Wang, G., Eskilsson, E., Hu, J., Mikkelsen, T., DePinho, R.A., Muller, F., Heimberger, A.B., Sulman, E.P., Nam, D.H., Verhaak, R.G.W., 2017. Tumor Evolution of Glioma-Intrinsic Gene Expression Subtypes Associates with Immunological Changes in the Microenvironment. Cancer Cell 32, 42-56 e46.

Wang, Q., Li, H., Sun, Z., Dong, L., Gao, L., Liu, C., Wang, X., 2016. Kukoamine A inhibits human glioblastoma cell growth and migration through apoptosis induction and epithelial-mesenchymal transition attenuation. Sci Rep 6, 36543.

Wang, X., Chen, Y., Zhang, S., Zhang, L., Liu, X., Zhang, L., Li, X., Chen, D., 2015b. Co-expression of COX-2 and 5-LO in primary glioblastoma is associated with poor prognosis. J Neurooncol 125, 277-285.

Wassall, S.R., Stillwell, W., 2009. Polyunsaturated fatty acid-cholesterol interactions: domain formation in membranes. Biochim Biophys Acta 1788, 24-32.

Watanabe, A., Toyota, T., Owada, Y., Hayashi, T., Iwayama, Y., Matsumata, M., Ishitsuka, Y., Nakaya, A., Maekawa, M., Ohnishi, T., Arai, R., Sakurai, K., Yamada, K., Kondo, H., Hashimoto, K., Osumi, N., Yoshikawa, T., 2007. Fabp7 maps to a quantitative trait locus for a schizophrenia endophenotype. PLoS Biol 5, e297.

Watanabe, M., Tanaka, R., Takeda, N., 1992. Magnetic resonance imaging and histopathology of cerebral gliomas. Neuroradiology 34, 463-469.

Watkins, P.A., 1997. Fatty acid activation. Prog Lipid Res 36, 55-83.

Weil, S., Osswald, M., Solecki, G., Grosch, J., Jung, E., Lemke, D., Ratliff, M., Hanggi, D., Wick, W., Winkler, F., 2017. Tumor microtubes convey resistance to surgical lesions and chemotherapy in gliomas. Neuro Oncol 19, 1316-1326.

Weller, M., Weber, R.G., Willscher, E., Riehmer, V., Hentschel, B., Kreuz, M., Felsberg, J., Beyer, U., Loffler-Wirth, H., Kaulich, K., Steinbach, J.P., Hartmann, C., Gramatzki, D., Schramm, J., Westphal, M., Schackert, G., Simon, M., Martens, T., Bostrom, J., Hagel, C., Sabel, M., Krex, D., Tonn, J.C., Wick, W., Noell, S., Schlegel, U., Radlwimmer, B.,

Pietsch, T., Loeffler, M., von Deimling, A., Binder, H., Reifenberger, G., 2015a. Molecular classification of diffuse cerebral WHO grade II/III gliomas using genome- and transcriptome-wide profiling improves stratification of prognostically distinct patient groups. Acta Neuropathol 129, 679-693.

Weller, M., Wick, W., Aldape, K., Brada, M., Berger, M., Pfister, S.M., Nishikawa, R., Rosenthal, M., Wen, P.Y., Stupp, R., Reifenberger, G., 2015b. Glioma. Nat Rev Dis Primers 1, 15017.

Wen, P.Y., Kesari, S., 2008. Malignant gliomas in adults. N Engl J Med 359, 492-507.

Weylandt, K.H., Kang, J.X., Wiedenmann, B., Baumgart, D.C., 2007. Lipoxins and resolvins in inflammatory bowel disease. Inflamm Bowel Dis 13, 797-799.

Whelan, J., Fritsche, K., 2013. Linoleic acid. Adv Nutr 4, 311-312.

Wick, W., Platten, M., Meisner, C., Felsberg, J., Tabatabai, G., Simon, M., Nikkhah, G., Papsdorf, K., Steinbach, J.P., Sabel, M., Combs, S.E., Vesper, J., Braun, C., Meixensberger, J., Ketter, R., Mayer-Steinacker, R., Reifenberger, G., Weller, M., Society, N.O.A.S.G.o.N.-o.W.G.o.G.C., 2012. Temozolomide chemotherapy alone versus radiotherapy alone for malignant astrocytoma in the elderly: the NOA-08 randomised, phase 3 trial. Lancet Oncol 13, 707-715.

Wick, W., Weller, M., van den Bent, M., Sanson, M., Weiler, M., von Deimling, A., Plass, C., Hegi, M., Platten, M., Reifenberger, G., 2014. MGMT testing--the challenges for biomarker-based glioma treatment. Nat Rev Neurol 10, 372-385.

Wiktorowska-Owczarek, A., Berezinska, M., Nowak, J.Z., 2015. PUFAs: Structures, Metabolism and Functions. Adv Clin Exp Med 24, 931-941.

Wolf, D.M., Segawa, M., Kondadi, A.K., Anand, R., Bailey, S.T., Reichert, A.S., van der Bliek, A.M., Shackelford, D.B., Liesa, M., Shirihai, O.S., 2019. Individual cristae within the same mitochondrion display different membrane potentials and are functionally independent. The EMBO Journal 38, e101056.

Woo, J.S., Kim, S.M., Jeong, C.H., Ryu, C.H., Jeun, S.S., 2013. Lipoxygenase inhibitor MK886 potentiates TRAIL-induced apoptosis through CHOP- and p38 MAPK-mediated up-regulation of death receptor 5 in malignant glioma. Biochem Biophys Res Commun 431, 354-359.

Wu, C., Su, J., Wang, X., Wang, J., Xiao, K., Li, Y., Xiao, Q., Ling, M., Xiao, Y., Qin, C., Long, W., Zhang, F., Pan, Y., Xiang, F., Liu, Q., 2019. Overexpression of the phospholipase A2 group V gene in glioma tumors is associated with poor patient prognosis. Cancer Manag Res 11, 3139-3152.

Wu, M., Guan, J., Li, C., Gunter, S., Nusrat, L., Ng, S., Dhand, K., Morshead, C., Kim, A., Das, S., 2017. Aberrantly activated Cox-2 and Wnt signaling interact to maintain cancer stem cells in glioblastoma. Oncotarget 8, 82217-82230.

Xu, L.Z., Sanchez, R., Sali, A., Heintz, N., 1996. Ligand specificity of brain lipid-binding protein. J Biol Chem 271, 24711-24719.

Xu, W., Yang, H., Liu, Y., Yang, Y., Wang, P., Kim, S.H., Ito, S., Yang, C., Wang, P., Xiao, M.T., Liu, L.X., Jiang, W.Q., Liu, J., Zhang, J.Y., Wang, B., Frye, S., Zhang, Y., Xu, Y.H., Lei, Q.Y., Guan, K.L., Zhao, S.M., Xiong, Y., 2011. Oncometabolite 2-hydroxyglutarate is a competitive inhibitor of alpha-ketoglutarate-dependent dioxygenases. Cancer Cell 19, 17-30.

Xu, X., Wang, Y., Choi, W.S., Sun, X., Godbout, R., 2021. Super resolution microscopy reveals DHA-dependent alterations in glioblastoma membrane remodelling and cell migration. Nanoscale 13, 9706-9722.

Yamagata, K., Andreasson, K.I., Kaufmann, W.E., Barnes, C.A., Worley, P.F., 1993. Expression of a mitogen-inducible cyclooxygenase in brain neurons: regulation by synaptic activity and glucocorticoids. Neuron 11, 371-386.

Yan, H., Parsons, D.W., Jin, G., McLendon, R., Rasheed, B.A., Yuan, W., Kos, I., Batinic-Haberle, I., Jones, S., Riggins, G.J., Friedman, H., Friedman, A., Reardon, D., Herndon, J., Kinzler, K.W., Velculescu, V.E., Vogelstein, B., Bigner, D.D., 2009. IDH1 and IDH2 mutations in gliomas. N Engl J Med 360, 765-773.

Yang, C., Cao, M., Liu, Y., He, Y., Du, Y., Zhang, G., Gao, F., 2019. Inducible formation of leader cells driven by CD44 switching gives rise to collective invasion and metastases in luminal breast carcinomas. Oncogene 38, 7113-7132.

Yang, C., Iyer, R.R., Yu, A.C., Yong, R.L., Park, D.M., Weil, R.J., Ikejiri, B., Brady, R.O., Lonser, R.R., Zhuang, Z., 2012. beta-Catenin signaling initiates the activation of astrocytes and its dysregulation contributes to the pathogenesis of astrocytomas. Proc Natl Acad Sci U S A 109, 6963-6968.

Yang, H., Chen, C., 2008. Cyclooxygenase-2 in synaptic signaling. Curr Pharm Des 14, 1443-1451.

Yang, L., Zhang, H., 2018. Expression of Cytosolic Phospholipase A2 Alpha in Glioblastoma Is Associated With Resistance to Chemotherapy. Am J Med Sci 356, 391-398.

Yasumoto, Y., Miyazaki, H., Vaidyan, L.K., Kagawa, Y., Ebrahimi, M., Yamamoto, Y., Ogata, M., Katsuyama, Y., Sadahiro, H., Suzuki, M., Owada, Y., 2016. Inhibition of Fatty Acid Synthase Decreases Expression of Stemness Markers in Glioma Stem Cells. PLoS One 11, e0147717.

Yi, Y., Hsieh, I.Y., Huang, X., Li, J., Zhao, W., 2016. Glioblastoma Stem-Like Cells: Characteristics, Microenvironment, and Therapy. Front Pharmacol 7, 477.

Young, R.M., Jamshidi, A., Davis, G., Sherman, J.H., 2015. Current trends in the surgical management and treatment of adult glioblastoma. Ann Transl Med 3, 121.

Yu, J., Fischman, D.A., Steck, T.L., 1973. Selective solubilization of proteins and phospholipids from red blood cell membranes by nonionic detergents. J Supramol Struct 1, 233-248.

Yun, E.J., Song, K.S., Shin, S., Kim, S., Heo, J.Y., Kweon, G.R., Wu, T., Park, J.I., Lim, K., 2016. Docosahexaenoic acid suppresses breast cancer cell metastasis by targeting matrix-metalloproteinases. Oncotarget 7, 49961-49971.

Zahonero, C., Aguilera, P., Ramirez-Castillejo, C., Pajares, M., Bolos, M.V., Cantero, D., Perez-Nunez, A., Hernandez-Lain, A., Sanchez-Gomez, P., Sepulveda, J.M., 2015. Preclinical Test of Dacomitinib, an Irreversible EGFR Inhibitor, Confirms Its Effectiveness for Glioblastoma. Mol Cancer Ther 14, 1548-1558.

Zamarreno, F., Herrera, F.E., Corsico, B., Costabel, M.D., 2012. Similar structures but different mechanisms: Prediction of FABPs-membrane interaction by electrostatic calculation. Biochim Biophys Acta 1818, 1691-1697.

Zaugg, K., Yao, Y., Reilly, P.T., Kannan, K., Kiarash, R., Mason, J., Huang, P., Sawyer, S.K., Fuerth, B., Faubert, B., Kalliomaki, T., Elia, A., Luo, X., Nadeem, V., Bungard, D., Yalavarthi, S., Growney, J.D., Wakeham, A., Moolani, Y., Silvester, J., Ten, A.Y., Bakker, W., Tsuchihara, K., Berger, S.L., Hill, R.P., Jones, R.G., Tsao, M., Robinson, M.O., Thompson, C.B., Pan, G., Mak, T.W., 2011. Carnitine palmitoyltransferase 1C promotes cell survival and tumor growth under conditions of metabolic stress. Genes Dev 25, 1041-1051.

Zhang, Q., Zhu, B., Li, Y., 2017. Resolution of Cancer-Promoting Inflammation: A New Approach for Anticancer Therapy. Front Immunol 8, 71.

Zhu, M., Wang, X., Hjorth, E., Colas, R.A., Schroeder, L., Granholm, A.C., Serhan, C.N., Schultzberg, M., 2016. Pro-Resolving Lipid Mediators Improve Neuronal Survival and Increase Abeta42 Phagocytosis. Mol Neurobiol 53, 2733-2749.

Zong, H., Espinosa, J.S., Su, H.H., Muzumdar, M.D., Luo, L., 2005. Mosaic analysis with double markers in mice. Cell 121, 479-492.

Zou, Y., Watters, A., Cheng, N., Perry, C.E., Xu, K., Alicea, G.M., Parris, J.L.D., Baraban, E., Ray, P., Nayak, A., Xu, X., Herlyn, M., Murphy, M.E., Weeraratna, A.T., Schug, Z.T., Chen, Q., 2019. Polyunsaturated Fatty Acids from Astrocytes Activate PPARgamma Signaling in Cancer Cells to Promote Brain Metastasis. Cancer Discov 9, 1720-1735.

Zwinkels, H., Dirven, L., Vissers, T., Habets, E.J.J., Vos, M.J., Reijneveld, J.C., van den Bent, M.J., Taphoorn, M.J.B., 2016. Prevalence of changes in personality and behavior in adult glioma patients: a systematic review. Neurooncol Pract 3, 222-231.